DOKUZ EYLÜL UNIVERSITY

GRADUATE SCHOOL OF

NATURAL AND APPLIED SCIENCES

VOLCANO-SEDIMENTARY EVOLUTION OF
THE UŞAK-GÜRE BASIN, WESTERN ANATOLIA

by

Özgür KARAOĞLU

March, 2012

İZMİR

VOLCANO-SEDIMENTARY EVOLUTION OF THE UŞAK-GÜRE BASIN, WESTERN ANATOLIA

A Thesis Submitted to the
Graduate School of Natural and Applied Sciences of Dokuz Eylül University
In Partial Fulfillment of the Requirements for the Degree of Doctor of
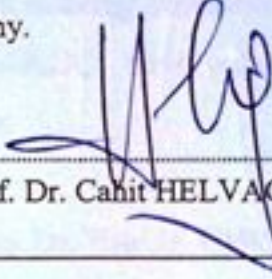**Philosophy in Geological Engineering, Applied Geology Program**
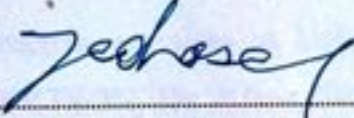
by
Özgür KARAOĞLU

March, 2012
İZMİR

Ph.D. THESIS EXAMINATION RESULT FORM

We have read the thesis entitled **"VOLCANO-SEDIMENTARY EVOLUTION OF THE UŞAK-GÜRE BASIN, WESTERN ANATOLIA"** completed by **ÖZGÜR KARAOĞLU** under supervision of **Prof. Dr. CAHİT HELVACI** and we certify that in our opinion it is fully adequate, in scope and in quality, as a thesis for the degree of Doctor of Philosophy.
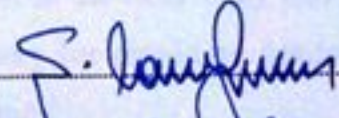
....

Prof. Dr. Cahit HELVACI

Supervisor

....

Prof. Dr. Hasan SÖZBİLİR   Prof. Dr. Kadir YURDAKOÇ
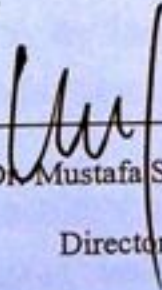
Thesis Committee Member   Thesis Committee Member

....

Prof. Dr. Uğur İNCİ   Prof. Dr. Ş. Can Genç

Examining Committee Member   Examining Committee Member

....

Prof. Dr. Mustafa SABUNCU

Director

Graduate School of Natural and Applied Sciences

ii

VOLCANO-SEDIMENTARY EVOLUTION OF THE UŞAK-GÜRE BASIN, WESTERN ANATOLIA

ABSTRACT

The Uşak-Güre basin is a well-preserved NE–SW-trending basin located on the northern part of the Menderes Massif, in western Anatolia. The basin contains a Lower to Upper Miocene volcano-sedimentary succession that records the un-roofing of the metamorphic rocks of the Menderes Massif. The new 40Ar/39Ar radiometric data demonstrate that Cenozoic volcanism commenced (17.29 Ma) with the emplacement of the Elmadağ volcano, synchronously with deposition of the İnay group. The youngest radiometric age is obtained from the Beydağı volcano (12.15 Ma) in the south, indicating that the volcanic activity migrated from north to south with time.

Low-angle detachment surfaces are clearly defined in the basin for the first time. Photomicrographs of the metamorphic rocks of the Menderes Massif as a footwall unit of the Simav Detachment Fault (SDF), show that transition of the ductile to brittle deformation.

Three stratovolcanoes has been described in the Uşak-Güre basin. These stratovolcanoes display the features of subaqueous-subaerial environments, and all volcanic sequences consist of complex successions of effusive-extrusive and explosive phases. The products of the explosive volcanism and related magma-water interactions have been described for the first time in the western Anatolia.

Three distinct volcanic unit are classified in the Uşak-Güre basin: (1) the Beydağı volcanic unit composed of shoshonite, latites and rhyolitic lavas followed by dacitic and andesitic pyroclastic deposits; (2) the Payamtepe volcanic unit composed of potassic intermediate composition lavas (latites and trachytes); and (3) the Karaağaç dikes composed of andesite and latite. Volcanic rocks of the basin are characterized by strong enrichment in LILE and LREE and depletions of Nb-Ta and Ti on MORB-

normalized multi-element diagrams. Geochemical features of the volcanic rocks suggest that they experienced mixing processes between mafic and felsic end-members and also fractional crystallization of dominantly plagioclase and pyroxenes from mixed magma compositions.

Keywords: Western Anatolia, NE–SW-trending basins, Uşak-Güre basin, physical volcanology, magmatic petrogenesis

UŞAK-GÜRE HAVZASININ VOLKANO-SEDİMANTER EVRİMİ, BATI ANADOLU

ÖZ

Uşak-Güre havzası Batı Anadolu'da Menderes Masifinin kuzeyinde yer alan KD–GB uzanımlı iyi korunmuş bir havzadır. Uşak-Güre havzası, Menderes Masifi Çekirdek Kompleksine (MMÇK) ait metamorfik kayaçlarının yüzeylemesine ait kayıtlar içeren Alt ve Üst Miyosen volcano-sedimanter istifler içermektedir. Yeni 40Ar/39Ar radyometrik yaş verileri Senezoyik volkanizmasının İnay grubuyla eş zamanlı olarak (17.29 My) Beydağı volkanın yerleşimiyle başladığını göstermektedir. En genç yaş verisi güneydeki Beydağı volkanından (12.15 My) elde edilmiş olup, volkanik aktivenin kuzeyden güneye doğru göçüne işaret etmektedir.

Düşük açılı sıyrılma fay düzlemleri havzada ilk defa tanımlanmıştır. Simav Sıyrılma Fayının (SSF) taban bloğunda kalan Menderes Masifi Metamorfik kayaçlarına ait incekesit görüntüleri sünümlü-kırılgan deformasyon geçiş özelliklerini göstermektedir.

Uşak-güre havzasında üç stratovolkan tanımlanmıştır. Stratovolkanlar karasal-yarı karasal ortam özellikleri sunarken volkanik istifler efüzif, ekstrüzif ve eksplozif faz özelliklerine sahiptir. Eksplozif volkanizma ürünleri ve bununla ilişkili magma-su etkileşimleri Batı Anadolu'da ilk defa tanımlanmıştır.

Ayrıca, Uşak-Güre havzasında üç farklı volkanik birim sınıflandırılmıştır: bunlar (1) şoşonit, latit ve riyolitik lavlar ile dasitik ve andezitik piroklastik kayaçlardan oluşan Beydağı volkanik birimi; (2) potasik ortaç bileşimli lavlardan oluşan (trakit ve latitler) Payamtepe volkanik birimi ve (3) andezit ve latitik dayklardan oluşan Karaağaç daykları. Uşak-Güre havzasındaki volkanik kayaçlar MORB-normalize çoklu element diyagramlarında, Nb-Ta ve Ti tüketilmesi ile LILE ve LREE elementlerinin zenginleşmesiyle karakterize edilmektedir. Volkanik kayaçların jeokimyasal özellikleri, mafik ve feslik uç üyeleri ile aynı zamanda karışım özelliği

gösteren magma bileşiminden baskın olarak piroksenlerin ve plajiyoklazların ayrımsal kristallenme süreçlerine maruz kaldıklarını göstermektedir.

Anahtar kelimeler: Batı Anadolu, KD–GB-uzanımlı havzalar, Uşak-Güre havzası, fiziksel volkanoloji, magmatik petrojenez

CONTENTS

ix

CHAPTER ONE
INTRODUCTION

The Anatolide belt of western Turkey, which is part of the Alpine-Himalayan orogenic system formed as a consequence of Eocene collision tectonics (Gessner et al., 2001). Following the Eocene collision between the Anatolide-Tauride block to the south and the Sakarya Zone to the north, the Neogene geodynamic evolution of the Anatolian-Aegean area was mainly controlled by (1) continental collision between Arabia and Eurasia to the east since the middle Miocene (ca. 13 Ma; McKenzie, 1978; Dewey et al., 1986; Jackson & McKenzie, 1988; Ring & Layer, 2003); (2) retreating subduction of the African plate under the Aegean-Anatolian plates along the Hellenic and Cyprean trenches (LePichon & Angelier, 1979; Jackson & McKenzie, 1988; Kreemer et al., 2003; Okay et al., 2010; Ring et al., 2010) followed by back-arc spreading (e.g. Boccaletti et al., 1974; LePichon & Angelier, 1979). According to van Hinsbergen et al. (2005), from the Early Cretaceous to the present, Africa–Eurasia convergence produced the continuous subduction of short alternating segments of continental and oceanic lithosphere; (3) post-collisional extensional processes as a consequence of the complex kinematic microplate interactions that developed after the latest Oligocene (Seyitoğlu & Scott, 1991, 1992).

1.1 Scope and Layout of Thesis

The dissertation aims to resolve the structure and volcanological evolution of the Uşak-Güre basin in western Anatolia since Early Miocene. The approach taken has been to field-based studies, and consists of (1) detailed mapping of geological structures at a scale of 1/25.000 (2) documentation of outcrop of-scale faults and their kinematic relationships and (3) revised stratigraphy and a new tectonic model. Comparatively, the evolution of the Uşak-Güre basin provides a synopsis of relevant data from various stratigraphic units in the basin. The data consist of recently published $^{40}Ar/^{39}Ar$ radiometric age data (Karaoğlu et al., 2010) with geological mapping. The work also documents new kinematic evidences using the three well-

identified extensional phases. I will further discuss the implications of this structural data in terms of the geodynamic evolution of the Uşak-Güre basin in order to better understand of the exhumation history of Menderes Massif Core Complex and related extensional tectonics in the province.

In addition, in order to better understand of the physical volcanologic processes of three volcanic centers (Elmadağ, İtecektepe and Beydağı) within Uşak-Güre basin, the work present all the eruptive phases via using detailed volcanologic maps (1/25.000 in scale), many columnar sections, simplified geologic sections, and many well-selected photographs from the field. Many visual materials have been used through the manuscript because of that the study area has complex geologic problems and in order to obtain the correct volcanologic approach of these volcanic centers. The dissertation also proposes main volcanic depressions in western Anatolia for the better understanding mechanism of the destruction processes of these volcanic centers.

The thesis is divided into five Chapters: the introductory chapter is followed by three Chapters (Chapters II, III and IV) which each represent self-consistent research manuscript, which have been published and submitted to scientific journals. A fifth Chapter summarises the conclusions of Chapters II, III and IV.

In the Chapter I, previous work is reviewed which is taken into proper to the regional tectonics of the western Anatolia. As the successive Chapters contain detailed introductory sections themselves, only a general picture is given to avoid unnecessary repetition.

Chapter II addresses the stratigraphic and sedimentologic setting via using new radiometric age data ($^{40}Ar/^{39}Ar$) of the Uşak-Güre basin. The most prominent Cenozoic basin fill deposits around western Anatolia was clearly determined, like Hacıbekir Group, İnay Group and Asartepe formation within Uşak-Güre basin. Most of researchers, who proposed different views with regard to exhumation processes of Menderes Massif Core Complex since early Miocene, refer to Cenozoic basin fill

sediments such as those found in Hacıbekir and İnay Groups with Asartepe formation. However, the previous works have not supplied any adequate and sufficient sedimentologically evidence concerning with aforementioned deposits up to the present. For this reason, the chapter will also exhibit some characteristic fabric and textural properties of Hacıbekir and İnay Groups supported with several photographs and cross-sections.

Chapter III documents Structural evolution of the Uşak-Güre basin since Oligo-Miocene. The chapter proposes a new structural mechanism via using a combination of geological mapping and detailed kinematic fault analysis from each of the evolutionary phases. This has allowed us to characterise the temporal and spatial evolution of footwall and hanging-wall deformation, which I interpreted in the context evolution of the Uşak and Güre basins. Chapter III also presents: (1) for the first time, low-angle detachment surfaces that define both the Uşak and Güre margins and (2) three different tectonic stages documented since the Early Cenozoic: the Early Miocene Deformation phase (D_2); the Middle Miocene Deformation Phase (D_3) and the Late Miocene Deformation Phase (D_4). Each of these phases indicates that the Uşak-Güre basin was affected by NE–SW-trending progressive extensional tectonics. Finally, the work suggests an alternating "Uşak-Muğla Transtensional Transfer Zone" (UMTZ) at the eastern part of the Menderes Massif since Middle Miocene. Chapter III is largely identical with the revised version of a manuscript submitted to 'Journal of Geological Society (London)' entitled "Structural evolution of the Uşak-Güre supra-detachment basin during Miocene extensional denudation in western Turkey". Co-author is Cahit Helvacı.

Chapter IV deals with physical volcanologic evolution of the volcanic centers in the basins. Proverbially, many geologist/volcanologists mention about interfingering properties between volcanic materials and sedimentary fillings in western Anatolia, however most of them could not clearly present proof-positive regard to these. The chapter documents exhaustive subaqueous-subaerial records for three stratovolcanoes. The importance of the Chapter IV is the products of the explosive volcanism and related magma-water interactions have been described for the first

time in western Anatolia. In addition, I have supplied new evidence about the occurrence of volcanism and related gold bearing porphyry system in Beydağı caldera and destructive areas of Elmadağ and İtecektepe are tectonically controlled by the combined influence of the NE–SW oblique, strike-slip and high-angle faults on-land propagating destruction of these stratovolcanoes. The largely part and improved version of the Chapter IV has been submitted to 'Journal of Volcanology and Geothermal Research' entitled "Growth, destruction and resurgence of three volcanic centers in the Miocene Uşak-Güre basin, western Turkey: subaqueous-subaerial volcanism in a lacustrine setting". Co-author is Cahit Helvacı.

The subject of Chapter V is to constrain the petrogenesis of the volcanic rocks in the Uşak and Güre basins. In order to resolve petrogenetic evolution of the Neogene Volcanic rocks and to develop a better understanding of the geodynamic evolution of the basin, it has been studied the whole rock geochemical data, and compared the results with previously published data from the Miocene Selendi volcanic rocks which represents the western adjacent; and coeval Afyon-Kırka-Isparta volcanic rocks, locating easternmost part of the Uşak and Güre basins. This chapter was published by 'Lithos' in July 2010, entitled "Petrogenesis and ^{40}Ar/^{39}Ar geochronology of the volcanic rocks of the Uşak-Güre basin, western Türkiye". Co-authors are Cahit Helvacı and E. Yalçın Ersoy.

1.2 An Overview of Neogene Tectonic Framework of Western Anatolia

The Aegean region is one of the best- studied continental extensional provinces in the world. However, much controversy still exists as to the detailed timing of the extension and observed metamorphism in the Menderes Massif. The general consensus is that lithospheric extension in the Aegean and west Anatolian region started approximately 25 Ma ago (Gautier et al., 1999; Jolivet, 2001; Tirel et al., 2009; Ring & Glodny, 2010; Ring et al., 2010). Crustal-scale extensions in the western Türkiye since the early Miocene have created numerous basins within the hanging-walls of low-angle normal faults (Gessner et al., 2001; Lips et al., 2001; Ring et al., 2003; Işık et al., 2004; Seyitoğlu et al., 2004; Catlos & Çemen, 2005;

Thompson & Ring, 2006; Çemen et al., 2006; Catlos et al., 2008). The depocenters in these supra-detachment basins have received much attention in the geological literature in recent years (Bozkurt, 2003; Bozkurt & Sözbilir, 2004; Çiftçi & Bozkurt, 2009, 2010; Ersoy et al., 2010; Ersoy et al., 2011). The most crucial reason for this the attention is that these supradetachment basins and the tectonics in this province are directly associated with domal uplift of the Menderes Core Complex in the lower plate and the formation of the asymmetric supradetachment basins (e.g. Early Miocene NE–SW-trending and Late Miocene E–W-trending basins) in the upper plate.

The formation of the NE–SW-trending basins (e.g. Uşak-Güre, Selendi, Demirci and Gördes basins) was one of the most prominent extensional processes during early Miocene in western Anatolia (Figure 1.1). Widespread Miocene volcanism is also one of the most important characteristics in these NE-SW-trending basins. In order to understand the origin of the basin's evolution and related Neogene volcanism in the frontal extensional area of the Menderes Massif, the extensional and geodynamic processes of the NE–SW-trending basins must be manifested. Five different geodynamic models have been suggested for the genesis of NE–SW-trending basins as summarized below: (i) NE–SW-trending basins are 'Tibet-type cross-grabens' developed during N–S post-Palaeocene compression and filled by a lower middle Miocene volcano-sedimentary succession. Later N-S extension prevailed and resulted in the E–W-trending grabens (e.g. Gediz, Büyük Menderes, Küçük Menderes grabens) of Tortonian age (Şengör et al., 1984, 1985; Şengör, 1987; Görür et al., 1995; Yılmaz et al., 2000, 2001), (ii) both NE–SW-trending basins and E–W-trending grabens began to develop simultaneously during the latest Oligocene– early Miocene under a N–S extensional tectonic regime, and this is attributed to the orogenic collapse of the over thickened Aegean crust (Seyitoğlu & Scott, 1992, 1994; Seyitoğlu, 1997), (iii) these basins are intramontane depressions which resulted from a slowly developed post-orogenic subsidence (İnci 1998) and filled with Miocene sediments (Helvacı & Yağmurlu, 1995). (iv) Purvis & Robertson (2004) proposes a new three-phase "pulsed extension" model for western Turkey. The authors also envisaged that the NE–SW-trending basins were formed in tens of

kilometre scale corrugations of a regional-scale, top-to-the-north extensional detachment fault via orogenic collapse, which unroofed the central Menderes Metamorphic Core Complex in the late Oligocene (Purvis & Robertson, 2004, 2005). (v) Ersoy et al. (2010) has modified all of the proposed geodynamic models that are available. The authors presented that the NE–SW-trending basins located on the northern side of the Menderes Massif were developed in response to different stages of extensional faulting, including two-stage detachment faulting and related strike-slip faulting during exhumation of the massif and later normal faulting during a rift-type extension (Ersoy et al., 2010).

van Hinsbergen et al. (2010) have recently reported a large set of new paleomagnetic data from western Turkey. He concluded that the lower volcanics from Lesbos to Uşak, including the NE–SW-trending basins on the northern Menderes Massif (NMM), underwent no significant rotation since middle Miocene. However, the Lycian Nappes and Bey Dağları are shown to rotate ~20° between 16 and 5 Ma, defining the eastern limb of the Aegean orocline. This occurred contemporaneously with the exhumation of the central Menderes Massif (along extensional detachments) and after the latest Oligocene to early Miocene exhumation of the northern and southern Menderes Massifs.

A number of workers have sought to better characterize the complex structural and stratigraphic history of the basin (Ercan et al., 1978; Şengör, 1987; Seyitoğlu, 1997; Gessner et al., 2001; Purvis & Robertson, 2004, 2005; Ersoy et al., 2010; Karaoğlu et al., 2010; van Hinsbergen, 2010). A considerable amount of debate has been generated concerning the exact nature and timing of tectonic and depositional events regarding the NE–SW-trending basins (e.g. Ercan et al., 1978; Seyitoğlu, 1997).

1.3 An Overview of the Neogene Magmatic Activity in the Region

The magmatism propagated from north to south with time and there were two major episodes (Yılmaz, 1989; Yılmaz et al., 2001; Aldanmaz, 2002). The first

episode during the Eocene to Oligocene–Miocene times produced medium to high-K calk-alkaline granitoids and widespread volcanic rocks. The volcanic products of this phase have high $^{87}Sr/^{86}Sr$ and low $^{143}Nd/^{144}Nd$ ratios, characteristic of a subduction metasomatized lithospheric mantle source (Aldanmaz et al., 2000, 2009; Innocenti et al., 2005). The second episode is mildly alkaline in nature, displaying gradually decreasing amount of crustal contamination and was active during the Middle Miocene (16–14 Ma) (Aldanmaz et al., 2000; Altunkaynak, 2007; Dilek & Altunkaynak, 2007). During the late Miocene to Pleistocene, an OIB-type volcanism yielded mafic alkaline and finally sodic products (Güleç, 1991; Alıcı et al., 2002; Aldanmaz et al., 2009) that accompanied the most recent extensional phase in the Anatolian-Aegean region. The Late Miocene to Quaternary lavas have low $^{87}Sr/^{86}Sr$ and high $^{143}Nd/^{144}Nd$, indicating a sub-lithospheric mantle origin.

Innocenti et al. (2010) grouped the late Eocene–Holocene volcanic products in the Aegean region into three categories according to their geochemical–isotopic features and age distribution: group A, Late Miocene–Pleistocene alkali basalts which were generated in the subslab asthenosphere; group B, calc-alkaline rocks of the Pliocene–Holocene active arc (south Aegean active volcanic arc) which were generated in an asthenospheric supra-slab mantle wedge (e.g. Francalanci et al., 2005); and group C, high-K calcalkaline to shoshonitic rocks belonging to the Late Eocene–Middle Miocene belt.

Different hypotheses have been developed to describe the Cenozoic volcanism across the Aegean region-western Anatolia. One hypothesis postulates that the magmatism is directly related to subduction events (Fytikas et al., 1984; Okay & Satır, 2000; Agostini et al., 2007; Doglioni et al., 2009; Innocenti et al., 2010; Ring et al., 2010; Ustaömer et al., 2009). The second hypothesis suggests that the magmatic events developed in response to a post collisional extensional tectonic regime with respect to the Eocene collision between the Anatolide-Tauride block and the Sakarya Zone (Yılmaz, 1989; Aldanmaz et al., 2000; Aldanmaz, 2002; Altunkaynak, 2007; Dilek & Altunkaynak, 2007).

According to the first view, Eocene to Quaternary volcanic rocks in the Aegean are the products of a single subduction system that migrated to the south over time (Fytikas et al., 1984; Okay & Satır, 2000; Agostini et al., 2007; Doglioni et al., 2009; Innocenti et al., 2010; Ring et al., 2010). Innocenti et al. (2010) claim that the geochemical differences among the Aegean volcanic rocks are not only closely related to different subduction enrichments but are also linked to different pre-subduction mantle features north and south. According to these authors, Eocene to Miocene volcanic rocks are the products of melting of a heterogeneously enriched lithospheric mantle on flatly subducted African oceanic lithosphere. The formation of the OIB-type volcanic rocks (such as Quaternary Kula volcanic rocks) is explained by slab tearing that allowed the rise of asthenospheric mantle.

The Neogene post-collisional extensional tectonic regime and related Cenozoic volcanism in western Anatolia has been described by three different models: (1) westward extrusion of the wedge-shaped Anatolian which is accommodated by two major faults: the right-lateral strike-slip North Anatolian Fault (NAF) and the left-lateral strike-slip East Anatolian Fault (EAF) (Şengör et al., 1985; Koçyiğit et al., 1999); (2) the difference between the velocity of the Greek microplate and that of the Anatolian microplate in overriding the African plate (Doglioni et al., 2002; Agostini et al., 2010); (3) postorogenic collapse, inwhich the Aegean–western Anatolian extension results primarily from 'gravitational collapse', following orogenic crustal shortening and overthickening within the Western Anatolian crust. During this postorogenic collapse, throughout the late Cenozoic, mid-crustal units of several metamorphic massifs were exhumed along low-angle detachment faults (Seyitoğlu & Scott, 1996; Gautier et al., 1999; Gessner et al., 2001; Işık & Tekeli, 2001; Jolivet, 2001; Lips et al., 2001; Sözbilir, 2001). Neogene exhumation of the metamorphic massifs formed the Menderes Massif Core Complex, on which several NE–SW-trending volcano-sedimentary basins were developed synchronously with the exhumation. One of the NE–SW-trending basins in the region is the Uşak and Güre basins, which is the major topic of this paper, located on the eastern side of western Anatolia (Figure 3.1). The Uşak-Güre basin contains well-preserved Neogene

volcanic units, whose geochemical characteristics have not yet been well documented.
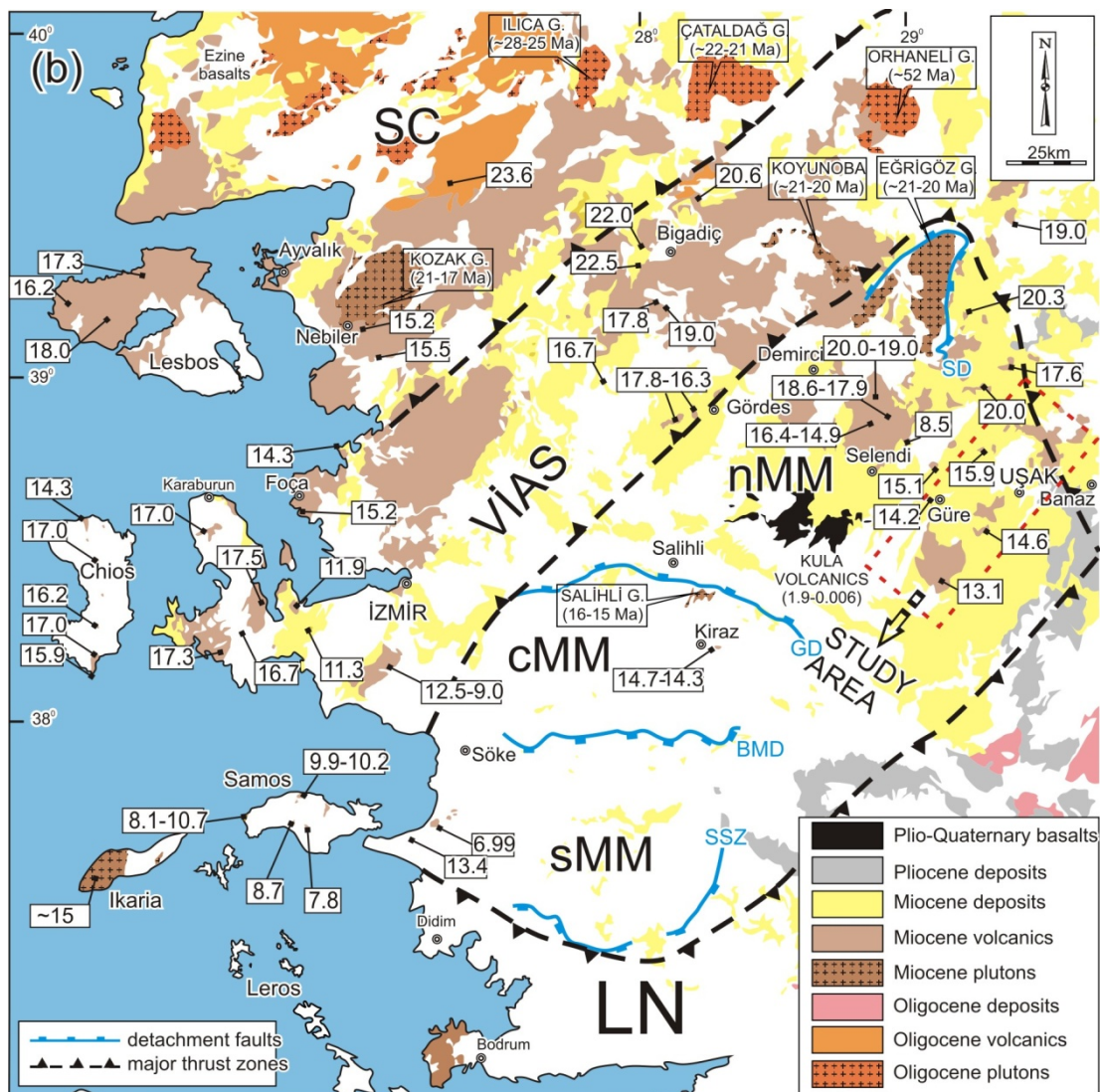
Figure 1.1 Generalized map of Western Anatolia, showing the Neogene volcanic and sedimentary rocks and main tectonic structures. The detachment faults are indicated by blue solid lines and comprise (from north to south) the Simav detachment (SD), Gediz detachment (GD), Büyük Menderes detachment (BMD) faults, Selimiye shear zone (SSZ), Sakarya continent (SC), northern Menderes Massif (nMM), central Menderes Massif (cMM), southern Menderes Massif (sMM), Vardar-İzmir-Ankara sture zone (VİAS), Lycian nappes (LN).

1.4 An Overview of the Major Volcanic Destruction Structures in the Region

The Köroğlu caldera (Aydar et al., 1998) and Afyon Stratovolcano (Aydar et al., 2003), Bodrum caldera (Ulusoy et al., 2004), Ezine volcano-plutonic complex (Karacık & Yılmaz, 1998) were defined by limited studies however these volcanic centers have not discussed in detailed within volcanologic framework. In addition, no detailed study of the processes of the physical volcanology has been studied on Demirci, Yağcıdağ, Elmadağ, Beydağ, İtecektepe and Karşıyaka volcanic depressions. The relationship between eruptive mechanism and chemical compositions is therefore, unclear, as is the possible correlation with dynamics of the volcano-tectonic background during late Cenozoic at the western Anatolia (Figure 1.2).

The Köroğlu Caldera is located north of the Afyon city, affected by NE–SW-strike slip faults which was active the pre-caldera stage, while NW–SE-trending faults after the ignimbrite eruption, and triggered the lava flow activity at the post caldera stage since Early Miocene (Aydar et al., 1998). The authors claim that the Köroğlu caldera is a resurgent type caldera, 13 X 18 km in diameter, produced low aspect ratio ignimbrites, which have been transported up to 50 km away from the volcanic source. The volcanological evolution of the caldera exhibits four distinct stages: (1) updoming; (2) ignimbrite eruption and caldera collapse; (3) resurgent doming; and finally (4) post-caldera lava extrusions (Aydar et al., 1998). The authors also suggested that the corresponding ignimbrites cover 1100 km^2 and the estimated volume is about 77 km^3. The ignimbritic eruptions also occurred in two stages which are preserved as 'Lower Seydiler' and 'Upper Seydiler' units (Figure 1.2a)

The volcanological evolution of the Afyon Stratovolcano commenced with lava flows and domes, lahars and block-and-ash flows since middle Miocene (Aydar et al., 2003). The authors suggest that after recharge of the volumunious ignimbrites and coeval onset of the caldera which exceeds 4 km in diameter, megasanidine-bearing (up to 5 cm) trachytic lava domes and dome flows, associated with block-and-ash flow, debris avalanches and autobrecciated lava flow deposits (Figure 1.2).

At the final of the volcanism, Hydrovolcanic activity, lamprophyric lava flows and phlogopite-bearing dyke intrusions dominated over the volcanic area (Aydar et al., 2003).

The Bodrum volcanic area is one of the best studied caldera structure in south-western Anatolia (Figure 1.2b). The Middle-Late Miocene Bodrum volcanic complex of the Aegean region, south-western Turkey, is mainly represented by intermediate stocks, lavas, pyroclastic and volcaniclastic deposits (Genç et al.. 2001; Karacık, 2006). Ulusoy et al. (2004) and Karacık (2006) is recent studies that agree with the caldera structure of the Bodrum Peninsula. Ulusoy et al. (2004) suggested that the Bodrum volcano developed as a result of a complex collapse and resurgence mechanism during four successive events: pre-caldera activity, caldera-forming eruptions, resurgence and post-caldera activity, based mainly on the interpretation of aerial photographs using remote-sensing techniques and digital elevation models (DEM). Ulusoy et al. (2004) reported that the emplacement of two ignimbritic sequences was responsible for the collapse of the NE–SW, the topographic caldera area covers about 98 km^2, 18.7 X 7.7 km wide. The collapsed area is estimated at 58 km2, and the average overall slope of the inner topographic walls is 16°. Karacık (2006) also documents detailed measured columnar sections around the volcano-magmatic complex. The authors claim that her evidence indicates that this region is the centre of a stratovolcano and consists of different types of magmatic rocks, such as monzonite, rhyolite and hypabyssal rocks in contrast to Ulusoy et al. (2004) who argued that the Dağbelen domain formed the centre of a caldera and was represented by hydrothermally altered rhyolitic domes.

The Ezine volcano-plutonic complex is located to the north of one of the E–W-trending grabens of Western Anatolia, the Edremit graben (Figure 1.2c). The first magmatic activity started with Kestanbol granite, which surrounded by hybabyssal rocks and volcanic successions (Karacık & Yılmaz, 1998). Lavas and lahar deposits dominate the northern sector while ignimbrites emplace the southern sector of the complex (Karacık & Yılmaz, 1998).
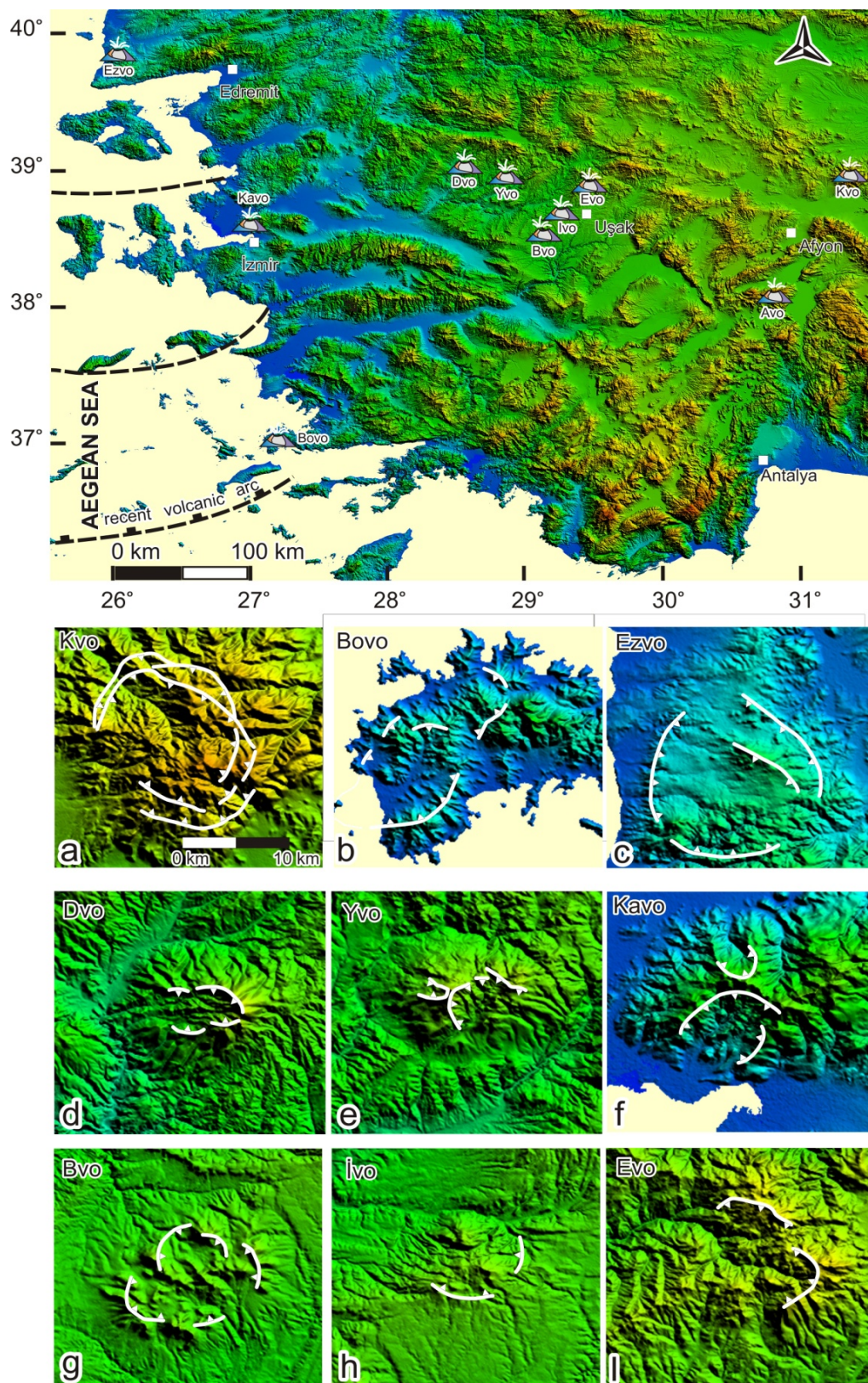
Figure 1.2 Simplified map showing some prominent Neogene volcanic centers which are destructive in character, over topography of western Türkiye derived from 90 m SRTM

digital (see overleaf) (figure caption continued) elevation model. Key volcanic centers are labelled: Kvo: Köroğlu; Avo: Afyon; Bovo: Bodrum; Kavo: Karşıyaka; Ezvo: Ezine; Dvo: Demirci; Yvo: Yağcıdağ; Evo: Elmadağ; Ivo: İtecektepe; Bvo: Beydağı stratovolcanoes.

The authors claim that the ignimbrite eruptions which have been associated in a caldera collapse environments were formed partly simultaneously with the plutonic and the associated volcanic rocks during the early Miocene. The Demirci (Figure 1.2d), Yağcıdağ (Figure 1.2e) and Karşıyaka-Yuntdağ (Figure 1.2f) volcanic centers have moderate scale semi-circular volcanic deformational area however no any evidence physical volcanologic processes for these stratovolcanoes. The Beydağı (Figure 1.2g), İtecektepe (Figure 1.2h) and Elmadağ (Figure 1.2i) volcanic centers have also experienced destruction processes since Early Miocene within Uşak-Güre basin. Here, I describe the time–space volcanologic evolution of three volcanic centers in the Uşak-Güre basin.

CHAPTER TWO
STRATIGRAPHY, SEDIMENTOLOGY AND TIMING OF THE UŞAK-GÜRE BASIN

2.1 Geological Outline of the NE–SW-Trending Basins

The NE–SW-trending Miocene basins in the western Anatolia, from west to east, Bigadiç (Helvacı, 1995; Helvacı & Yağmurlu, 1995; Erkül et al., 2005a,b), Soma (İnci, 1998), Gördes (Seyitoğlu & Scott, 1994a,b; Purvis & Robertson, 2004; Ersoy et al., 2011), Demirci (Yılmaz et al., 2000; Ersoy et al., 2011), Selendi (Ercan et al., 1983; Seyitoğlu, 1997a; Westaway et al., 2004; Purvis & Robertson, 2004, Ersoy & Helvacı, 2007; Ersoy et al., 2010a) and, Uşak-Güre basin (Ercan et al., 1978; Seyitoğlu, 1997a; Westaway et al., 2004; Seyitoğlu et al., 2009; Karaoğlu et al., 2010) dominated north-facing of the Menderes Massif (Figure 2.1). Although, these basins dominantly display similar sedimentary sequences from west to east (Figure 2.1) the field relationships between the sediments of these basins and basement rocks have also been still disputed.

One of the most crucial problems is if presence of tectonic controls via detachment faults between unroofed the Menderes Massif and sediments later accumulated or major unconformities between basement and cover rocks. Some authors report that unroofing process of the Massif occurred purely by erosion from depth (Yılmaz et al. 2000; Westaway et al. 2004). Some other previous authors (e.g. Ercan et al. 1978; İnci 1984; Seyitoğlu & Scott 1994; Seyitoğlu 1997; Yılmaz et al. 2000) suggesting that metamorphic rocks of the Menderes Massif are unconformably overlain by Miocene sediments of clastic, lacustrine and tuffaceous facies in different NE–SW-trending basins. Alternatively, Purvis & Robertson (2004; 2005) and Ersoy et al. (2010) for Selendi and Demirci basins; Karaoğlu et al. (2010) for Uşak-Güre basin, and in this study I propose that these basins ensue of late Oligocene-early Miocene, low-angle normal faulting and ductile shear that created basin scale corrugations are directly controlling the basin evolutions, early Miocene sediments overlay over the Metamorphic rocks by tectonically (Figure 2.1).
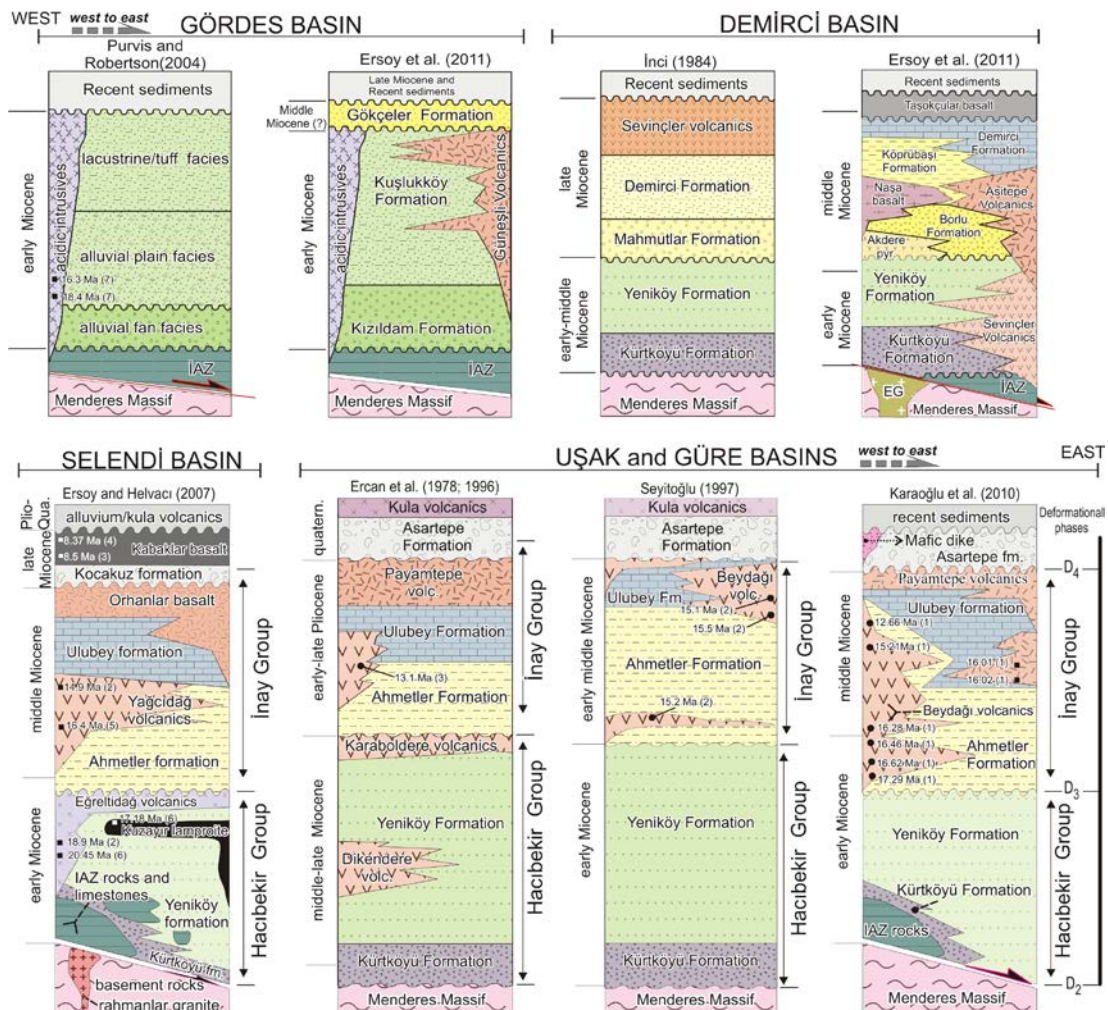
Figure 2.1 Comparison of stratigraphic sections proposed for the NE–SW-trending Gördes, Demirci, Selendi, Uşak-Güre basin . İAZ-İzmir-Ankara Zone rocks, EG-Eğrigöz granitoid.

Much as, Ersoy et al. (2011) reported that no evidence by for presence of detachment fault in Gördes basin between the rocks of Menderes Massif and early Miocene sedimentary rocks. According to authors, Gördes basin was opened by strike- to oblique-slip movements on the basin-bounding faults as a result of dextral transtension, such that the transtensional Gördes basin formed where extension is oblique to the margin that bounded the basin. The Demirci, Selendi, Emet, and Gure basins, have similar stratigraphic and tectonic features, and began to develop as supra-detachment extensional basins on an early Miocene corrugated detachment fault (the Simav detachment fault, SDF) Ersoy et al. (2011).

2.2 Previous Studies of the Uşak-Güre Basin

The Miocene stratigraphy of the Uşak-Güre basin was studied and documented by Ercan et al. 1978; Seyitoğlu 1997; Karaoğlu et al. 2010. Ercan et al. (1978) is the first study of the geological history of the basin, proposing that the basin stratigraphy commenced with the Middle-Upper Miocene Hacıbekir Group which is overlain, with an angular unconformity by the Lover-Upper Pliocene İnay Group (Figure 2.1). According to Ercan et al. (1978), Quaternary Asartepe Formation unconformable overlay all of these sedimentary packages. Ercan et al. (1978) displayed that the Hacıbekir Group interfinger with, and is conformably overlain by felsic volcanic rocks, namely the Dikendere and Karaboldere volcanic rocks, respectively. Bingöl (1977) also noted that the K-Ar dates of the Muratdağı volcanic rocks which are located in the NE-edge of the basin lie between 16.9±0.2 and 20.9±0.5 Ma.

Seyitoğlu (1997) indicated that the deposition of the Hacıbekir Group began at the early Miocene on the basis of palynological and radiometric age data of felsic volcanic rocks (18.9±0.6 Ma K-Ar age) which cut the Hacıbekir Group in the Eskin area, which is in the adjacent-Selendi basin (see Figure 2.1). Seyitoğlu (1997) also show that the İnay Group is early Middle Miocene in age, on the basis of palynological data collected from the sedimentary rocks and radiometric ages from the dacitic rocks interfingering with the İnay Group. Ercan et al. (1978) and Seyitoğlu (1997) highlighted that Hacıbekir and İnay Groups, unconformable overlie the basement rocks (Figure 2.1). These studies argue that structural evolution of the Uşak-Güre basin is dominated by N–NNE-trending normal faults which have also controlled the volcanic activity in the basin.

Çemen et al. (2006) provided more detailed systematic strike and dip measurements of foliation surfaces in the Northern Menderes Massif. Foliation surfaces documented in the Uşak area indicate that the presence of major antiformal and synformal structures.

Karaoğlu et al. (2010) presents the petrogenesis evolution and ^{40}Ar/^{39}Ar geochronology of the volcanic rocks from the Uşak-Güre basin using new mapping and radiometric age data. Karaoğlu et al. (2010) put forward three different volcanic units (Beydağı and Payamtepe volcanic units and Karaağaç dikes) which were recognized within the Uşak-Güre basin , as well as the geochemical features of the volcanic rocks are comparable with those of the other volcanic areas in western Anatolia.

2.3 Geological Outline of the Uşak-Güre Basin

2.3.1 Pre-Miocene Rock Units

2.3.1.1 Metamorphic Rocks of the Menderes Massif

It were originally divided into a Precambrian "core" and Mesozoic–Cenozoic "cover" (e.g. Şengör et al., 1984; Bozkurt & Oberhaensli, 2001; Rimmele et al., 2003; Erdoğan & Güngör, 2004). The core of high grade rocks are comprised of granitic gneisses and high-grade schists, was thought to have formed during the Pan African orogeny (Cambro-Ordovician; Şengör et al., 1984), whereas the cover consists of Paleozoic mica schists and Mesozoic–Cenozoic platform marbles that experienced regional metamorphism during the Alpine orogeny (Şengör et al., 1984).

Field studies have documented the presence of nappes that formed during the formation of the İzmir-Ankara suture zone (see Ring, 1999; Gessner et al., 2001). I clearly observed that the boundary between the core and cover rocks of the Menderes Metamorphic rocks are overlapped by marbles at the vicinity of northeast of the Uşak and eastern side of the Ulubey. The orthogneisses are cut by quartz veins and aplitic intrusions. Dominant foliation trending of the schist and gneiss is in NE–SW-direction (017°-054°), nevertheless dip direction of the rocks rest on NE–SW-trending antiform and synform geometries of the metamorphic rocks. Large-scale asymmetric folds and associated crenulations, and cleavage are commonly described in Menderes Metamorphic rocks in the Uşak–Güre area. These large antiforms and

synforms are first identified by Ercan et al. (1978), and after that are detailed by Çemen et al. (2006) which have NE–SW-oriented axes (Figure 2.2). The Menderes Massif is also tectonically overlain by upper Cretaceous ophiolitic mélange rocks of the İzmir-Ankara zone and the Hacıbekir Group (Figures 2.3, 2.4 and 2.5).
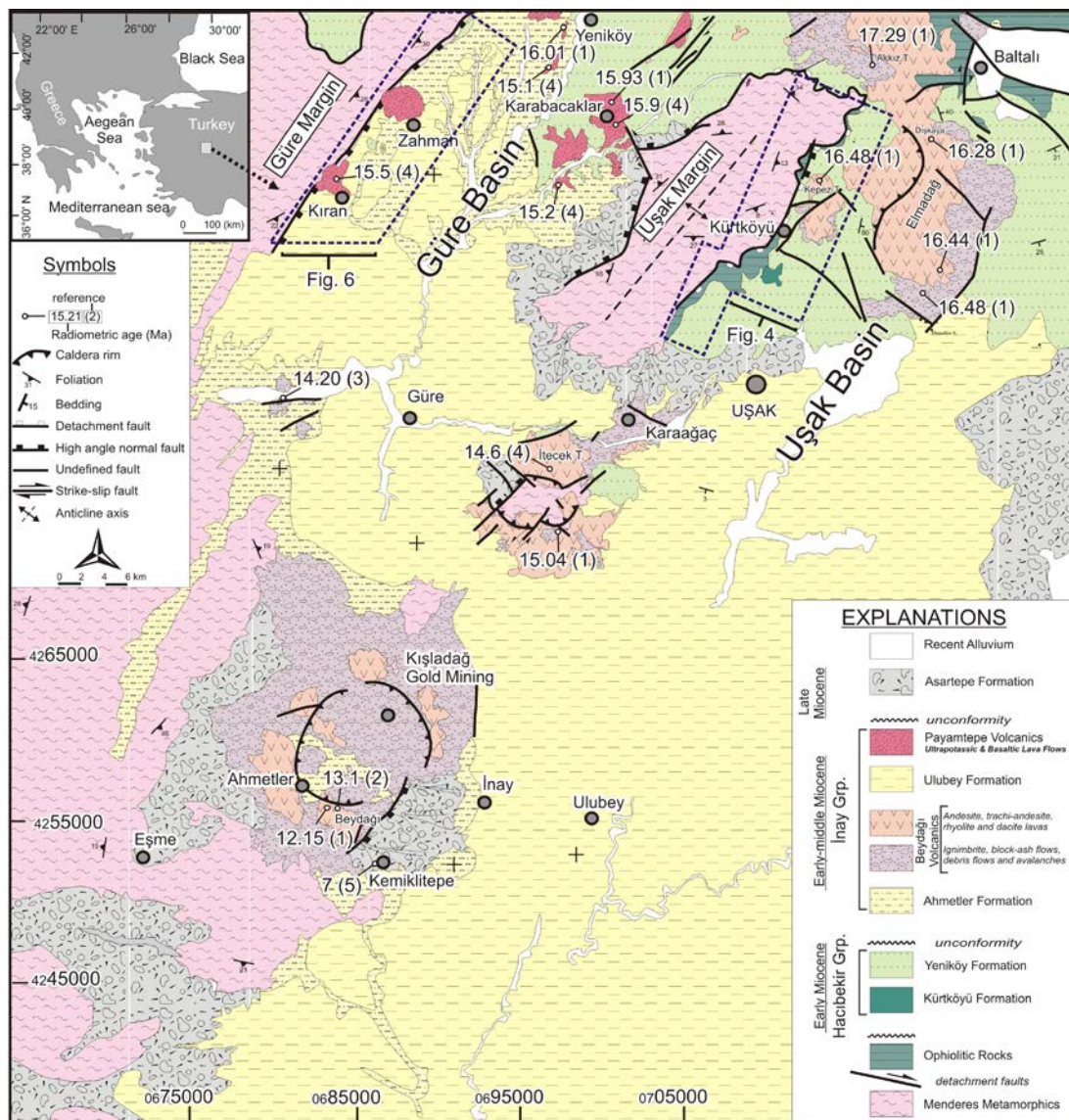
Figure 2.2 Geological map of the Uşak-Güre basin including the radiometric age data from the volcanic rocks and a mammalian age from Asartepe formation (modified from Karaoğlu et al. (2010); see Fig. 1 for location of the map). References: 1–Karaoğlu et al. (2010); 2–Ercan et al. (1996); 3–Innocenti et al. (2005); 4– Seyitoğlu (1997); 5– Seyitoğlu et al. (2009).

2.3.1.2 Mélange Rocks of the İzmir-Ankara Zone

Vezirler mélange of Ercan et al. (1978), are not the focus of the present study but occupy a key tectonic position in the exhumation process in late Oligocene-early Miocene interval. There is a general agreement about the contact relationship between the rocks of ophiolitic mélange and Menderes Massif. Robertson et al. (2009) reported that the Bornova mélange has a very low metamorphic grade and is separated from the Menderes Massif to the south by high-angle neotectonic faults.
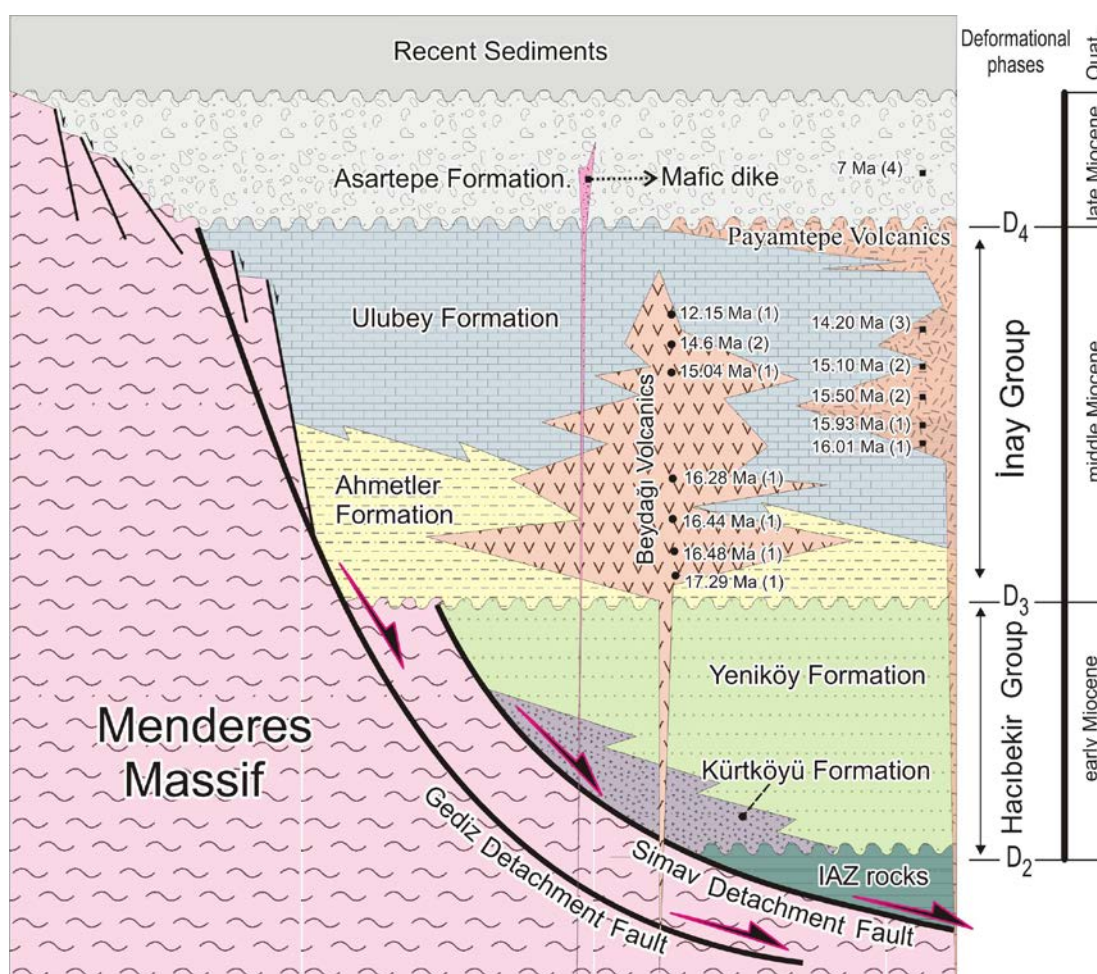
Figure 2.3 Tectono-stratigraphic columnar section of the NE–trending Uşak-Güre basin (D_2-D_4 refers to deformation phase). Age data: (1) Karaoğlu et al. (2010); (2) Seyitoğlu (1997); (3) Innocenti et al. (2005); (4) Seyitoğlu et al. (2009).

In general, this melange is dominated by blocks of thick-bedded neritic carbonate and thin-bedded pelagic carbonate (up to several kilometer sized), together with

subordinate basic extrusive rocks set within a terrigenous matrix (Robertson et al., 2009). In the Vezirler area, the mélange is mainly made up of unmetamorphosed ultramafic rocks, radiolarites and highly altered silicic rocks. The mélange rocks directly and tectonically overlie on the inner and outer metamorphic subunits along a low-angle normal fault in the area.

2.3.2 Basin Fill Units (Summary of Sequences and Age Estimates)

These deposits contain a record of early to late Miocene syn-extensional sedimentation and volcanism that accompanied exhumation of the metamorphic core complex (Menderes Massif).

Uşak-Güre basin is filled by fluvio-lacustrine deposits assigned to three unconformity-bounded sequences: (1) the Hacıbekir Group; (2) the İnay Group; and (3) the Asartepe Formation.

The Hacıbekir Group is composed of dark yellow conglomerate, sandstone and mudstone deposits of fluvio-lacustrine environments. I obtained also some pumice fall deposits in the Group. However the major volcanic source could not be determined contrary to documentation of by Ercan et al. (1978) in the Uşak-Güre basin. Seyitoğlu (1997); Ersoy & Helvacı (2007) who proposed an early Miocene age (19-20 Ma) on the basis of radiometric age data from Eğreltidağ volcanic unit and Kuzayır lamproite in the adjacent Selendi basin that have similar stratigraphy with Uşak-Güre basin. The thickness of the Hacıbekir Group in the study area is also not well constrained.

Measured sections, will be presented elsewhere, are up to ~800 m thick have been mapped within fault blocks of the northern side of the Uşak-Güre basin (see Figures 2.6 and 2.7; e.g. Ercan et al., 1978), but the whole formation is considerably thicker than that and may be more than 1000 m thick.
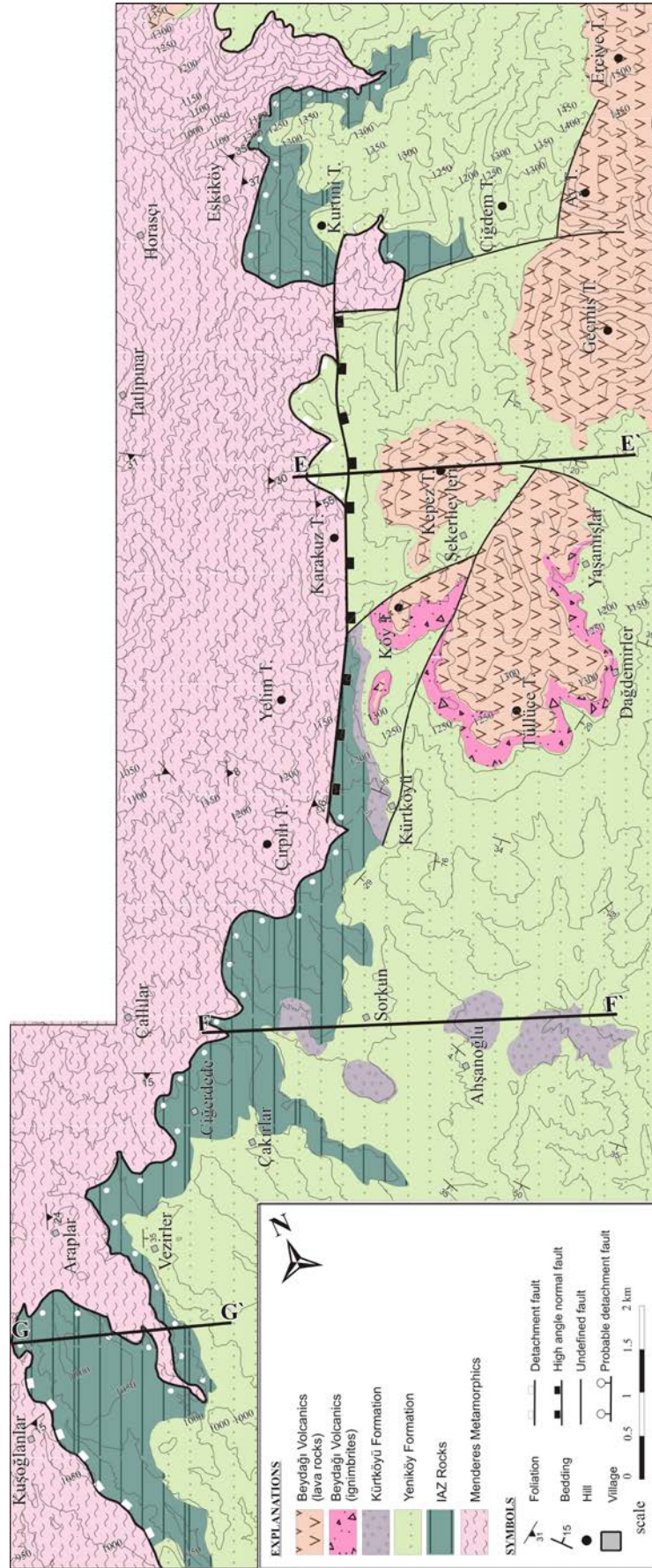
Figure 2.4 Geological map of the eastern margin of the Uşak-Güre basin.
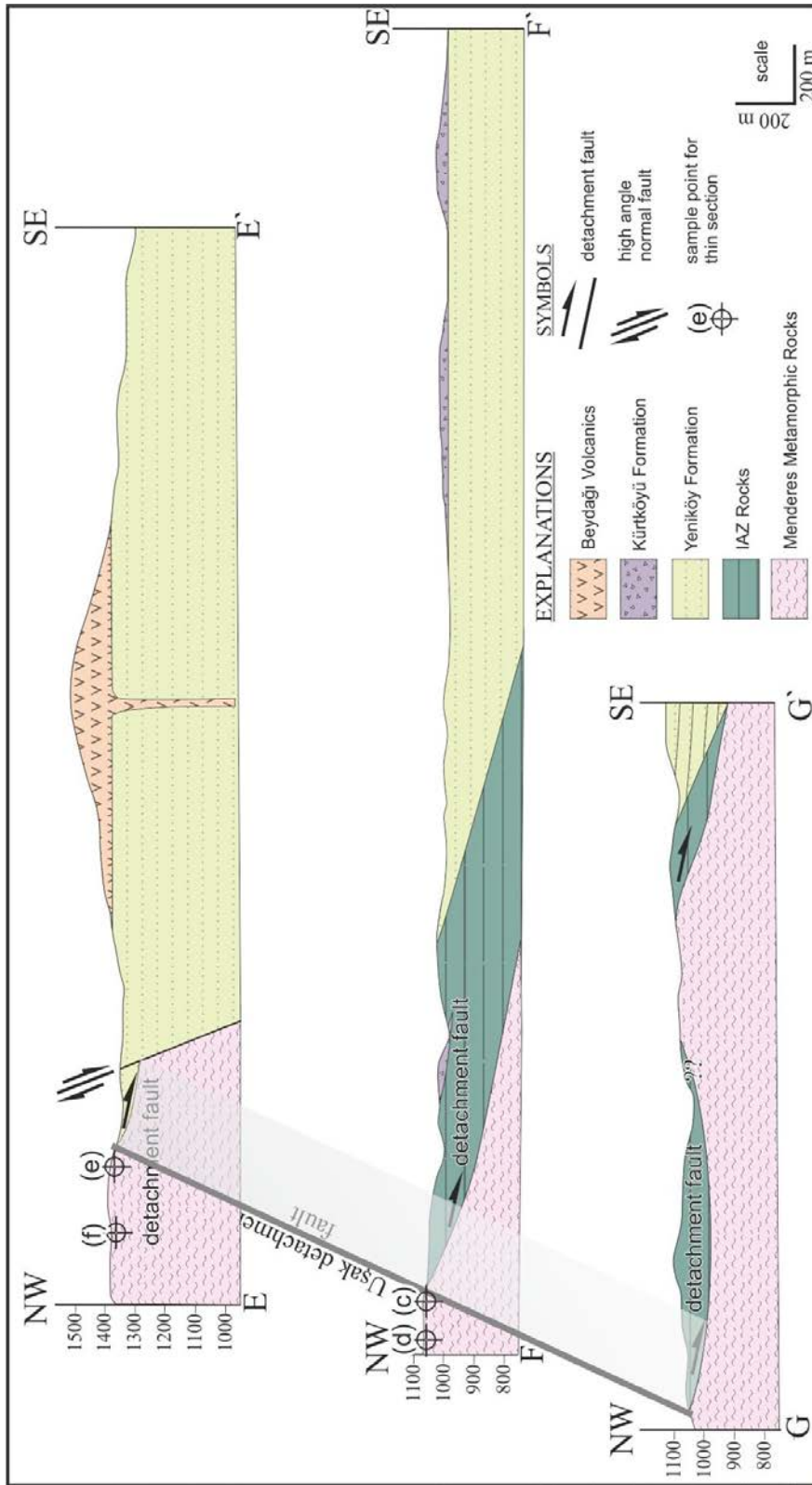
Figure 2.5 Cross-sections of the Uşak-Güre basin from eastern margin also including sample points for Fig. 3.7 (c, d, e and f).

The İnay Group is a thick volcano-sedimentary package, interfingering with Beydağı and Payamtepe volcanic rocks. The İnay Group crops out at southern side of the Güre-Uşak-Banaz and eastern side of the basin.

The İnay Group is composed of conglomerate, sandstone, tuff, mudstone marl and limestone of fluvio-lacustrine setting, and is accompanied by volcanic rocks. Seyitoğlu (1997) and Ersoy et al. (2010) suggest that the İnay Group was deposited under the control of NE–SW-trending strike- to oblique-slip faults. Seyitoğlu (1997) also proposed that the volcanic rocks are intercalated with the İnay Group based on their stratigraphic position and the radiometric age of the volcanic rocks (dated as 15.5 ± 0.4 to 14.9 ± 0.6 Ma, K/Ar ages).

Ercan et al. (1978) and Seyitoğlu (1997) propose a completely different basin stratigraphy and the existence of certain volcanic units (e.g. Dikendere and Karaboldere volcanic according to Ercan et al., 1978) in Hacıbekir Group has been a matter of debate. Recently, new radiometric age data were presented by Karaoğlu et al. (2010). Age determinations were carried out on 7 samples from the Beydağ volcanic unit and 2 samples from the Payamtepe volcanic unit. The authors proposed that Cenozoic volcanism in the Uşak-Güre basin started (17.29 Ma) with the Beydağı volcanic unit, which is located in the northern part of the basin where it interfingers with the İnay Group. The data indicate that volcanism was active since the late early Miocene (Burdigalian). The youngest radiometric age from the Beydağı volcanic unit is from the Beydağı caldera (12.15 ± 0.15 Ma) in the south. Also, the $^{40}Ar/^{39}Ar$ dates of the Payamtepe volcanic unit restrict it to a period between 16.01 ± 0.08 and 15.93 ± 0.08 Ma.

Additionally, Karaoğlu et al. (2010) indicate that the deposition mechanism of the volcano-sedimentary infill (İnay Group) of the Uşak-Güre basin confined to the north of the asymmetrically uplifted Menderes Core Complex. Bingöl (1977) also noted that the K-Ar dates of the Muratdağı volcanic rocks which not shown in any figures, are located in the NE-edge of the Uşak-Güre basin between 16.9 ± 0.2 and 20.9 ± 0.5 Ma.
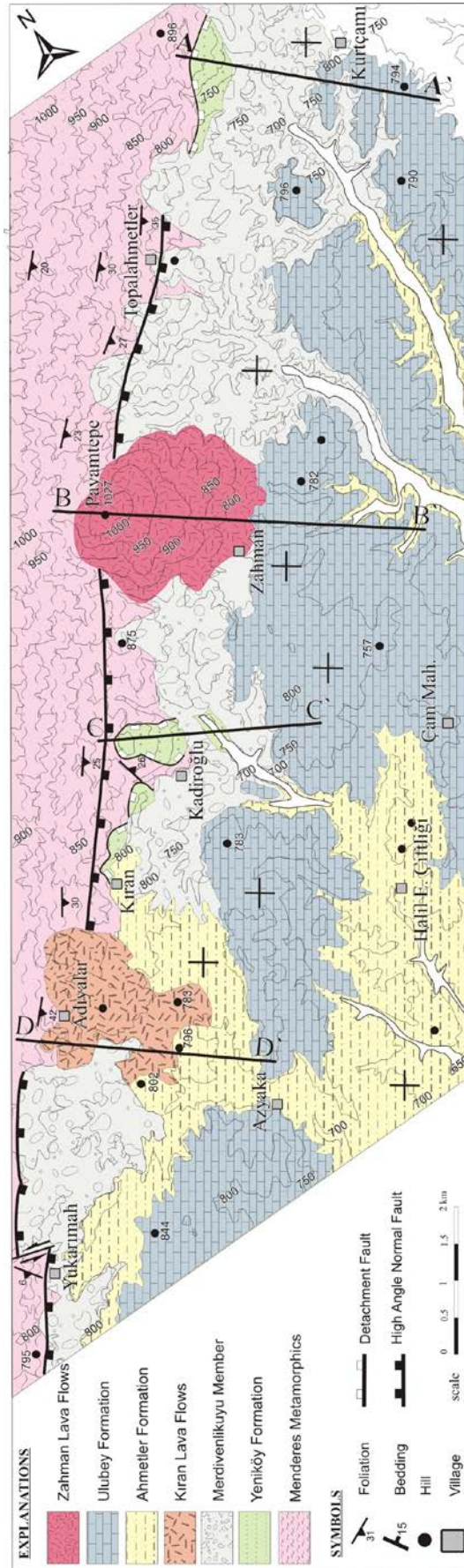
Fig.ure 2.6 Geological map showing geological setting of the effusive payamtepe volcanic rocks in the western margin of the Uşak-Güre basin
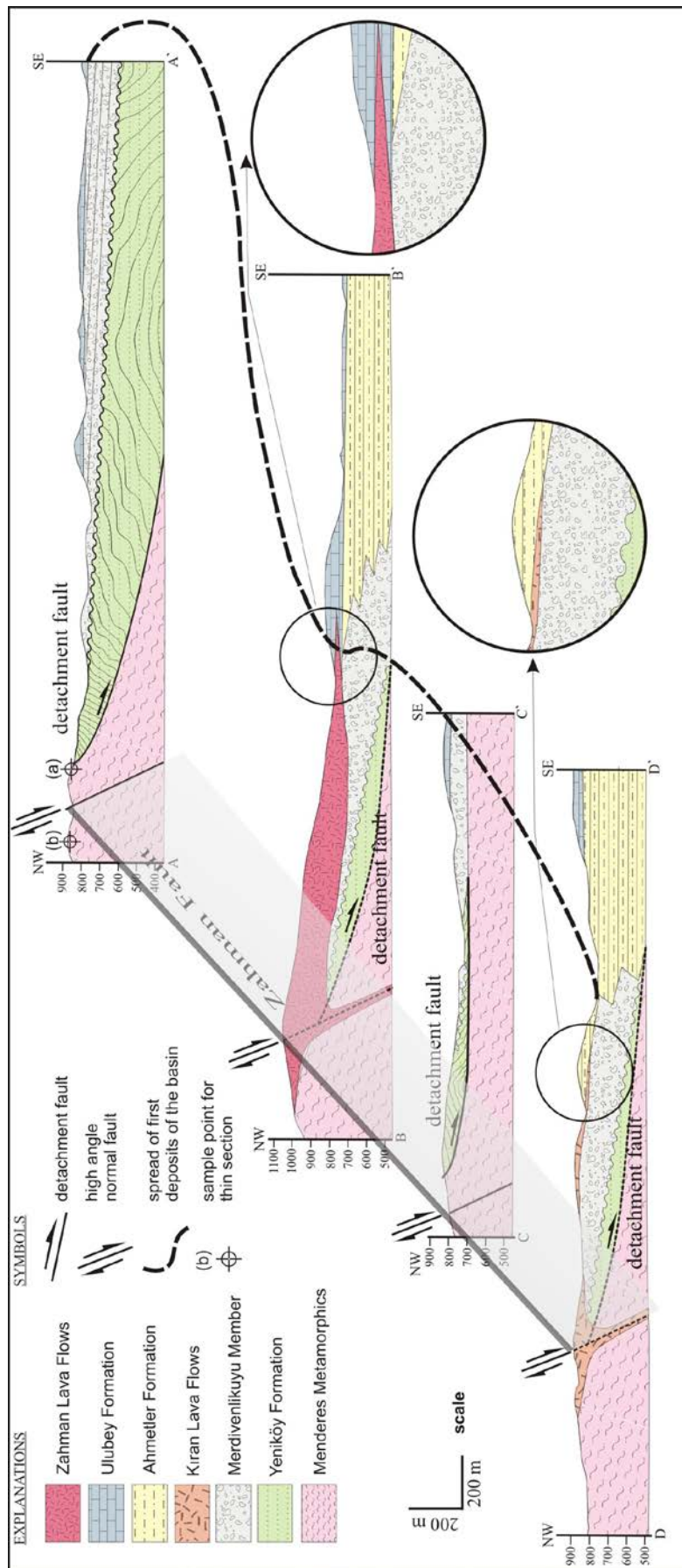
Figure 2.7 Cross-sections of the Uşak-Güre basin from western margin with sample localities for Figure 3.7 (a, b).

2.3.2.1 Hacıbekir Group

The Hacıbekir Group is exposed in north of the Güre-Uşak-Banaz trend (Figure 3.3) respectively and laterally variable, subdivided into interfingered Kürtköyü and Yeniköy formations. Many researchers have manifested that Menderes Massif is a core complex occurs on the footwall of the SDF zone that is now mostly covered by Cenozoic sediments (Figure 2.3). The coupling of metamorphic core complexes and supra-detachment basins are supremely exhibited in the vicinity western of the Uşak and Güre basin margins (Figure 2.3). Yeniköy formation tectonically overlies the Menderes Massif along a low-angle normal detachment fault. Whole foliation surfaces along the detachment fault surfaces are in NE–SW direction. Also, while the angles of detachment fault is 9°, 4° showing the more low angle (N60°E/32°SE) at western side of the Uşak margin compare to western side of the Güre basin which showing detachment angles of 19°, 21°. The contact between the Yeniköy formation and the Menderes metamorphic rocks is a low-angle normal fault (N40–55°E/19–29°NW) that can easily be traced in the Kıran–Kadıoğlu–Kurtçamı area. Also has observed ~10 m thick highly altered silicic zone through the low angle normal fault surface between hanging wall and footwall rocks. Detailed kinematic analysis will be presented at Chapter 3.

2.3.2.1.1 Kürtköyü formation (Thf). The Kürtköyü formation mostly crops out in the vicinity of Kürtköyü (the type locality), Baltalı and Çukurağıl villages (Figure 2.2) and consists of monolithic grey, reddish brown boulder conglomerates. The boulder conglomerates are composed of moderately to poorly sorted and coarse clast size. The Kürtköyü formation also consists of thin-bedded massive conglomerate with moderately to well-rounded clasts of ultramafic (harzburgites and pyroxenites) ranging from pebble to boulder grade and minor unmetamorphic clasts of the Lycian rocks.

The Kürtköyü formation unconformably overlies the İAZ rocks at the type locality with bedding shear bands in 8-39° and the NNE-trending. I have observed these NE-trending shear bands on the Kürtköyü formation at many locations and

indicate that following of the Kürtköyü alluvial fan deposition unconformably over the İAZ, the basin-bounding fault must have been reactivated entirely in the hanging wall of the Simav detachment fault (SDF).

2.3.2.1.2 Yeniköy formation (Thy). Yeniköy formation widely exhibits exceptional sedimentary structures such as tabular cross-beddings, channel structures, ball and pillow, ripple, flaser beddings (Figures 2.8a-e). The early Miocene Yeniköy formation is composed of three fabric and architecture sequences: 1) parallel laminated bedsets; 2) tabular cross-stratified bedsets; 3) architecture of parallel-laminated and cross-stratified sandstone and conglomerate (Figure 2.3). All of the sequences are dominantly made up sandstone, claystone, mudstone, limestone and coal lenses. Medium-grained, yellow-brown sandstone with occasional pebble lenses dominate much of the section; thin, lenticular grey mudstones and siltstone are also common.

Coal lenses are especially observed in the transition zone of Kürtköyü formation to Yeniköy formation (Figures 2.8f and 2.9). Bituminous and coal lenses reflect the interaction between swamp and fluvial depositions (Figures 2.9 and 2.10). The lower part of the Yeniköy formation was most probably formed in extensive mires with claystone and sandstone deposition in ephemeral small and shallow lakes and ponds (e.g. in Soma coalfield; İnci, 2002). Lithofacies features associated with the coal seams suggest that mire terminations were created by relatively rapid crevasse-splay sedimentation. According to İnci (2002), this type of coal deposition may be attributed to the 'ephemeral-lacustrine floodplain delta' setting as proposed by Blair & McPherson (1994).

Yeniköy formation was most probably deposited in huge alluvial fans and fan-deltas along the Simav detachment fault (SDF) prior to exhumation of the Menderes Massif and/or basin margin. Interrelation between Hacıbekir Group (Kürtköyü and Yeniköy formations) and base of the margin that is Menderes Massif is one of the most debatable subjects.

Figure 2.8 Field photographs of Yeniköy formation. (a) Planar cross bedding in pebbly sandstones of Yeniköy Formation near Yeniköy town. Note the dip directions in the two cross-bedded units, suggesting possible deposition. (b) Channel slightly incised fill conglomerate A similar coarse grained architecture are interpreted as representing 'autoconfining leve´es' in Rosario Formation, Mexico by Kane et al., 2009. (c) Ball and pillow structures. They exhibit hemispherical shaped of sandstone that shows internal lamination. They show complete isolation from the bed and were enclosed in the underlying mud. Ball and pillow structures are believed to form as a result of foundering and break up semi-consolidated sand, or limey sediment, owing to partial liquefaction of underlying mud, possibly caused by an earthquake shocking (e.g. Bogs, 1987). (d) Plan view of oscillation (wave generated) ripples on the upper surface of a fine grained sandstone bed, north of Uşak. Individual lamination sets exceed 7-8 cm in thickness. (e) Flaser bedding in sandstone, near Aşağıkaracahisar village. Thin

streaks of mud occur between sets of massive sandy sediment. (f) Coal bearing sandstone, near Kürtköyü village.

The Kürtköyü formation passes laterally and vertically into the Yeniköy formation in the Uşak-Güre basin (Figure 2.9). Soft sediment deformation structures occurred in the transitional zone of the Kürtköyü and Yeniköy formations (Figure 2.9). The soft sediment intruded structures include pillars, dykes and cusps. These structures result from a complex combination of processes, mostly including reverse density gradients, fluidization and liquefaction. Reverse density gradients, promoted by differential liquefaction associated with different degrees of sediment compaction, led to the genesis of convolute folds. Pillars, cusps and dykes have been widely interpreted to represent flow paths with fluidized sediments being injected from surrounding strata as a result of increasing interstitial pore pressure (e.g. Daley, 1971).

All these soft sediment deformations might be triggered by a seismic agent as suggested by a combination of criteria, including (1) the position of the study area at the edge of the Simav detachment fault zone relating with exhumation of Menderes Massif that was reactivated several times from the late Oligocene to the early Miocene; (2) a relative increase in the degree of deformation in sites located closer to the fault zone; (3) recurrence through time; and (4) similarities to many other earthquake-induced deformational structures (e.g. Rosetti, 1999). An example of an isolated "cusp" into a conglomerate bed is illustrated in Figure 2.9. There, a shear zone branches off the basal glide plane of the conglomerate bed. Isoclinal folding with axial planes parallel to the basal shear zone and subsequent boudinage of isoclinals folds can be seen as an effect of progressive simple shear (e.g. Northern Calcareous Alps, Ortner, 2007). Initially, folds above the glide plane formed with SW-dipping axial planes, but were progressively rotated into parallelism with the shear zone and then extended.
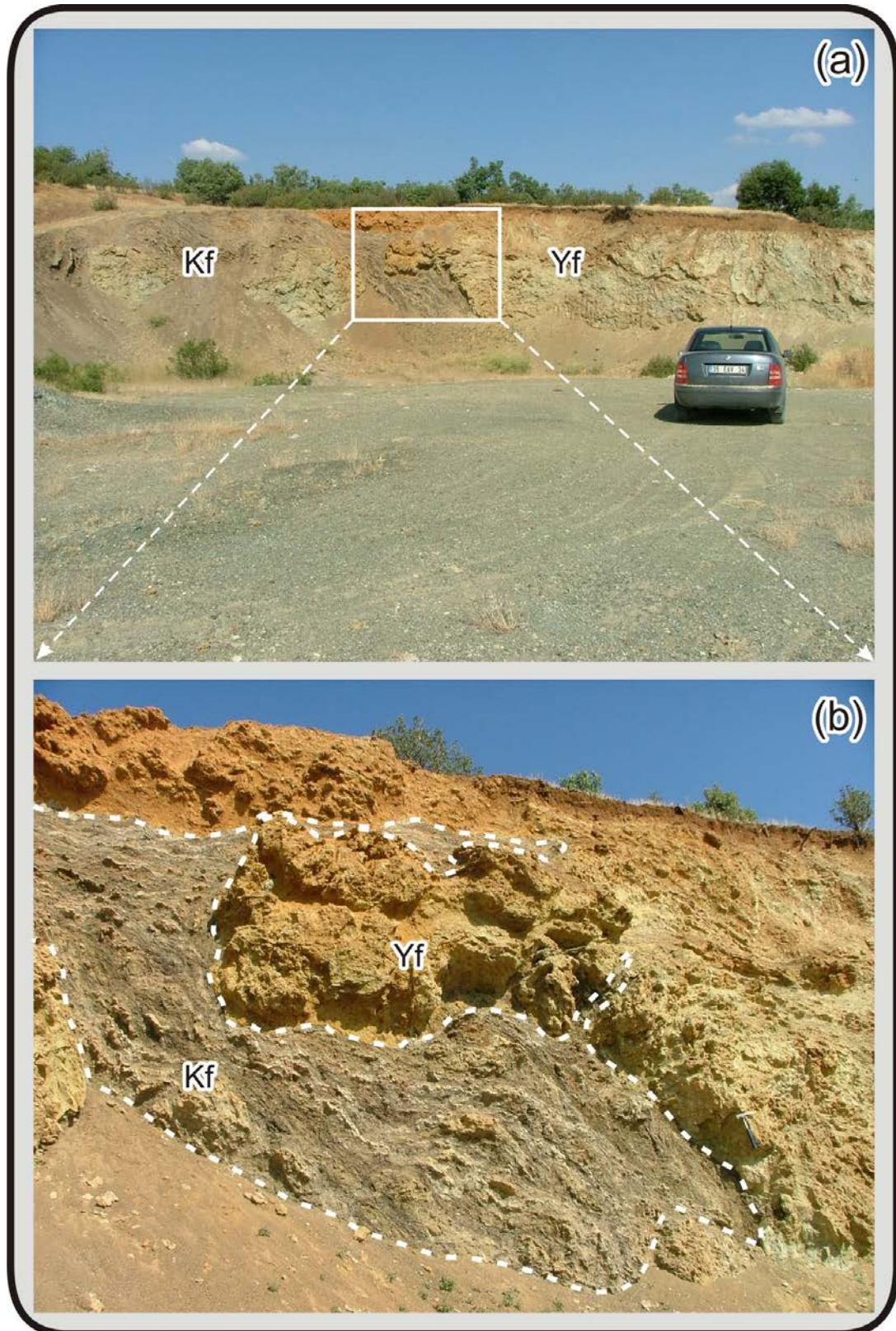
Figure 2.9 The soft sediment deformation and intercalation structures between Yeniköy (Yf) and Kürtköyü formations (Kf) of the Hacıbekir Group.
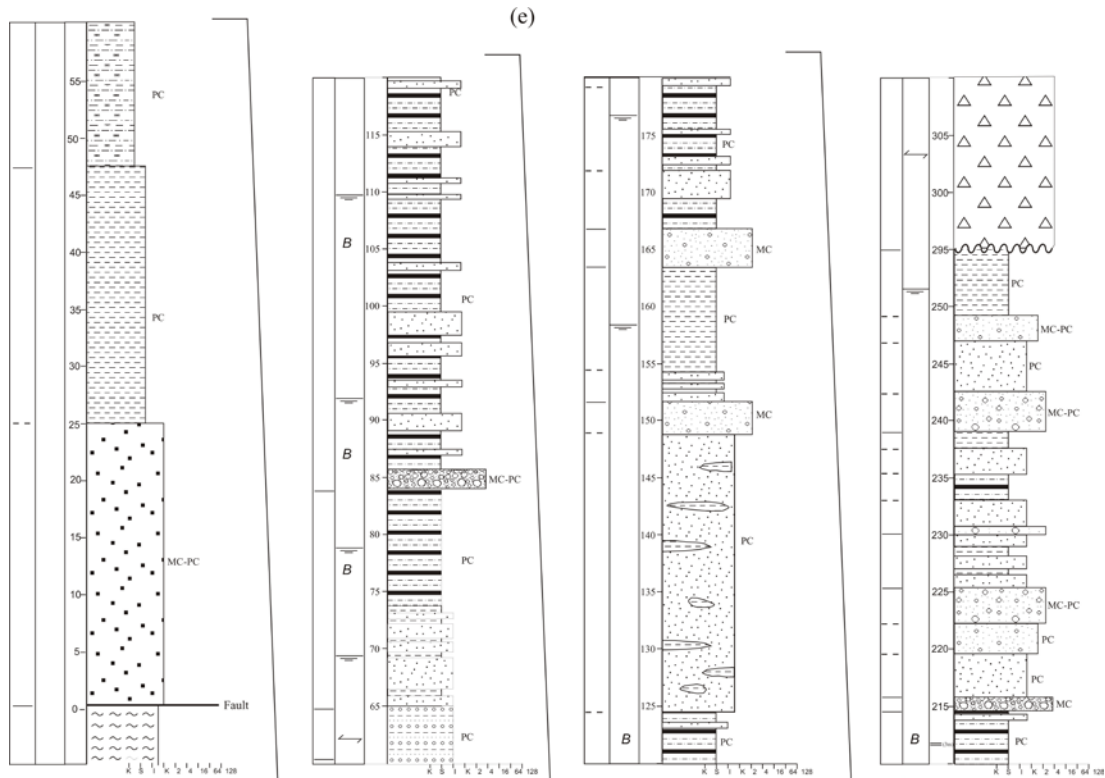
Figure 2.10 Measured cross-section of the Hacıbekir group. Represented by Section 1 on Figure 2.2 for location of the stratigraphic position. See the explanations and symbols on Figure 2.12.

2.3.2.2 İnay Group

The early Middle Miocene İnay Group is divided into two sedimentary units called the Ahmetler and Ulubey formations. The Group mainly presents a volcano-sedimentary package, and the dating was obtained from the volcanic rocks. The İnay Group, also unconformably overlies the older rocks of the Menderes Massif, the İzmir-Ankara zone and the Hacıbekir Group (Karaoğlu et al., 2010). The internal characteristics of the Inay Group have much in common with alluvial fans dominated by sediment gravity flow (e.g., debris flow, rock avalanche, rock slide facies, Merdivenlikuyu member); fluvial and lacustrine deposits (Balçıklıdere member) and fluvial deposits (Gedikler member), also are interstratified with volcanic rocks of Uşak-Güre basin (Figure 2.11a-g).

Seyitoğlu (1997) and Ersoy et al. (2010) suggest that the İnay Group was deposited under the control of NE–SW-trending strike- to oblique-slip faults.

Seyitoğlu (1997) also proposed that the volcanic rocks are intercalated with the İnay Group based on their stratigraphic position and the radiometric age of the volcanic rocks (dated as 15.5±0.4 to 14.9±0.6 Ma, K/Ar ages).

Ercan et al. (1978) and Seyitoğlu (1997) propose a completely different basin stratigraphy and the existence of certain volcanic units (e.g. Dikendere and Karaboldere volcanic according to Ercan et al., 1978) in Hacıbekir Group has been a matter of debate.

2.3.2.2.1 Ahmetler Formation (Tia). Ahmetler formation is represented by fluvia-lacustrine deposits and subdivided into three Merdivenlikuyu, Balçıklıdere and Gedikler member. Merdivenlikuyu member consists primarily of single- and multistory depositional units of matrix-supported breccia and conglomerates originated from metamorphic rocks, with subordinate clast-supported conglomerate, and clast-supported breccia facies. Matrix-supported breccias and conglomerate beds range from 5–12-m-thick, contain poorly sorted, angular to sub rounded gravel clasts (maximum diameter = 1.2 m) are massive (unstratified), and are ungraded to coarse-tail normally and inversely graded (Figures 2.11a and b). A fine- to coarse-grained, crystal-lithic sand-rich matrix supports gravel clasts. Clast-supported conglomerate beds are 2–7 m thick and consist of weakly stratified, normally graded breccia and conglomerate in gradational contact with matrix-supported facies (Figure 2.11b). Clast-supported breccia facies consist of pervasively fractured, boulder- and block-rich beddings that form a single 16–20-m-thick depositional unit near the Güre margin (Figures 2.11a and b). Merdivenlikuyu member lacks volcanic flows, in addition, monolithologic blocks and blocky units are common in Merdivenlikuyu (Figure 2.11b), and is most commonly composed of rocks of Menderes Massif. Boulder and block in rich units are interpreted as catastrophically emplaced glide blocks and rock avalanche deposits.

Balçıklıdere member that is a sequence of fluvial facies up to 250-m thick which is typically present in the western part of the Güre margin (Figure 2.11c).
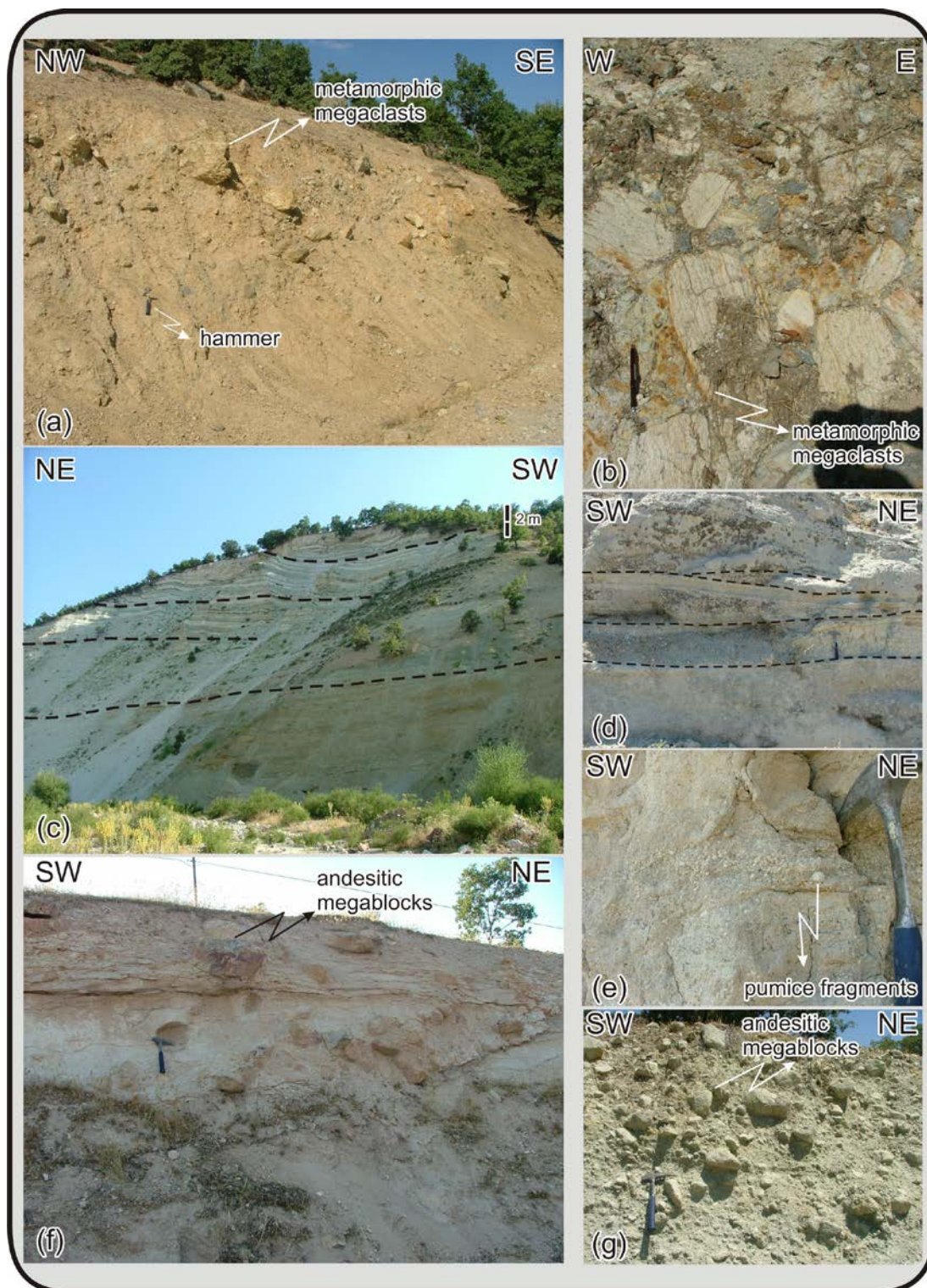
Figure 2.11 Three distinct members of the Ahmetler formation. (a) Photograph showing matrix-supported Merdivenlikuyu block member which reflecting basal layer of the Ahmetler formation, in the western margin of the Güre basin. (b) Close-up view of Merdivenlikuyu member showing subordinate matrix-supported metamorphic breccias and blocks, near the western margin. (c) Balçıklıdere member with siltstone and mudstone horizontal bedding, near Kıran village-western side

of the basins. (d) Close-up view of Balçıklıdere member, western side of the Beydağı volcano, showing fine-grained sandstone within horizontal bedding and small scale channel structures. (e) Pumice bearing sandstone demonstrating syndeposition of Balçıklıdere member-İnay Group with explosive eruptions within Uşak-Güre basin. (f) Gedikler member is characterised with matrix-supported volcanic conglemarate bearing mainly andesitic blocks which most probably originated from Beydağı volcanic unit. (g) Volcanic blocks from Gedikler member.

The Balçıklıdere member is conformable with the Merdivenlikuyu member and consists of claystone, mudstone, tuffaceous sandstone and siltstone with rare carbonate layers and channel conglomerate (Figure 2.11d). They show generally horizontal beddings. The volcanic intercalations with İnay Group are commenced with this member in Uşak-Güre basin (Figure 2.11e). Volcanic successions will be given Chapter 4 in detail.

Gedikler member is mainly exposed north of the Beydağı volcanic centre (in the Gedikler village) and consists of greenish and yellowish tuffaceous sandstone. The member which is 50-60-m thick conformable with the previous member and includes andesitic blocks and agglomerates belongs to Beydağı volcanism (Figures 2.11f and g).

2.3.2.2.2 Ulubey Formation (Tiu). The Ulubey formation is a carbonate rock-dominated sequence. The formation comprises of nearly horizontal beds (Ercan et al., 1978), consisting lacustrine fossils (Gastrapoda, Lamelli branchiata and Ostracoda). The thickness of the Ulubey formation is reaching ca. 300 m that shows a contrasting varying in accordance with position of the basin. While the thickness reaches 350-m near centre of the basin, the thickness is 35-40-m along the western margin of the Güre basin (Figure 2.10). This unit conformably overlies the Ahmetler formation and is overlain unconformably by the Asartepe formation. Although, the Ulubey formation shows interfingering with ultrapotassic Payamtepe volcanic rocks from which two radiometric age data are obtained (15.93 ± 0.08 and 16.01 ± 0.08). There are also some dike settings in the Ahmetler formation and lava flows at the vicinity of Yeniköy village in western part of the basin.
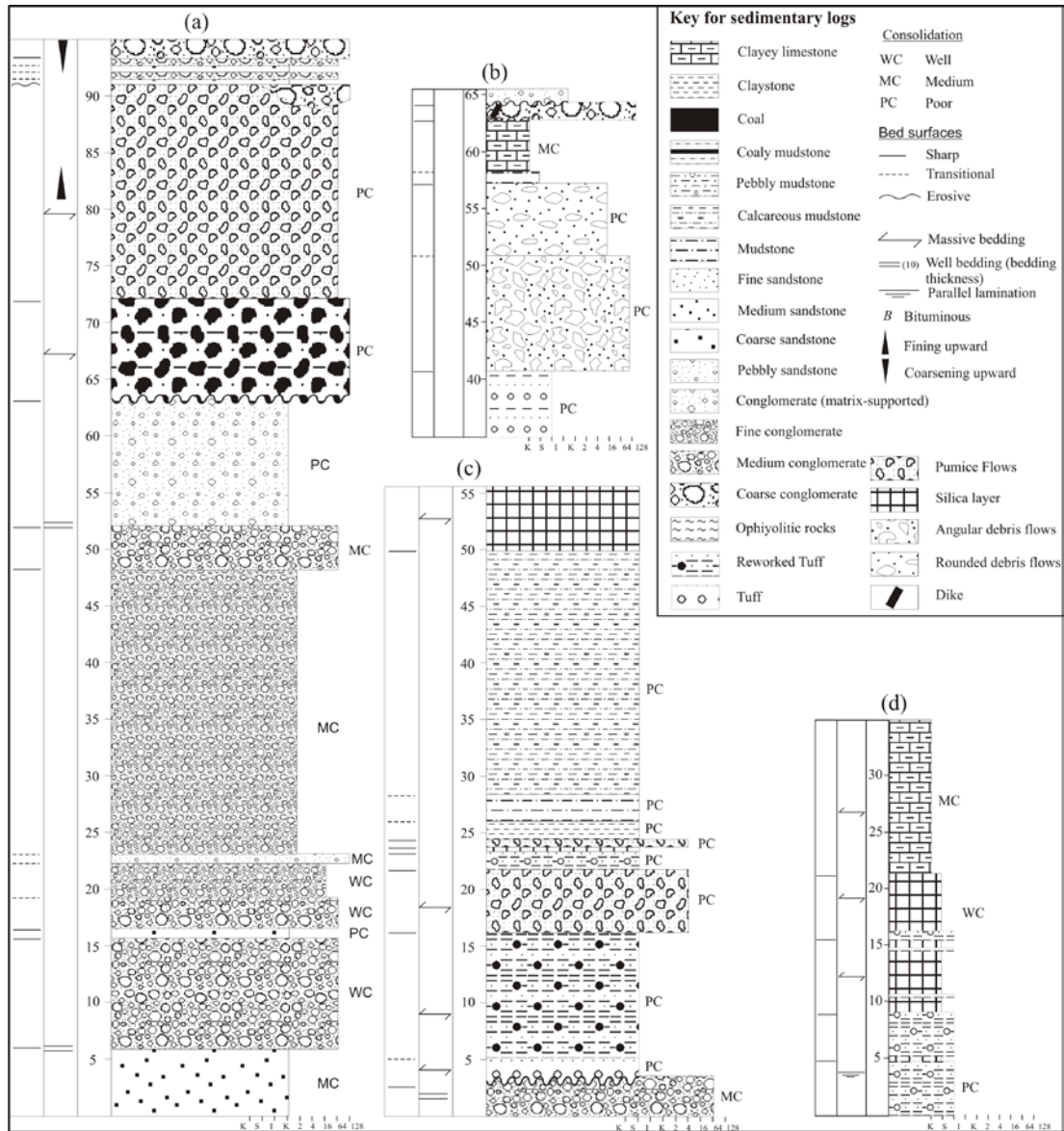
Figure 2.12 Measured cross-sections from volcanic rocks and associated with the sedimentary packages of the basin. You can see represented section numbers on Figure 2.2 for location of the stratigraphic sections. Section 2 for Figure 2.12a; Section 3 for Figure 2.12b; Section 5 for Figure 2.12c; Section 4 for Figure 2.12d.

2.3.2.3 Asartepe Formation (Tf)

The Asartepe formation is represented by reddish, coarse-grained fluvial and subaerial sediment gravity flow deposits, and is unconformable and overlies the older units in the Uşak-Güre basin. The flow deposits grade down a depositional dip, into mass-flow dominated deposits. The redbeds sequence is a thick package of laterally

variable and interfingering lithofacies that include: boulder breccias, conglomerate and sandy conglomerates. The Asartepe formation displays rapid lateral fining away from the Uşak margin faults at the north and the NW–SE-trending fault over the Beydağı at south of the basin. The thickness of the redbeds sequence is estimated from map relationships and cross-sections as approximately 300-350 meter. Our observations show that the Asartepe Formation has placed only along the structurally active NE–SW-trending boundaries and volcanic highlands of Uşak-Güre basin (Figure 2.2). There is no radiometric age data from volcanic rocks which related with the Asartepe formation in the literature from the Uşak-Güre basin.

In order to obtain a better stratigraphic position of the Asartepe formation, I have used published radiometric age data from adjacent Selendi basin. The Asartepe formation is also observed in the Selendi basin where the Upper Miocene Kabaklar basalt (8.37-8.5 Ma, Ercan et al., 1996; Innocenti et al., 2005) conformably overlies the unit. Ersoy & Helvacı (2007) proposed that the Kocakuz formation, which is correlated with the Asartepe formation, is late Miocene in age according to stratigraphic relations in the Selendi basin. Recently, Seyitoğlu et al. (2009) documented biostratigraphic and magnetostratigraphic age of 7 Ma for the Asartepe formation in the Uşak-Güre basin.

2.4 ^{40}Ar-^{39}Ar Geochronology

In order to obtain the timing of the volcanism and coeval sedimentation in the basin, I carried out radiometric analysis from those nine volcanic rocks. Detailed analytical procedures and result have been presented at further pages.

2.4.1 Analytical Procedure

Age determinations were carried out on 7 samples from the Beydağ volcanic unit and 2 samples from the Payamtepe volcanic unit. The samples from the Beydağı volcanic unit are three andesitic-dacitic lava flows (#U-31, U-70, U-132), two andesitic-dacitic rocks from lava domes (#U-161, U-164), one rhyolitic pyroclastic

rock (#U-168) and one andesitic dyke. The trachytic/trachydacitic samples from the Payamtepe volcanic unit comprise a lava flow (#U-144) and a dike sample (#U-153). All were analyzed by the $^{40}Ar/^{39}Ar$ incremental heating method in the Nevada Isotope Geochronology Laboratory at the University of Nevada, Las Vegas.

Samples analyzed by the furnace step heating method utilized a double vacuum resistance furnace similar to the Staudacher et al. (1978) design. Sanidine standard 92-176 (Fish Canyon sanidine), with a calibrated age of 28.10±0.04 Ma (Spell & McDougall, 2003), was used as the fluence monitor. Details of the analytical methods and data treatment are given in Justet & Spell (2001) and Spell & McDougall (2003). The results of nine age determinations (details are given in Table 2.1) are summarized in Table 2.2 and selected age spectra plots are illustrated in Figure 2.13.

2.4.2 Results

The biotite phenocrysts of rhyolite sample U-31 (from the Elmadağ volcanic rocks) yielded a total gas age of 16.37±0.08 Ma (equivalent to a conventional K/Ar age), which is indistinguishable from the plateau age of 16.28±0.09 Ma at steps 5–13 (Figure 2.13a).

Moreover, this sample yielded a well-defined isochron age of 16.28±0.05 Ma. The isochron age, however, indicates that a small amount of excess argon is present. The isochron age is used, and as all 3 methods give essentially identical ages, the age of this sample can be considered as highly reliable (Figure 2.8b).

^{40}Ar–^{39}Ar analyses of biotite phenocrysts from the rhyolitic tuff sample U-68 (Elmadağ volcanic unit) produced an ideal flat age spectrum, with the exception of older ages for the first 3 steps. The total gas age is 17.20±0.12 Ma. Steps 4–15 define a slightly younger plateau age of 16.62±0.12 Ma (Figure 2.13c).

Table 2.1 Argon isotopic data for the representative lava samples from the Uşak-Güre basin (Note: Errors in age include J error and all errors 1 sigma. [36]Ar through [40]Ar are measured beam intensities, corrected for decay for the age calculations (see overleaf).

Steps	36Ar	37Ar	38Ar	39Ar	40Ar	%40Ar*	cumulative %39Ar	Ca/K	40Ar*/39ArK	Age (Ma)	1s.d.
Sample-U-31 (biotite)		J=0.002114 ± 0.10%									
1	4.330	0.440	1.030	8.790	1221.280	3.300	0.500	0.635	4.632	17.58	3.98
2	3.150	0.490	1.190	33.070	1026.610	16.600	2.300	0.188	5.191	19.69	0.73
3	0.710	0.700	2.150	81.740	537.810	65.900	6.700	0.109	4.313	16.37	0.17
4	0.490	0.880	3.770	116.190	636.990	80.500	12.900	0.097	4.407	16.73	0.15
5	0.350	0.950	4.220	126.700	636.410	86.600	19.800	0.096	4.341	16.48	0.14
6	0.340	1.100	5.380	162.530	782.510	89.200	28.600	0.087	4.302	16.33	0.13
7	0.270	1.090	4.460	134.270	639.060	90.000	35.800	0.104	4.278	16.24	0.13
8	0.240	1.350	3.630	105.720	505.090	91.000	41.500	0.164	4.248	16.13	0.13
9	0.270	2.170	4.690	131.930	626.880	91.500	48.600	0.211	4.279	16.25	0.13
10	0.410	3.540	8.210	228.070	1072.200	91.000	60.900	0.199	4.268	16.20	0.13
11	0.530	5.870	13.120	360.610	1676.400	92.000	80.400	0.209	4.300	16.33	0.13
12	0.370	3.140	9.850	288.820	1325.840	93.300	96.000	0.140	4.289	16.28	0.13
13	0.110	0.330	0.970	34.680	171.670	97.100	97.900	0.123	4.293	16.30	0.13
14	0.150	0.390	1.360	39.840	199.060	91.100	100.000	0.125	4.144	15.74	0.13
									Total gas age:	16.37	0.08
									Plateau age (5-13)	16.28	0.09
									Isochron age (1-8):	16.28	0.05
									MSWD:	1.70	
Sample-U-68 (biotite)		J=0.001869 ± 0.49%									
1	10.810	0.200	2.110	3.800	3062.030	3.500	0.100	0.601	28.282	92.93	15.71
2	13.790	0.160	2.700	4.550	3935.680	4.200	0.300	0.416	36.792	119.98	16.71
3	15.320	0.330	3.490	23.190	4544.690	7.800	1.100	0.164	15.476	51.44	4.09
4	12.230	1.300	5.470	129.850	4015.910	16.600	5.600	0.116	5.206	17.47	0.66
5	4.000	1.500	4.400	154.190	1869.180	41.600	10.900	0.112	5.113	17.16	0.27
6	1.870	1.780	4.080	162.010	1324.680	61.500	16.500	0.127	5.089	17.08	0.20
7	1.500	1.760	3.450	133.460	1073.360	62.200	21.000	0.152	5.054	16.96	0.20
8	1.270	1.550	3.620	142.620	1043.620	67.200	26.000	0.126	4.967	16.67	0.19
9	1.750	1.930	5.470	219.180	1555.160	69.300	33.500	0.102	4.977	16.70	0.18
10	1.880	2.690	6.060	235.370	1657.340	68.900	41.600	0.132	4.915	16.50	0.18
11	1.520	3.350	5.390	200.690	1390.620	70.500	48.500	0.193	4.929	16.54	0.18
12	0.790	7.750	7.430	267.220	1508.130	86.000	57.700	0.334	4.900	16.45	0.16
13	0.520	11.830	11.040	395.370	2068.510	93.300	71.400	0.345	4.936	16.57	0.15
14	0.350	6.170	11.050	454.170	2301.450	95.700	87.000	0.157	4.909	16.48	0.15
15	0.320	1.950	8.220	377.310	1920.550	95.900	100.000	0.060	4.914	16.49	0.15
									Total gas age:	17.20	0.12
									Plateau age (4-15)	16.62	0.12
									Isochron age (5-15):	16.48	0.08
									MSWD:	1.60	
Sample-U-70 (groundmass		J=0.001882 ± 0.43%									
1	1.740	0.470	0.420	4.670	506.490	7.100	0.300	1.303	7.742	26.10	2.26
2	0.760	1.670	0.510	24.950	331.510	40.000	1.800	0.875	5.246	17.73	0.30
3	0.290	7.020	1.920	151.170	840.370	91.900	10.700	0.607	5.139	17.36	0.16
4	0.170	9.100	3.270	268.850	1356.060	96.900	26.700	0.442	4.940	16.70	0.15
5	0.120	8.880	5.090	415.920	2042.160	98.300	51.400	0.279	4.889	16.52	0.14
6	0.130	7.220	5.260	424.350	2071.900	98.400	76.600	0.222	4.859	16.42	0.14
7	0.110	4.330	3.060	239.860	1174.020	98.000	90.800	0.236	4.834	16.34	0.14
8	0.120	2.650	1.140	85.120	432.850	96.100	95.900	0.407	4.835	16.34	0.15
9	0.110	1.700	0.340	20.460	121.390	89.700	97.100	1.082	4.872	16.47	0.16
10	0.110	2.640	0.300	13.290	98.070	99.200	97.900	2.601	5.858	19.78	0.19
11	0.220	6.780	0.390	13.160	114.360	72.500	98.700	6.740	4.970	16.80	0.20
12	0.240	17.590	0.530	17.120	131.330	72.500	99.700	13.476	4.772	16.13	0.18
13	0.190	8.990	0.210	5.440	65.960	56.300	100.000	21.733	4.771	16.13	0.50
14	1.740	0.470	0.420	4.670	506.490	7.100	0.300	1.303	7.742	26.10	2.26
15	0.760	1.670	0.510	24.950	331.510	40.000	1.800	0.875	5.246	17.73	0.30
									Total gas age:	16.63	0.11
									Plateau age (4-9)	16.46	0.13
									Isochron age (5-9):	16.44	0.07
									MSWD:	0.92	

Steps 5–15 also yielded a well defined statistically valid isochron, which gives an age of 16.48±0.08 Ma (Figure 2.13d), indistinguishable from the plateau age, and indicates that a small amount of excess argon is present. The isochron age for this sample is highly reliable.

Table 2.1 (Continued).

Steps											
	36Ar	37Ar	38Ar	39Ar	40Ar	%40Ar*	cumulative %39Ar	Ca/K	40Ar*/39ArK	Age (Ma)	1s.d.
Sample-U-132 (biotite)			J=0.002078 ± 0.08%								
1	13.920	0.380	3.400	30.390	4202.700	9.400	3.000	0.146	13.208	48.85	3.14
2	0.590	0.160	0.160	3.890	173.110	10.700	3.400	0.487	4.652	17.35	1.17
3	0.510	0.260	0.390	19.300	225.570	42.400	5.300	0.156	4.895	18.26	0.32
4	0.240	0.340	0.600	32.810	207.150	74.200	8.600	0.119	4.617	17.22	0.17
5	0.200	0.320	0.950	44.920	259.860	82.900	13.100	0.081	4.719	17.60	0.16
6	0.290	0.310	2.320	99.880	529.150	86.500	23.100	0.036	4.590	17.13	0.14
7	0.380	0.250	2.890	120.800	636.320	84.800	35.100	0.024	4.486	16.74	0.14
8	0.320	0.220	2.560	105.540	552.380	85.700	45.700	0.024	4.496	16.78	0.14
9	0.190	0.190	1.900	79.040	400.960	89.200	53.600	0.028	4.504	16.81	0.14
10	0.200	0.190	1.730	69.760	354.540	88.500	60.500	0.032	4.412	16.46	0.14
11	0.190	0.170	1.650	65.830	335.360	88.600	67.100	0.030	4.420	16.49	0.14
12	0.180	0.170	1.560	61.820	316.250	88.700	73.300	0.032	4.432	16.54	0.14
13	0.190	0.170	1.500	58.490	304.070	88.000	79.100	0.033	4.461	16.65	0.14
14	0.250	0.180	2.170	82.620	425.660	87.100	87.400	0.025	4.431	16.54	0.14
15	0.400	0.220	3.130	126.390	660.830	86.100	100.000	0.020	4.444	16.58	0.14
									Total gas age:	17.76	0.08
									Plateau age (7-15)	16.62	0.09
									Isochron age (7-15):	16.48	0.33
									MSWD:	1.60	
Sample-U-144 (groundmas			J=0.001856 ± 0.55%								
1	55.390	0.790	1.020	10.170	15234.570	-0.200	0.400	1.030	-2.650	-8.90	-33.86
2	23.520	0.610	4.550	5.420	6813.350	4.900	0.600	1.505	62.426	197.78	24.15
3	20.040	2.310	4.020	11.940	5893.660	6.400	1.100	2.577	32.033	104.19	10.27
4	14.440	4.940	3.230	34.340	4415.230	10.000	2.500	1.913	13.088	43.30	2.72
5	12.620	4.690	3.880	118.640	4284.030	18.900	7.200	0.526	6.909	22.99	0.78
6	4.660	8.320	5.030	345.850	3031.080	57.500	21.000	0.320	5.108	17.02	0.22
7	1.280	10.110	7.580	592.270	3198.630	88.600	44.700	0.227	4.850	16.17	0.17
8	0.570	5.870	5.350	415.680	2129.030	92.600	61.300	0.188	4.791	15.97	0.16
9	0.520	4.780	4.510	333.480	1719.770	91.900	74.600	0.191	4.781	15.94	0.16
10	0.480	3.740	3.480	230.700	1220.900	89.900	83.800	0.215	4.787	15.96	0.16
11	0.440	3.550	2.800	160.340	877.390	87.300	90.200	0.294	4.789	15.96	0.16
12	0.640	6.200	3.560	143.040	847.360	80.500	95.900	0.576	4.780	15.93	0.17
13	0.460	11.360	3.220	62.600	422.240	75.600	98.400	2.415	4.930	16.43	0.19
14	0.510	14.800	3.230	37.720	303.970	62.200	99.900	5.226	4.752	15.84	0.20
15	0.140	2.470	0.710	2.720	40.930	90.800	100.000	12.145	13.836	45.74	0.68
									Total gas age:	17.62	0.13
									Plateau age (7-14)	16.02	0.13
									Isochron age (3-13):	15.93	0.08
									MSWD:	1.60	
Sample-U-153 (sanidine)		J=0.002038 ± 0.10%									
1	0.060	0.230	0.990	74.660	330.170	97.000		0.047	4.355	15.94	0.13
2	0.070	0.250	0.710	58.310	262.560	96.300		0.065	4.396	16.09	0.13
3	0.060	0.240	0.910	72.570	319.740	97.000		0.049	4.336	15.87	0.12
4	0.090	0.250	1.000	79.920	360.100	95.400		0.048	4.368	15.99	0.13
5	0.070	0.220	0.680	53.090	238.030	95.900		0.062	4.357	15.95	0.13
6	0.060	0.240	0.910	72.370	315.470	97.000		0.051	4.292	15.71	0.12
7	0.060	0.240	1.010	81.220	360.660	97.400		0.045	4.388	16.06	0.13
8	0.060	0.270	1.000	79.770	353.620	97.600		0.051	4.389	16.07	0.13
9	0.120	0.320	1.400	108.180	490.460	94.700		0.045	4.361	15.96	0.13
10	0.080	0.250	0.870	70.480	319.550	95.100		0.054	4.376	16.02	0.13
11	0.060	0.270	0.990	78.160	345.960	97.300		0.052	4.370	16.00	0.12
12	0.070	0.220	0.750	58.720	264.740	95.600		0.057	4.353	15.93	0.13
13	0.070	0.300	1.270	101.620	451.820	96.900		0.046	4.375	16.01	0.13
14	0.070	0.270	1.120	89.590	402.360	96.800		0.046	4.416	16.16	0.13
									mean:	15.98	0.10
									Weighted mean age (14 crystals):	15.98	0.03
									Isochron age (14 crystals):	16.010	0.080
									MSWD:	1.20	

Groundmass from the latite sample U-70 (Elmadağ volcanic rocks) produced a generally flat age spectrum, with somewhat older ages for the first 3 steps and some discordance in the final 4 steps. The total gas age is 16.63±0.11 Ma and steps 4–9 define a statistically indistinguishable plateau age of 16.46±0.13 Ma (Figure 2.13e). Steps 5–9 yield a valid isochron, which gives a nearly identical age of 16.44±0.07

Ma. The isochron does not suggest that excess argon is present (initial $^{40}Ar/^{36}Ar=287\pm20$, indistinguishable from atmospheric argon).

Table 2.1 (Continued).

Steps	36Ar	37Ar	38Ar	39Ar	40Ar	%40Ar*	cumulative %39Ar	Ca/K	40Ar*/39ArK	Age (Ma)	1s.d.
Sample-U-159 (biotite)		J=0.001990 ± 0.10%									
1	1.160	0.290	0.540	4.170	331.640	6.500	0.200	0.809	5.171	18.47	1.73
2	5.630	0.690	1.530	19.280	1668.310	7.900	1.300	0.423	6.965	24.83	1.90
3	0.450	0.810	2.430	68.050	419.760	75.500	5.200	0.140	4.644	16.59	0.15
4	0.410	0.780	5.000	142.220	723.080	85.400	13.400	0.065	4.366	15.61	0.13
5	0.380	0.740	7.160	208.850	993.520	89.900	25.400	0.042	4.313	15.42	0.13
6	0.520	1.050	12.960	384.520	1768.010	91.700	47.400	0.032	4.272	15.27	0.12
7	0.450	1.310	12.950	383.840	1746.490	92.600	69.500	0.040	4.269	15.26	0.12
8	0.420	0.890	9.830	294.960	1358.340	91.800	86.400	0.036	4.260	15.23	0.12
9	0.240	0.810	5.030	146.770	673.610	94.800	91.800	0.065	4.207	15.04	0.12
10	0.130	0.800	1.930	54.520	255.770	92.700	97.900	0.173	4.204	15.03	0.12
11	0.090	0.580	0.560	14.080	73.750	91.500	98.700	0.487	4.032	14.42	0.13
12	0.080	0.510	0.270	5.740	36.810	86.900	99.100	1.042	3.700	13.23	0.15
13	0.120	0.840	0.660	16.300	91.170	91.100	100.000	0.608	4.039	14.44	0.12
									Total gas age:	15.42	0.08
									Plateau age (5-10)	15.21	0.10
									Isochron age (3-10):	15.04	0.10
									MSWD:	2.10	
Sample-U-161 (biotite)		J=0.001897 ± 0.38%									
1	2.220	0.580	2.160	28.090	738.030	18.600	3.100	0.242	4.931	16.80	0.56
2	0.270	0.240	0.230	9.970	107.530	40.600	4.200	0.280	4.188	14.28	0.25
3	0.190	0.590	1.530	51.670	245.530	83.400	9.900	0.135	3.892	13.27	0.12
4	0.210	0.700	2.970	79.160	348.940	86.600	18.600	0.105	3.790	12.92	0.12
5	0.250	0.740	3.850	106.740	456.460	87.100	30.300	0.082	3.721	12.69	0.12
6	0.400	1.140	7.780	218.950	913.340	88.200	54.400	0.062	3.711	12.66	0.11
7	0.290	1.490	6.640	186.920	757.950	90.800	75.000	0.094	3.679	12.55	0.12
8	0.180	1.420	3.130	85.180	356.660	90.200	84.400	0.197	3.707	12.64	0.11
9	0.130	0.720	2.120	58.460	245.510	91.700	90.800	0.146	3.714	12.67	0.11
10	0.110	0.510	1.810	50.510	209.760	92.500	96.400	0.120	3.672	12.52	0.11
11	0.100	0.570	1.060	28.250	120.030	91.700	99.500	0.240	3.542	12.08	0.11
12	0.070	0.330	0.160	2.820	20.470	95.700	99.800	1.371	2.638	9.01	0.25
13	0.090	0.390	0.120	1.730	22.470	99.900	100.000	2.642	1.291	4.41	0.87
									Total gas age :	12.79	0.08
									Plateau age (4-10)	12.66	0.09
									Isochron age (3-10):	12.15	0.15
									MSWD:	1.80	
Sample-U-164 (amphibole)		J=0.002022 ± 0.10%									
1	1.180	9.200	1.180	72.210	700.750	55.300	14.500	1.724	5.396	19.58	0.25
2	0.110	1.840	0.290	20.680	116.220	86.300	18.700	1.202	4.591	16.67	0.16
3	0.210	4.970	0.870	51.520	290.060	84.400	29.000	1.307	4.697	17.05	0.16
4	0.140	1.560	0.400	12.570	85.720	69.800	31.600	1.684	4.382	15.91	0.18
5	0.110	1.240	0.380	5.930	48.490	57.500	32.800	2.833	3.976	14.44	0.20
6	0.110	1.670	0.480	4.530	40.580	50.500	33.700	4.982	3.675	13.36	0.54
7	1.250	8.340	2.350	25.390	463.910	28.000	38.800	4.450	5.119	18.58	0.46
8	4.200	74.020	18.870	179.950	2009.250	44.100	75.000	5.575	4.988	18.10	0.28
9	0.870	83.420	13.370	69.970	498.030	61.000	89.000	16.209	4.343	15.77	0.18
10	0.690	108.090	7.940	48.220	326.590	59.500	98.700	30.603	4.002	14.54	0.17
11	0.150	21.490	0.750	5.130	44.470	58.600	99.800	57.631	3.748	13.62	0.40
12	0.100	5.520	0.200	1.200	20.030	41.100	100.000	63.331	2.584	9.40	1.29
									Total gas age :	17.29	0.13
									No plateau		
									No isochron		

The isochron data are dominantly near the x-axis, which defines the age, thus the age is very precise, but the y-axis intercept (initial $^{40}Ar/^{36}Ar$) is less precise. The isochron age, therefore, is used for this sample, and it is also accepted as highly reliable (Figure 2.13f).

Table 2.2 Summary of step heating ^{40}Ar/^{39}Ar data for the dated samples. (BVU: Beydağı volcanic unit; PVU: Payamtepe volcanic unit).

Sample	Unit	UTM coordinates 35 S	Material used	Preferred age	Total gas age	Weighted mean Plateau age (Ma)	Isochron age
U-31	BVU (lava flow)	7 18618/42 98122	biotite	16.28±0.05	16.37±0.08	16.28±0.09	16.28±0.05
U-68	BVU (pyroclastic flow)	7 17824/42 88588	biotite	16.48±0.08	17.20±0.12	16.62±0.12	16.48±0.08
U-70	BVU (lava flow)	7 18072/42 90168	groundmass	16.44±0.07	16.63±0.11	16.46±0.13	16.44±0.07
U-132	BVU (lava flow)	7 11777/42 95468	biotite	16.48±0.33	17.76±0.08	16.62±0.09	16.48±0.33
U-144	PVU (lava flow)	6 99775/42 99080	groundmass	15.93±0.08	17.62±0.13	16.02±0.13	15.93±0.08
U-153	PVU (dike)	6 96875/43 04825	sanidine	16.01±0.08	no age	15.98±0.03	16.01±0.08
U-159	BVU (dike)	6 96863/42 73805	biotite	15.04±0.10	15.42±0.08	15.21±0.10	15.04±0.10
U-161	BVU (lava dome)	6 83603/42 55465	biotite	12.15±0.15	12.79±0.08	12.66±0.09	12.15±0.15
U-164	BVU (lava dome)	7 15183/43 02517	amphibole	17.29±0.13	17.29±0.13	no plateau	no isochron

The biotite phenocrysts from the shoshonite sample U-132 (Elmadağ volcanic rocks) yielded a total gas age of 17.76±0.08 Ma. Steps 7–15 define a younger plateau age of 16.62±0.09 Ma (Figure 2.13g) and also a statistically valid isochron, which yields an indistinguishable and less precise age of 16.48±0.33 Ma (Figure 2.13h). Due to the very tight clustering of the isochron data of this sample, it should not be considered reliable. Therefore, plateau age is used and is considered reliable.

The groundmass of the latite sample U-144 (Payamtepe volcanic unit) also produced a nearly ideal flat age spectrum, with the exception of generally older initial steps. The total gas age is 17.62±0.13 Ma. Steps 7–14 define a significantly younger plateau age of 16.02±0.13 Ma (Figure 2.13i).

Moreover, steps 3–13 define an extremely well constrained, statistically valid isochron, which gives an indistinguishable age of 15.93±0.08 Ma (Figure 2.13j). The isochron indicates that some excess argon is present, which is also evidenced by the form of the age spectrum. The concordance between the plateau and the isochron, along with the very well defined isochron, gives high confidence in the age of this sample. The isochron age is preferred for this sample and is considered to be highly reliable.
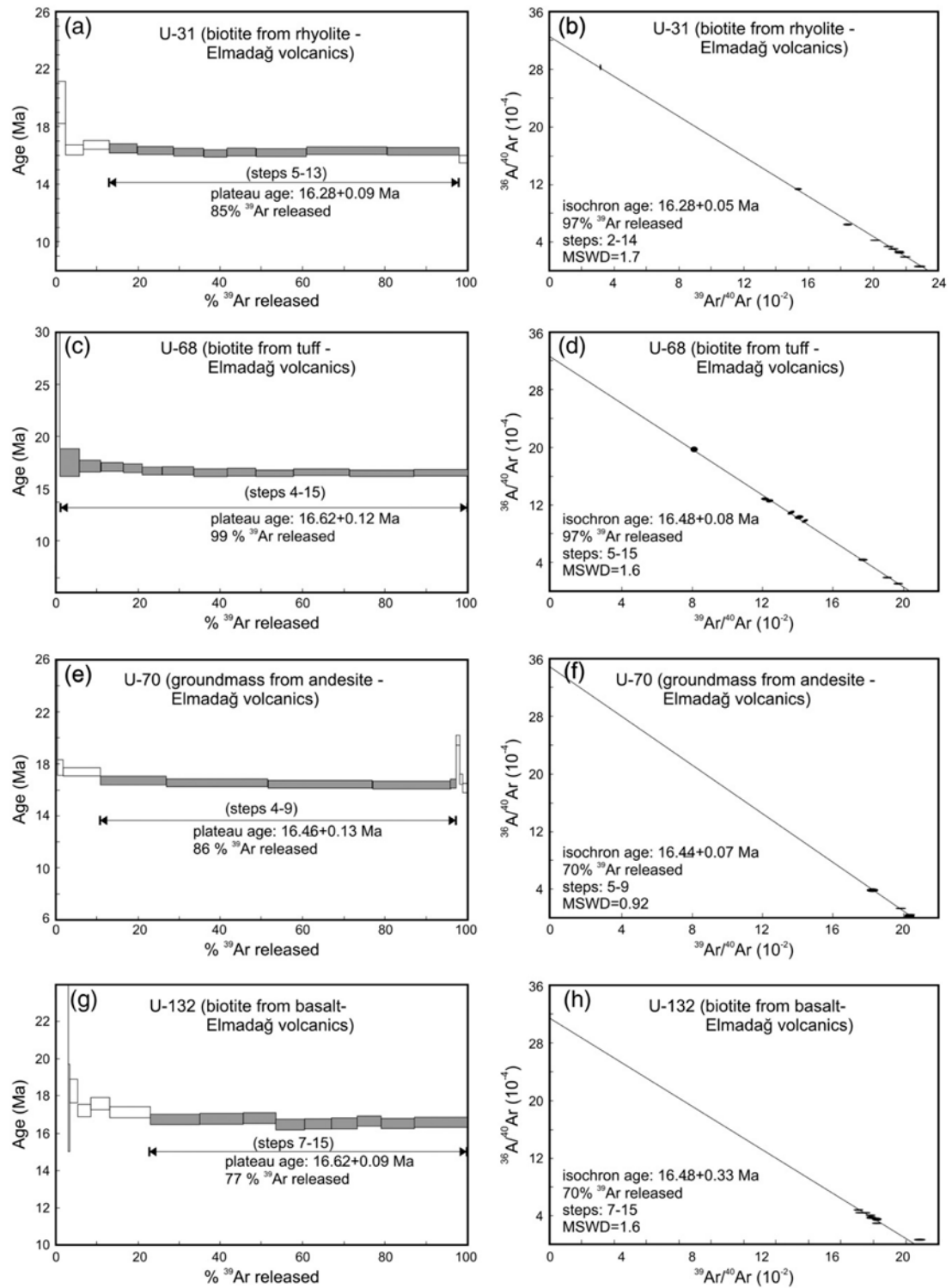
Figure 2.13 Apparent age spectra for the dated volcanic rocks in this study (a-h). See text for discussion.

^{40}Ar–^{39}Ar analyses of biotite phenocrysts from the dacite sample U-159 (from the İtecektepe volcanic rocks) yielded a nearly ideal flat age spectrum, with the

exception of some higher ages in the first 3 steps. The total gas age for this sample is 15.42±0.08 Ma.
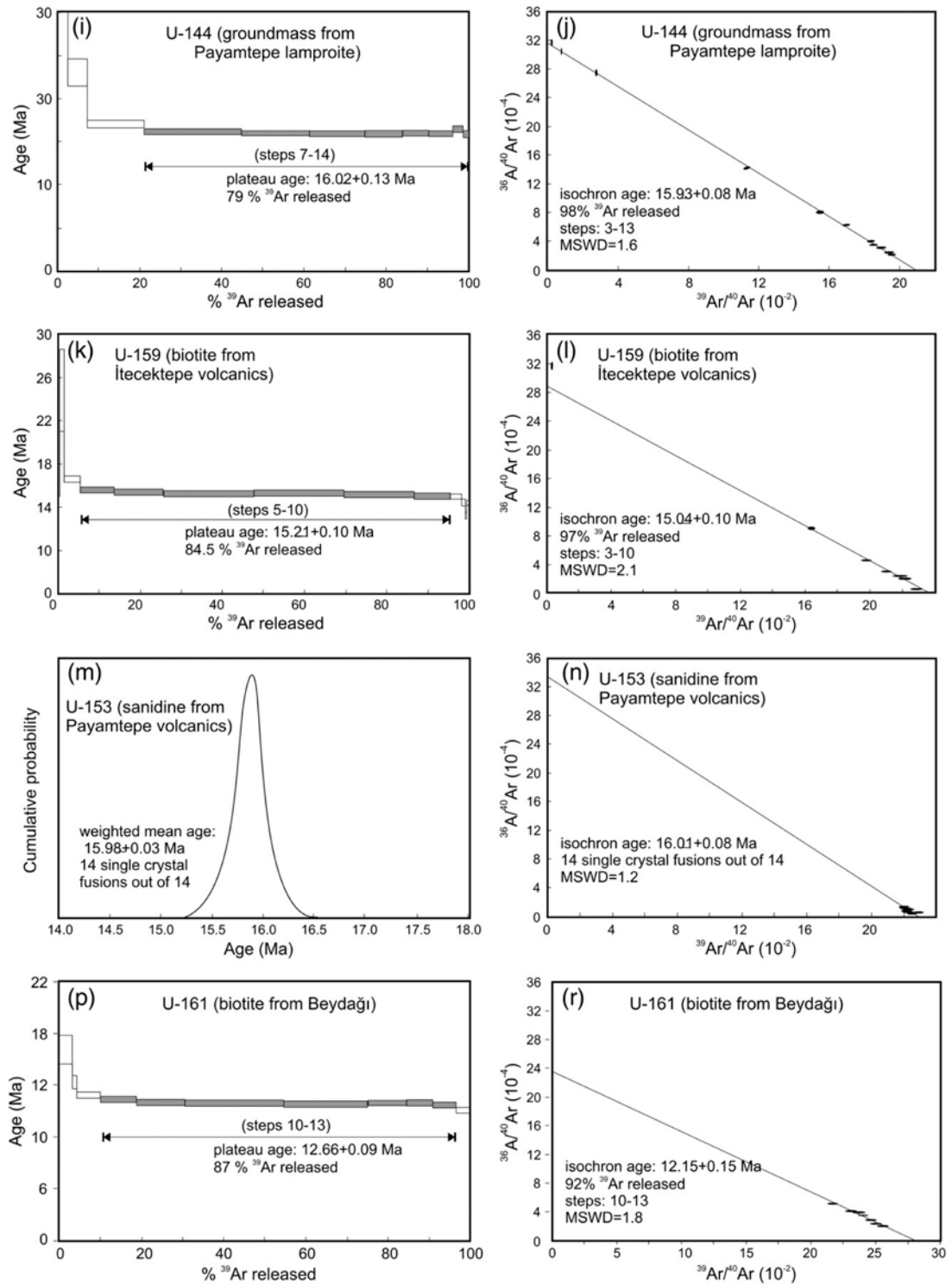
Figure 2.13 (Continued; i-r).

Steps 5–10 define a plateau age of 15.21±0.10 Ma, which is indistinguishable from the total gas age at 2σ analytical uncertainty (Figure 2.13k). Steps 3–10 define a statistically valid isochron, which yields a significantly younger age of 15.04±0.10 Ma (Figure 2.13l) and indicates that some excess argon is present. The isochron age is considered reliable for this sample.

^{40}Ar–^{39}Ar analyses were conducted on sanidine phenocrysts from the trachyte sample U-153 (Payamtepe volcanic unit) by single crystal laser fusion. A total of 14 crystals were analyzed. All 14 defined a single, coherent population with no outliers such as older xenocrysts. These analyses yield a mean age of 15.98±0.10 Ma and a weighted mean age of 15.98±0.03 Ma (Figure 2.13m). Single crystal analyses can be utilized to define an isochron as can the individual steps from a step heating experiment. All 14 analyzed crystals for this sample define an isochron, which yields an age of 16.01±0.08 Ma (Figure 2.13n) and suggests that there is no excess argon in this sample. Although his isochron is statistically valid, note that all analyses cluster very tightly near the x-axis. This is due to the consistent and high radiogenic yields (%^{40}Ar*) which is common for sanidine. Thus, the isochron only serves to validate the age and the y-intercept (initial ^{40}Ar/^{36}Ar) is very imprecise. Clearly, all of these 3 ages are indistinguishable. Therefore, the weighted mean age is preferred for this sample and it is considered as highly reliable.

The biotite phenocrysts from the andesite sample U-161 (Beydağı volcanic unit) yielded a nearly ideal flat age spectrum, with the exception of some higher ages in the first 3 steps and lower ages in the last two steps. The total gas age is 12.79±0.08 Ma. Steps 4–10 define a plateau age of 12.66±0.09 Ma, which is statistically indistinguishable from the total gas age (Figure 2.13p). Steps 4–10 define a plateau age of 12.66±0.09 Ma, which is also indistinguishable from the total gas age. Moreover, steps 3–10 define a valid isochron, which yields a younger age of 12.15±0.15 Ma. The isochron indicates that some excess argon is present in the dated biotite, as the initial ^{40}Ar/^{36}Ar is 420±27. Note that the intercepts on the isochron regression are somewhat imprecise due to the fact that the steps defining the isochron are of similar radiogenic yield and thus cluster in a relatively restricted region.

Regardless, this is a reliable isochron for this sample, defined by a large portion of the analyses and should be considered valid. Overall, the isochron age of this sample is considered to be reliable (Figure 2.13r).

Amphibole phenocrysts from the trachyte sample U-164 (Elmadağ volcanic unit) produced a very discordant age spectrum. The total gas age is 17.29±0.13 Ma. There is no plateau or isochron age defined by these data. This may be due to alteration, intergrowths of other minerals, and impurities in the mineral separates or excess argon. The total gas age is used for this sample.

CHAPTER THREE
STRUCTURAL EVOLUTION OF THE UŞAK-GÜRE SUPRA-DETACHMENT BASIN DURING MIOCENE EXTENSIONAL DENUDATION IN WESTERN TURKEY

3.1. Structural Studies of the NE–SW- Trending Basins

The Uşak-Güre basin is bounded by metamorphic rocks of the Menderes Massif on its northwestern and southeastern sides. Neogene exhumation of these rocks has been attributed to the activity of extensional detachments, with preserved NE–SW to N-S stretching lineations (Şengör et al., 1984; Hetzel et al., 1995; Bozkurt 2000; Bozkurt & Oberhanslı 2001; Işık & Tekeli 2001; Ring et al., 2003; Seyitoğlu et al., 2004; van Hinsbergen 2010). Many works suggest the timing of the exhumation and related detachment faults. van Hinsbergen (2010) reported that Northern and Southern Menderes Massifs were recorded as late Oligocene to latest Early Miocene zircon and apatite fission track ages (~27–16 Ma, with zircon fission track ages generally 2–3 Ma older than the apatite fission track ages), and that the Central Menderes Massif was exhumed mainly between ~16 and 5 Ma (Gessner et al., 2001; Ring et al., 2003; Thomson & Ring, 2006).

The general consensus associated with the contact relationships between basement rocks, exists is that unmetamorphosed ophiolitic mélange rocks structurally overlie the Menderes metamorphic rocks. van Hinsbergen (2010) reported that the Massif is surrounded by metamorphosed and nonmetamorphosed older, structurally higher thrust slices. These are (1) the Bornova Flysch zone in the NW, a chaotic mélange of late Cretaceous age that formed during accretion and subduction prior to underthrusting of the Menderes Massif (Okay & Altıner, 2007); (2) the HP–LT metamorphic Afyon zone (Candan et al., 2005) and (3) in the west, the Menderes Massif is overthrusted by the HP–LT Dilek Nappe (Ring et al., 2007) and in the south, the top of the Menderes Massif is formed by a metasedimentary sequence including upper Paleozoic to lower Mesozoic rocks (Erdoğan & Güngör, 2004).
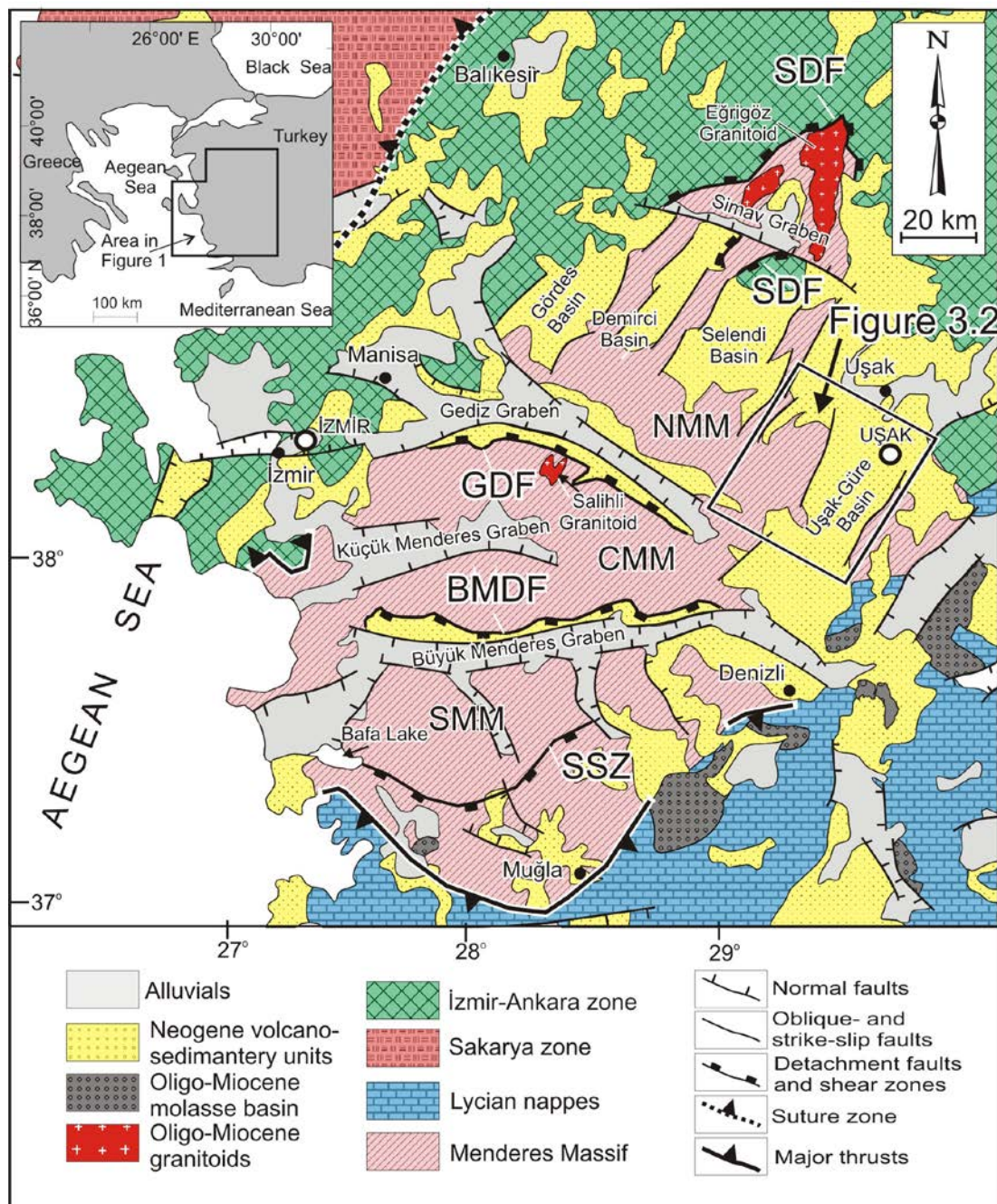
Figure 3.1 Geological map of western Anatolia showing the major tectono stratigraphic units on which the Neogene and Quaternary sedimentary basins developed. SDF—Simav detachment fault, GDF—Gediz detachment fault, BMDF—Büyük Menderes detachment fault, SSZ—Selimiye shear zone, NMM—Northern Menderes Massif, CMM—central Menderes Massif, SMM—Southern Menderes Massif. The map is compiled from Bozkurt (2004); Bozkurt & Park (1994); Sözbilir (2001); Sözbilir (2005); Bozkurt & Sözbilir (2004); Işık et al. (2004); Collins & Robertson (2003); Okay & Siyako (1993); Özer & Sözbilir (2003).

The hinge lines of the major and minor folds trend between N10°E and N30°E and are parallel to the trend of the stretching lineations. The author claimed that this geometry suggests a genetic relationship between the stretching lineations and the small and large folds. These folds were probably formed by the contractional component of the N30°E-directed extension, because their axes are parallel to the extension direction in the province.

Dating and assessment of the tectonic style of the late Cenozoic NE–SW trending sedimentary basins for northern side of the MMCC shed light on the role of crustal extension and subsidence associated with exhumation of the MMCC. However, fault kinematic evidence for understanding tectonic evolution of these sedimentary basins is quite limited. Ersoy et al. (2010), is one of the rare works that has presented detailed kinematic evidence for the Selendi basin. The authors stated that four phases of deformation (D_2 to D_5) have been established within the Selendi basin on the basis of stratigraphic, sedimentologic and structural data.

3.2 Kinematic Analysis of the Basin

In order to establish the surface expressions of extensional deformation, field structural data were collected at seventeen localities (for locations see Figure 3.2) that occur over both of two main areas: the Uşak basin and the Güre basin. The relative age of the different sets of faults was established by cross-cutting and offset relationships using (1) mapping of geological structures; (2) measurement of outcrop-scale faults and kinematic relationships and (3) published radiometric age data. Although, I documented most of the outcrop scale of faults in the field in simplified geological maps (Figure 3.3), not all the faults can be shown. The most important reason is that the space and time correlations of some of these faults could not be determined clearly and some of these faults are not directly responsible for the evolution of the basin.

I have selected the main faults for structural re-construction of the basin. Measurements have been subdivided in three datasets which represent D_2 (Early

Miocene deformations); D$_3$ (Middle Miocene deformations) and D$_4$ (Late Miocene deformations).
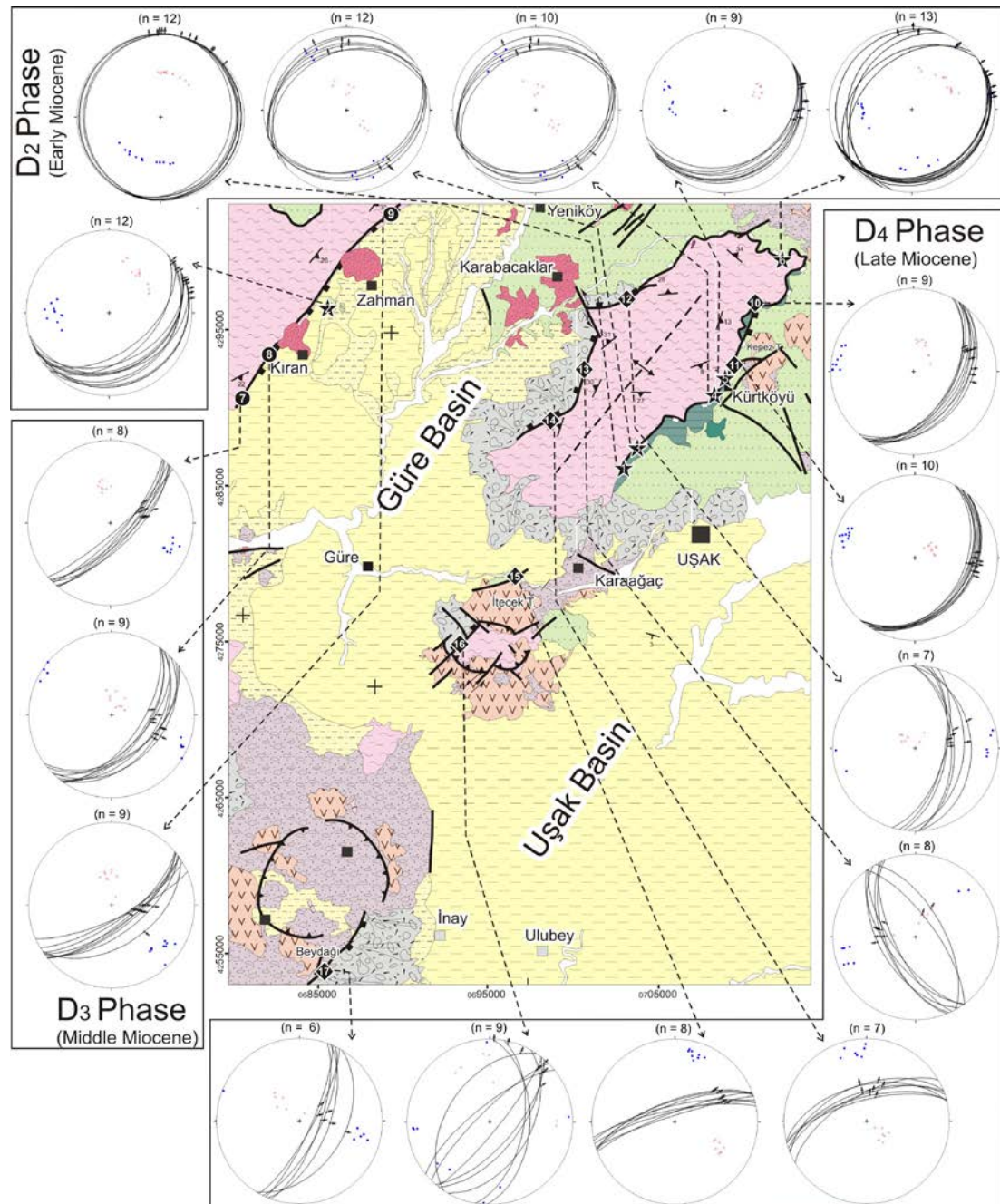
Figure 3.2 Stereographic projections (equal area, lower hemisphere) showing orientations of faults in outcrops of the Uşak-Güre basin. Note that the faults of D$_2$ (represented by 1-6) have lowest dip angles, the faults of D$_3$ (from 7 to 9) and D$_4$ (from 10 to 17) contains structures pointing to dip to oblique slip indicating NE-SW directed extension.

The D_1 deformation phase refers to the pre- Miocene tectonic history of the region, which is beyond the scope of this paper and readers are referred to Şengör & Yılmaz (1981), Şengör *et al.* (1984), Ring *et al.* (2003), Hetzel *et al.* (1995), and Gessner *et al.* (2001) for further information.

3.2.1 Faults of the D_2 (Early Miocene Deformations)

Five measurements were taken from the western margin of the Uşak basin and one from the eastern margin of the Güre basin (see Figure 3.2). These deformational surfaces (shear zones) separating brecciated-rock volumes with differentiated tectono-metamorphic characteristics, represent brittle-ductile transitions. The brittle deformation under decreasing P-T conditions is characterised by a brittle-ductile transition in deformation towards the low-angle fault. The shear zones are commonly detached on the contact between (1) the Palaeozoic–Metamorphic rocks and the Yeniköy formation for the Güre margin (Figure 3.3) and (2) Palaeozoic–Metamorphic rocks and ophiolithic rocks with the Yeniköy formations in the Uşak basin margin (Figure 3.4).

The structural relationship between the metamorphic rocks and the basin fill units is best shown in the western Uşak and Güre basin margins (Figures 2.2, 2.4 and 2.6). The Yeniköy formation tectonically overlies the Menderes Massif along a low-angle normal detachment fault (Figures 2.4 and 2.6). Foliation surfaces along the detachment fault plane are consistent with a nearly NE–SW-directed extension in the area (Figures 3.3 and 3.4). The angles of the detachment fault are inclined with a low angle, 9° and 4° (N60°E/32°SE) (Figure 3.3) on the western side of the Uşak margin compared to the western side of the Güre basin which shows detachment angles of 19° and 21° (Figures 2.4, 2.6 and 2.7).

The contact between the Yeniköy Formation and the metamorphic rocks is a low-angle normal fault (N40–55°E/19–29°SE) that can easily be traced in the Kıran–Kadıoğlu–Kurtçamı area (Figures 2.6 and 3.3). I have also observed a ~10 m thick highly altered silicic zone through the low angle normal fault surface between

hanging wall and footwall rocks (Figure 3.5). The beds of the Yeniköy formation are cut and displaced by this fault (Figure 2.5).

Figure 3.3Structural relations between Menderes Massif and Yeniköy formation (Hacıbekir group). Note that layers of the Yeniköy formation almost vertically overlay tectonically on Metamorphic rocks through the detachment fault near Kadiroğlu village.

One of the master detachment outcrops is represented by Station 2 (Figure 3.2), which strikes in an NNE-direction and extends laterally from the Güre margin. While the dip angles of the fault scarp vary from 12° to 50°, the rakes show a maximum of 9°. The more detailed data have supplied from the Uşak basin margin with respect to those of the Güre margin for the D_2 deformation. The shear zone strike shows a dominantly NE-direction and extends laterally for over 30 km towards the western Uşak basin margin. While the outcrop patterns of the Station 1 and 3 indicate lower rake angles; Stations 4, 5 and 6 present higher rake angles than Stations 1 and 3. The rake angles of Station 4 display very high values from 72° to 81°. The outcrop pattern of the major detachment fault is probably influenced by fold-like primary

corrugations in the detachment fault that are oriented parallel to the northeast direction of MMCC exhumation and coeval extension. In many places, the detachment faults were cut and tilted by high angle normal faults in both the Güre and Uşak basin margins.
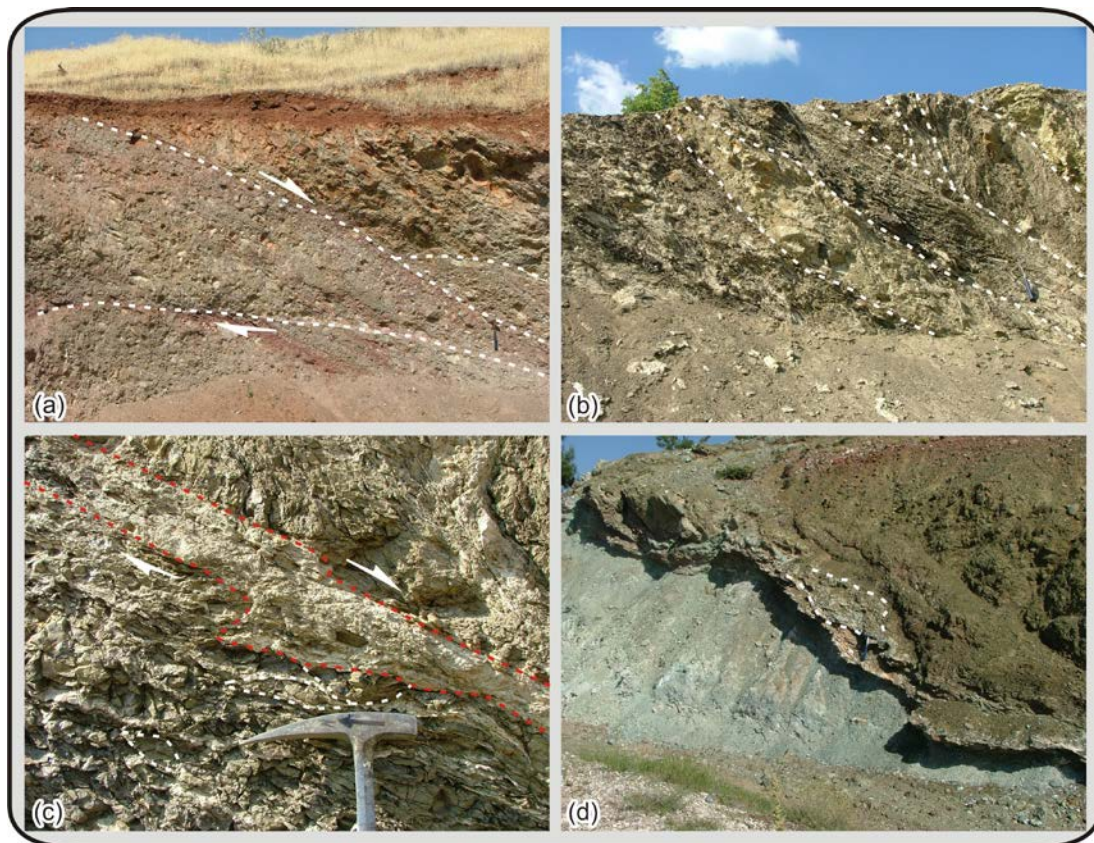
Figure 3.4 Early Miocene structural deformations (D_2) over the Kürtköyü formation from Uşak Margin.

3.2.2 Faults of the D_3 (Early-Middle Miocene Deformations)

The D_3 deformational phase was responsible for the start of the deposition of the İnay Group (Merdivenlikuyu Member, according to Ercan *et al.* 1978), as represented by the clastic boulder sediments that accumulated during this period in the Güre basin. The D_3 phase is characterised by NE–SW- striking range-front fault zones developed in an extensional tectonic regime. The normal faults are dip-to oblique-slip and are well-exposed. At three locations in the footwall-metamorphic rocks of the Güre margin (Figure 3.2), a single set of vertical to near vertical NE-

trending faults extending over 28 km, with well-developed antithetic strike slip faults, was observed. Our observations show that the source of the Kıran and Zahman lava flows overlies the fault of D_3, and are also consistent with the NE–SW directed extension.

Our observations show that Kıran and Zahman lava flows directly controlled by the fault of D_3 (Figure 2.6). Moreover, Seyitoğlu (1997) reported K/Ar dating, 15.5±0.4 Ma trachyandesitic lavas interfingers with the upper levels of the İnay group, from Kıran (Adıyalar) lava flows. Three stations of D_3 exhibit high angle fault surfaces and with a measured rake of the faults, which are between 52° and 81°. Fault sets display well-preserved slickensides, with stereographic plots showing oblique-normal offsets dipping at an average of 68°. Fault dip and dip azimuth versus rake plots shows similar clustering in three locations. NNE–SSW-trending sets of conjugate normal faults suggest the existence of a NE–SW directed tensional stress field during the D_3 deformation phase. These faults truncate the Early Miocene detachment faults through a few small scale locations.

3.2.3 Faults of the D_4 (Late Miocene Deformations)

I have mentioned earlier some references related to the age of the Asartepe formation in the Uşak basin as well as the adjacent Selendi basin. Ercan et al. (1996) and Innocenti et al. (2005) reported two radiometric age data, 8.37 and 8.5 Ma for Selendi basin, while Seyitoğlu et al. (2009) presented the magnetostratigraphic age data, 7 Ma from Asartepe formation, for Uşak Güre basin. It is unlikely that the magnetostratigraphic age data from Asartepe formation is so trustable with respect to radiometric age data from lava rocks; the magnetostratigraphic age value for Uşak-Güre basin is similar to that of the radiometric age data from the Selendi basin. Therefore, I presume the deposition age of Asartepe formation, to be at least in the Late Miocene. Our observations show that the D_4 phase was responsible for initiation and deposition of the Asartepe formation and refers to Late Miocene extensional phase. The fault zone is presumed to have formed during this stage.

I have made eight sets of fault surface measurements in the Uşak basin and along the displacements of three stratovolcanoes. Measurements from the Asartepe Formation at the Uşak basin margin indicate different strikes and, strike-dip angles owing to the geometrical shapes of the basement rocks of the Uşak margin. In addition, these D_4 faults are truncated by younger splays. While Stations of 12, 13 and 14 show WNW strikes on the western side, stations of the eastern side as well as Stations 10 and 11 display NE-trending strikes (Figure 3.2).

At the axis of the fault zone on eastern side of the Uşak margin, I found two well-exposed slickenside fault surfaces, whose average strike is N35°E with rakes of 52° for Station 10 and 65° for Station 11. The western Uşak margin fault is characterised by a curvilinear range front fault. Stereographic plots (for Stations 12-13 and 14) show nearly dip-slip normal offset with attitudes averaging N5°E/51°NW; N60°W/63°SW and N70°W/76SW, where the rakes of slip lines are 77°NNE; 72°N and 76°N, respectively. One of the sets of the İtecektepe stratovolcano (Station 15) shows NEE strike directions and has lesser rake angles (37-47°) with respect to measurements of the Uşak margin.

However, a second location of the İtecektepe stratovolcano displays scattered dip quadrants and rake measurements from 2° to 36° for the D_4 deformation phase (Figure 3.2). The fault zone extending along the İtecektepe (Stations 15-16) shows oblique-slip normal faults dipping at an average of 27° with a major dextral strike-slip component. In addition, the NE-striking fault segment cutting the Beydağı stratovolcano in southern part of the Uşak-Güre basin, suggest a high angle component normal fault with strikes averaging N25°E, with a 76°NE higher average rake of slip lines (Figure 3.2). All the kinematic evidence of the D_4 deformation phase, suggests that the predominant NE–SW-trending extensional tectonics was active and progressive during the late Miocene.
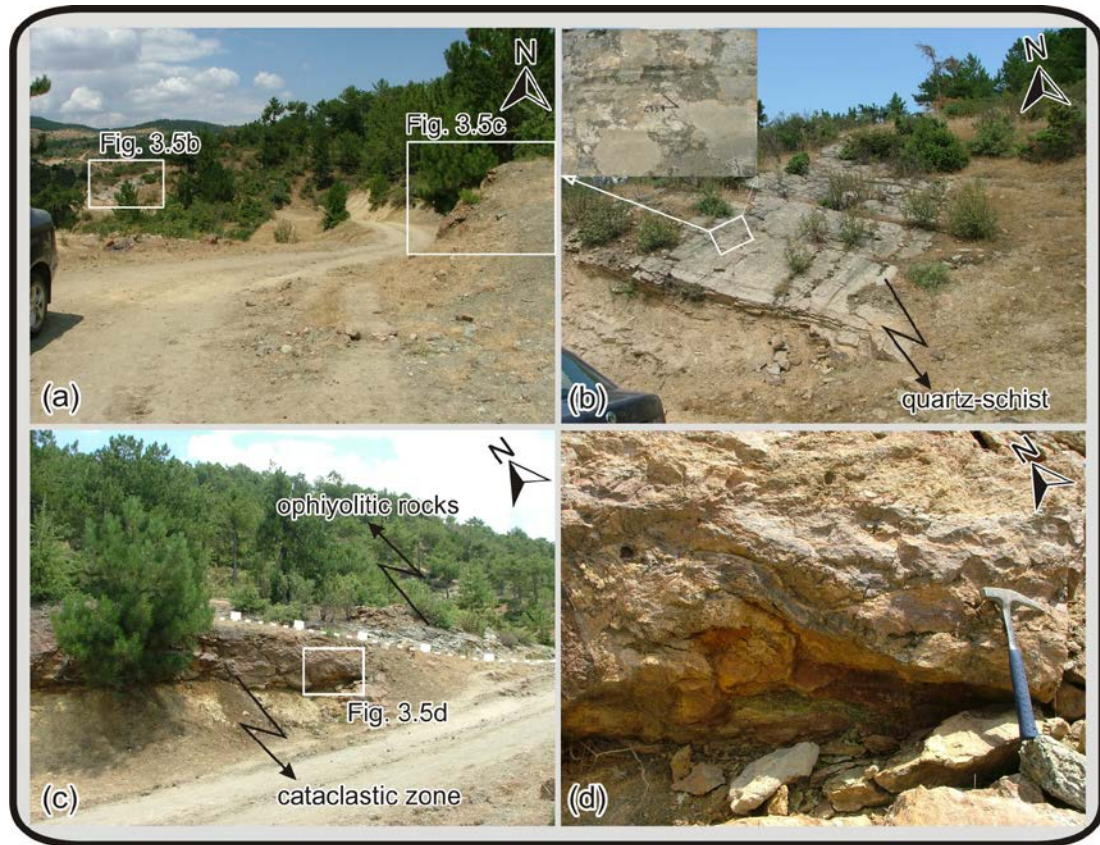
Figure 3.5 Early Miocene deformations (D_2) between metamorphic basement rocks and the ophiolithic rocks (İAZ) of the Hacıbekir group. Note that (a) detachment tectonic relationships between footwall and hanging wall rocks are well preserved at the Uşak margin vicinity, (b) footwall rocks showing low angle fault scarps, (c) silica rich cataclastic zone is nearly extending horizontally, (d) also this cataclastic rock exhibits asymmetric deformation textures.

3.3 Deformation and Rock Fabrics

Işık et al. (2004) and Ring & Collins (2005) reported that the ductile deformation along the SDF occurred at the beginning of the Miocene. Işık et al. (2004) also obtained mica age ($^{40}Ar/^{39}Ar$) of 22.86 ± 0.28 Ma from the mylonitic gneisses; in addition Ring & Collins (2005) obtained a SHRIMP-U/Pb–zircon age of 20.7±0.5 Ma that dates the intrusion of the Eğrigöz granite. Each of two studies indicates the timing of ductile deformation. I have also observed ductile to brittle deformation structures of Menderes metamorphic rocks at both margins of the basin (Figure 3.16). There is also insufficient evidence of rock fabrics on Menderes Metamorphic rocks near Uşak-Güre basin. Purvis & Robertson (2004) reported that beneath the

adjacent Selendi Basin, the Menderes metamorphic rocks exhibit pervasive deformation, marked by a gently dipping foliation and an extensional lineation consistently plunging to the NE or SW according to Verge (2000). Top-to-the- NNE shear-sense indicators (e.g. rotated feldspar porphyroblasts) are ubiquitous. The authors interpreted these shear fabrics as the result of ductile to brittle extension related to unroofing of the Menderes Massif.

Although the detachment fault is not well exposed in the NE-trending Uşak margin, I obtained the data regarding exhumation of the basement rocks (Figures 2.4 and 2.5). The ductile to brittle deformation along the detachment fault in the Uşak-Güre basin is evidenced by petrographic data (Figure 3.6). Mica fish and flattened feldspar structures synkinematic to the stretching event show mostly north-eastward shearing (see ductile kinematic vectors and porphyroblast in Figure 3.6). S (S_1 foliation) and C' (S_2 foliation) planes are frequently cut by extensional cleavage and by low-angle ductile shear bands that indicate mostly top-to-the-NE shearing.

Further extension was accommodated by brittle deformation with the same NNE tectonic transport at the eastern part of the Menderes Massif Core Complex. As a result, the Menderes metamorphic rocks experienced polyphase deformation giving rise to superimposed folding events and related tectonic foliations (Hetzel, 1995; Işık et al. (2004); Ring & Collins (2005). A synkinematic HP/LT metamorphic mineral association consisting of quartz ± feldspar ± micas ±c hlorit ± albite ± carbonates ± oxides ± garnet is associated with S_1. At the microscopic scale, S_1 relates to a continuous schistosity mainly defined by elongate feldspar and mica grains. This ductile deformational phase and associated folds are also defined in the province. The successive brittle deformational phase and folding event which is typified by meso-to map scale folds (see Figure 3.2 for an anticlinal example), produced pervasive tectonic foliation (S_2).

All the data show that the low-angle tectonic contact separating the metamorphic rocks in the footwall from the ophiolitic rocks and the Hacıbekir Group in the hangingwall is correlated with the Simav detachment fault (SDF). Işık *et al.* (2004)

and Ring & Collins (2005) reported that the ductile deformation along the Simav detachment fault (SDF) occurred at the beginning of the Miocene. Işık *et al.* (2004) also obtained mica age ($^{40}Ar/^{39}Ar$) of 22.86 ± 0.28 Ma from the mylonitic gneisses; in addition Ring & Collins (2005) obtained a SHRIMP-U/Pb–zircon age of 20.7±0.5 Ma that dates the intrusion of the Eğrigöz granite. I believe that both dates constrain the timing of ductile deformation.

3.4 Paleogeography and Basin Evolution

I summarize the stratigraphic and structural results and framework of the Uşak-Güre basin in relation to regional tectonic elements in a five-step evolutionary palaeogeographic model (Figure 3.2). Three phases of deformation have been obtained within the Uşak-Güre basin, and I will also refer to same notation by Ersoy et al. (2010) for content integrity such as D_2, D_3 and D_4 phases.

3.4.1 Early Miocene Deformation (D_2 Phase)

The fundamental tectonic control on the supra-detachment Uşak-Güre basin commenced with activation of the SDF pre-late Oligocene (Figure 3.7a). The D_2 deformation phase is characterised with low-angle normal faulting (SDF) in the Uşak-Güre basin, which marks the initiation of the extensional tectonics during the latest Oligocene. The Kürtköyü Formation (Hacıbekir Group) represents the first sediments to be deposited in this deformation phase and was mainly derived from the mélange rocks of İAZ with lesser contributions from the rocks of the Lycian Nappes. Ersoy *et al.* (2010) reported that in the Selendi basin the ophiolitic and cherty limestone bodies occurred as local olistoliths in the Kürtköyü Formation. However, the cherty limestone (most probably sourced of from the rocks of the nappes) could not be clearly observed in the Kürtköyü Formation in the Uşak-Güre basin. The deposition of the Yeniköy formation, which is interfingered with Kürtköyü formation, started to be deposited in the Early Miocene (Figure 3.6b).
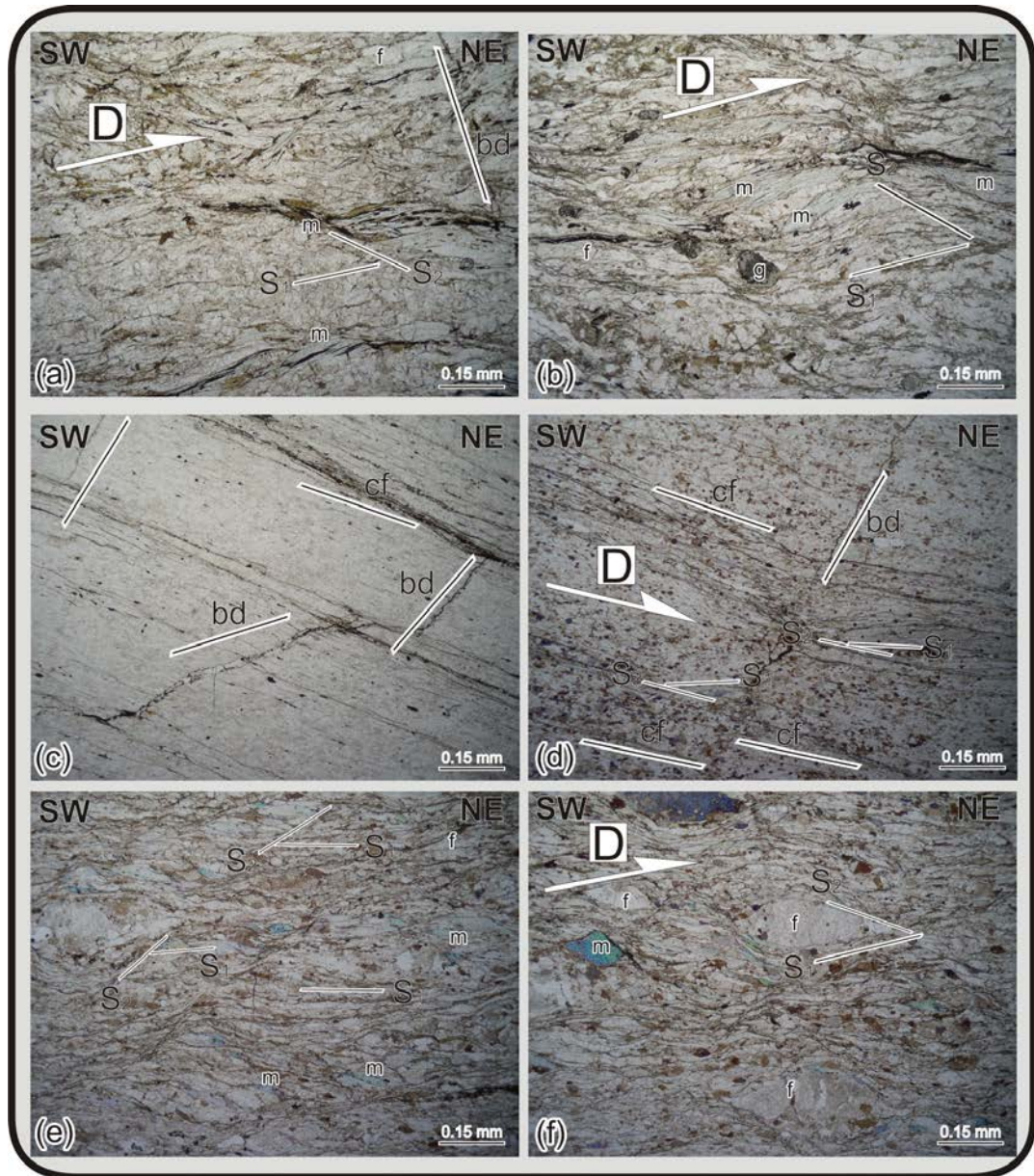
Figure 3.6 Photomicrographs of the metamorphic rocks of the Menderes Massif in the western basin margin of the Uşak-Güre basin. S (S$_1$ foliation) and C' (S$_2$ foliation) planes are defined by feldspar porphyroclasts and aligned micas respectively. (a) Meta-granite showing ductile structure which is overprinted by brittle structures. (b) The sample represents deeper level of the metagranite with respect to "Fig. 3.6 a". (c and d) Quartz-schist showing asymmetrical microstructures indicating that ductile structures are overprinted by brittle structures (//N). (e and f) Microstructure of ductile deformed meta-granite. Feldspar porphyroclasts have been flattened. Mica fish structures and flattened feldspars are showing deformation direction. Ductile structures are overprinted by brittle structures. Thin sections of the Menderes metamorphic rocks placed at the eastern margin of the Uşak-Güre basin. All photographs are parallel to the stretching lineation and normal to the foliation. m=mica, f=feldspar, g= granat, cf=cataclastic foliation, D=direction of the main shear zone.

In the neighbouring Selendi Basin, Işık et al. (2004) reported radiometric age data of the Eğrigöz granite, which is related with Simav detachment fault, (20.19 Ma); and Ersoy et al. (2008; 2010) documented that volcanic rocks from Selendi basin (from 20.45 Ma to 17.18 Ma) which are interfingered with the Yeniköy formation.

Purvis & Robertson (2004) suggest that the Selendi basin and the other NE–SW-trending basins were passively deposited throughout the Miocene in a depocenter that formed at the depressed part of the large-scale corrugations of a north-facing detachment fault. The accumulation of these deposits in the Uşak-Güre started using large scale corrugations of the supra-detachment Uşak-Güre basins (which are referred to as NE-SW trending basins) started in the early Miocene (Figure 3.7b) as mentioned by Purvis & Robertson (2004). However, I believe that the field evidence indicates that the Menderes Massif had not been exhumed around the Uşak-Güre basin area during this time because the Hacıbekir Group (Kürtköyü and Yeniköy Formations) does not contain any rock clasts of the Menderes Massif. The detachment fault surfaces can be traced throughout both basin margins (Figure 3.7b), so this causes contrasting transverse drainage catchments to evolve on newly created footwall and hanging wall uplands over the SDF (e.g. Gawthorpe & Leeder, 2000). The detachment fault surfaces can be observed through each of the basin margins (Figures 2.4 and 2.6).

However, despite the fact that the MMCC was exhumed to a shallow depth following an extensional system on a footwall over the SDF, there is no evidence for initiation of volcanism during Early Miocene deformation phase (D_2). Our mapping studies and kinematic evidence for early Miocene deformation phase in Uşak-Güre basin completely support the model proposed by Purvis & Robertson (2004, 2005), but the Early-Middle Miocene İnay Group was likely deposited after the cessation of activity on the SDF.

3.4.2 Early-Middle Miocene Deformation (D₃ Phase)

Deposition of the Ahmetler and Ulubey formations (İnay Group) commenced with first volcanic activation (17.29 Ma; age data from Karaoglu et al., 2010) of the Uşak-Güre basin. Moreover, I would like to highlight the age data from the İnay group for the adjacent Selendi basin for a comparison with Uşak-Güre basin. Purvis & Robertson (2005) obtained 15.61, 16.42 and 18.89 Ma ^{40}Ar/^{39}Ar biotite ages from the volcanic intercalations of the İnay group from the Selendi basin. The age data which are very important refer to the D_3 deformation phase, compared to the age data from Karaoglu et al. (2010) and Purvis & Robertson (2005) which are widely consistent.

The D_3 deformation phase refers to volcano-tectonic activities during accumulation of the İnay Group. The first volcanic activities interfinger with the Ahmetler Formation around the basin (Figure 3.7c). Three volcanic centres were built up during this phase. The western margin of the basin was responsible for deposition of the İnay Group. During the D_3 phase, the basin geometry was like a half-graben. The large mega-block and mega-breccia units of the Ahmetler Formation can be traced back to the Güre margin. Ersoy et al. (2010) reported similar alluvial fan deposits with boulder conglomerates deposited at the western side of the Selendi basin. The high angle normal fault surfaces are well exposed along the western margin of the Uşak-Güre basin. The syn-sedimentary faults generally strike N55°E to N60°W and dip 67° to 79° southward. The D_3 deformation phase was controlled by these fault activities from the late early Miocene to middle Miocene in the western margin of the basin. In addition, volcanic centres and dyke emplacements are conformable with NE–SW-trending extensional structures (Figure 3.7). Figures 2.6 and 2.7 indicate that the volcanic centre of the shoshonitic rocks of Zahman and Kıran lava flows lie on the high angle normal fault zone. The dyke intrusions have similar orientations and are conformable with the main early to middle Miocene extension trending.

3.4.3 Late Miocene Deformation (D₄ Phase)

The D_4 deformation phase refers to late Miocene tectonic activity widely responsible for deposition of the late Miocene Asartepe formations and uplift of the metamorphic rocks in the Uşak margin (Figure 3.7e). The late Miocene fault systems at the Uşak margin are classified as high-angle faults. The D_4 phase has caused the minor uplift of the Güre margin with respect to the Uşak basin margin. The tectonic activity most probably led to exhumation of the buried rocks of the Hacıbekir Group and some prominent detachment fault surfaces over both margins of the basin (Figure 3.7e). The data indicate that the D_4 phase occured predominately along the long axis of the basin, which extends in a NE–SW-direction. The D_4 phase deformation is characterised by higher rake angles at the northern part of the basin compared to the southern part. Hence, I suggest that the basin experienced southwest dipping asymmetric major scale uplift during the D_4 deformation phase.

3.5 Discussion

Many authors have noted that Menderes Massif is a core complex that occurs on the footwall of the SDF zone that is now mostly covered by Cenozoic sediments (Bozkurt & Park, 1994; Hetzel et al., 1995; Koçyiğit et al., 1999; Gessner et al., 2001; Işık & Tekeli, 2001; Lips et al., 2001; Bozkurt & Sözbilir, 2004; Seyitoğlu et al., 2004; Catlos & Çemen, 2005; Ring & Collins 2005; Glodny & Hetzel, 2007; van Hinsbergen, 2010) (Figures 3.6 and 3.7). The deformation history of the Hacıbekir Group and exhumation of the core complex of the massif are associated with the Early-Miocene (18-20 Ma) in time deformation and asymmetric uplift of the massif which is basin margin in recent time.

The author have also observed ductile to brittle deformation structures in Menderes metamorphic rocks at both margins of the basin (Fig. 3.6), but there is insufficient rock fabric evidence in the metamorphic rocks near the Uşak-Güre basin.
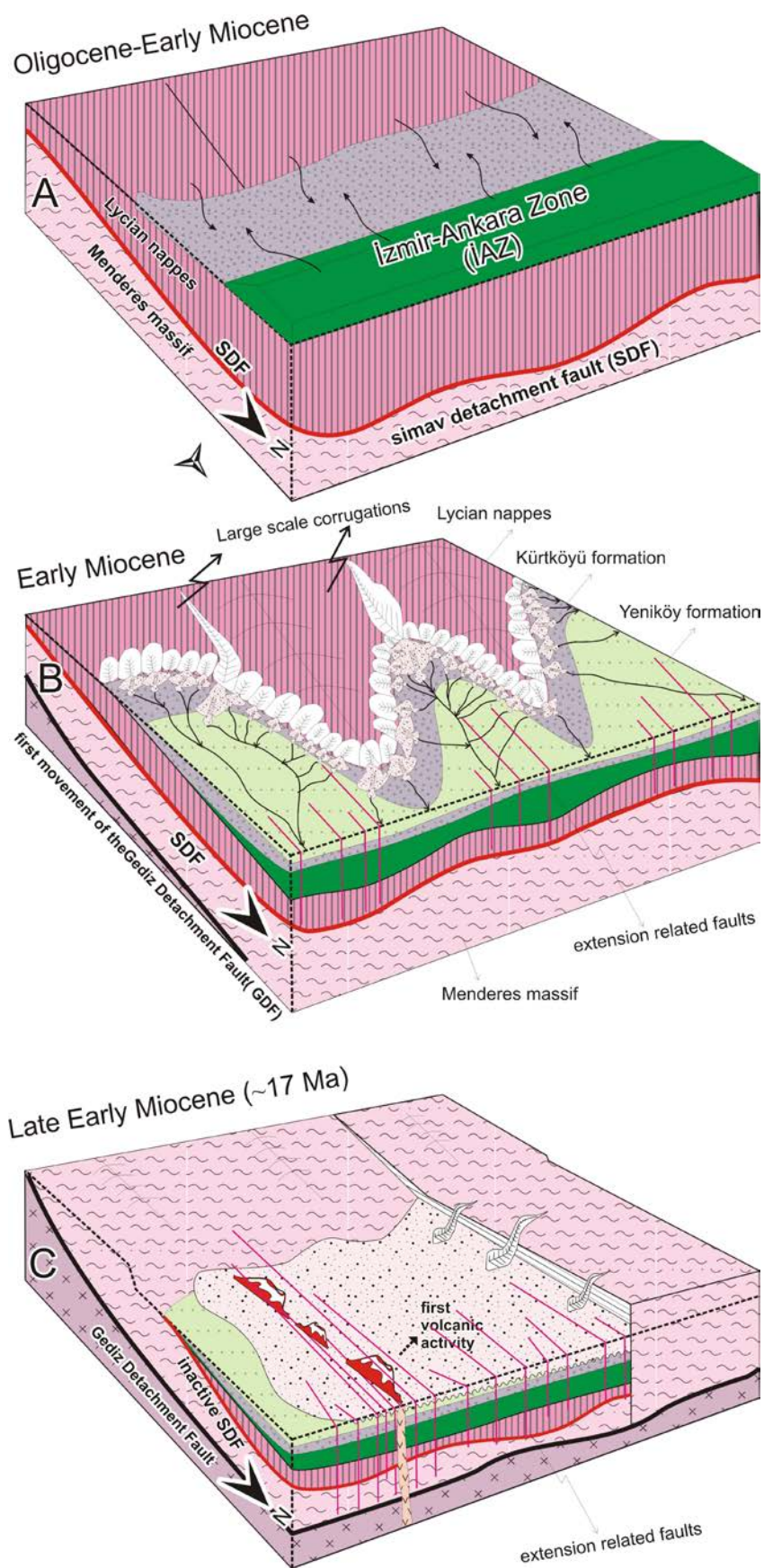
Figure 3.7 (Figure caption will present at the further pages, see overleaf).
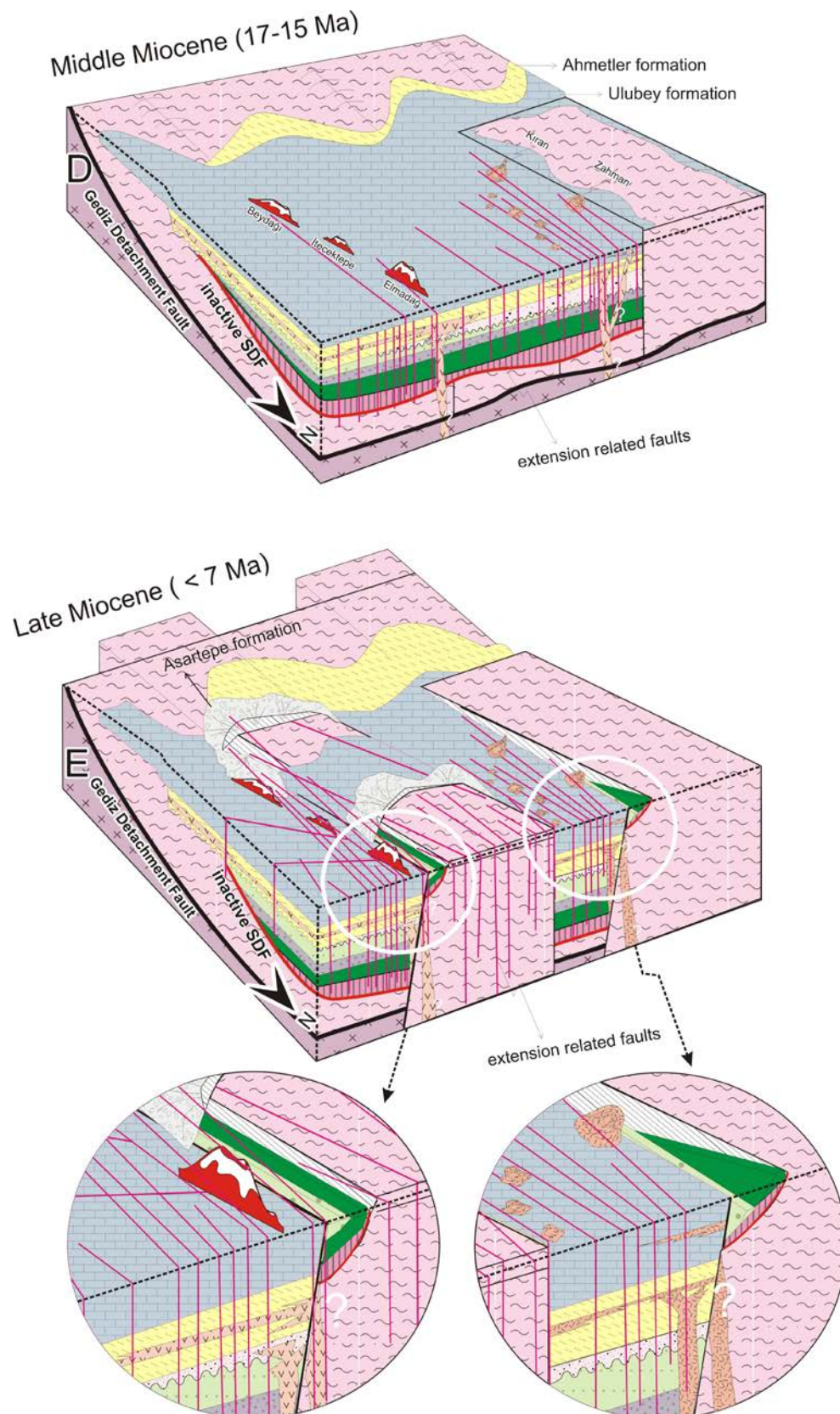
Figure 3.7 Cartoon showing the evolution of the NE–SW-trending Uşak-Güre basin from late Oligocene to late Miocene: (a) movement of the Lycian nappes with the İzmir–Ankara (see overleaf)

(figure caption continued) Zone as hangingwall of the SDF through late Oligocene-early Miocene interval (b) the early Miocene exhumation of the Menderes Massif, which commenced during the late Oligocene (e.g. Seyitoğlu et al. 2004), is represented by the Simav detachment fault (SDF) that juxtaposed the Menderes Massif. Rocks in the footwall of the SDF comprise the gneisses-dominated Lycian nappes of the Menderes Massif. A corrugated fault plane formed a supra-detachment basin in which early Miocene sedimentary units were deposited. The corrugations gave rise to formation of intrabasinal highs. (c) Orogenic collapse of Menderes during the late early-middle Miocene sedimentary units deposited in association with volcanism occurred along the Gediz detachment fault (GDF), located further south massif of the SDF. The footwall units of the GDF comprise the schist-dominated nappes. The hanging wall of the GDF comprises the footwall rocks of the SDF, including gneiss-dominated metamorphics of the Menderes Massif, the rocks of the İzmir–Ankara zone and the Hacıbekir group. Differential stretching in the hanging wall of the GDF formed a number of NE–SW-trending oblique-slip accommodation faults that controlled deposition of the middle Miocene İnay group in association with volcanic rocks. (d) This phase is including lack of tectonism and the deep depositional area filled by carbonates fluids of the Ulubey formation. (e) Last phase of the NW–SE extension was responsible for formation of the exhumation of the Uşak basin-margin causing to accumulation of the Asartepe formation via oblique and/or high-angle normal faults.

Purvis & Robertson (2004) reported that beneath the adjacent Selendi Basin, the metamorphic rocks exhibit pervasive deformation, marked by a gently dipping foliation and an extensional lineation consistently plunging to the NE or SW. Top-to-the- NNE shear-sense indicators (e.g. rotated feldspar porphyroblasts) are ubiquitous. The author interpreted these shear fabrics as the result of ductile to brittle extension related to unroofing of the Menderes Massif.

The Uşak-Güre area presents an asymmetrical basin shape with a NE-trending axis (overview in Figure 3.2), contains two distinct basins which developed in different geological periods. These consist of the Uşak basin, located on the east and the Güre basin placed on the west side of the study area. In geological-section, the Güre basin has a symmetric open synform over a 17-km scale. In contrast, the Uşak basin is fault-bounded along its western side, whereas at its eastern margins the Asartepe Formation lies unconformably on the basement rocks.

After the main extension, determination of the final dome geometry of the MMCC was initiated by the early Miocene northeast-directed shortening, and resulted in a

high degree of folding of the basement and deposition of the early Miocene sediments. These structural elements were further accentuated by Serravalien-to-Pliocene high-angle faulting. Three distinct extensional tectonic phases and associated fault sets of high-angle normal faults with NE–SW-trending faulted the previous northeast trending low-angle normal faults, and determined the configuration of the western boundaries of the Menderes Massif and related volcanic centres. Finally, the NE–SW-trending tectonic elements resulted in the final shape of the Uşak-Güre basins (see Figures 2.4, 2.5, 2.6, 2.7 and 3.7). The deformational features, stratigraphic, sedimentologic and structural evidence of the low- angle detachment fault in the Uşak-Güre basin can be correlated with the SDF. Early Miocene basin fill deposits (Hacıbekir Group) of the basin are separated from footwall basement rocks of Menderes Massif by the SDF. The Hacıbekir Group was deposited in large-scale corrugations on the SDF and tectonically emplaced onto metamorphic rocks of the MMCC along the SDF.

Şengör (1987) proposed that NE–SW-trending basins are 'Paleotectonic Tibet-type cross-grabens' developed during N–S post-Palaeocene compression and filled by a lower middle Miocene volcano-sedimentary succession. Later, this was terminated by Neotectonic Aegean-type cross-grabens. Differential stretching in the hanging wall of the GDF may have resulted in formation of the NE–SW-trending oblique-slip faults (accommodation faults) that cut both the footwall and hanging wall units of the SDF. These accommodation faults would only cut the hangingwall units of the GDF (Figure 3.7d). This is important for explain why the middle Miocene NE–SW trending oblique-slip faults (accommodation faults) that cut both the footwall and hanging wall units of the SDF (e.g. Selendi Basin, Ersoy et al. 2010). During the late Miocene, the exhumation history of Uşak margin is well-constrained along high-angle faults (Figure 3.7e).

This study demonstrates that Uşak-Güre basin was affected by different deformational phases resulting in different basin fills: (1) early Mioecene supradetachment basin fill, (2) middle Miocene Aegan type cross basin fill and (3) late Miocene half-graben basin fill along Uşak basin margin.

3.5.1 A Discussion About a Probable Uşak-Muğla Transtensional Transfer Zone

van Hinsbergen et al. (2010) proposed that the two-stage successive exhumation of the Menderes massif is constrained by two observations: (1) the NMM is bounded in the north by the Simav detachment that separates the Menderes Massif from the blueschist facies Afyon zone and the unnmetamorphosed ophiolitic mélange of the Izmir-Ankara suture; and (2) the NMM is bounded in the east and west by discrete lineaments (which may be transform faults) from the Afyon zone and the unnmetamorphosed Bornova flysch.

The İBTZ is bounded by the western-border of the Neogene NE–SW-trending basins, and has been described by Sözbilir et al. (2003), Erkul et al. (2005) and Uzel & Sozbilir (2008). While, Ring et al. (1999) suggested that the zone was also active during the Miocene as a sinistral wrench corridor, Erkul (2010) also presented evidence for NE–SW-trending crustal-scale strike-slip deformation further to the northeast of this zone around the Alaçamdağ granitoid. Recently, Ersoy et al. (2011) concluded that the eastern margin of the Gördes basin, which also remarks the western margin of the MMCC, is characterized by NE–SW-trending oblique- to strike slip faults that controlled the deposition of the early Miocene sedimentation. The eastern side of the NMM may be bounded by a sustained driven fault zone, as proposed by Çemen et al. (2006). In this respect, it appears that the first-stage exhumation of the massif was controlled by (1) top to the N-NE SDF in the north, and (2) NE–SW-trending transfer faults along its eastern and western margins during the early Miocene.

Our observations show that the late Miocene Asartepe Formation, which is controlled by a series of NE–SW-trending strike-slip and oblique-slip normal faults extends southwards towards Buldan (Figure 3.8). I am unable to determine whether the fault zone is terminated by Plio-Quaternary Alaşehir graben (Gediz graben) related faults or extends further around the south-east edge of the Menderes Massif.
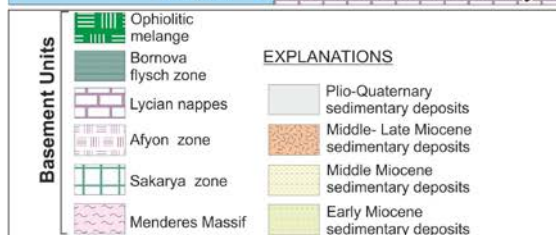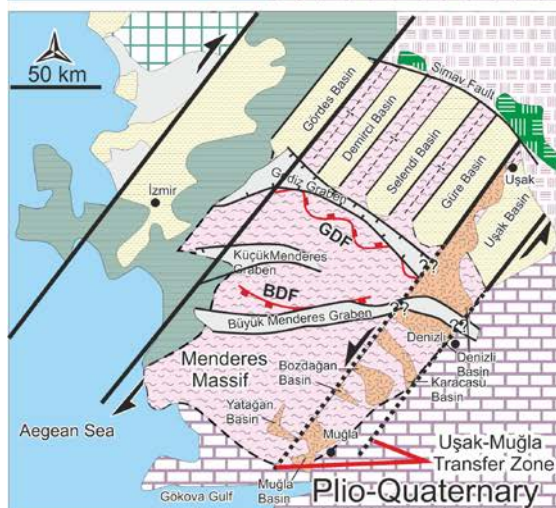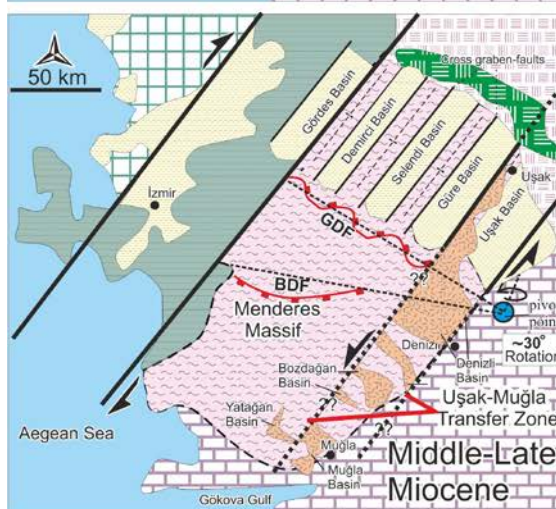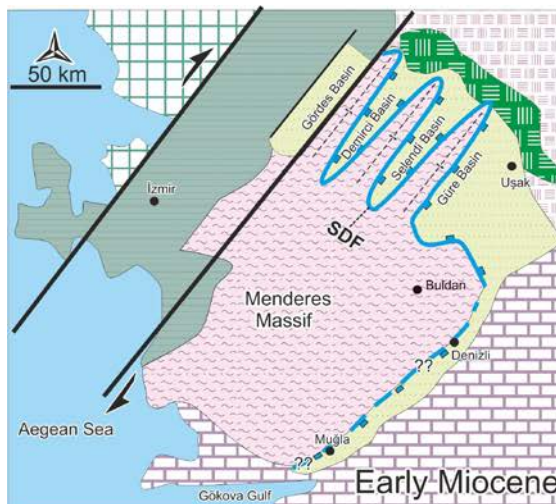
Figure 3.8 A schematic scenario of illustrating the Uşak-Muğla Transtensional Transfer Zone (UMTZ). (a) Early Miocene represents the relationships between Simav Detachment Fault and NE–SW-trending basins. SDF also refers to Kale-Datça main breakaway fault for eastern margin of the MMCC proposed by Seyitoğlu et al. (2004). (b) The UMTZ accommodated the differential stretching caused by crustal-scale extension in collaboration with different Tectonic elements during Middle-Late Miocene. Vertical axis rotation (~ 30° rotation difference from 16 Ma to 5 Ma) and pivot point taken from van Hinsbergen (2010). (c) The UMTZ was terminated by the Simav Fault since Plio-Quaternary. (Regional Map and Simplified Faults compiled from Şengör et al., 1985; Bokurt, 2004; Bozkurt & Sözbilir, 2004; Sözbilir et al., 2010; Alçiçek, 2010; Ersoy et al., 2011).

In addition, this fault zone could not be followed further to the north side of the Uşak basin margin as it is cut by the active dextral strike- slip Simav fault (Figure 3.8c). van Hinsbergen et al. (2010) have recently reported a large set of new paleomagnetic data from western Turkey. These authors concluded that the exhumation of the central Menderes Massif was associated with a vertical axis rotation around a pivot point near Denizli, difference between the northern and southern massifs of ~25° –30° between 16 and 5 Ma (van Hinsbergen, 2010). According to van Hinsbergen (2010) the westward motion of Anatolia (the reconstructed 85 km) along North Anatolian Fault zone lead to a counterclockwise rotation of ~2° since 11 Ma.

Alçiçek (2010) recently defined most of the Neogene extensional grabens and half-grabens of eastern margin of the MMCC in southwestern Anatolia which are NW–SE-trending Early to middle Late Miocene Denizli and Yatağan; late Miocene to Pliocene Karacasu and Bozdoğan basins. Kaymakçı (2006) and ten Veen et al. (2009) have documented several NE–SW-trending strike- to oblique-slip faults cutting the basin fill units especially since middle Miocene.

Thus the study infers that the fault zone commenced its activity in the Oligocene-Miocene, however the NE-SW direction of extension was presumably accommodated by a transfer zone. A deep crustal extensional phase linked to back-arc extension in the eastern part of the Aegean back arc during the Oligocene-Miocene later acted as a transtensional transfer fault zone since the middle Miocene. I also suggested that the probable transfer fault zone (Uşak-Muğla Transfer Zone)

was the most active during the late Miocene with regard to deposition of late Miocene Asartepe Formation, which may be controlled by NE-SW trending strike-slip and oblique slip normal faults (Figure 3.8). Note that each of Neogene basins located in the south-eastern part of the Menderes Massif, extend our proposed Uşak-Muğla Transtensional Transfer Zone in Figure 3.8. Although, I have insufficient evidence with regard to the tectonic controls on these aforementioned basins extending probable NE-SW trending a transtensional zone, I would like to propose a transtensional transfer zone. I think that the UMTZ accommodated the differential stretching caused by crustal-scale extension in collaboration with "back arc extension of the Aegean Arc", "westward extrusion of the Anatolian plate" and "anti-clockwise rotation of the Menderes Massif" during Middle-Late Miocene.

CHAPTER FOUR

GROWTH, DESTRUCTION AND RESURGENCE OF THREE VOLCANIC CENTERS IN THE UŞAK-GÜRE BASIN, WESTERN TURKEY: SUBAQUEOUS-SUBAERIAL VOLCANISM IN A LACUSTRINE SETTING

With exception of a few volcano-stratigraphy studies (Aydar et al., 1998; Karacık & Yılmaz, 1998; Genç et al. 2001; Ulusoy et al., 2004; Karacık, 2006), previous works on the western Anatolian volcanics was mainly geochemically oriented (e.g., Yılmaz, 1989; Güleç, 1991; Aldanmaz et al., 2000; Innocenti et al., 2005; Ersoy et al., 2008; Karaoğlu et al., 2010), and focused on overall evaluation of post collision-related volcanism at a regional scale, rather than a systematic study of individual volcanic centers and their petrology (see Figure 4.1 for location of the volcanic centers).

In this chapter, I aim to present the evolution of the physical volcanologic processes of three volcanic centers (Elmadağ, İtecektepe and Beydağı) within Uşak-Güre basin. In order to re-construct the eruptive phases, we will present detailed volcanologic maps (1/25.000 in scale), several columnar sections, simplified geologic sections, and numerous well-selected photographs from the field. Many visual materials used through the manuscript show the complex geological problems in order to obtain an accurate volcanologic approach of these volcanic centers. I will also propose the main volcanic depressions in western Anatolia for the better understanding mechanism of the destruction processes of these volcanic centers.

4.1 Volcanologic Evolution of the Volcanic Centers

According to their eruptive history, two main volcanic forms can basically be classified as monogenetic and polygenetic. Monogenetic volcanic forms (or monogenetic volcanoes) are defined as volcanoes formed during single events (eruptions) of short-lived (days to years) volcanic activity, without subsequent eruptions (Lexa et al., 2010). Such a definition fits especially volcanic forms found in basaltic monogenetic volcanic fields and satellite edifices distributed on flanks of

larger composite volcanoes. However, the same definition is applicable also to volcanic forms made of intermediate and felsic lavas – monogenetic volcanic cones of explosive, stratovolcano or effusive type, solitary extrusive domes and solitary intrusions (Lexa et al., 2010).
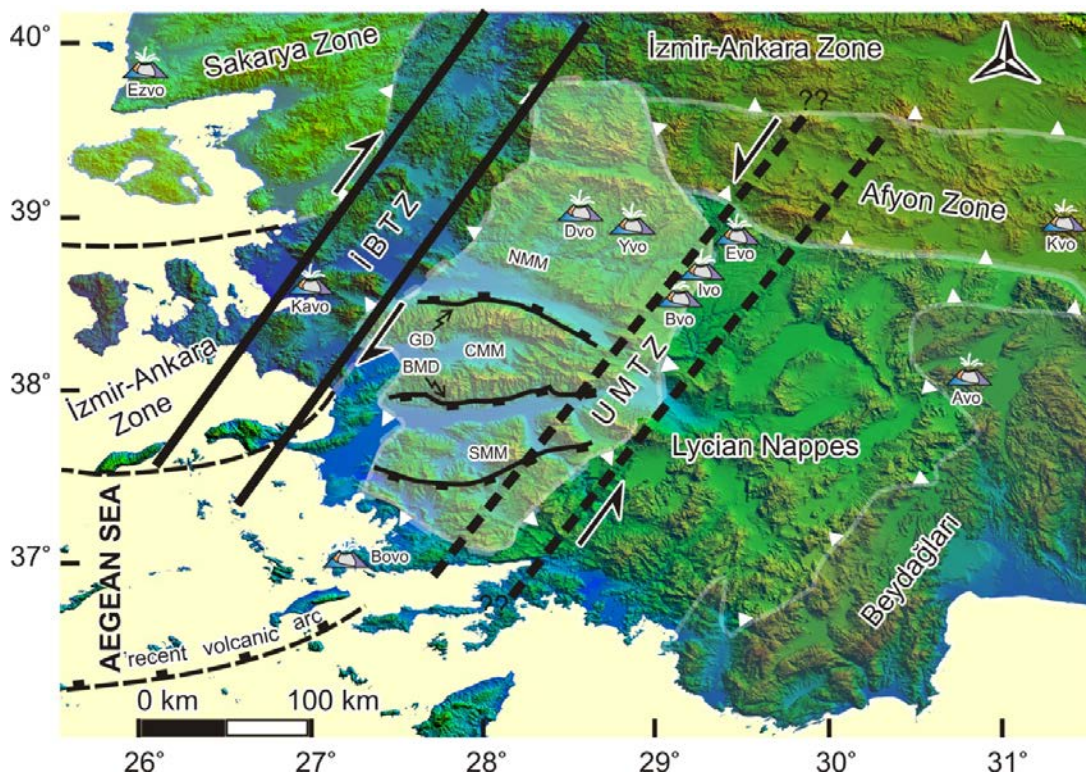
Figure 4.1 Simplified map showing some prominent Neogene volcanic centers, over topography of western Türkiye derived from 90 m SRTM digital elevation model. Key volcanic centers are labelled: Kvo: Köroğlu; Avo: Afyon; Bovo: Bodrum; Kavo: Karşıyaka; Ezvo: Ezine; Dvo: Demirci; Yvo: Yağcıdağ; Evo: Elmadağ; Ivo: İtecektepe; Bvo: Beydağı stratovolcanoes. İzmir-Balıkesir Transfer Zone (IBTZ) is modified from Uzel & Sözbilir (2008); Uşak-Muğla Transfer Zone (UMTZ) is modified from Karaoğlu & Helvacı (in press).

Polygenetic volcanic forms (polygenetic volcanoes) have experienced more than one, usually many, eruptive events during their history. They usually associate with a long lasting and complex eruption history of a volcanic system. Such volcanic systems can either consist of a single volcanic edifice, or nested volcanic edifices (Lexa et al., 2010). Polygenetic volcanoes have a sufficiently large and persistent magma supply rate that an ascending magma batch will preferentially follow the still-hot pathway of the preceding batch. Conversely, a volcano is monogenetic if the

magma supply is so limited or episodic that any pathways have cooled down and are no longer favoured routes for the next magma batch (Walker, 2000).

In the light of such volcanologic background while Elmadağ, İtecektepe and Beydağı volcanic centers in Uşak basin could be classified as typical polygenetic volcanic forms (or stratovolcanoes), the volcanic edifices within Güre basin (Payamtepe volcanic rocks, for both volcanic unit see geological section on Figure 4.2). These volcanic centers are located in the Uşak basin, and exhibit a within-basin type volcanism during 17.29 Ma–12.15 Ma interval. The volcanic centers show a NE–SW-trending along the tectonic alignments which was active since early Mioecene. I have more information from the Elmadağ volcano compared to İtecektepe and Beydağı, because it has clear outcrops and geological interrelations.

4.2 Elmadağ Volcanic Center

The Elmadağ is 12 km away and NE part of the Uşak city and covers approximately 210 km^2 (Figure 4.2). The Elmadağ reflects a typical stratovolcano which lies within a > 700 m –thick succession of predominantly subaerial calc-alkaline lavas. However, some parts interfinger with the lacustrine sediments and seem to suffered from moderate-level intrusions. The volcano exhibits a deeply eroded and semi-circular area ca. 5 km in diameter (Figures 4.3 and 4.4) which will be discussed with all evidence at further. It is overlain by very thick-lacustrine limestone (Ulubey formation), and the volcanic rocks have been affected by locally pervasive hydrothermal alteration.

Karaoğlu et al. (2010) presents several distinct ^{40}Ar/^{39}Ar radiometric age data. 16.44 Ma corresponds to the andesitic lavas; 16.28 Ma is from rhyolitic intrusion; 17.29 Ma is from a dacitic dome. Andesitic lavas and rhyolitic intrusions overlie the pyroclastic flow deposits (16.48 Ma) at the southern sector of the volcano (Figure 4.3).
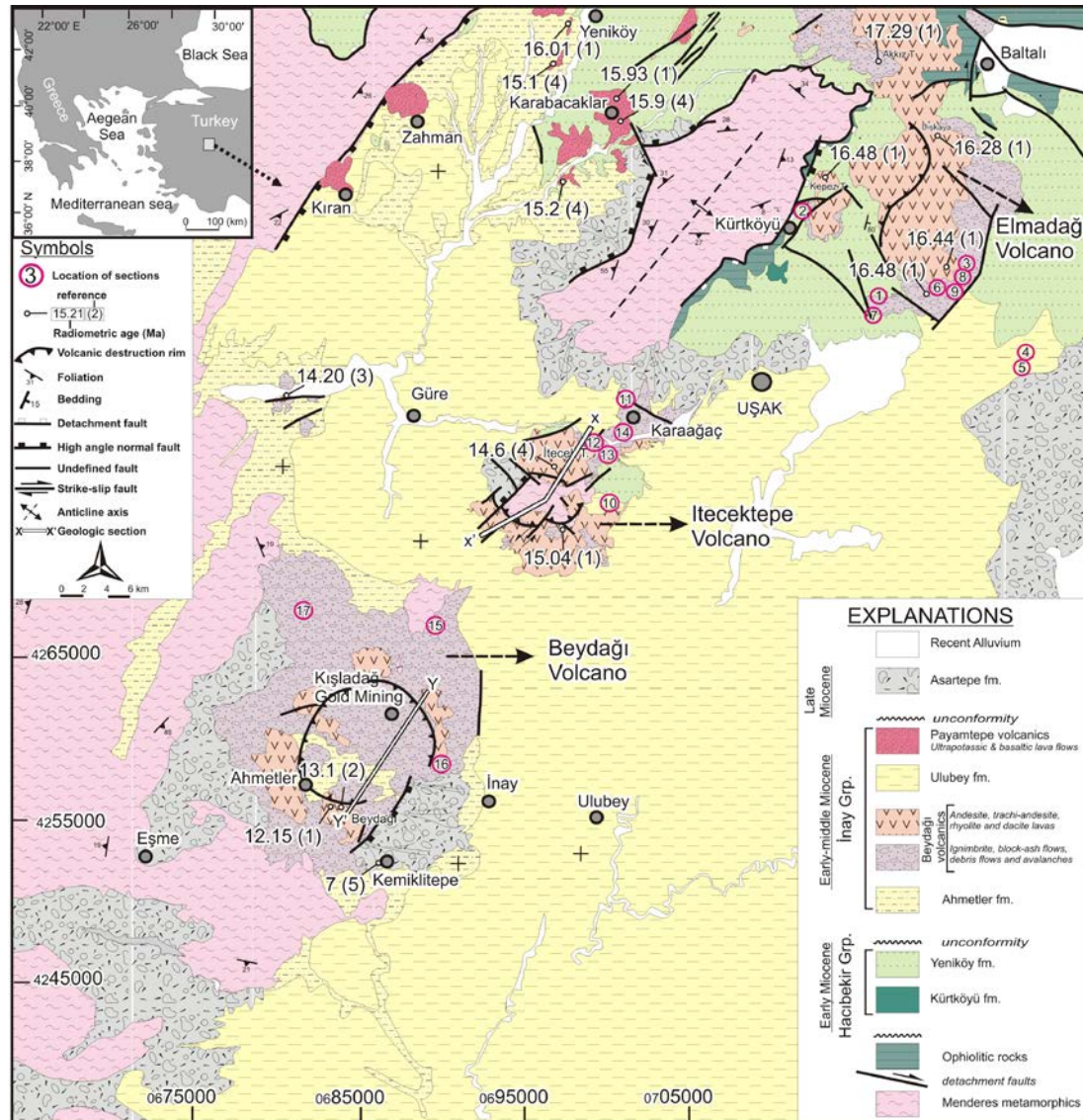
Figure 4.2 Geological map of the Uşak-Güre basin and related stratovolcanoes (modified from Karaoğlu et al. 2010).

4.2.1 Effusive Volcanism

4.2.1.1. Lava Flows

4.2.1.1.1. Cone Building Andesites. Many successive andesitic lava flows have been recognized during construction of the stratovolcano. Andesitic lava flows are distinguished in successions each other by their compositional differences and colours, exposing pink, pinkie-red, greenish-grey and brownish-black.
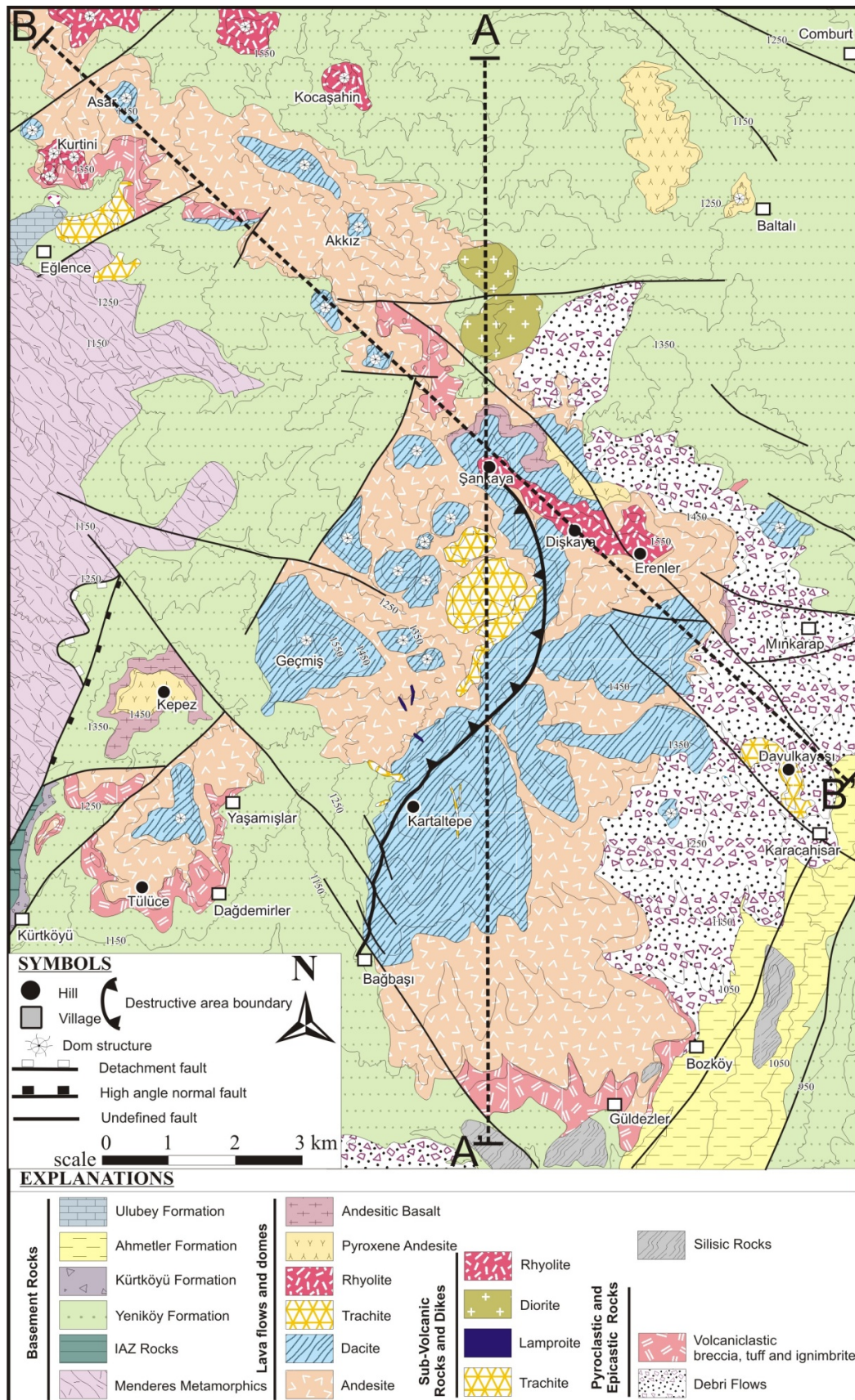
Figure 4.3 Geology map of the Elmadağ stratovolcano.

Bottom levels of these andesitic sequences, include plagioclase-rich andesitic lava flows, rarely displaying increasing amount of sanidine. The top level of lavas shows SE-dip direction, has abundant volcanic glass within matrix and less crystal contents that cause to more fluid behaviour. Good exposures of flow textures could be seen to the easternmost part of the volcano, near Güldezler village.

The lava edge is ca. 2 m, while the apparent margin of the lava flows is enveloped in crudely stratified, oxidized coarse breccias representing probably the proximal source of the debris flow deposits or debris avalanche deposits (e.g. Oregon Cascades; Fierstein et al., 2011). Hydrothermal alterations are very pervasive in the whole andesite sequence, visible along the flow bending and cracks, which resulted from extensive tectonic deformation.

Chlorite and epidote replace feldspar and biotite crystals along these weaknesses. The most significant hydrothermal alterations are exposed inside of eroded structure, especially contact zone between the very steep cliffs of the main cone. Cross-cutting valleys follow violent hydrothermal alterations throughout the several fault zones. Andesitic lava flows around Yaşamışlar village are dominating the western part of the volcano; several lava sequences north of Eğlence village (for location see Figure 4.3), display massive texture.

4.2.1.1.2. Draping Dacite Flows. Dacite flows are overlying the andesitic lavas at the top of the volcano through the boarder of the eroded structure. Dacites at the peak of the Elmadağ volcano consist mainly of hackle fractures (strongly fragmented). These fractures show brown-blackish alterations and cross-cut deformations. They are caused by NE–SW-trending strike-slip and oblique fault zone that has a minor extending inside of the volcano. Along the moderate eastern flanks of the Elmadağ edifice has exposed a thick younger series of deposits made up of debris flows, debris avalanches and pyroclastic flows and associated volcaniclastic units, which is up to 100 m thickness. These pyroclastic and volcaniclastic sequences were mainly fed by andesitic source, however rarely from dacitic lavas. The circumferential distribution of dacite clasts presents glassy-rich texture, however I could obtain any

holohyalin texture through the outcrops of the rhyolitic lava. These glassy rocks were probably from the source of the volcaniclastic rocks, are surfaced upper levels of the volcanic edifice. In addition, the lower level of the dacites overlies the aforementioned volcaniclastic sequences. These glassy lava flows should be represent the last stage of the dacitic lavas.

4.2.1.1.3. Rhyolite Flows. These lavas are white to gray, porphyritic, including 20-30 % quartz phenocrysts, generally 0.1–0.3 mm in size and less abundant amphibole phenocryst (%15), up to 0.2 mm in length, that are semi-aligned in the matrix. Blocky lava flows occur more commonly. They form narrow (< 1 km), lengthy flows through NW–SE-oriented fault zone on the main-cone's northeast part of the flank (Figure 4.4).

4.2.1.1.4. Pyroxene Andesite Lava Flows. These flows have mainly recognized in two distinct areas such as near at Baltalı and Kepez (Figure 4.4). These flows overlay of the andesitic basalts at the Kepez area, while descending as an individual body near Baltalı village. Petrographically the andesites are identical, containing < %15 pyroxene phenocrysts within the matrix with quartz and feldspar in a dominated microcrystalline to somewhat vitreous groundmass.
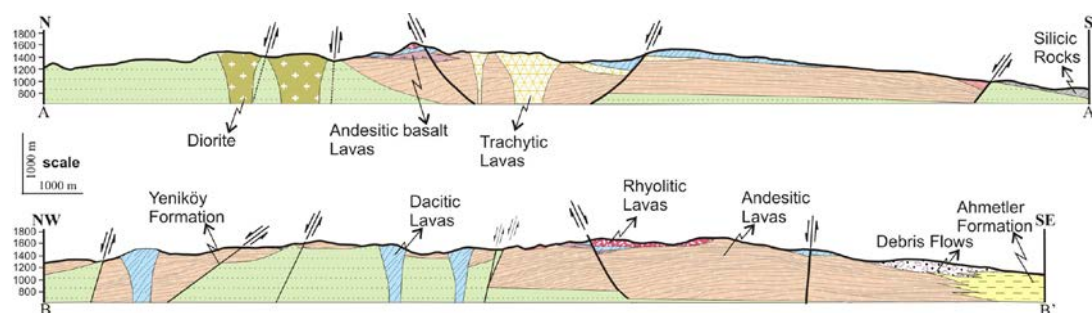
Figure 4.4 Geological cross-sections across the Elmadağ stratovolcano (see Figure 4.3 for localities and legends).

4.2.1.1.5. Andesitic-Basalt Lava Flows. They form a suite of flows that are characterised by the pyroxene-rich (> 15 % in vol.) with abundant plagioclase (40-45 % in vol.) within the volcanic matrix. They are observed at two different places, not only basement of the Kepez peak but also vicinity of Şenkaya area, which is summit

of the Elmadağ volcano. Both of lava flows were truncated by NE–SW trending faults. These form ca. 30 cm in thickness bedding at the base of the edifice, which is located at the vicinity of top levels (Figure 4.4).

4.2.1.1.6. Monogenetic Lava Flows. More than eight remnants of monogenetic volcanoes of lamproite composition are placed over within Güre basin (Figure 4.2). The volcanism shows mostly potassic in character which occurred during Middle-Miocene time (ca. 15–16 Ma; Karaoğlu et al., 2010). The lamproite rocks effusive in character dominate up to 16 km^2 in the area. These lava flows show intercalating with sedimentary rocks of the İnay Group and some of them display vertical columnar jointing. Some of the related fault planes are cutting the columnar jointing. This evidence suggests that effusive lavas were experienced intense deformation throughout a NE–SW-oriented fault zone (Figure 4.2).

Two individual shoshonotic lava flows are extended throughout NW–SW-trending "Zahman fault," up to 25 km in length, westernmost of the Güre basin (Figure 4.2). Both look like a small scale shield volcano. The first one is located in Zahman village, bearing many gase pipes, black in colour. Phenocrysts are less abundant within the volcanic matrix (< % 10 in vol.). Very clear and obvious peperite textures are observed between these effusive lavas and host carbonatic rocks (Ulubey formation).

4.2.1.2. Intrusive Rocks

4.2.1.2.1 Lamproite Rocks. The western margin of the flank of the eroded structure was also intruded by three distinct lamproitic dikes (Figure 4.5d). Two of them intrude the andesitic rocks, while the other one cuts the andesitic and dacitic lava sequences throughout the steep cliff of the flank. Intrusive bodies present a curved, semi-circular array and exhibit similar petrographic features and structures inside of the eroded area (Figure 4.5f). Dikes are extended throughout NW–SE-orientation. Lamproite dikes were also observed in the Güre basin, somewhat intruded in the lacustrine sediments of the İnay Group (Figure 4.5d).

4.2.1.2.2 Rhyolite Rocks. The wide-scale rhyolite intrusions dominate the top of the Elmadağ volcano and extend to the NW-SE- direction, as the last stage for the intrusive rocks (Figures 4.5c and i). In addition, some of rhyolitic intrusions are observed near Akkız peak, northernmost of the Elmadağ volcano. This intrusion may be coeval with the rhyolitic lava flows through the uppermost level of the volcano such as locations of Şenkaya, Dişkaya and Erenler (Figure 4.4) and cross-cutting relations show a repetition in itself. Rhyolitic intrusions occur as necks and plugs that pass upward and laterally into dacitic and andesitic lavas and lava domes. They are commonly offset by faults mostly occurring at the basement of the rhyolitic intrusions. The orientation of the biggest body of them is uniform with the NW–SE- trending of strike-slip and oblique faults. The rocks are white to gray in colour having abundant glassy matrix.

4.2.1.2.3 Trachyte Rocks. The widest outcrops of trachytic intrusives were exposed around the Davulkayası area (Figure 4.4). These rocks are observed ca. 2 km^2 in the area and show a NW–SE orientation (Figure 4.6b). Indeed, the entire region experienced NW–SE- trending faulting. The intrusive body is over 100 m high from its basement, showing from black to brown colour, and vertical columnar jointing, which exceed 5 m in diameter. Rocks are mainly composed of sanidine mega-crystals, up to 1 cm large (Figure 4.5h), small-scale trachytic dikes intrude into andesite and dacite lavas at the eastern part of the Kartaltepe. Two different dikes were recognized in this locality, located at the eastern part of eroded structure of the Elmadağ volcano, and are followed through 1 km in length, while two individual bodies are situated westernmost of Kartaltepe, inside of the eroded area (Figure 4.5g). Concentration of these intrusive bodies may indicate a dike swarm structure fed from the same compositional magma chamber.

4.2.1.2.4 Micro-Diorite Intrusive (Plutonic Facies). The only exposed small body is the crudely layered mafic intrusion with an estimated area extent of < 2 km^2 and showing 200 m in height from the basement. Physical contact is obvious and intruded pervasively into altered andesitic lava flows (Figure 4.5e). Intense hydrothermal alterations are present throughout the contact zone.

Figure 4.5 Field photographs from well-exposed and characteristic intrusions around the Elmadağ volcano: (a) ultrapotassic dikes cutting the lacustrine sediments of the İnay group, in the Güre basin; (b) intrusions at the Davulkayası showing hexagonal trachytic columns; (c) rhyolitic dike at the vicinity of Akkız peak, at the northern Elmadağ volcano; (d) lamproitic dike from the inside of the Elmadağ eroded structure; (e) micro-diorite intrusion at the northern part of the Elmadağ volcano; (f)

lamproitic-semi circular dike from the inside of the Elmadağ volcano; (g) trachytic dike outcropping westernmost of the Kartaltepe; (h) sanidine megacrystals up to 1 cm in size within a trachytic intrusion, western part of the Kartaltepe; (i) rhyolitic intrusive rocks are located at the top of the Elmadağ.

The body exhibits black colour and blocky jointing. This intrusive body was truncated by an E–W directed fault.

4.2.1.3 Lava Domes

More than nineteen dacitic, two trachytic and four rhyolitic/rhyodacitic individual volcanic domes have been recognized around the Elmadağ in the Uşak basin. More than ten of them have been observed related to the wide-spread lamproitic lava flows in the Güre basin. They mostly expose as circular and rarely semi-circular shape. Most of them also prevail in the eroded area of the Elmadağ volcano; in addition, this area was affected by the faint multi-stage hydrothermal alteration in space and time. The oldest age was obtained from the Akkız peak as 17.29 Ma, which is a dacitic dome at the northern part of the volcano (Karaoğlu et al., 2010).

Both of dacite and rhyolite dome structures at the north of the Eğlence village presents in a semi-circular trend (Figure 4.3). Well-preserved "hydraulic breccias" are present at the top of the rhyolite dome which consists of very thick silicic lavas, near Kurtini (Figure 4.6).

Figure 4.6 (a) Dome structures at the vicinity of Eğlence sector, northern part of the volcano; (b) uppermost silicic rocks with "hydraulic breccias.

These lavas are glassy and bearing more abundant quartz crystals. Hydraulic breccias are extending in vertical direction. Presents of these breccias indicate that the geothermal system and aquifer were active; brecciation was resulted by the steam water, as a mixture of hydrothermal and meteoric water (Cas & Wright, 1987).

4.2.2 Subaqueous-Subaerial explosive volcanism

4.2.2.1 Pyroclastic Flow Deposits (P_1–P_8)

Eight major explosive eruption phases (P_1-P_8) were identified around Elmadağ volcano, based on their lateral distributions, thickness variations and stratigraphic relations: (i) four different ash-fall layers; (ii) three distinct debris-flows; (iii) and stratigraphic position with respect to lake sediments and silica layer (Figures 4.7 and 4.8)

4.2.2.2.1 Eruption Phase (P_1). The first major explosive eruption on Elmadağ volcano generated an andesitic ignimbrite preserved widely in the southern part (Figure 4.10). P_1 (Phase 1) overlies the Early Miocene sedimentary rocks (Yeniköy Formation) by angular unconformity. The ignimbrite is about 15 m thick and forms a prominent cliff at the base of the volcano. This phase exhibits compositionally two different layers (L_1 and L_2). L_1 is characterised by large pumices, exceeds 40 cm in diameter and andesitic and dacitic lithic fragments up to 4 cm (Figure 4.9e). The lowest phase (P_1) is buff to gray and unlithified whereas the upper phase (P_2) shows compositionally colour changing, which is pink, brown and gray sillar. L_2 is mainly composed of pumice reach 10 cm in diameter, and less abundant lithics. The first phase is truncated by a debris flow deposit D_1 (Figure 4.9d).

4.2.2.2.2 Eruption Phase (P_2). Following eruption phase (P_2) exposes different textural and thickness properties basis on distance of the source. Phase 2 including 25 cm in diameter pumices, up to 1 cm lithic fragments and fewer crystals in proximal, while 5 cm pumices and ash matrix increases in volume in the medial zone extend southern part of the volcano (Figures 4.10c and d). Thickness changes

dramatically from proximal part, is 2.5 m thick with medial part, up to 6 m thick. The medial section (Sec. 7 in Figure 4.7) is crudely bedded while the proximal presents massive outcrop.
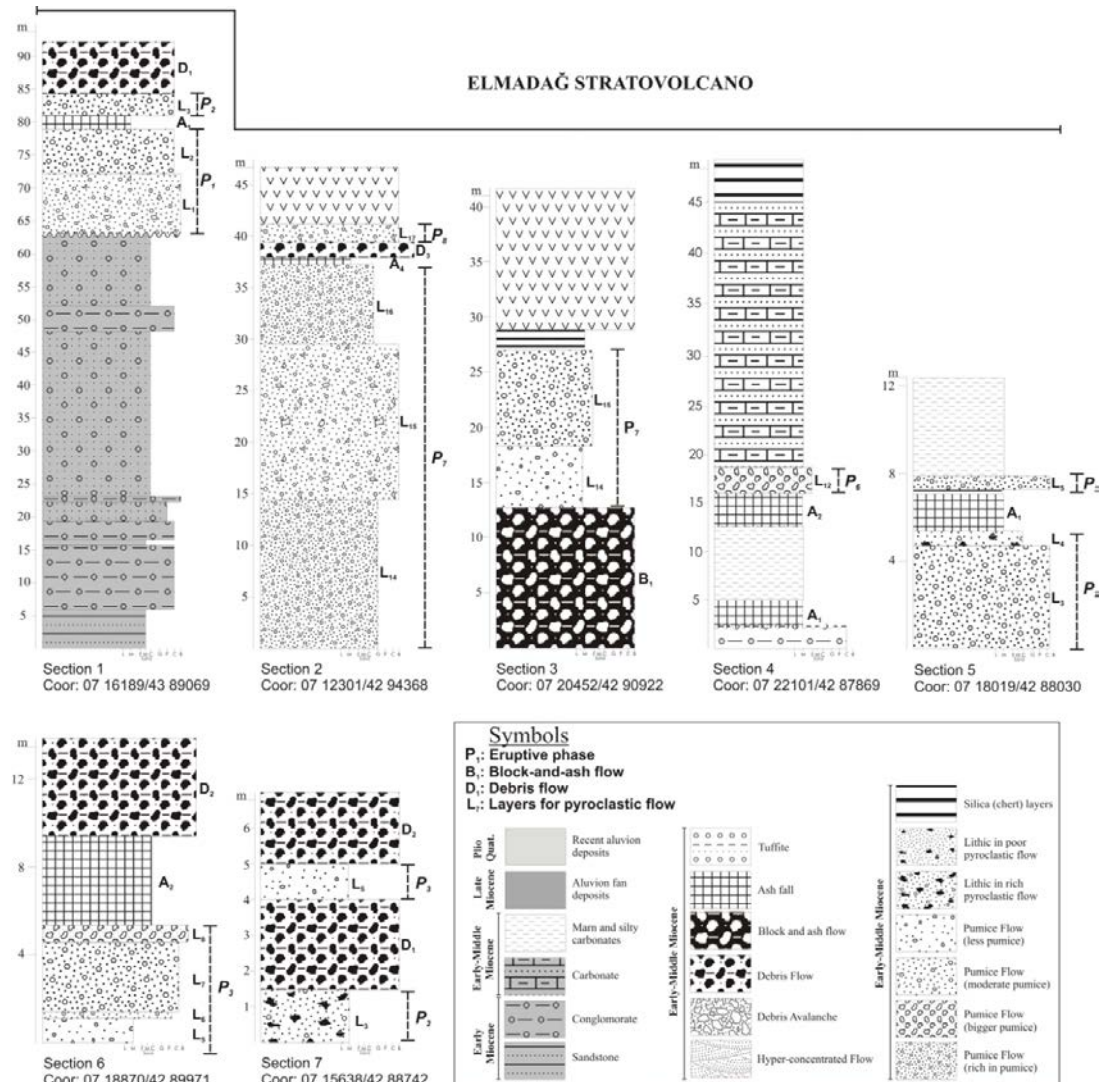
Figure 4.7 Typical columnar sections of the Elmadağ stratovolcano (Sections 1–7; see Figure 4.2 for locations).

4.2.2.2.3 Eruption Phase (P₃). P₃ is one of the most wide spread eruption phases between all of them, preserved extensively in south-eastern Elmadağ (Figures 4.3 and 4.12). This phase directly overlies Phase 2, separated only by a single ash layer (A_1) at Sec. 5 in Figure 7 dominated by brownish ignimbrite (Figure 4.10a). Pumices are up to 3 cm in diameter and show normal grading, and terminated by lacustrine sediments at the same section.
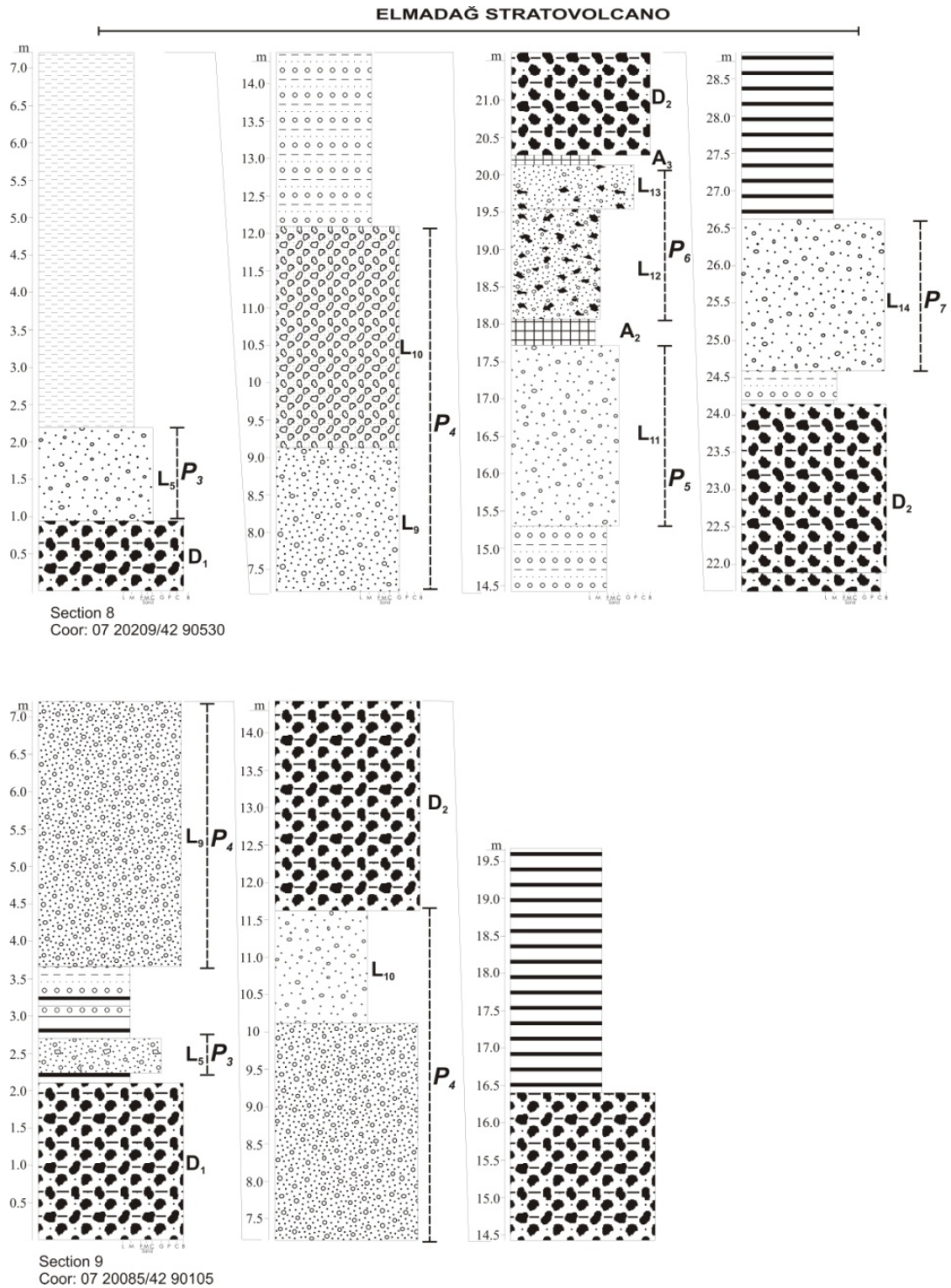
Figure 4.8 Typical columnar sections of the Elmadağ stratovolcano (Sections 8–9 see Figure 2 for locations and Figure 4.7 for legend).

The products of Phase 3 which have several distinct layers (L_5-L_8), present the thickermost, 5.5 m near Güldezler Village at Sec 6 (Figure 4.7). L_5 comprises of 3 cm pumices within a dominated ash matrix.
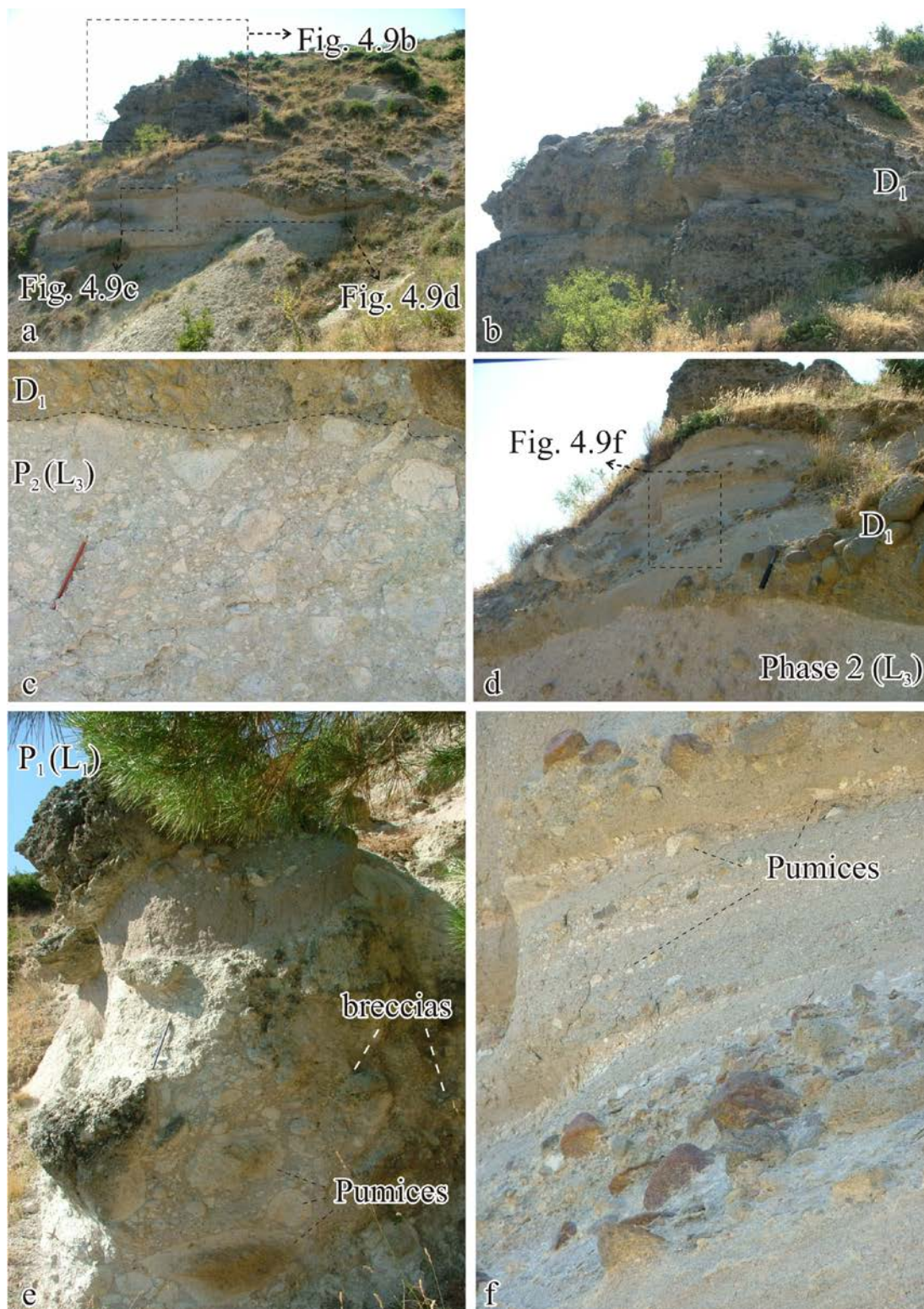
Figure 4.9 Field photographs showing characteristic outcrops from the early succession of pyroclastic flow and debris flow deposits. All photographs are taken from the Sec. 1 showing location on map in Figure 2. (a) General view and relationships between the D_1 and P_2, uppermost of this section; (b) D_1 in detail-view; (c) a clear contact zone between the D_1 and P_2; (d) P_2 is (see overleaf) (figure caption

continued) truncated by debris-flow and hyperconcentrated flow deposits; (e) typical texture of the P_1; (f) hyperconcentrated flow deposits.

There then followed a thin layer (L_6), including trachytic-and-andesitic lithic rich breccias, showing inverse grading. Following this, there was the accumulation of the pumice dominated (L_7) and pumice flow layer (L_8). This layer exposes large abundant pumices to exceed 30 cm in diameter and truncated by an ash fall deposit (A_2).

*4.2.2.2.4 Eruption Phase (P_4).*The next explosive phase commenced with emplacement of debris flow (D_1) and coeval lacustrine sediments, while culminated in the major debris flow (D_2). The basal levels of the P_4 are the most well-preserved outcrops for suabaerial-subaqueous transition at the eastern part of the volcano where they show a maximum thickness of ~ 8 m (Figures 4.8 and 4.11a, b). The sequences at sites 8 and 9 (Figure 4.8) begin with epiclastic levels (L_9), showing low-angle cross stratification and substrate erosion (volcaniclastic turbidite textures with re-worked pumice clasts (Figure 4.11a). The basal section indicates a subaqueous setting of the accumulation. The upper section reflects a subaerial setting basis on the texture of the deposit. This portion of the P_4 consists of, up to 2 cm in diameter pumice clasts and heterolithologic blocks and lithics (andesitic, latitic and rhyolitic in origin). The pumice size decreases whereas the lithic fragments are less abundant in the top part.

4.2.2.2.5 Eruption Phase (P_5). The Phase 5 observed in the area of Section 5 to the east of the volcano (Figure 4.6). The total thickness of the P_5 is 2.5 m, pumice to 8 cm long, no lithic fragments, white to light gray. The Phase 5 is distinctive in having a high proportion of pumice (60-70 %) through to top level, while bottom layer showing less abundant pumice (15-20 %) in locally. Pumice clasts present faint inverse or inverse-to-normal grading. This cycle is terminated by an ash fall deposit A_2 (Figure 4.11 c).
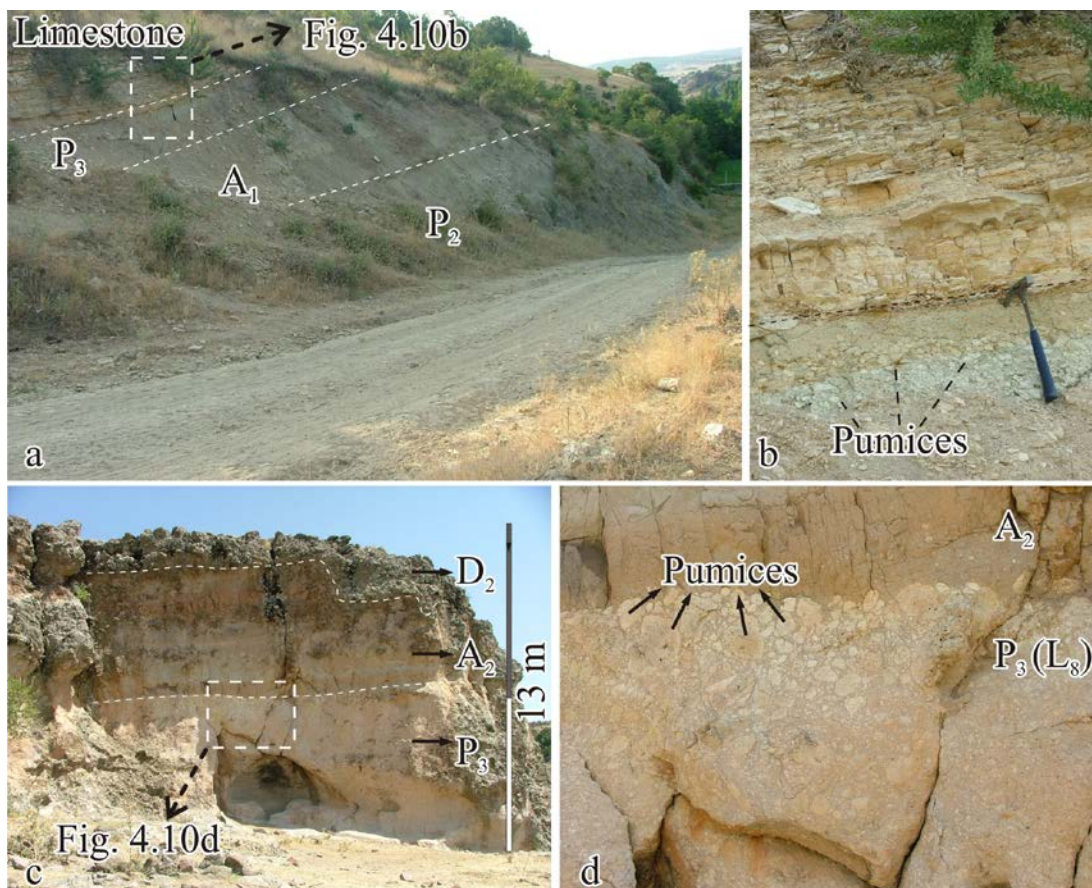
Figure 4.10 Field photographs showing outcrops of pyroclastic flow sheets and interactions of it's with lake sediments from southern part of the volcano. (a) Early-Middle Miocene limestone overlaying the volcanic successions; (b) close-view of transition from pumice in rich clay stone to limestone; (c) well-preserved relations between D_2 and P_3; (d) close-view of sharp contacts between P_3 dominated by pumice and related ash deposit (A_2) in a subaerial environment.

4.2.2.2.6 Eruption Phase (P_6). The P_6 crops out in the southern and south-eastern portion of the volcano. This phase was emplaced following to second Ash layer (A_2). Limestone from Ulubey formation overlies the P_6 in the south (Section 4). This cycle has abundant lithic fragments and less pumice contents.

Pumices reach 2 cm, lithics are 3 cm in large, gray, at the basement of the cycle L_{12}, while pumice is less than 1 cm and lithic fragments are up to 9 cm in size, brown, at the upper level- L_{13} (Figure 4.11d). Phase 6 contains heterolithologic lithics and rock fragments, which experienced different type and non-equally alterations. The eruption phase was ceased with an Ash layer (A_3).
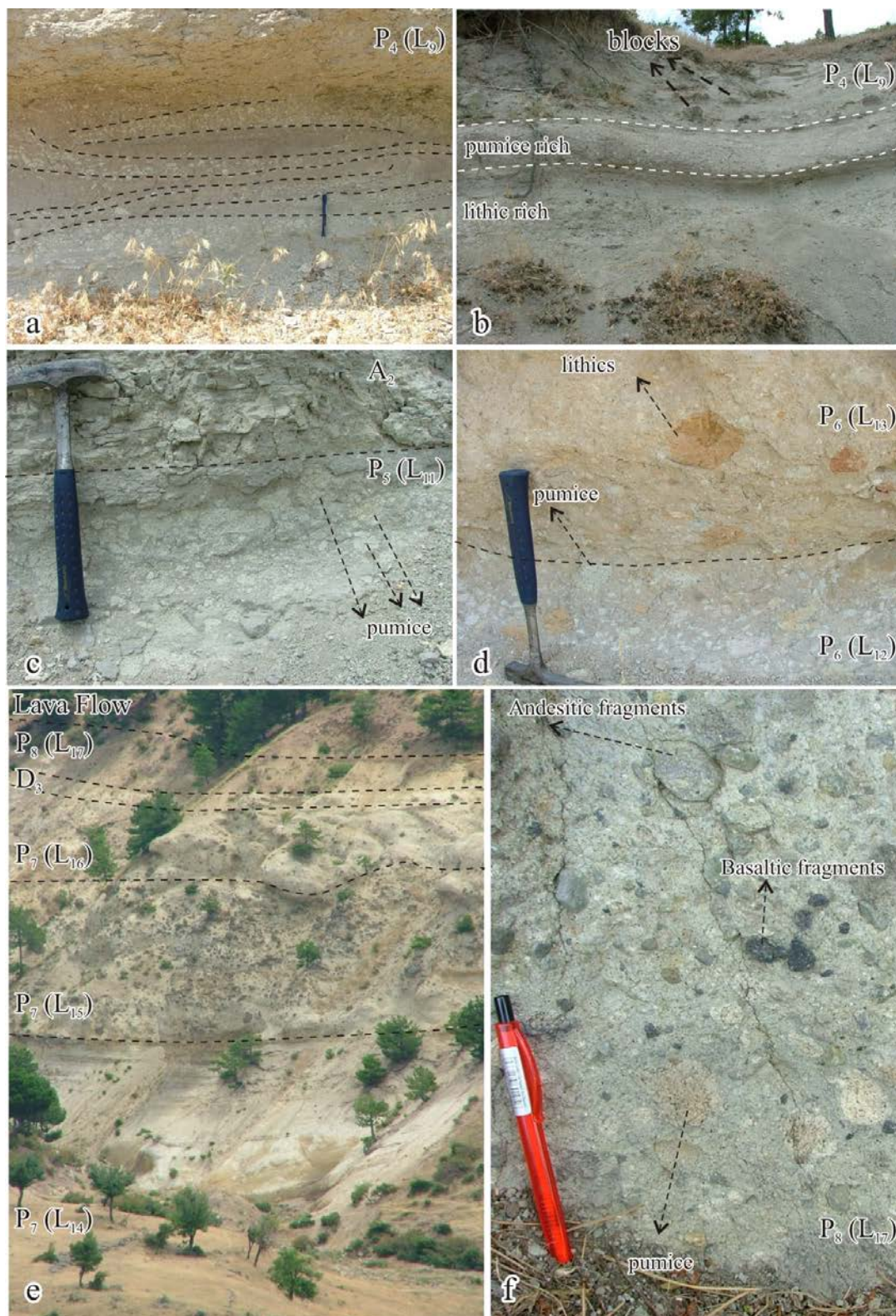
Figure 4.11 Field photographs of the last stages of the volcanic successions around the Elmadağ volcano. (a) Bottom level of the P_4, from Sec. 8 (see Figure 2 for locations); (b) P_4 containing different horizons such as pumice and lithic rich; (c) interrelations between P_5 and A_2; (see overleaf)

(figure caption continued) (d) different parts of the P_6 deposit; (e) full-view of the section 2, terminated by a lava flow; (f) close-view of the P_8, from west side of the Tüllüce Hill.

4.2.2.2.7 Eruption Phase (P_7). Phase 7 is the most widespread and thick pyroclastic flow deposit during the volcanic history of Elmadağ volcano. It is dominated on the western side of the volcano, but observed at a small scale in the Sections 3 and 8 (Figures 4.7 and 8). This phase can be seen in a deep valley, as consequence of an NE–SW-trending oblique fault near Tüllüce Hill (Figure 4.3). Thickness of the P_8 is up to 35 m, gray and white, poses distinct level's basis on compositional and textures. The bottom of the cycle initiated with L_{14} which has, up to 3cm in large pumice (40-50 %) and less abundant andesite-dominated lithics (5-10 %) in an ash matrix (Figure 4.11e). L_{14} exhibits pervasive stratification and faint normal grading in locally. The medial part of the phase 7 (L_{15}) is characterised by the high incidence of monolithologic volcanic blocks and lithic fragments, while pumice is less abundant. Andesitic blocks exceed 45 cm in diameter at the some part of the L_{15} (Figures 4.11e and f). The top-level exhibits same textural and compositionally in character with the L_{14} except that bearing further lava clasts. Phase 7 is concluded by the last ash falls A_4 (Figures 4.11e and f).

4.2.2.2.8 Eruption Phase (P_8). Following the accumulation of D_3, a pyroclastic flow deposited at the western part of the volcano at Sec. 5 was observed (Figure 4.7). The final phase 8 composed of pumice up to 4 cm in diameter and heterolithologic; sub angular–angular volcanic clasts which are compose of andesite, basalt and dacites. It exhibits gray to greenish in colour, ca. 2 m thickness and a massive structure.

4.2.2.2 Block-and-Ash Flow Deposits (B_1- B_2)

4.2.2.2.1 Block-and-Ash Flow Deposit (B_1). Compositionally two different block-and-ash flow deposits are observed within the northern side of the Uşak area. The first one is B_1 which is a light-gray massive monolithologic layer composed of subangular andesite blocks, locally clast-supported or set, rarely pumiceous in a coarse ash matrix, it's compaction is well (Figure 4.11a, Sec 3). Thickness of the B_1 increases away from the volcano from 0.9 to 14 m (Figures 4.7 and 4.8). The deposit

composed of in the lower part poorly sorted massive tuff breccias to lapilli tuff and in the upper part, normally graded and stratified lapilli to tuff. The B_1 comprise poorly vesicular lapilli and ash. Ash pyroclasts consist of angular to semi-angular crystal fragments (mostly amphibole and biotite). The diameter of blocks varies between 2–21 cm. This unit has a maximum extent of 3.1 km (elevation of 1.452 m).

4.2.2.2.2 Block-and-Ash Flow Deposit (B_2). B_2 refers to block and-ash-flow deposit around Kıran ultrapotassic lava rocks. The feeding system of the lava flows has been related with the NE-SW-trending oblique fault system (Figure 4.2). The deposits include several units over 8 m thick and each composed of poorly sorted mostly massive tuff breccias tuff to rarely lapilli tuff. The non- to poorly vesicular lamproitic blocks have cooling joints. The basal horizon (h_1) shows inversely graded part of the B_2 locally grooving and scarcely parallel-laminated part of the B_2. The basal part of the B_2 is coarse tuff, depleted in blocks and coarse lapilli, and grades upward into massive poorly sorted tuff breccias (e.g. Takayama volcano, SW Japan from Kano & Takarada, 2007).

The flow also consists of rarely juvenile glass shards at the upper part of the deposit. The B_2 is generally massive with monolithologic block and gravel-sized clasts, however, it shows a weak-bedded, and poorly-sorted, loose compaction. It has a coarse sandy matrix, sub-rounded and sometimes rounded large boulder, which exceeds 70 cm in diameter. Although the block-and-ash flow deposits do not generally show a systematic grading, the B_2 shows retreating to inverse grading (Figure 4.11b). This unit has a maximum extent of 1.1 km (elevation of 865 m).

4.2.2.3 Debris Flow Deposits (D_1-D_3)

4.2.2.3.1 Debris Flow Deposit (D_1). The occurrence of volcanic debris flows in this area is linked to the high concentration, poorly sorted, sediment-water mixtures during water-saturated lacustrine deposition of İnay Lake in a subaqueous environment.
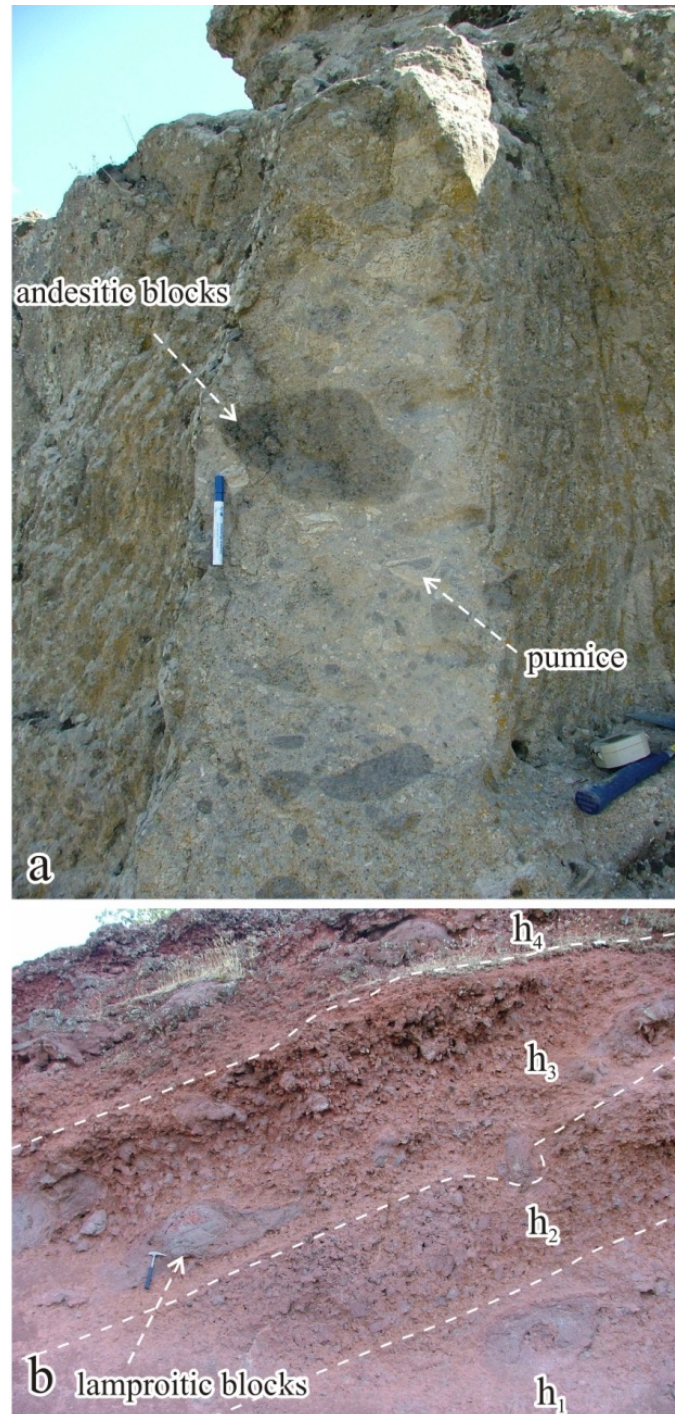
Figure 4.12 Field photographs of the block-and-ash flow deposits: (a) eastern side of Elmadağ volcano, Uşak basin; (b) front of Kıran lava flow from western margin of the Güre basin, h symbol shows different horizons.

D_1 is 2.5 m -6.5 m (Secs.7 and 2 in Figure 4.7) in thickness changing according to distance from the source. D_1 shows a transition from "hyperconcentrated-flow" to "debris flow" which characterized by water saturated mixture of debris and water having large sediment concentrations (Figure 4.7). The basal contact commences with hyperconcentrated-flow based on its feeding by different sources, shows very high detritic concentrations (up to 50 vol. % of sediment load) crudely laminated and pumiceous-crystal rich sandy matrix. The laminated sandstone may indicate traction of volcano-sedimentation associated with dilute flows. In addition, it exhibits many planar and gullied erosive basal contacts within the framework while displaying cross-cutting channels and lobes (Figure 4.9). The debris flow exhibits faint stratification, marked by concentrated bands of pumice clasts with local inverse or inverse-to-normal grading, is locally developed, and some beds have reworked and winnowed tops with concentrations of crystal–lithic sands (e.g. Taupa Volcanic Zone is from Manville, 2002). Manville (2002) documents that emplacement temperature of debris flows as < 100°C. It is very clear that the primary ignimbrite (Figure 4.9e) is terminated by the secondary debris- and hyperconcentrated-flow deposits (Figures 4.9c and d).

The deposits of D_1 are interpreted as the secondary phreatic explosions, coeval with ignimbrite emplacement in subaerial or subaqueous environments. I could not have clear observations of the contacts between hot ignimbrite and water-saturated interactions at this location (see Figure 4.9). Although the lake sediments buried the pyroclastic flow deposits (D_1) the explosions proceeded. Some turbiditic events which contain re-worked pumice fragments within silts, and sandy matrix may reflect phreatic explosions during sedimentation of lacustrine deposits (Figures 4.13a and b).

4.2.2.3.2 Debris Flow Deposit (D_2). Early remobilization processes on slopes and ridges were dominated by debris flows and high-sediment concentration streams, which eroded main cone or dome material and re-deposited it nearly on flat surfaces.
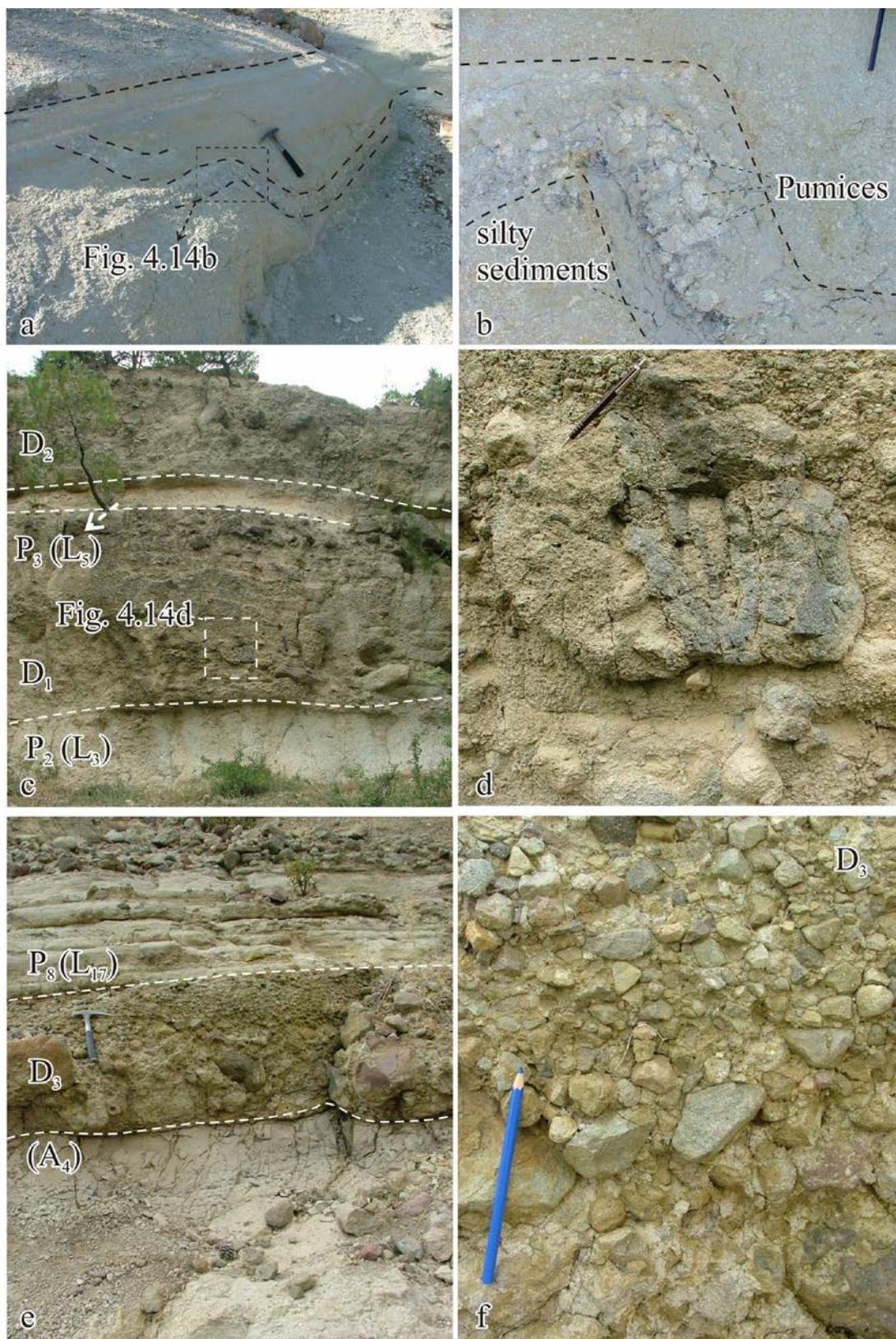
Figure 4.14 Field photographs of upper levels of pyroclastic, debris and hyperconcentrated flow deposits around the Elmadağ volcano. (a) Locally turbiditic flow within volcano-sedimantary successions, from Sec. 9 (see Figure 2 for the location); (b) close-view of turbiditic events at the same

locality; (c) relationships between different debris and pyroclastic flow deposits from Sec. 7; (d) bomb-like lava clast within D_1, from Sec. 7; (e) and (f) upper part of the pyroclastic and debris flows, from western part of the Tüllüce Hill (see Figure 2 for location).

D_2 is heterolithologic, its clasts and lava megaclasts (> 40 cm) are mainly andesitic with minor lamproitic and dacitic in composition. The main characteristic of these lava megaclasts are that they commonly display a subcircular shape. The thickness of D_2 exceeds 4 m at Sections of 6 and 8 which should be the proximal region; however, it is 2 m at Section 7, which reflects characteristics of the medial region (Figures 4.13c and d). In addition, two distinct debris flow deposits D_1 and D_2 are clearly observed at Section 7. Both of the D_1 and D_2 show juvenile lava clasts, which indicate a hot emplacement from nearby source (Figures 4.13c and d).

4.2.2.3.3 Debris Flow Deposit (D_3). D_3 has just only seen in the western part of the main volcano (Tüllüce Hill). D_3 is distinguished from the other debris flow deposits on some properties (Figures 4.11e and f). The first one is that the D_3, overlay directly on an ash fall deposit and the next is that D_3 is heterolithologic composed of the many different kinds of volcanic rocks. Dacite, andesite and latite are very common. D_3 includes massive to crudely oriented volcanic clasts. It is medium to thick bedded (~1.8 m), ungraded to locally crudely inverse graded. Internal truncation surface is rare. Clasts are subangular to subrounded, mostly pebble to cobble sized; boulder-size clasts are abundant with sandy and muddy matrix (Figures 4.11e and f).

4.3 İtecektepe Volcanic Center

The İtecektepe is located 11 km SW of the Uşak city. It has NE–SW-oriented, 6 x 7 km elliptical shape volcanic center (Figures 4.2 and 4.14). The volcano was constructed mainly by andesite with minor latite and trachytes, with explosive products rich in ignimbrites and pyroclastic flows. The volcano has experienced intense tectonic deformation and erosion. The tectonic deformation was insignificant on flanks around of the volcano and the basement rocks of Menderes Massif and İzmir-Ankara Zone in the center of the volcano. The İtecektepe volcano presents a

volcanic deformational structure which was tectonically uplifted by the basement rocks (Figure 4.14). Two radiometric age data were obtained from the İtecektepe volcano: the first one is 14.6 Ma (K–Ar age) from summit of the İtecektepe (Seyitoğlu, 1997), while the other one is 15.04 Ma (^{39}Ar–^{40}Ar) from an andesitic dike cutting the main cone lavas (Karaoğlu et al., 2010).
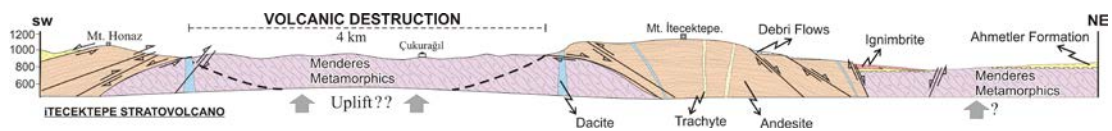
Figure 4.14 Geological cross-sections across the İtecektepe volcanic center (see Figure 2 for localities).

4.3.1 Effusive Volcanism

Andesitic volcanic sequences dominate on the İtecektepe volcanic center, while obtained the minor dacite, latite, rhyolite, trachite. The following the explosive phase has been identified: (1) lava flows and lava domes (2) dike structures and intrusive bodies piercing the effusive phase of the volcano (Figure 4.15). The lava sequences are uniform. The İtecektepe presents a destructive area in the middle of the volcanic center. The area has metamorphic basement rocks, which display some reverse faults. These faults have been also crudely observed crossing the volcanic rocks, especially at contact with the basement rocks. İtecektepe takes the name of the highest hill in the northern part of the volcano. This edifice is a big lava dome, up to 3.2 km in diameter. The data indicates that the dome emplacement occurred at 14.6 Ma (K-Ar age was taken from hill of İtecektepe, Seyitoğlu, 1997), following the dike emplacement (15.04 Ma, Ar-Ar dating is from Karaoğlu et al., 2010) which are cutting the basement lavas within the assumed vent area (Figure 4.14). The İtecektepe dome show flow-foliated lavas, has as much as 1249 m, thickness is ca. 250 m. Andesitic eruptions and several lava sequences, some of which flowed up to 1.5 km radially, drape the flanks of the dome structure. Intense hydrothermal alterations are observed at the southern part of the edifice, and destructive center of the volcano has subjected by magma - water interactions. The contact zones between the lava flows and lacustrine deposits are well preserved, including baking surface

and related textures. The existence of the lake sediments of İnay Group and associated contacts suggest that the volcanism was active following the deformation period of the İtecektepe volcano. Western and south-western part of the volcanic center was affected by excessive deformation since middle Miocene, especially during late Miocene. Several strike-slip and oblique faults cut the complex through NE-SW alignment.
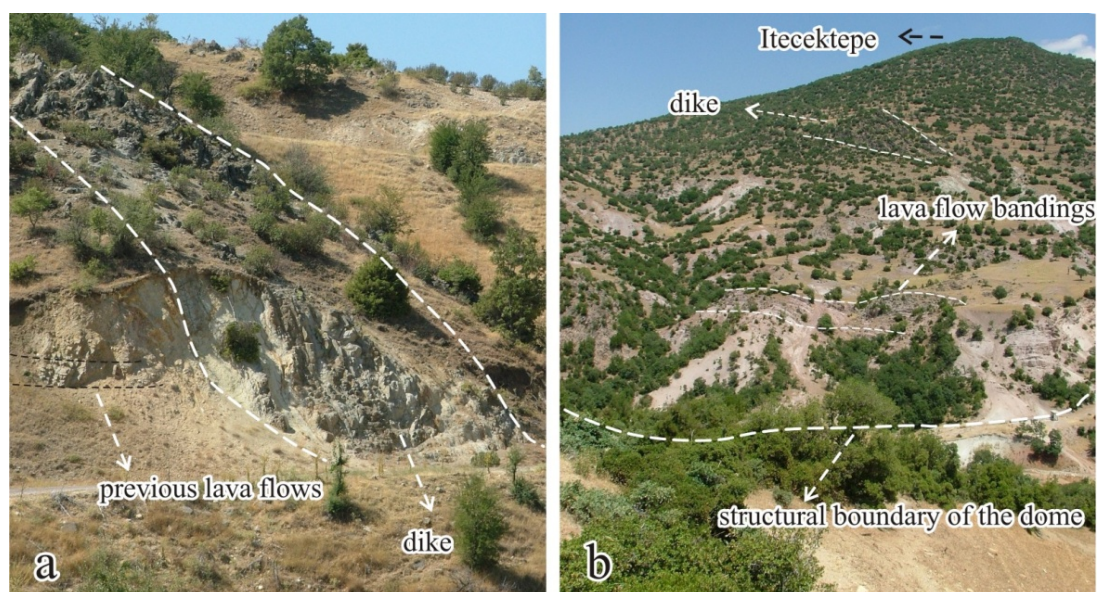
Figure 4.15 (a) Field photos of a dike propagation at the southern part of the İtecektepe volcano; (b) and İtecektepe dome structure and related dike, from northern part of the volcano.

4.3.2 Subaqueous-Subaerial Explosive Volcanism

Here, I present five distinct sections of representative sites of accumulation during the subaqueous-subaerial transition condition that was taken place in the vicinity of the İtecektepe volcano (Figure 4.16). Pyroclastic flow deposits (ignimbrites) present with huge voluminous products occur around the volcano. The İtecektepe volcano is different from the Elmadağ volcano, as distinguished by producing high-volume debris avalanche deposits with minor debris flow deposits. The first volcanic activity commenced with phreatoplinian eruptions (A_1). The most important evidence of these ash fall deposits which are bearing abundant accretionary lapilli and vesicular cohesive ash texture are observed northern part of the İtecektepe volcano. Spherical aggregates of fine ash that forms the 1.5 m thick level (Figure 4.17a). This level also

includes < 1mm heterolithologic accidental fragments. This level unconformably overlies the basement rocks of the Yeniköy formation. This locality indicates a very strong evidence of interaction between magma and water of a large lake (İnay Lake).
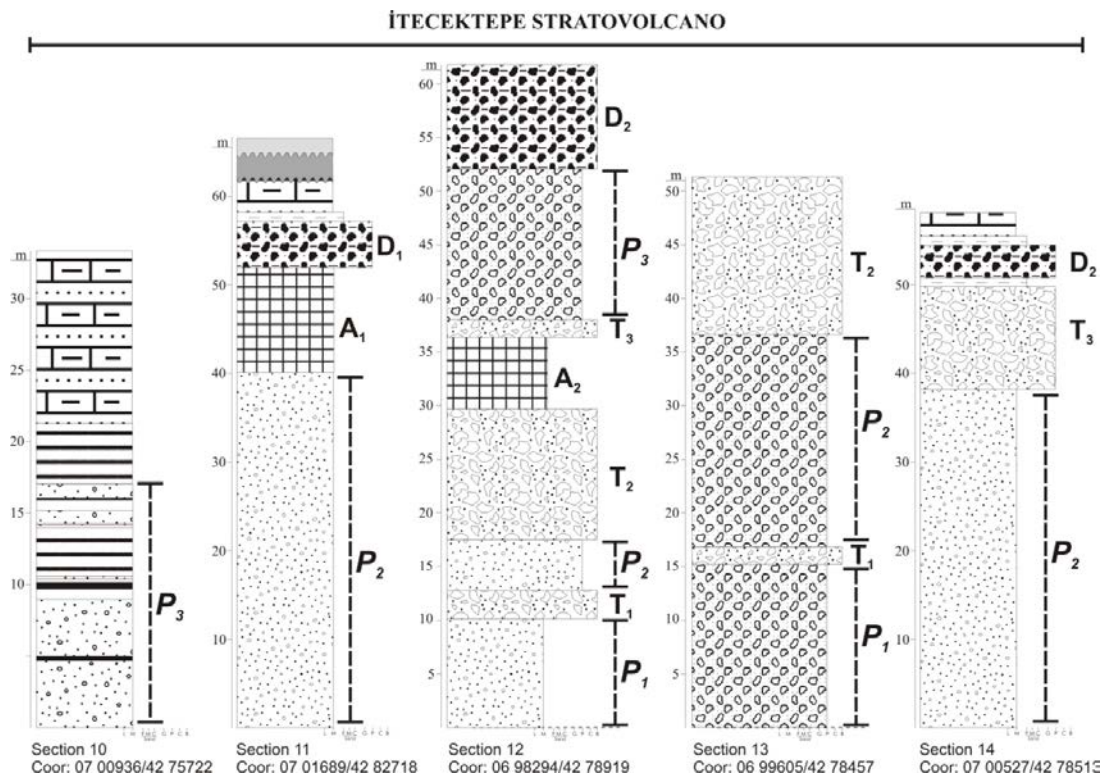
Figure 4.16 Typical columnar sections of the İtecektepe volcanic center (Sections 10–14; see Figure 2 for locations).

4.3.2.1 Pyroclastic Flow Deposits (P_1–P_3)

4.3.2.1.1 Eruption Phase (P_1). The first pyroclastic flow (P_1) is up to 15 m thick and comprises a distinctive layered pumice flow succession is overlain by an extensive massive phase (P_2). The bottom levels display a massive texture, while their stratification tending to increase upwards through the unit. The basal phase (P_1) comprises pale grey pumice up to 9 cm in diameter in a medium- to a coarse-ash matrix. The subrounded pumice clasts and lapilli are uniform in colour. Pumices are semi-vesicular and scarcely banded. Lithic fragments which are mostly dark grey dense andesits, up to 4 cm in diameter are rich abundant throughout the unit, and their concentrations are stable. The initial phase includes lesser abundant accidental fragments from the basement rocks (Figure 4.18a).
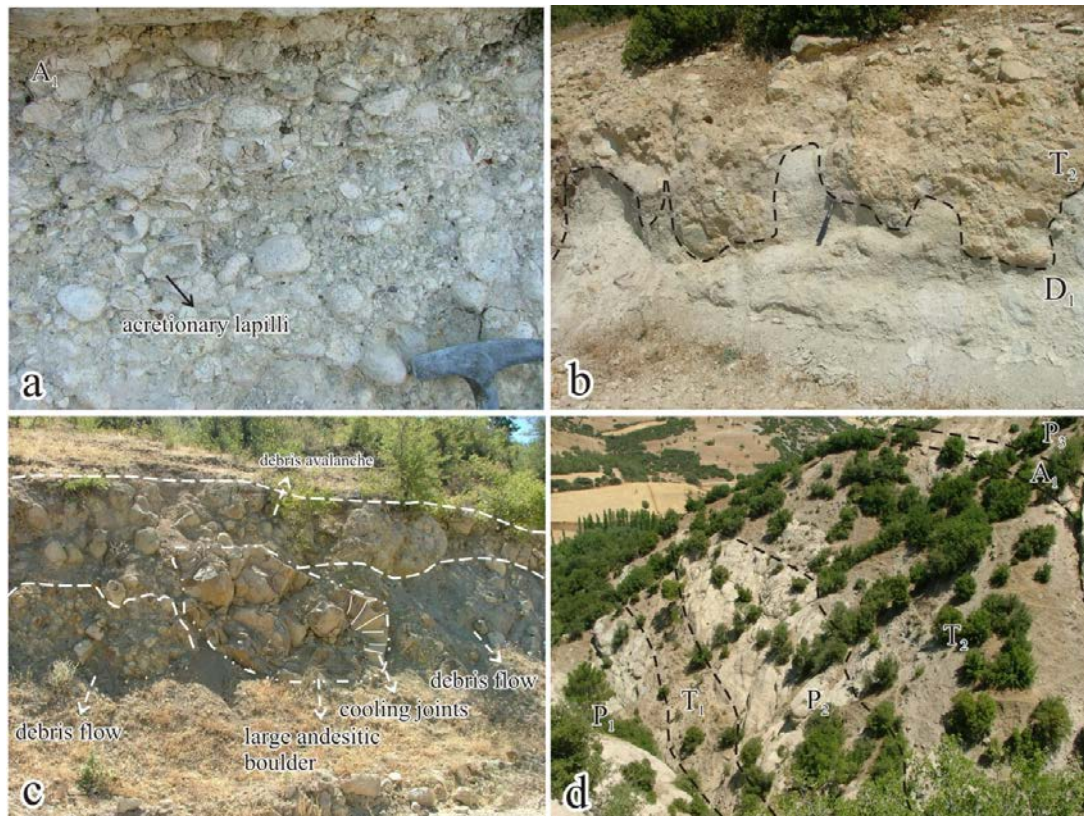
Figure 4.17 Field photographs are showing volcanic outcrops from the succession of the İtecektepe volcanism. (a) Spherical accretionary lapilli within an ash fall deposits, northern part of the İtecektepe; (b) interrelationships between a debris flow (D_1) and debris avalanche deposit (T_2), from Sec. 11; (c) well-preserved contacts between a debris flow (D_2) and debris avalanche deposit (T_2) from inside of the volcanic center; (d) full-view of the Sec. 12 is showing the pyroclastic flow and debris flow sequences (see Figure 2 for location).

4.3.2.1.2 Eruption Phase (P_2). P_2 is the most extensive and ubiquitous phase of the pyroclastic deposits of the İtecektepe volcano. This unit shows significant lateral thickness variations from > 15 m to 10 m thick in the sections 12 and 13 (Figure 4.16), while P_2 exceeds 35 m thickness at south-eastern part of Karaağaç village at Sec 14 and northern part of Sec 11. The P_2 is predominantly formed by massive ignimbrites, although surge deposits (Figure 4.17b) are sparsely intercalated in some localities of Sec. 12 (e.g. the Amazcala caldera; Aguirre-Diaz & Lopez-Martinez, 2001). P_2 is white in colour with abundant white pumice lumps and a pumiceous matrix with lesser crystal rich, including feldspar and quartz, both make up 6 vol. % as the only mineral components. Individual pumice fragments can be up to 12 cm long in pumice concentration zones, also exhibit very intense vesiculation fabrics.

Alteration and fiamme texture could not be observed on individual pumice fragments, while some of them have crystal rich. Andesitic lithic fragments are scarce (< % 5 in vol.) and small (<1 cm long). P_2 displays a transition massive to successive crudely stratified levels from base to upper parts that have andesitic boulders within the same matrix. Eventually, the pyroclastic flow at Section 12, terminated by a debris avalanche deposit T_2 (Figure 4.16b). This eruption phase also was obtained from the western side of the volcano, experienced a deformation to where hanging wall of the NE–SW-trending high angle normal fault (see Figure 4.2 for location). As a result, stratification of the pyroclastic units was disrupted by the fault (Figure 4.18d).

4.3.2.1.3 Eruption Phase (P_3). The most distinctive event for the P_3, including andesitic blocks up to 50 cm large at the basement of the unit. Andesitic lavas are dark gray, sub-angular and poorly sorted within the base level of 1.5 m thickness. Clast and block rich level displays faint stratification locally. This portion of the P_3 contains rare to absent virtually absent (<2 %) pumice clasts, while lithic clasts are common (<20 %) in an ash matrix. Pumice fragments exceed 13 cm in their average length. However, lithic concentration and length of sizes decrease dramatically through the middle part of the D_3. Concentration of andesitic clast and blocks increases towards the top of the unit. Nevertheless, pumice ingredients are the same with the middle level.

4.3.2.2 Debris Flow Deposits (D_1–D_2)

*4.3.2.2.1 Debris Flow Deposit (D_1).*The first debris flow deposits are observed outside of the destruction area of the volcano which represents the medial facies. D_1 includes matrix supported (40-50 vol. % of a matrix < 2mm) with some sand-sized clasts and angular andesitic blocks (< 40 cm wide) were generally observed. The matrix composed of few lithics (andesite, pumice and calcareous sediments) and abundant free crystals (sub-euhedral micas and feldspar). The basal contact is difficult to observe, nevertheless I could obtain a small-scale contact relation with an

ash deposit in the Section 11. D_1 is overlaid by a debris avalanche deposit (T_2) around Section 11 (Figure 4.17b).

4.3.2.2.2 Debris Flow Deposit (D_2). The second debris flow deposit is clearly observed inside of the volcanic depression, and the locations of Sections 12 and 14. D_2 and D_1 have very similar facies but D_2 presents differences with lesser matrix content, proximal characteristics. Their contacts are also truncated by a debris avalanche. D_2 contains matrix supported (25-30 vol % of a matrix < 2 mm) and contains less abundant sand sized clasts (< 20 vol. %). Angular and sub-angular andesitic blocks which exceed 30 cm wide, dominates the D_2. The debris flow 2 is distinguished the previous one with its clear cooling joint texture over the andesite blocks (Figure 4.17c). Both D_1 and D_2 debris flow deposits reflect a soft sediment deformation structure with the debris avalanche deposits. These could indicate the sustained accumulation processes during explosive phases of the İtecektepe volcano. Matrix of the D_2 at Sec. 14 including sand, clay and marl intercalated of a mixture material, D_2 has also more sub-rounded andesitic clasts and blocks respect to inside of the accumulation. These fabrics for Sec 14 indicate properties of medial or distal facies.

4.3.2.3 Debris Avalanche Deposits (T_1–T_3)

4.3.2.3.1 Debris Avalanche Deposit (T_1). Good exposures occur on the edges of the valley, where whole subaerial facies accumulates are best seen at the Section 12, which is taken from the sheer cliff's north-eastern side of the volcano (Figures 4.17, 4.17d and 4.18a). T_1 consists of breccias panels and lava blocks. It is heterolithologic; clasts (< 15 cm large and 35-40 vol %) and megaclasts (< 40 cm large and 15-20 vol %) are mainly andesitic lavas with minor unstratified trachytic and trachyandesitic breccias. T_1 deposits are very poorly sorted, and matrix supported, and there is no obvious bedding. However, it presents a faint successive inverse grading. Component sizes decrease toward distal parts of the deposits. The light coloured matrix is fine-grained and rich in pumice, crystals and angular andesitic lithics. Clasts and blocks of the avalanche deposit are fractured and display

obvious jigsaw puzzle geometry. Clasts and blocks present angular shaping; while rare of them have sub-angular crests (e.g. Schnieder & Fisher, 1998).
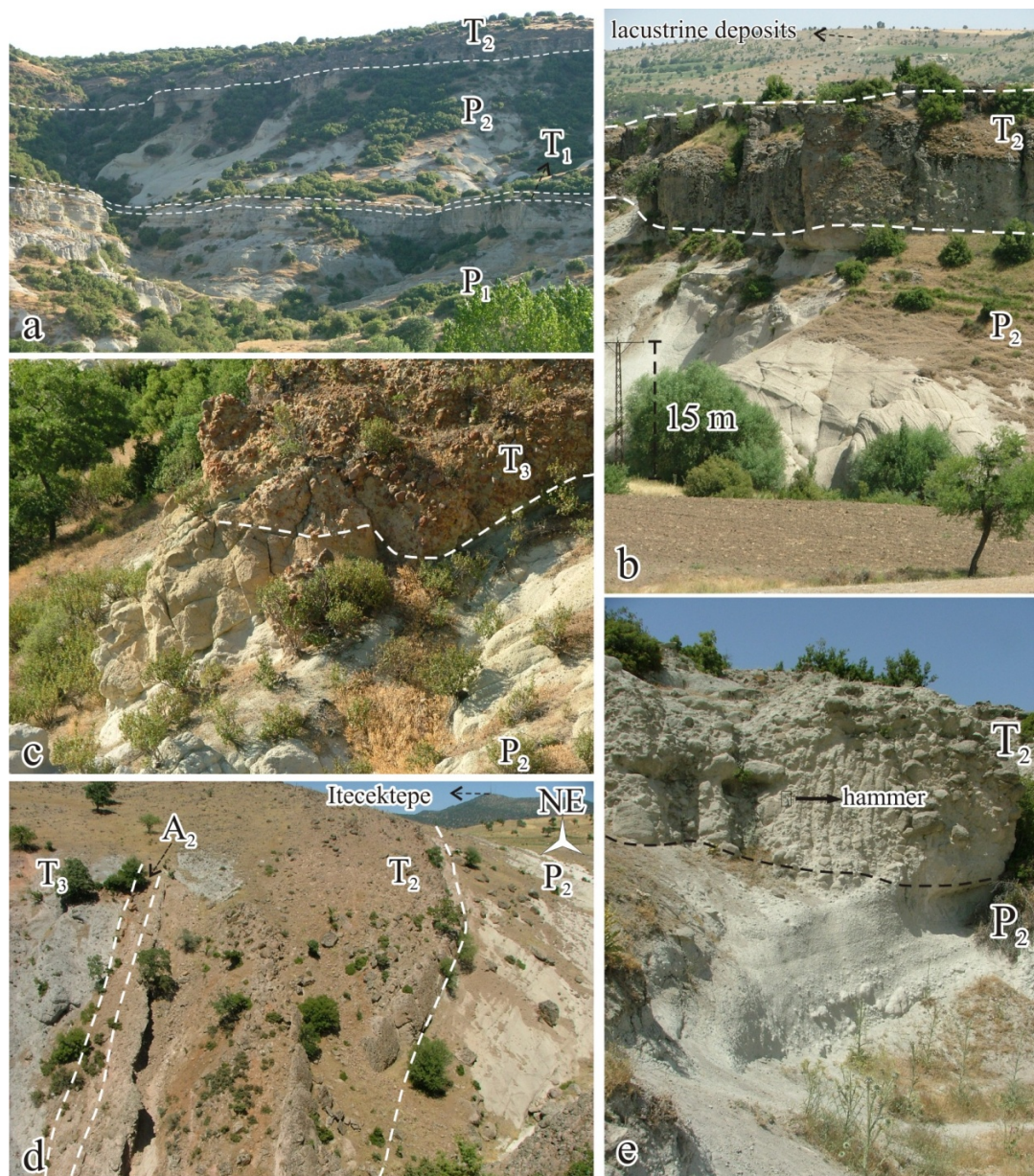
Figure 4.18 Field photographs of volcanic successions around the İtecektepe volcano. (a) Well-preserved exposure showing thick pyroclastic deposits (P_1 and P_2; with T_1 and T_2); (b) interrelation between T_2 and P_2, bottom level of the P_2, displaying phreatomagmatic textures within surge deposits; (c) P_2 is terminated by T_3, from Sec. 14 (see Figure 2 for location); (d) good-exposure from the western side of the volcano showing interrelation between P_2 and debris avalanche deposits, is divided by an ash fall (A_2). The volcanic succession is truncated by a fault, which is placed at the eastern side of the photograph (not visible); (e) a dramatic transition from P_2 to T_2.

4.3.2.3.2 Debris Avalanche Deposit (T_2). T_2 could be clearly seen in two sections, numbers 12 and 13. Section 12 displays the medial features of the zone (Figure 4.18d); while Section 13 presents characteristics of a distal zone (Figure 4.17b, Figure 4.18b and Figure 4.18e). The fabric inside of the medial zone (Sec. 12) has avalanche blocks which is generally massive. Rare of clasts show a faint stratification and inverse grading within both of sections, while distal section (Sec. 13) is characterised by matrix supported but some very poorly fragmented blocks have clast-supported fabric, massive structure and components exhibit more sub-angular and sub-rounded morphology, have more jig-saw cracks on blocks. T_2 generally includes andesitic clast and blocks (90-95 vol %) with less abundant trachy-andesite and trachyte context. Individual avalanche blocks show yellow and brownish colours at the distal zone (Figure 4.17b), which depend on the degree of oxidation and hydrothermal alteration of source rocks (e.g. Shiveluch volcano, Kamchatka; Belousov et al., 1999).

4.3.2.3.3 Debris Avalanche Deposit (T_3). Thickness of the T_3 is up to 12 m in the location of Sec 14 and overlay a thick pyroclastic flow deposit (P_2). It consists of coarse-grained, matrix-supported breccias of dominated andesitic lava fragments. Individual clasts are mostly angular with lesser sub-angular (Figure 4.18c). Clasts show little signs of abrasion and there is a typically little matrix in the breccias, except near the basement (e.g. Parinacota debris avalanche, Chile; Clavero et al., 2001). T_3 display two different andesitic individual breccias, the first one is experienced by any hydrothermal alteration; and the other one is extremely altered. Whole components present pervasively jig-saw crack puzzles. Sub-angular and sub-rounded breccias are generally in the altered clasts (Figure 4.18c).

4.4 Beydağı Volcanic Center

Beydağı is a 16.5 x 9 km^2 in a large volcanic basement, while have 12.5 x 5.5 km^2 in scale destruction area that displays ~300 m elevation difference from the basement to top, in the middle of the volcano (Figure 4.19). The volcano rises about 1170 m. Lacustrine sediments (Ahmetler formation of İnay group) are observed within this deformation area. This indicates that the lake was the present during the post-

destructive phase, so sediments related accumulated within the center of the volcano. Multi-stage intense hydrothermal alterations which are observed at margin of the destructive area, occurring as intrusive bodies, dike swarms, wide range of volcanic rocks, pervasive pyroclastic deposits both inside and outside of the destructive plane, are very distinctive for the Beydağı stratovolcano.
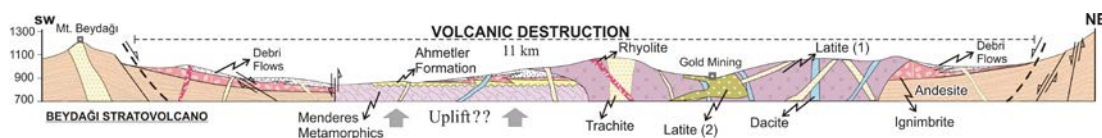
Figure 4.19 Geological cross-sections across the Beydağı volcanic center (see Figure 2 for localities).

4.4.1 Effusive Volcanism

This volcanic edifice has constructed by many kinds of lavas, domes and intrusive bodies prior to destructive stage. The presence of the well-preserved flanks of the volcano is the most cynosure respect to the other volcanic complexes. The whole lava and dome lava sequences, which drape the topography around the Beydağı volcano (northern and western flanks of the remnants of the cone) up to a distance of about 2 km's from the margin of its own flanks, present multi-stage lava flow events. Andesite, latite, trachyte, dacite, rhyodacite and fewer basalt flows and dome structures are recognized within the volcanic complex (Figure 4.20).

This complex was experienced intense deformation since middle Miocene such as the other volcanic edifices. NE–SW-oriented oblique fault dissected the southern flank of the volcano which caused the accumulation of late Miocene coarse grained Asartepe formation (mammalian age data is available by Seyitoğlu et al., 2009).

Metamorphic basement is exposed, which was uplifted by several faults, inside of the depression area. This evidence may be related with the regional uplift of the metamorphic basement, which has documented in detail by Karaoğlu et al. (2010).
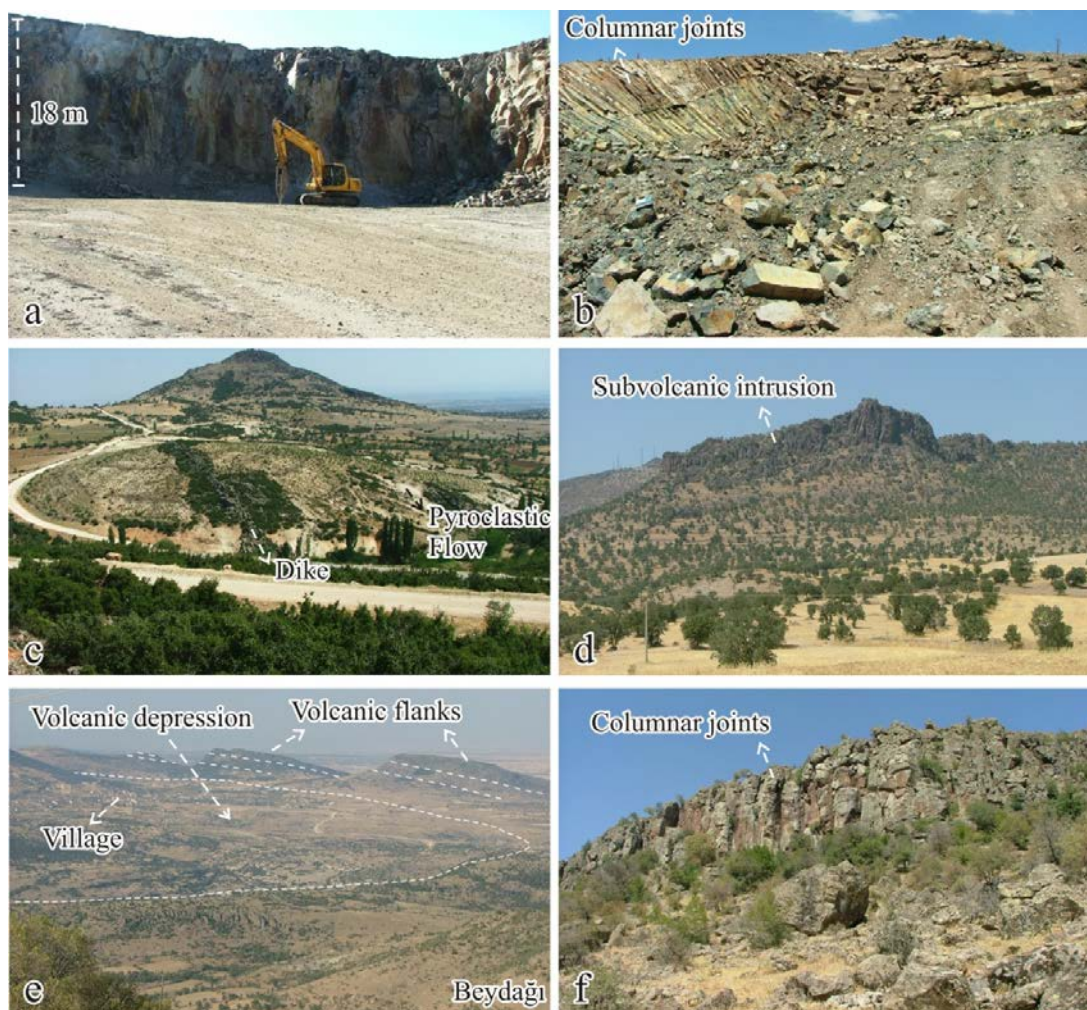
Figure 4.20 Field photographs showing the prominent volcanic edifices of the Elmadağ volcano. (a) Thick andesitic lava flow from the southern part of the volcano; (b) basaltic lavas showing columnar joints, in front of Mt. Beydağı; (c) NW–SE-trending latitic dike, which is cutting pyroclastic flow deposits at the inside of the volcanic depression; (d) subvolcanic intrusions, from southern part of the Mt. İtecektepe; (e) volcanic depression and volcanic flanks of the Beydağı, from Mt. Beydağı; (e) andesitic lavas showing columnar joints at the center of the volcano.

Emplacement of the intrusive bodies and related mineralizations are pervasively observed inside of the deformed area. The intrusive bodies present scarcely sub-volcanic textures petrographical, while bottom levels of them also show clearer aplitic textures. In addition, the Beydağı volcanic depression hosts a gold deposit (Kışladağ Gold Mining) which located on the northern part of the volcanic center, produced 30 tons gold ore during the last five years. The type of gold mineralisation shows a transition of porphyry to the epithermal system, and is directly related with latitic intrusive bodies.

4.4.2 Subaqueous-Subaerial Explosive Volcanism

The products of the explosive volcanism and related facies are not well exposed outside of western part of the edifice, respect to the other volcanic centers. Two different radiometric age data are available, 12.15 Ma (^{40}Ar/^{39}Ar method by Karaoğlu et al., 2010) and 13.1 Ma (K/Ar method by Seyitoğlu, 1997) in range from summit of Beydağı, which is located southern part of the volcano. I obtained three distinct and typical stratigraphic sections from the study area. Beydağı volcano produced huge volume of pyroclastic flow, debris flow and debris avalanche deposits. I describe here the complex stratigraphic sequences, observed in the subaqueous and subaerial exposures of the volcano (Figure 4.21). This stratigraphy provides a record of the eruptive history of volcanism in the area and its effects on the lacustrine evolution of the Uşak-Güre basin (e.g. Caballero et al., 2001).

4.4.2.1 Pyroclastic Flow Deposits (P_1–P_7)

Although, I have obtained seven distinct pyroclastic flow deposits, around the Beydağı volcano, I summarize all shortly due to the they lack of knowledge of well preserved pyroclastic flow deposits in this area (Figures 4.22a,b and f).

I examined pyroclastic flow deposit P_3 which is most extensive and omnipresent phase between pyroclastic deposits of this volcano. It is un-welded and varies in colour from a pink and light yellow oxidized groundmass with pumice clasts (Figure 4.22f), to gray groundmass depend of the distance of the source. This unit shows significant lateral thickness variations from < 11 m at the depression center and northern part of the volcano, to 50 m in thickness at the north-eastern portion of the volcano. It is noted that topography is very smooth over the area covering pyroclastic and related debris flows, it may have been removed many voluminous pyroclastic materials by erosion. P_3 consists of pumice fragments with 7 cm in diameter, very abundant crystals (feldspar, quarts and minor biotite) with lesser lithic components in the pervasive altered matrix at proximal zone (at the center of the volcano). The unit is characterized by a high proportion of accidental lithic and clasts (andesite, latite,

basalt and rhyolite fragments), 5cm in large angular pumices and mineral components (primarily quartz with lesser feldspar).
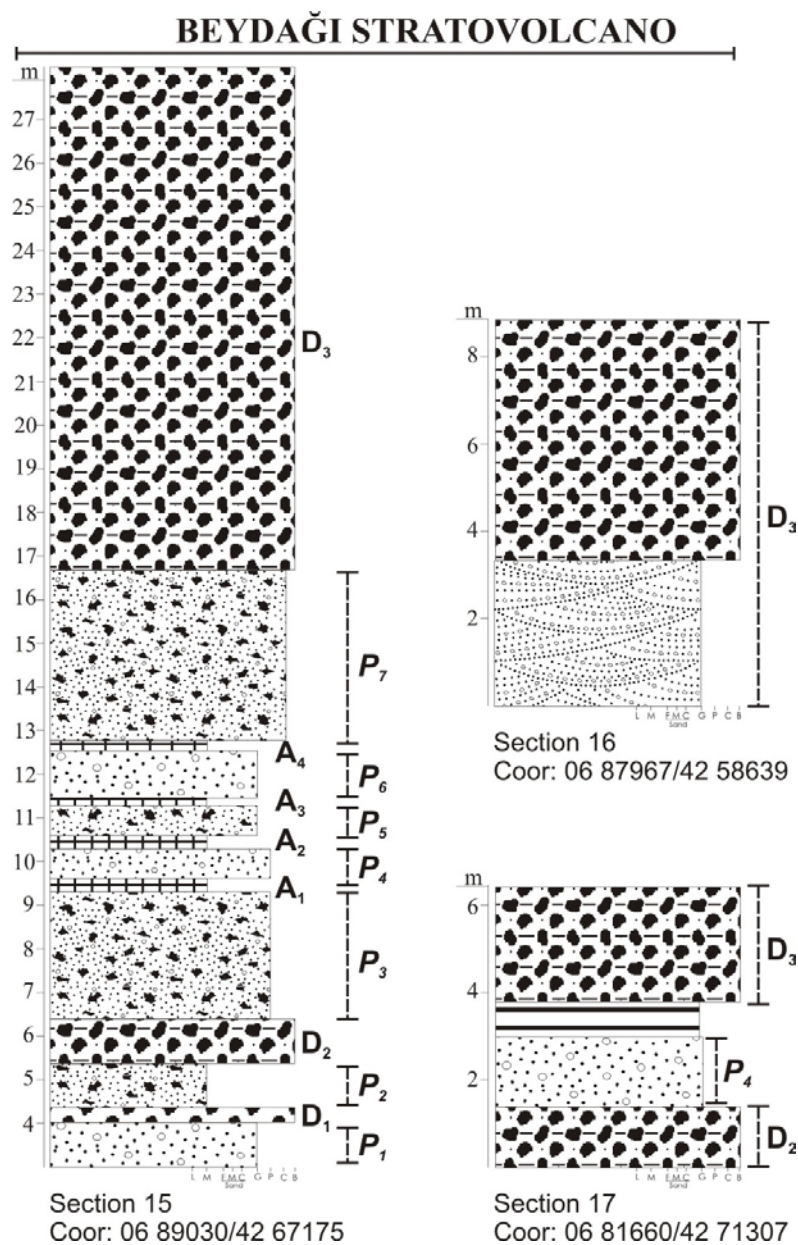
Figure 4.21 Typical columnar sections of the Beydağı volcanic center (Sections 15–17; see Figure 4.2 for locations).

4.4.2.2 Debris Flow Deposits (D_1–D_3)

The base of the volcanic succession of the edifice at Sec 15 is started with D_1 following a pyroclastic flow deposit (P_1). D_1 is composed of heterolithologic blocks

(40 cm in diameter; <60 %) and with less abundant clasts (3-4 cm in size; <10 %) within a sandy-clayey matrix (<30 %). Components are mostly latite and andesites. D_2 consists of latite block (20 cm; <10 %) and clats (5 cm; 60 %) with rare re-worked pumice clasts in a same sandy matrix (30 %). Blocks are up to 25 cm in size, poorly sorting, and display scarcely inverse grading.

The last debris flow deposit (D_3) covers all around the Beydağı volcano, but the western part of the volcano is widely dominated by D_3. The sequence and related pyroclastic deposits (P_4) form good exposure plains at the same portion (Figures 4.22a and b). Thickness of the D_3 exceeds 50 m at some places of the edifice. In the D_3 sequence, a series of inverse grading, sandy, silty and clayey horizons are present. Concentration of angular and sub-angular megaclast and clasts dramatically decreases from inside of the deformation area to outside of the volcanic center (Figure 4.22). Juvenile clasts could observe at southern side of the volcano, in locally throughout the sequence of D_3 (Figure 4.22c). Basaltic juvenile clasts and blocks indicate a hot emplacement inside of the volcano; as well as obtained outside of the volcano. Baked surface and hyaloclastite textures are seldomly observed between unconsolidated-lacustrine sediments (Ahmetler formation of İnay Group) and debris flow deposits D_3 (Figure 4.22d).

The occurrence of debris flow in this area is linked to the saturated volcaniclastics in the form of soil slip, rapidly turning into flows (e.g. Pareschi et al., 2002). I observed hyperconcentrated flow deposits between lacustrine sediments and debris flow D_3 at the volcanic center. This flow displays very high sediment concentrations (up to 70 vol. % of sediment load) crudely laminated pumiceous-crystal sand. The basal contact of the deposit presents cross-cutting channels and lobes (Figure 4.22e). This evidence indicates that the interaction between lake water and volcanism continued at the deformed plane following to post-deformation stage of the stratovolcano.

Figure 4.22 Field photographs of the volcanic successions of the pyroclastic deposits around the Beydağı volcano. (a) The sheet of pyroclastic flow deposits are covered by the debris flows, north-western part of the volcano, and lacustrine deposits covers all at the back-side of the photo; (b) upper part of the pyroclastic deposits is divided by an ash fall (A_4); juvenile basaltic block within D_3; (d) a good-exposure of the baked-surface between the debris flow (D_3) and lacustrine deposit of the İnay group; (e) the basal contact of the D_3 at the inside of the caldera showing of the hyperconcentrated flow texture; (f) pyroclastic deposits (P_3 and D_3) and intense hydrothermal alterations at the inside of the volcanic center.

4.5 Discussion

Uşak-Güre basin presents the complex volcanic successions that formed on three distinct volcanic centers, with several individual volcanic products. These volcanic centers exhibit strong similarities in terms of the mechanism of main-cone construction and destruction processes.

Subaerial pyroclastic density currents or subaqueous eruption-fed density currents that result directly from the generation of particulate material by eruptive activity are key components of volcaniclastic sedimentation (Manville et al., 2009). The components in pyroclastic deposits of three volcanic complexes reflect a spectrum of eruptive conditions and fragmentation mechanisms and provide information on grain, origin and constraints on the dynamic reconstruction of eruptive systems on a detailed scale (e.g. De Rosa, 1999). The subaqueous-subaerial explosive phase for three volcanic centers in Uşak-Güre basin generated a succession of pyroclastic flows, pyroclastic falls, and rarely surge deposits associated with debris flow deposits, sometime of mixed volcanogenic and terrestrial origin (e.g. Sirinia Basin, Romania; Seghedi, 2011). I have obtained strong evidence about accumulation of the debris flow and debris avalanche deposits occurred in a subaqueous environment by explosive fragmentation in the presence of water (İnay Lake). The products of the explosive volcanism and related magma-water interactions have been described for the first time in western Anatolia. The magma-water interactions have also exposed within destruction areas of İtecektepe and Beydağı volcanic centers on the contrary these features are looking at the Elmadağ volcano. The evidence indicates that accumulation of the lake sediments was going on during the post-destructive stage of the Elmadağ volcano. Secondly, the timing of these destructive phases should be considered to be between the range of ca. 17 Ma-15 Ma, as the present dating of volcanic materials support the deposition range of the sedimentary sequence of İnay group.

On the other hand, I have also supplied strong proofs for subaqueous-subaerial effusive phase. Peperitic textures have been observed within Güre basin, especially

in the Zahman village, evidenced by the jig-saw fit breccias clasts, lobate contacts with host rocks (lacustrine Ulubey formation, İnay Group) and occurrence at both the bottom and top of the coherent lava facies (Zahman lava flows).

I have also determined bedded silica (chert) layers through the whole columnar sections (Figures 4.7, 4.16 and 4.21). Discrete layers of silica interbedded with carbonates, siltstones, mudstones and intercalated volcano-sedimentary sequences. The overall geologic setting is similar to those of lakes in the whole NE–SW-trending Neogene basins (Demirci, Gördes Selendi) and borate rich basins (e.g. Bigadiç, Emet and Kırka; Helvacı & Yağmurlu, 1995; Helvacı & Alonso, 2000), in western Anatolia; East African Rift (e.g. Lake Magadi, Lake Bogoria) and Bolzano volcanic complex, northern Italy (e.g. Krainer & Spötl, 1998). I interpret the cherts (silica layers) within the intervolcanic sediments as abiogenic in origin and suggest that they formed in a physicochemical environment under the influence of acidic explosions around proximal and medial areas, similar to that of modern Lake Magadi and Bolzano complex (e.g. Krainer & Spötl, 1998). Similar to those aforementioned areas, chert bearing sedimentation most likely reflects fluctuations in the semiarid climatic conditions during middle Miocene. Thickness of the individual silica layers around Elmadağ (Sections 3 and 4; Figure 4.7) is up to 10 m, quite differently from the İtecektepe volcano. The data may indicate that the volume of the Elmadağ products of the explosive volcanism (e.g. ignimbrite and ash falls) was more vast in respect to discrete and thin silica-bearing sediments around İtecektepe, at that time.

Although there are similarities among these volcanic complexes, they have also experienced by different constructive and destructive processes, which will be briefly presented below.

4.5.1 Elmadağ Volcano

The existence of three superimposed breccias units may implies at least three successive sector collapse events during evolution of this stratocone attested by volcaniclastic debris flow and hyper-concentrated stream deposits. Rounded clastic

components of these debris flow deposits strongly suggest an elevated source (e.g. Schenieder & Fisher, 1998). The distribution and character of sedimentary facies in columnar sections (Figure 4.7) suggest that all debris flow deposits accumulated in proximal to medial zone near an active volcanic center. The unstratified, coarse grained, inversely graded and poorly sorted, and heterolithologic distribution of the blocky and gravel fragments with a sandy to conglomerate dominated matrix support the rapid deposition from non-cohesive volcanogenic debris flow. Crudely stratified, inverse to normal graded, clast-supported deposits are defined hyper-concentrated flood flows by McClaughry & Gaylord (2005). Transitions between the matrix- and clast supported conglomerate likely reflects the fluctuating stags of debris flow transport and accumulation (e.g. White Lake Basin, British Colombia; McClaughry & Gaylord, 2005). The other kinds of volcaniclastic deposits are interbedded with the Elmadağ volcanic breccias successions. They consist of ignimbrite sheets, debris flows and volcaniclastic fluvial deposits. Block-and-ash flows are typically produced by the gravitational or explosive dome collapse or a combination of these processes (Sato et al., 1992; Freundt et al., 2000). Block-and-ash flows could also be produced by the magma encounters an aquifer or surface water and dynamically interact with the water (e.g. O'e Takayama volcano, Japan; Kano & Takarada, 2007). The first block-and-ash flows (B_1) may indicate that magma interact with the water, while B_2 does not reflect such as processes. The whole evidence obtained that there was a complex succession of eruptive phases, sector collapses and erosional intervals during the growth of the volcanic edifice. Debris flows, and hyperconcentrated flows are the most significant evidence about the magma and lake water (İnay Lake) interaction during the cone-building period. Eight distinct of pyroclastic flows (ignimbrites) dominates at the south-eastern part of the volcano. The occurrence of a main destructive area in the middle of the volcanic complex, with rare horseshoe-shaped craters seems to be problematic (Figure 4.23). Thickness and distributions of pyroclastic flow deposits look like not enough to produce a caldera structure. However, small-scale sector collapse of the flank of the volcano was probably the main source of the debris avalanche and debris flow deposits.
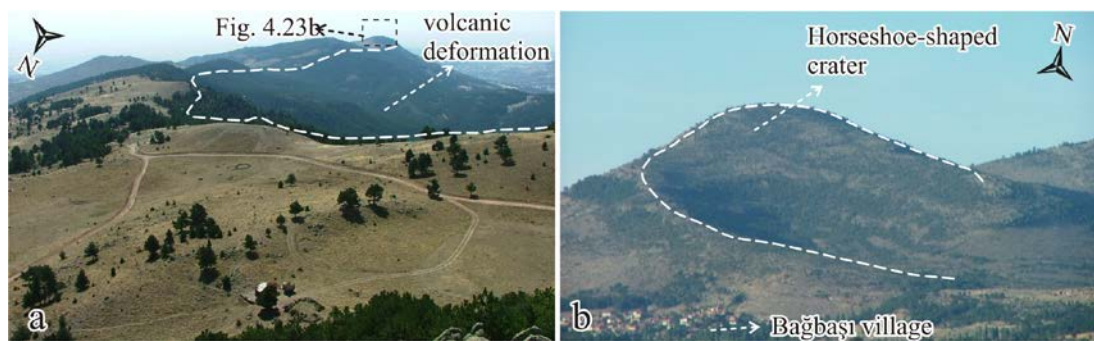
Figure 4.23 Volcanic depression structures over the Elmadağ volcano. (a) Photo was taken from NW to SE across the edifice; (b) one of the small-scale (ca. 300 m in diameter) horse shoe-shaped flank collapse of the Elmadağ volcano.

4.5.2 İtecektepe Volcano

Debris flows deposits are mostly composed of angular clasts which are the direct results of tectonic activity (Muleller & Corcoran, 2001). The present of the wide-spread and successive debris avalanche deposits support the tectonic activity. Several faults and the presence of metamorphic basement rocks inside of the volcanic center were mapped. It is suggested that the massif was outcropped as a result of uplift. Accumulation processes of the debris flows and avalanche deposits may have been triggered by aforementioned tectonic activity. Many volcanic products are interbedded with the lacustrine sediments while pyroclastic flow deposits do not show any water interaction. These data indicate that subaqueous-subaerial volcanism is one of the prominent characteristics of the Elmadağ volcanic center. In addition, there are accretionary lapilli within a base-ash deposit; pyroclastic flow deposits occasionally enclose accretionary lapilli. They are, however, more characteristic of the fallout deposits closely associated with pyroclastic flows in a proximal environment (e.g. Seghedi, 2011; Edmonds et al., 2006). The fallout deposits are crudely stratified, mantling the dominated former morphology of the basement rock deposits (early Miocene fluvial deposit, Yeniköy formation).

Pyroclastic flows (ignimbrites) display thick sections and are present all around the volcano, except its center. This evidence may indicate that İtecektepe present a complex succession of eruptive phases, sector collapses and erosional intervals

during the growth of the volcanic edifice such as the Elmadağ volcano. However, its destructive area most probably was the source of the explosions which triggered the sector collapse shape area at the upper part of the volcano. The existence of the metamorphic rocks inside of the volcano indicates that post-tectonics took place after the sector-collapse stage.

4.5.3 Beydağı Volcano

Although, two radiometric age data documented by younger intrusive body of Beydağı between 12 Ma to 13 Ma, the volcanic successions are coeval with accumulation of the İnay group since Early-Middle Miocene (Karaoğlu et al., 2010). It is constructed multistage of volcanic activity, separated by long intervals of quiescence. The evolution of the Beydağı volcano reflects different types and degrees of interaction between magma and external lake water during both cone-building periods and subsequent the destructive period. The middle part of the volcanic complex is dissected deeply enough to uncover intrusive bodies, indicating the volcano's central vent area. These lava clasts within the debris avalanche underwent pervasive hydrothermal alteration, which could be related to pre-failure magma intrusion. I propose that Beydağı destructive area display such as nested large volcano structure based on its elongated circular shape, surrounding and widespread thick pyroclastic flow deposits (e.g. ignimbrites) which interacted with the lacustrine deposits (Ulubey formation).

The gold deposits are dominantly hosted by volcanic rocks and contemporaneous volcano-sedimentary successions of the Kışladağ (Beydağı) mining. Exposing processes should be controlled by three different constraints: (i) erosion; (ii) tectonics; (iii) periods of onset of the intrusive event.

Erosion rate differs greatly among the various volcanic environments. Island arcs have high erosion rate due to rapid uplift (from 0.1 mm/yr. at Kyushu to New Guinea) and high rainfall, whereas continental environments have lower erosion rate (generally about 0.01 mm/yr.), except during periods of volcanic collapse (e.g.

Marcoux & Milési, 2000). The Beydağı destructive area should be occurred at least since ca. 17 Ma, because the oldest age data indicates this period. It could be easily calculated the probable thickness as 170 m for the Beydağı during interval of 16 Ma for the western Anatolia, which shows typical continental environment. I assume that during its construction, the stratovolcano has been estimated to culminate at > 4000 m, by comparing the modern stratovolcanoes (e.g. Mts. Ağrı, Süphan and Erciyes, in Türkiye). Individual erosional processes irrespective of the tectonics are not enough to form this destructive area and expose ore deposits, in spite of official report of Elderado Gold (Juras et al., 2010).

Mineralisations might be controlled by major structural constraint in the Beydağı volcano. Many authors have pointed out the importance of large-scale structural constraints which serve as major drainage pathways where subsequently enable pluton emplacement and hydrothermal circulation. Karaoğlu & Helvacı (in press) documented the intense tectonic deformation since Middle Miocene within Uşak-Güre basins including Beydağı volcanic complex. The authors reported that NE–SW strike slip and oblique faults dominated the Uşak-Güre basins since Oligo-Miocene. Following the Early-Miocene extensional phase, fluvio-lacustrine İnay Group initiated their own deposition (17-15 Ma). NE–SW directed oblique accommodation faults deformed and cut the hanging wall of the Gediz Detachment Fault. These faults were responsible for the NE–SW trending Uşak-Güre basins (e.g. Selendi, Gördes, Demirci basins) with an accompanying huge volume of calc-alkaline and ultrapotassic volcanism. The main faults are extending in the both of Güre basin margin and within the Uşak basin. In addition, NE–SW oblique faults which were sustained and progressive faults, as a consequence of extension were triggered by the isostatic uplift and exhumation of the Menderes core complex from Oligo-Miocene to late Miocene. Since the late Miocene NE–SW oblique and high-angle faults uplifted the margin of the Uşak basin. These faults were responsible for the deposition of the Asartepe formation and also exhumation of the buried units of the basin, such as the location of south-eastern part of the Beydağı (see Figure 4.2). Besides these, Karaoğlu & Helvacı (in press) propose a probable transfer fault zone (Uşak–Muğla Transfer Zone) directly controlled by NE–SW-trending strike-slip and

oblique slip normal faults which led to successive extensional deformations, cross-cutting the Beydağı stratovolcano, since the middle Miocene on the eastern edge of the Menderes Massif Core Complex (Figure 4.1). This evidence indicates that the Beydağı complex was subjected the crustal-scale structural deformations.

Many volcanoes are located along regionally important fault zones. In mineralized volcanic edifices, the ore deposits are controlled by structures developed during intrusive formation and by regional faults which intersect and reactive the edifice-related structures (Rytuba, 1994). The Beydağı volcanic center is controlled by structural edifice boundary via high-angle normal fault (Figure 4.19). Elderado Gold's report reveals that high density of low-displacement brittle fractures on volcanic settings and NNE–striking joints are the most pervasive observations at the eastern portion of the open pit. Two sets of structural evidence may relate with radial-ring faults and fractures which led to low-to moderate scale deformation on the inside of volcano and extending outside. Ring and radial faults and fractures developed during caldera may also be important in localizing ore deposits such as in the gold allunite deposits within the caldera complex (e.g. Rodalquilar caldera complex; Rytuba et al., 1990). I claim that several porphyry intrusive bodies are directly associated with batholiths in depth. The caldera setting reflects a resurgent caldera together with intrusive bodies and uplifting of the metamorphic basement (Figure 4.19). Ore deposits may form very late in the onset of the large volcano edifice (post-volcanic stage), and porphyry-gold bearing stocks emplaced in ring and resurgent cores of calderas (e.g. calderas in Arizona; Lipman & Sawyer, 1985). The present of the hydrothermal alteration and dike systems near the structural boundary is very significant. Ultimately, I think that evolution of ore deposits in this destructive setting accommodated by the differential processes caused by regional-scale extensional tectonic in association with onset of the caldera and minor erosional stage during Middle-Late Miocene.

CHAPTER FIVE
PETROGENESIS OF THE VOLCANIC ROCKS OF THE
UŞAK-GÜRE BASIN

5.1 Geological and Volcanological Settings

Western Anatolia is characterized by wide-spread Neogene continental volcanic activity that was accompanied by fluvio-lacustrine sedimentation in several continental basins. The volcanic rocks and related Neogene sediments rest on continental blocks and suture zone rocks which were amalgamated during Paleogene continental collision events. The continental blocks are the Anatolide-Tauride block to the south and the Sakarya Zone to the north, which were joined along the İzmir-Ankara Suture Zone. The suture zone represents the northern branch of the Neo-Tethys Ocean which was consumed by northward subduction beneath the Sakarya Zone, giving rise to development of the Pontide magmatic arc on the southern margin of Eurasian (e.g. Şengör & Yılmaz, 1981).

The volcanic rocks in western Anatolia are not restricted to the Neogene, as they were preceded by Eocene to Oligocene volcanic activity further north and succeeded by Quaternary intra-plate alkali basaltic volcanism (Kula volcanic rocks) in the central part of the region. The origin and the evolution of the Eocene volcanism in the north are debated. Some authors claim that these volcanic rocks represent the beginning of the post-collisional volcanic activity in the region with respect to the collision between the Anatolide-Taurides and the Sakarya Zone (e.g. Genç & Yılmaz, 1997; Dilek & Altunkaynak, 2007). On the other hand, it has recently been proposed that the Eocene magmatic activity may represent the end of subduction, as some granites show northward imbrications, which have been dated at 47.6 Ma (Lutetian) by zircon U-Pb ages (Ustaömer et al., 2009).

The main NE–SW-trending Neogene basins in the region are, from west to the east, the Bigadiç basin (Erkül et al., 2005), the Gördes basin, (Seyitoğlu & Scott, 1994), the Demirci basin (Yılmaz et al., 2000), the Selendi basin (Ersoy et al., 2010)

and the Uşak-Güre basin (Ercan et al., 1978; Seyitoğlu, 1997). The volcanic activity in these basins is characterized by (1) early Miocene high-K calc-alkaline dacites and rhyolites and their pyroclastics with small amounts of shoshonitic and ultrapotassic-lamproitic occurrences (e.g. Erkül et al., 2005; Ersoy & Helvacı, 2007), (2) middle Miocene high-K calcalkaline dacites and andesites with high-Mg shoshonitic to ultrapotassic lavas (Innocenti et al., 2005; Ersoy et al., 2008), (3) late Miocene K-trachybasalts (Innocenti et al., 2005) and (4) Plio-Quaternary strongly sodic-alkaline, OIB-type basic lavas (the Kula volcanic rocks, e.g., Alıcı et al., 2002).
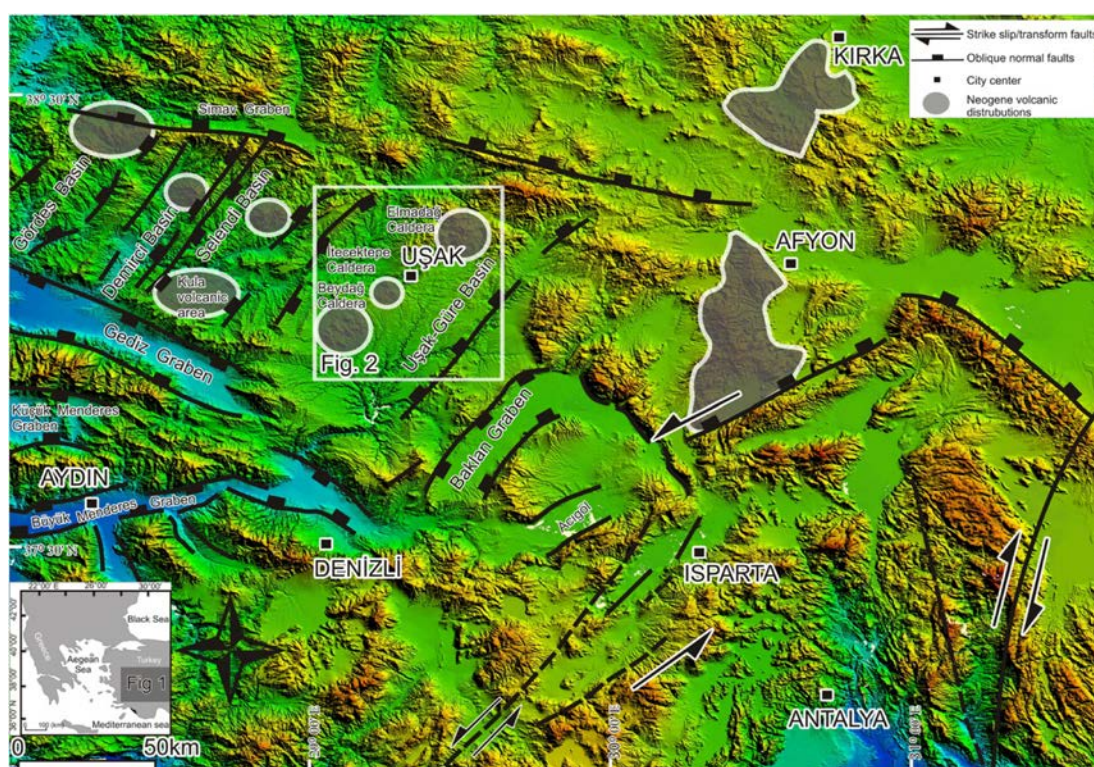
Figure 5.1 Simplified map showing Neogene major structural elements over topography of western Türkiye derived from 90-m SRTM digital elevation model. Key regions and volcanic centers are labeled. Strike slip/transform faults and oblique normal faults are shown with symbols on the footwall (modified from Bozkurt 2003 (for Neogene and Quaternary basins of Western Anatolia); Alçiçek et al., 2006; Çemen et al., 1999 (for Isparta Angle and major structural elements of south-western of Türkiye); Koçyiğit et al., 2000 (for Afyon fault), Çoban & Flower, 2007; Francalanci et al., 2000; Yağmurlu et al., 1997 (for Neogene volcanic rocks of Kırka, Afyon and Isparta) and the volcanic centers of western Anatolia modified from Geological Map of Türkiye, 2002; 1:500 000), references therein.

The amount of the more mafic volcanic products in the region increases from early Miocene to Quaternary. This variation is mainly interpreted to result from lithospheric thinning in response to extension (e.g. Yılmaz, 1989, 1990; Seyitoğlu, 1997; Ersoy et al., 2008). The first two volcanic episodes in the region, together with the Oligocene volcanism to the north, represent the first stage of volcanism in western Anatolia and are widely accepted to result from melting of a metasomatized sub-continental lithospheric mantle beneath the Anatolian plate (Yılmaz, 1990; Güleç, 1991; Aldanmaz et al., 2000; Innocenti et al., 2005; Ersoy et al., 2008; Helvacı et al., 2009). The last episode of volcanism, which produced the Kula volcanic rocks, is interpreted to be largely derived from asthenospheric mantle (Güleç, 1991; Aldanmaz et al., 2000; Alıcı et al., 2002; Agostini et al., 2007). Thus, the late Miocene volcanism likely represents the transition between the lithospheric mantle-derived orogenic or post-orogenic extensional magmas and the intra-plate OIB-type alkaline magmas (e.g. Innocenti et al., 2005).

The Uşak-Güre basin is a key area among the NE–SW-trending basins as (1) it contains a large amount of volcanic rocks developed in three major volcanic centers located on a NE–SW trend; (2) it is located in the easternmost part of the NE–SW-trending basins, and the westernmost part of the N–S-trending Kırka-Afyon-Isparta area, and hence, the geochemical feature of the Miocene volcanic rocks form an important tool in correlating the two volcanic areas; and (3) the volcanic activity in the basin is represented by a wide-spectrum of compositions ranging from high-K calc-alkaline andesites, dacites and rhyolites to ultrapotassic (ultra-K) shoshonites and lamproites. However, the Uşak-Güre basin is not well studied in terms of the geochemical evolution of the volcanic activity.

5.1.1 Field Relations of the Volcanic Units

In order to reconstruct the volcano-sedimentary history of the Uşak-Güre basin , I mapped ~2500 km^2 on a 1/25.000 of scale and revised the Miocene volcano-sedimentary units on the basis of field studies and $^{40}Ar/^{39}Ar$ geochronologic data from the volcanic rocks (Figure 5.2). Three distinct volcanic successions were found

in the Uşak-Güre basin: (1) the Beydağı volcanic unit made up of andesitic to rhyolitic lavas and pyroclastic deposits; (2) the Payamtepe volcanic unit, consisting of lava flows and dikes; and (3) the Karaağaç latite/andesite dikes.

The Beydağı volcanic unit occurs in three different NE–SW trending volcanic centers. These are the high-K calc-alkaline to shoshonitic Beydağı, İtecektepe and Elmadağ calderas from southwest to northeast, respectively. The Beydağı caldera is approximately 16×9 km in diameter and is represented by voluminous pyroclastic deposits. These deposits are block-and-ash flows, ignimbrites which are associated with onset of the caldera collapse and debris flows. The İtecektepe caldera is ~5×6 km in diameter and extensive dacitic ignimbrites were associated with the collapse of the İtecektepe caldera. Subsequent uplift of the caldera floor led to the exposure of metamorphic basement in the middle of the caldera. The eastern half of the Elmadağ caldera is preserved and the half-deformed caldera size is ~5×9 km in diameter.

Dacitic ignimbrites were formed during the collapse of the Elmadağ caldera. The oldest radiometric ages from the Beydağı volcanic unit were obtained from the Elmadağ volcanic center in the north and ranged between 17 and 16 Ma (Figure 5.2). The data indicate that volcanism was active since the late early Miocene (Burdigalian). The youngest radiometric age from the Beydağı volcanic unit was obtained from the Beydağı caldera (12.15±0.15 Ma) in the south. These data indicate that Beydağı volcanism was active until the late middle Miocene and that activity migrated from north to the south with time. The volcanic products of the Beydağ volcanic unit interfinger with the fluvio-lacustrine sediments of the İnay Group.

The Payamtepe volcanic unit consists of several lava flows and dikes. These are the shoshonitic Kıran rocks, Yeniköy latite dikes, ultrapotassic Güre lavas and Karabacaklar lava flows. The lava flows and locally developed dykes of the Payamtepe volcanic unit were emplaced along NE–SW-trending oblique-slip faults and are most abundant in the northeastern part of the Güre region. The Payamtepe volcanic unit also interfingers with the fluvio-lacustrine sedimentary rocks of the İnay group. Seyitoğlu (1997) proposed that the volcanic rocks of the Uşak-Güre

basin is intercalated with the İnay group based on their stratigraphic position and the radiometric age of the volcanic rocks (dated as 15.5±0.4 to 14.9±0.6 Ma, K/Ar ages). Bingöl (1977) also noted that the K-Ar dates of the Muratdağı volcanic rocks which are located in the NE edge of the basin lie between 16.9±0.2and 20.9±0.5 Ma.

The Karaağaç latite/andesite dikes were emplaced along a NE–SW direction and cut the late Miocene Asartepe formation. The Asartepe formation is also observed in the Selendi basin where the Upper Miocene Kabaklar basalt (8.37–8.5 Ma, Ercan et al., 1985; Innocenti et al., 2005) conformably overlies the unit. Ersoy & Helvacı (2007) proposed that the Kocakuz formation, which is correlated with the Asartepe formation, is late Miocene in age according to stratigraphic relations in the Selendi basin. Recently, Seyitoğlu et al. (2009) documented biostratigraphic and magnetostratigraphic age of 7 Ma for the Asartepe formation in the Uşak-Güre basin.

age		units	geochronologic data	rock types	SiO₂	K₂O/ Na₂O	Mg#	Eu/Eu*
		recent sediments						
Late Mioce.		Karaağaç dikes / Asartepe fm.	→*7 Ma	Andesite	60.11	0.75	75.7	0.71
		Payamtepe volcanics						
Middle Miocene	İnay Group	Ulubey fm.	→12.15 ± 0.15 Ma	Andesite	62.36	1.30	53.8	0.71
		Beydağı volcanics	→15.04 ± 0.10 Ma	Dacite	63.53	3.05	63.5	0.78
			→15.93 ± 0.08 Ma	Latite	63.76	2.40	63.8	0.76
			→16.01 ± 0.08 Ma	Trachyte	62.34	2.98	77.3	0.78
			→16.28 ± 0.09 Ma	Rhyolite	64.93	3.00	57.8	0.65
			→16.44 ± 0.07 Ma	Latite	58.11	2.17	73.2	0.77
		Ahmetler fm.	16.48 ± 0.08 Ma	Rhyolitic tuff	63.10	1.72	69.4	0.84
			16.48 ± 0.33 Ma	Shoshonite	—	—	—	—
			→17.29 ± 0.13 Ma	Trachyte	67.15	1.26	71.1	0.79
Early Miocene	Hacıbekir Group	Yeniköy fm.						
		Ophiyolitic rocks / Kürtköyü fm.						
		basement rocks	detachment fault					
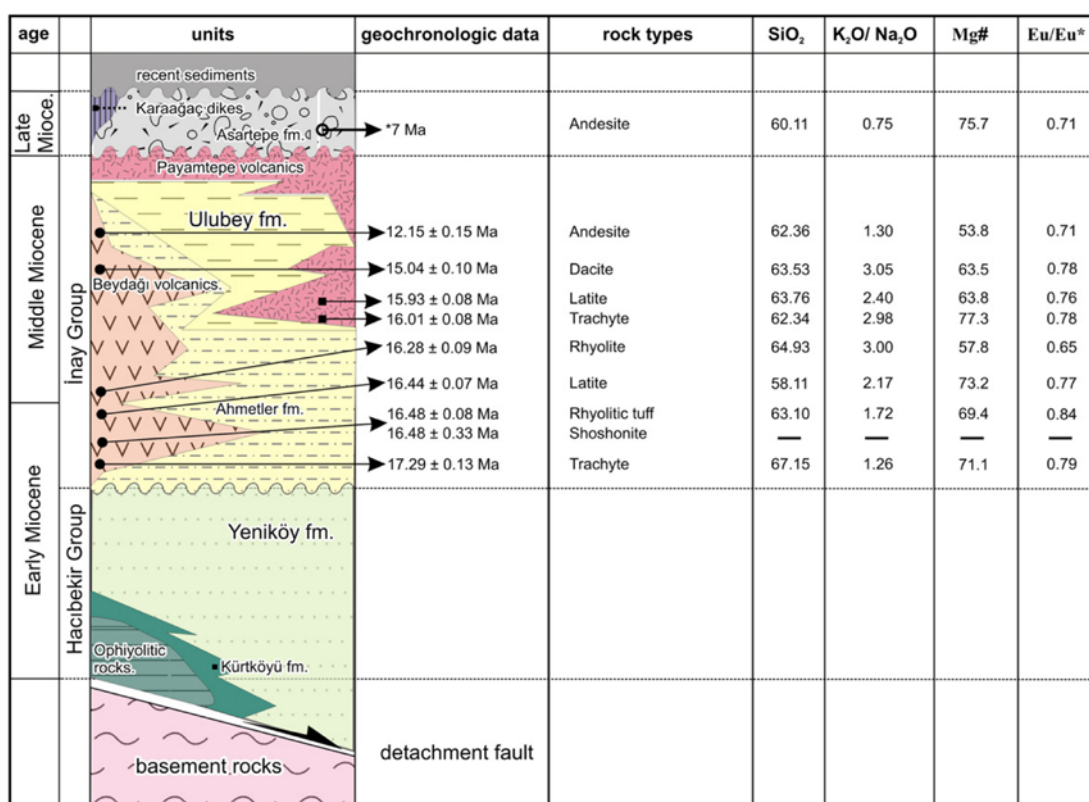
Figure 5.2 Stratigraphy and geochemical characteristics of the volcanic rocks from the Uşak-Güre basin. Age of the Asartepe formation is from Seyitoğlu et al. (2009).

5.1.2 Petrography and Mineralogy of the Volcanic Units

Petrographical studies are carried out as northern and southern part of the Uşak-Güre basin. Approximately 170 samples are collected for mineralogical and petrographical studies from the study area. These samples are grouped in terms of mineral paragenesis. Phenocryst ratios respect to matrix between are 8-60 % in volume and these samples show porphyric textures for all of the lava samples. These phenocryst ratios increase at some subvolcanic samples. Volcanic products are defined as lavas and ignimbrites.

Volcanic rocks of Beydağı volcanic unit can be divided into three main groups on the basis of phenocryst assemblage: those that include (1) quartz + plagioclase + biotite + hornblende ± kaersutite, (2) plagioclase + clinopyroxene + biotite, (3) plagioclase + clinopyroxene + orthopyroxene+ biotite. As shown in the next section, these three groups correspond to dacite and rhyolite, trachy-dacites and trachy-andesite, basaltic andesite basaltic trachy-andesite, trachy-andesites, respectively. Clinopyroxene and orthopyroxene bearing samples were determined as basalt or andesitic basalt petrographically by the polarised microscope studies. These volcanic rocks exhibit mainly hyalopilitic textures. Volcanic rocks of Payamtepe volcanic unit are characterised by two groups: (1) sanidine + phlogopite ± olivine ± hornblende, (2) olivine + plagioclase + clinopyroxene + biotite. Karaağaç volcanic rocks are composed of sanidine + biotite + plagioclase ± clinopyroxene.

Plagioclase is the most abundant phase, both as phenocrysts and in the groundmass. It is early phenocrysts in the early Miocene Andesites of Beydağı volcanic unit (Figure 5.3) vicinity of Elmadağ and İtecektepe volcanic area but was formed after olivine and clinopyroxene in the basalts and some of potassic rocks of Payamtepe volcanic unit. The plagioclase phenocrysts in Beydağı exhibit strong normal zoning, from core to rim. Oscillatory and reverse zoning are observed in the plagioclase crystals of Beydağı andesites. Ortho- and clinopyroxene coexist in rare of basaltic lavas in southern sector-Beydağı volcanic area. The orthopyroxene is generally hyperstene in the Beydağı basalts and rarely potassic lavas of Payamtepe

unit vicinity of Adıyalar-Kıran village. The clinopyroxene is normally augite, being diopside in a basaltic sample from Beydağı volcanic unit. Olivine is present in most basalts, basaltic andesites, and potassic samples (Figure 5.4).

Abundant basaltic and rare andesitic lavas comprise of olivine-basalt enclavas in the Beydağı volcano (Figure 5.4c, d). This may indicate a magma mixing for the Beydağı lavas. Most of the olvine phenocrysts show iddingsitic alteration both of basaltic and potassic (lamproite) samples. Amphibole and biotites are mostly abundant in andesitic and the other intermediate lavas. Most of their phenocrysts tend to opaque minerals. In addition reactions with liquid are observed conspicuously. Sanidine and phlogopite pheno and microcryts are dominantly observed in potassic lavas. While phlogopites predominantly rich in potassic lavas indivual but sometimes biotites accompanied to them. Rhyolites are highly vitrophyric, containing only 10% volume of plagioclase crysts together with biotite. Apatite, sphen and zircon are present as accessory minerals. Porphyry texture dominates whole of the lavas.

The ratios of the volcanic matrix, phenocrsysts and volcanic glass respect to each other's determine the the hipocrystaline or hipohyaline textures. Vitrophyric flow textures are observed mostly in dacitic and rhyolitic and rarely in basaltic rocks.
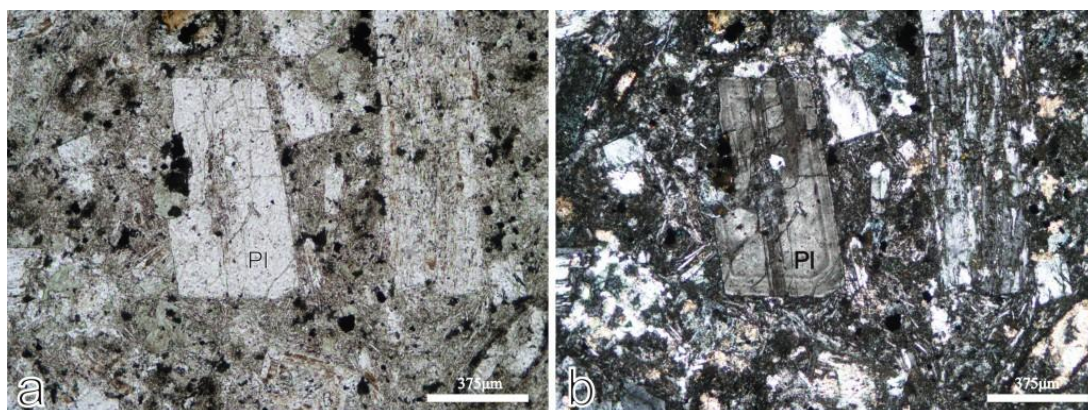
Figure 5.3 (a, b) Andesite. Hipocrystalline texture, P.N (plane nichols) ve C.N (crossed nichols) images, microlits are more dominated from volcanic glass and showing oscillatory concentring zoning in plagioclase. Pl: Plagioclase

Some of andesitic, rhyolitic and rhyodacitic lavas distinguished with glomeroporphric texture mostly in İtecektepe and Elmadağ volcanic regions. Mostly lavas consist of embayed, normally –inverse zoning and reaction bearing quartz sanidine and plagioclase phenocrysts.

In addition some of clinopyroxene crysts present intense eroding throughout the corner of the body themselves. Euhedral phenocrysts are mostly abundant in basaltic and potassic lava rocks such as euhedral olivine crysts are one of the prominent instance. Nevertheless, olivine and pyroxene crysts are dominantly in subeuhedral in forms throughout the Kışladağ gold mining region for Beydağı volcanic unit. Even skeleton and ghost olivine and pyroxene crysts are conspicuous in the same samples. Besides this, xenoliths and secondary quartz are observed in the basaltic samples of Payamtepe volcanic unit (Figure 5.5).
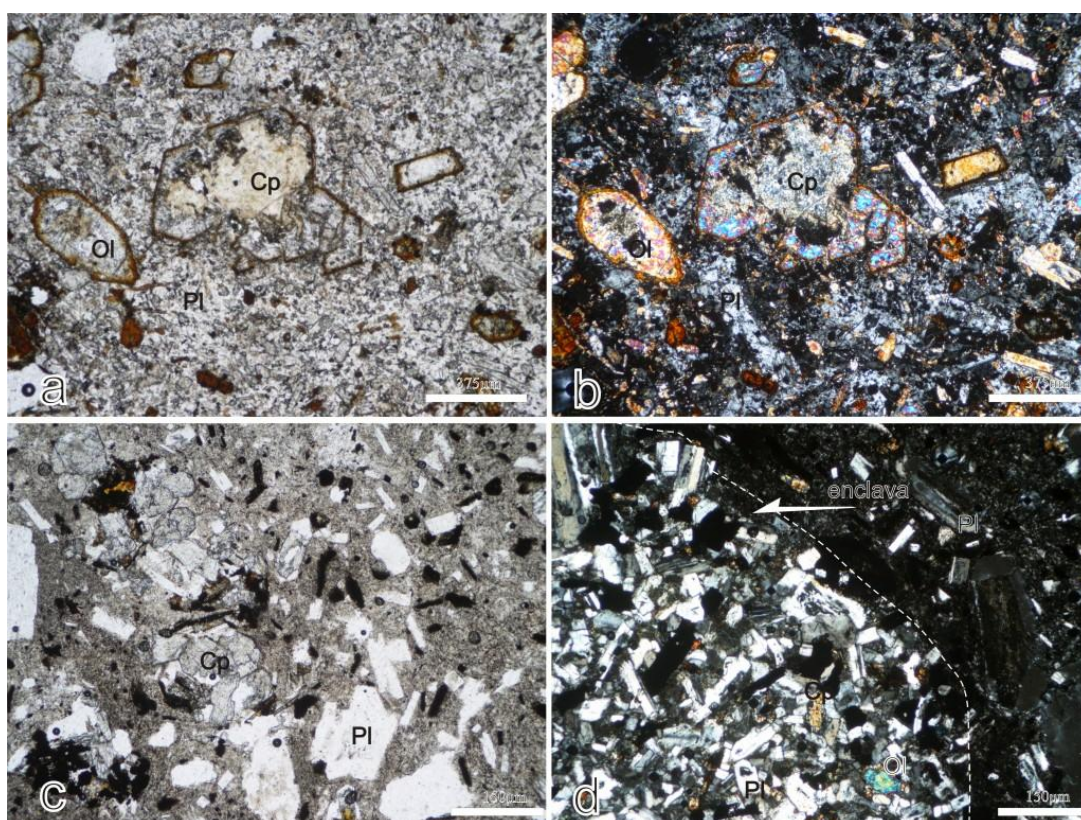
Figure 5.4 (a, b) Basalt and (c, d) olivine basalt enclava. Hipocrystalline porphyric texture, plane and crossed nichol images, iddingsitized euhedral olivine and opacitized biotites are very common. Enclave may reflect a sub-volcanic type textures more than a classical porphyric textures for the volcanic rocks. Ol: Olivine; Cp: cylinopyroxene; Pl: Plagioclase.

Potassic/ultrapotassic rocks outcrops at the area, between the Güre massive and Elmadağ volcanic complex. These rocks consist of Sanidine + Phlogopite (Ph) + Amphibole (Af) ± Biotite (Bi) phenocrysts. Sanidine and phlogopite are included the rocks both as phenocrysts and as microlits. Hornblendes are oppacitized in usually.
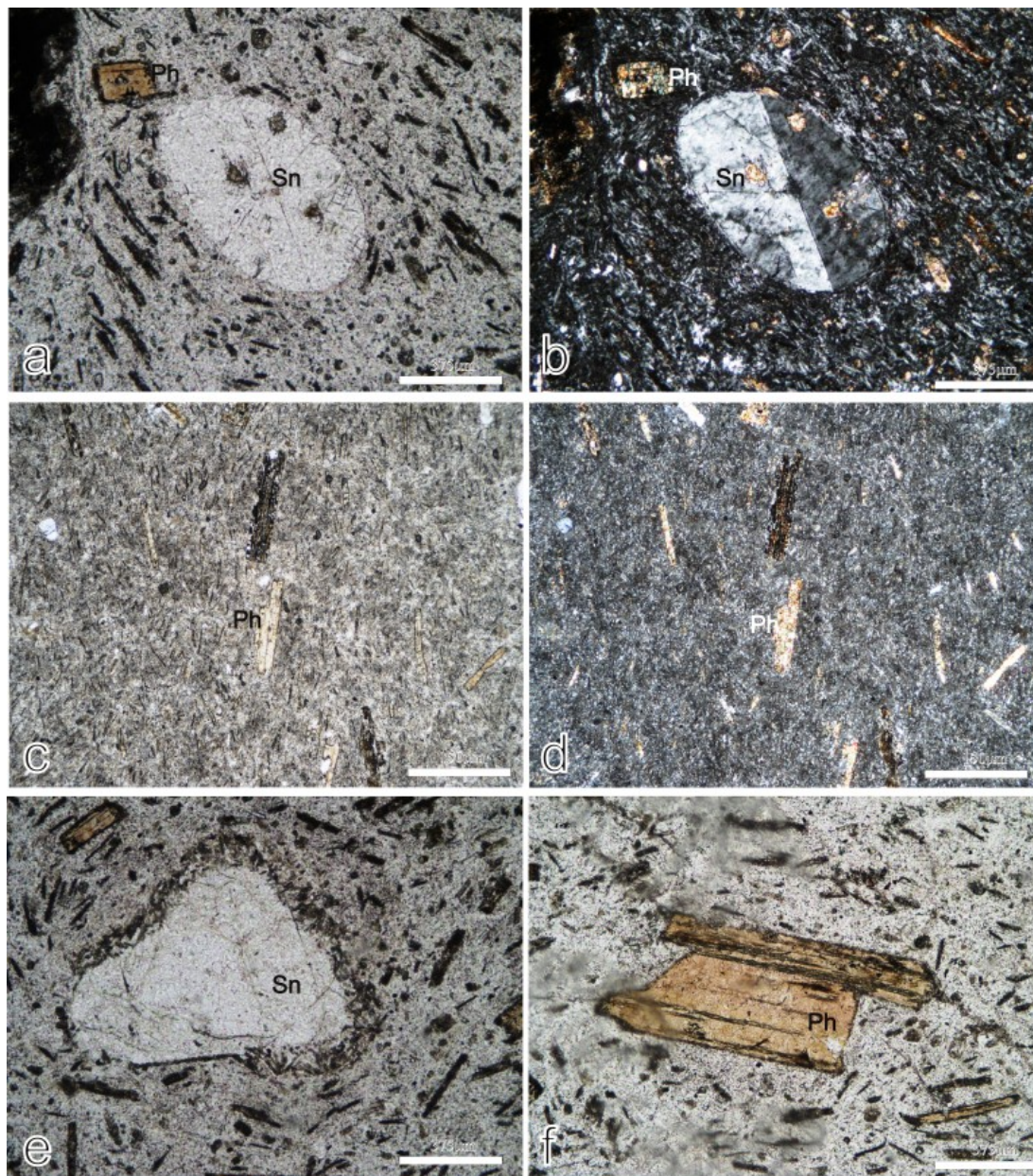
Figure 5.5 Lamproitic rocks of the Payamtepe volcanic unit. (a, b) The sample consists of eroded-spherical sanidine phenocrysts within also sanidine and phlogopite in rich microlite groundmass, plane and crossed nichol images; (c, d) phlogopites are within sanidine dominated microlithic groundmass, plane and crossed nichol images; (e) intense eroded sanidine showing reactions with

magma, plane nichol image; (f) phlogopite phenocrysts within its own and sanidine in abundant groundmass, plane nichol images. Sn: Sanidine; Ph: Phlogopite.

The samples of the pyroclastic flow rocks are subdivided into rhyolitic and dacitic in composition. While the embayed quartz and accidentally lithic fragments bearing ignimbrites are mostly observed close to eruption source (proximal zone), pumice in rich deposits is followed throughout the medial or distal zone of the main cone such as Elmadağ (Figure 5.6). In addition deformed biotites and quartz are clearly observed also pumice fragments in block-and ash flows and ignimbrites.
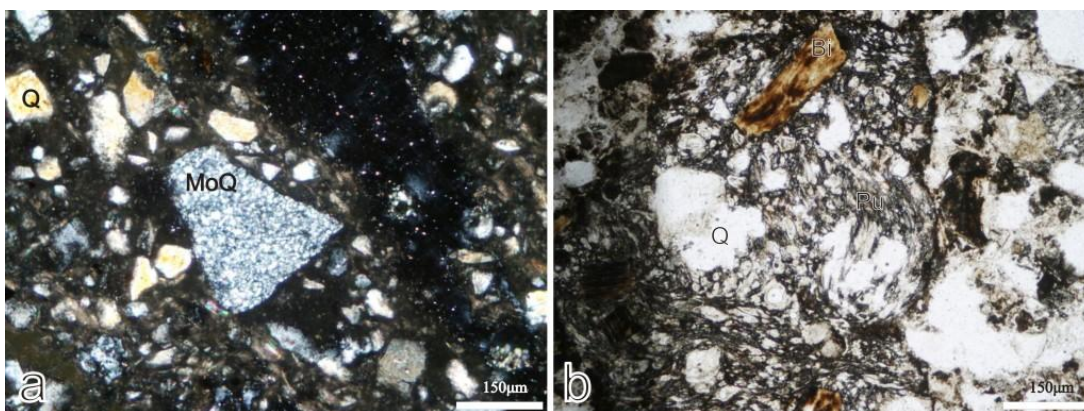
Figure 5.6 (a) Monolithic quarts (MoQ) within ignimbrites, crossed nichols, rhyolithic lithic tuff. Quartz (Q) + Biotite (Bi) + Amphibole (Amp) + Pumice + Lithic fragments; (b) Cellular pumice within ignimbrite, Biotite and euhedral and embayed quarts phenocrysts, crossed nichols.

5.2 Geochemistry of the Miocene Volcanic Units

5.2.1 Analytical Procedure

I selected forty one samples from the Beydağı and Payamtepe volcanic units and Karaağaç latite/andesite dikes. Rock powders of the fresh rock samples for major and trace element analysis were prepared by removing the altered surfaces in the Dokuz Eylül University sample preparation laboratories. Rock samples were crushed manually and then powdered using a tungsten carbide pulverizer. Whole-rock major element and trace-element analyses (by inductively coupled plasma mass spectrometry; ICP-MS) were performed at ACME Analytical Laboratories, Vancouver, Canada.

Table 5.1 Whole-rock major- and trace element data for the representative lava samples from the Uşak-Güre basin Fe₂O₃ is presumably Fe₂O₃ (total). Major oxides are wt.% and trace elements are in ppm. UTM coordinates are also given (E.C: Elmadağ Caldera; B.C: Beydağ Caldera; İ.C: İtecektepe Caldera; M.dağı: Muratdağı;Kb: Karabacaklar; Ka:Karaağaç; P.tepe:Payamtepe)

Sample#	U-31	U-32	U-52	U-58	U-68	U-70	U-80	U-96	U-98	U-104	U-118	U-122	U-124
Easting	718890	716206	713094	711875	718421	718094	721002	717545	716032	720955	710965	711773	711361
Northing	4296255	4296939	4292758	4293881	4292055	4290217	4298310	4200327	4300994	4303241	4302334	4305262	4305984
Unit	Beydağ	Beydağ	Beydağ	Beydağ	Beydağ	Beydağ	Beydağ	Beydağ	Beydağ	Beydağ	Beydağ	Beydağ	Beydağ
Center	E.C.	E.C.	E.C.	E.C.	E.C.	E.C.	E.C.	E.C.	E.C.	E.C.	E.C.	E.C.	E.C.
SiO₂	62.29	58.47	59.83	58.23	57.66	56.7	53.64	63.12	62.66	64.27	60.79	71.57	69.9
Al₂O₃	16.51	17.03	18.05	14.98	17.19	15.19	16.6	14.72	15.4	15.9	13.43	14.3	15.17
Fe₂O₃	4.11	5.02	3.55	4.28	3.78	5.97	6.9	4.27	3.82	4.43	4.83	0.64	2.32
MgO	1.28	2.84	1.86	3.63	1.95	3.71	4.3	1.48	1.53	0.77	3.36	0.13	0.85
CaO	1.55	4.28	2	5.96	3.57	5.69	7.91	3.96	4.05	2.69	4.47	0.19	2.34
Na₂O	2.15	2.63	1.44	2.44	2.11	2.65	3.13	2.3	2.46	2.91	2.47	0.81	3.4
K₂O	6.46	4.83	4.07	6.17	3.64	5.76	3.83	4.67	4.51	4.29	6.88	10.75	4.24
TiO₂	1	0.73	0.95	1.18	0.9	1.14	0.78	0.59	0.53	0.63	1.22	0.09	0.32
P₂O₅	0.55	0.29	0.23	0.71	0.44	0.69	0.44	0.22	0.21	0.26	0.7	0.06	0.11
MnO	0.03	0.1	0.03	0.06	0.13	0.07	0.1	0.07	0.06	0.12	0.08	<0.01	0.05
LOI	3.9	3.4	7.8	1.7	8.1	1.8	1.7	4.6	4.3	3.5	1.3	1.3	1.1
Total	99.82	99.67	99.83	99.39	99.49	99.42	99.38	99.98	99.55	99.77	99.57	99.84	99.78
Ba	1126	1330	1438	1760	1834	1713	1918	761	1028	1068	1214	709	935
Co	14.4	23.2	13.7	43.3	44.8	28.9	33.3	22	22.6	20.5	24.5	21.1	14.5
Cs	14.2	4.3	15.7	8.3	11.3	7.8	2.8	4.6	2.9	7.5	9.3	10.4	8.7
Hf	12.2	8.8	11.8	15.3	10.4	14.4	7.9	4.3	6	5.9	15.8	2.5	4.5
Nb	33	23.9	33.1	35.2	27.9	34.3	17	17.7	19.5	19.4	31.3	16.1	16.1
Rb	233	140	199	206	133	205	111	150	148	154	246	419	170
Sc	13	10	14	17	15	17	20	10	10	12	14	3	4
Cr	130.01	27.37	109.48	205.28	109.48	150.54	61.58	34.21	13.69	27.37	184.75	0	0
Sr	460	775	762	1085	1015	1129	1495	340	476	623	752	76	327
Ta	2.4	1.5	1.9	2.1	1.7	2.2	0.9	1.6	1.8	1.6	2	1.7	1.7
Th	36.2	26.5	32.6	25.6	30.8	34.1	26.2	26.8	30.5	31	28.7	17.8	24.7
U	16.6	8.6	9.7	9.1	18.9	9.7	7.5	4.3	9.5	9.1	11	6.1	6.5
V	85	105	131	145	204	130	203	33	75	52	131	<8	29
Zr	415	322	417	575	351	491	277	151	208	196	560	63	147
Y	61.6	23.3	20.3	33.1	25.4	26.4	29.2	19	22	30.1	25	20.2	18.5
La	64	62	68	76	76	81	76	40	44	61	67	31	39
Ce	110	117	134	152	151	162	152	74	84	126	134	53	73
Pr	15.3	13.4	14.4	18.6	17	19.1	18.54	8.5	9.9	15.29	16.1	6.3	7.9
Nd	55.4	46.2	48.9	68.6	61.4	71.4	70	30.8	35.8	57.8	62	21.4	26.7
Sm	10.1	7.6	8.3	11	10	11.2	11.1	5.2	6	9.5	9.5	3.9	4.9
Eu	2.07	1.71	2	2.51	2.39	2.47	2.81	1.11	1.4	2.05	2.05	0.76	0.94
Gd	9.13	5.52	5.9	8.2	7.44	8.43	8.5	4.14	4.79	7.42	7.13	3.4	3.87
Tb	1.43	0.79	0.84	1.13	1.05	1.09	1.09	0.59	0.7	1.07	0.88	0.57	0.58
Dy	8.06	4.17	4.21	5.72	5.04	5.24	5.47	3.26	3.75	5.73	4.57	3.29	3.11
Ho	1.71	0.78	0.72	1.02	0.9	0.92	0.96	0.6	0.73	1.03	0.78	0.62	0.59
Er	5.2	2.2	2.1	2.9	2.4	2.5	2.7	1.7	2.1	3	2	1.9	1.7
Tm	0.8	0.3	0.3	0.4	0.4	0.4	0.4	0.3	0.3	0.5	0.3	0.3	0.3
Yb	5	2.1	2	2.8	2.3	2.3	2.5	1.8	2.1	2.9	2.1	1.9	1.8
Lu	0.8	0.3	0.3	0.4	0.3	0.3	0.4	0.3	0.3	0.5	0.3	0.3	0.3
Pb	7.2	56.3	14.2	4.8	18.7	2	4.2	11.7	10.2	4.4	3.2	9	4.3
Ni	23	15	19	30	82	26	8	4	6	18	50	3	6
Mg#	57.8	71.4	69.8	78.9	69.4	73.2	73.3	60.4	63.8	43.4	75.4	47.2	61.7

Table 5.1 (Continued)

Sample#	U-125	U-162	U-163	U-164	U-100	U-101	U-165	U-1A	U-2	U-6	U-7B	U-8A	U-9
Easting	707481	711579	712825	715256	728504	729024	728081	679725	680022	679680	678302	681774	683398
Northing	4304526	4303606	4302780	4302750	4309002	4308651	4308796	4257800	4255923	4262981	4259019	4255201	4255644
Unit	Beydağ	Beydağ	Beydağ	Beydağ	Beydağ	Beydağ	Beydağ	Beydağ	Beydağ	Beydağ	Beydağ	Beydağ	Beydağ
Center	E.C.	E.C.	E.C.	E.C.	M.dağı	M.dağı	M.dağı	B.C.	B.C.	B.C.	B.C.	B.C.	B.C.
SiO_2	61.89	72.21	65.79	62.95	61.31	46.31	63.27	59.74	58.28	54.95	57.9	69.15	61.79
Al_2O_3	13.08	13.93	17.89	13.86	15.14	15.1	17.86	17.13	17.63	16.39	16.98	14.89	16.74
Fe_2O_3	4.4	1.75	3.12	4.22	4.61	6.57	3.54	5.25	4.79	6.61	5.52	2.53	4.99
MgO	3.18	0.71	1	2.36	2.51	2.12	0.74	1.94	1.89	3.95	2.85	0.82	2.32
CaO	3.85	1.51	0.82	3.54	4.12	10.3	1.19	5.17	5.11	8.17	5.99	2.21	4.51
Na_2O	1.69	2.79	2.17	2.63	2.49	2.56	4.78	3.47	3.21	2.61	2.85	3.08	2.8
K_2O	6.41	4.44	7.25	6.7	3.01	2.8	6.35	4.15	4.41	2.94	3.76	5.01	3.17
TiO_2	1.02	0.25	1.48	0.74	0.54	1.13	0.38	0.7	0.6	0.76	0.69	0.53	0.58
P_2O_5	0.65	0.09	0.47		0.2	0.75	0.25	0.33	0.3	0.35	0.34	0.24	0.2
MnO	0.07	0.02	0	0.05	0.07	0.27	0.06	0.06	0.08	0.1	0.08	0.02	0.1
LOI	3.2	2.1	5.8	1.3	5.8	12	1.2	1.7	3.3	2.8	2.6	1.2	2.4
Total	99.51	99.76	99.56	99.55	99.8	99.87	99.65	99.62	99.59	99.65	99.59	99.69	99.63
Ba	1137	843	1742	1225	530	677	1345	1273	1417	1303	1268	844	843
Co	26.8	10.9	11.2	41.2	20.5	27	17.2	21.5	39.1	25.6	48.4	21	22.6
Cs	15.9	17.9	10.1	12.4	6.7	5.7	5.1	4.6	11	8.9	7.8	12.4	6.5
Hf	14.4	4.2	16.6	15.4	4.4	8.1	8.8	8.8	9	5.6	7	8.1	5.4
Nb	32	16.3	39	31	15.6	23.6	26.8	20.9	22	12.9	17.3	29.2	12.3
Rb	244	196	238.5	233	111	112	259	126	132	93	113	221	120
Sc	12	16	22	11	14	25	3	13	10	22	16	7	15
Cr	205.28	41.06	177.91	20.53	41.06	54.74	0	41.06	20.53	177.91	123.17	27.37	41.06
Sr	708	219	918.1	753	580	550	557	860	1005	1017	873	573	663
Ta	2.4	2	16.6	2.2	1.5	2.1	1.9	1.2	1.3	0.8	1.2	2.4	0.8
Th	28.7	25.6	36.3	29.3	27.2	22	79.5	30.4	36.7	21.1	23.2	49.3	16
U	12.6	8.1	12.7	12.9	7.6	8.9	11.1	9	10.4	6.2	7.3	18.1	4.8
V	106	24	194	119	96	179	48	110	95	174	136	65	77
Zr	495	122	575.6	512	140	300	349	326	330	200	254	262	190
Y	22.5	18.4	28.5	21	17.7	31.9	18.2	27.4	23.9	23.9	24.8	25.5	22.4
La	61	27	90.8	64	44	47	117	69	79	61	62	94	43
Ce	125	49	187.5	124	84	99	207	128	148	113	117	164	85
Pr	14.9	5.9	22.47	14.5	9.6	12.8	21.3	14.2	15.9	13.5	13.4	16.5	9.6
Nd	55.5	20.7	88	53.4	34.8	51.9	70.3	51.1	56.5	48.5	46.6	52.8	34.9
Sm	8.9	4	14.53	8.5	5.7	9	8.8	7.9	8.4	7.9	7.5	8	5.7
Eu	1.9	0.75	3.3	1.91	1.23	1.85	1.82	1.83	1.97	1.93	1.74	1.54	1.4
Gd	6.76	3.31	11.67	6.42	4.55	7.2	5.62	6.05	6.08	5.97	5.71	5.82	4.68
Tb	0.88	0.55	1.57	0.87	0.66	1.05	0.67	0.77	0.74	0.82	0.84	0.8	0.72
Dy	4.33	2.98	7.36	4.21	3.5	5.68	3.27	4.28	4.02	4.34	4.42	4.07	3.79
Ho	0.75	0.57	1.2	0.69	0.65	1.08	0.58	0.9	0.8	0.79	0.82	0.77	0.75
Er	1.9	1.7	2.95	1.9	1.8	3.2	1.6	2.6	2.3	2.3	2.3	2.1	2.1
Tm	0.3	0.3	0.43	0.3	0.29	0.49	0.27	0.41	0.36	0.31	0.36	0.33	0.32
Yb	2	1.9	2.41	1.9	1.8	3.1	1.8	2.6	2.3	2.1	2.3	2.3	2.1
Lu	0.3	0.3	0.3	0.3	0.3	0.5	0.3	0.4	0.4	0.3	0.3	0.3	0.3
Pb	1.1	3.8	5	4	8.4	10.3	24.7	6.3	4.9	3.1	3.6	4	2.1
Ni	53	9	20.4	35	11	8	4	5	7	15	14	8	3
Mg#	76.1	64.1	67.2	71.1	70.6	58.7	47.9	61.9	63.5	72.5	69.4	58.8	67.2

Table 5.1 (Continued)

Sample#	U-11	U-12B	U-161	U-16	U-18	U-159	U-109	U-129	U-140	U-144	U-145	U-151	U-153
Easting	689154	686223	684976	699104	694208	700335	704002	700812	682025	699821	700219	798452	696902
Northing	4262995	4265117	4254692	4273348	4270965	4274259	4304552	4297446	4294992	4299059	4300394	4300031	4304774
Unit	Beydağ	Beydağ	Beydağ	Beydağ	Beydağ	Beydağ	P.tepe	P.tepe	P.tepe	P.tepe	P.tepe	P.tepe	P.tepe
Center	B.C.	B.C.	B.C.	I.C.	I.C.	I.C.	Kb.	Kb.	Kıran	K.b.	K.b.	K.b.	Yeniköy
SiO_2	62.01	56.53	62.36	61.63	56.9	63.95	57.83	61.93	52.42	61.35	61.56	61.46	61.49
Al_2O_3	17.24	17.05	17.89	15.85	19.24	17.93	15.57	15.68	12.4	14.02	15.17	14.95	13.67
Fe_2O_3	3.14	4.68	4.93	5.23	5.17	2.25	4.22	4.88	6.78	4.94	4.03	4.13	4.26
MgO	1.05	3.09	4.4	1.84	0.63	0.89	2.81	1.27	8.34	1.98	1.58	1.38	3.29
CaO	3.34	5.43	3.9	4.75	2.03	3.26	5.75	1.17	6.17	2.99	2.39	2.27	4.51
Na_2O	2.76	2.75	2.71	2.78	2.88	2.69	2.69	1.53	2.25	2.58	2.33	2.21	2.38
K_2O	4.27	3.82	3.54	4.58	6.35	3.39	5.76	9.86	6.34	6.2	6.98	6.72	7.09
TiO_2	0.58	0.7	0.79	0.82	0.96	0.67	1.21	1.11	1.8	1.02	1.18	1.13	1.2
P_2O_5	0.29	0.3	0.27	0.5	0.52	0.2	0.67	0.77	0.75	0.75	0.91	0.87	0.69
MnO	0.02	0.09	0.09	0.05	0.01	0.01	0.06	0.01	0.1	0.39	0.01	0.02	0.06
LOI	5.2	3.2	5.6	1.5	4.9	4.7	2.8	1.3	2	3.4	3.4	4.4	0.8
Total	99.88	99.59	99.68	99.52	99.59	99.9	99.4	99.55	99.49	99.66	99.62	99.54	99.51
Ba	1366	1348	1050	1740	2097	776	1894	2099	694	1324	1585	1543	1254
Co	13.9	22.1	19	23.7	15.8	6.7	58	15.6	40.5	29.5	15.6	16.5	31.3
Cs	8.9	11.2	7.1	10.9	10.3	8.3	6.4	11.3	9.5	65.9	11.9	15.3	14.9
Hf	6.2	6.1	6.8	10.3	13.6	5.8	14.7	15.1	24.7	14.3	16.8	15.7	16.5
Nb	16.6	16.8	20.8	26.5	40.6	14.5	28.3	24.3	55.1	23.3	27	25.9	33.8
Rb	149	133	113.1	173	222	129	193	355	248	223	226	233	300
Sc	11	15	12	15	11	23	21	6	20	10	10	10	12
Cr	54.74	47.9	34.21	205.28	88.95	88.95	164.22	0	513.19	0	0	0	205.28
Sr	937	927	485.6	865	884	514	1075	607	692	703	722	716	774
Ta	1.1	1.2	1.4	1.5	2.4	1	1.7	1.4	3.2	1.4	1.6	1.5	2.4
Th	27.4	29.7	21.3	22	39.3	18	27.9	16.2	25.7	15.7	17.5	17.6	31.9
U	8.6	9.1	6.5	6.7	9.6	6.3	9	7	5.6	7.1	6.5	5.9	13.5
V	87	111	101	68	124	44	188	86	149	99	103	102	107
Zr	228	208	238.4	354	513	204	497	551	886	497	610	560	569
Y	17.6	22.2	20.3	42.8	25.8	23.3	24.9	21.5	22.1	29.1	19.5	19.9	22.5
La	64	64	52.4	69	94	43	72	50	90	40	45	43	64
Ce	115	122	95.9	111	177	87	138	110	199	85	93	87	135
Pr	13	13.9	11.75	15.2	20.1	10.6	17	13.6	23.8	10.2	11.1	10.6	16.3
Nd	44.8	50.2	42.7	57.2	69	40.8	64.4	52.1	87.6	40.4	43.5	40.7	62.7
Sm	6.7	8	7.29	9.5	11.3	6.9	10.6	8.6	11.8	7	7.3	7	9.9
Eu	1.63	1.87	1.59	2.18	2.51	1.63	2.41	1.86	2.44	1.59	1.74	1.63	2.14
Gd	4.73	5.92	5.79	8.08	7.89	5.72	8.11	6.36	8.13	5.79	5.81	5.55	6.96
Tb	0.63	0.83	0.81	1.19	1.05	0.83	1.06	0.85	0.96	0.84	0.83	0.78	0.93
Dy	3.11	4.17	4.28	6.52	4.99	4.38	5.13	4.15	4.57	4.28	3.74	3.86	4.45
Ho	0.56	0.74	0.77	1.32	0.86	0.77	0.92	0.67	0.77	0.83	0.66	0.66	0.76
Er	1.6	2.2	2.18	3.9	2.4	2.1	2.5	1.9	1.9	2.3	1.6	1.7	2
Tm	0.23	0.31	0.34	0.57	0.35	0.35	0.38	0.29	0.3	0.35	0.23	0.26	0.3
Yb	1.6	2.2	2.05	3.6	2.2	2.2	2.2	1.8	1.7	2.1	1.4	1.6	1.9
Lu	0.2	0.3	0.31	0.5	0.3	0.3	0.3	0.3	0.3	0.3	0.2	0.2	0.3
Pb	3.4	2.9	10	5.5	3	4.3	3.2	11.4	0.6	1.4	3.5	2.1	3.3
Ni	4	6	16.6	23	21	3	51	31	269	35	59	60	39
Mg#	59.6	74.4	53.8	60.8	34.9	63.5	74.6	53.4	84.4	63.8	63.3	59.5	77.3

Table 5.1 (Continued)

Sample#	U-82	U-85	Standarts	
Easting	725156	702429		
Northing	4287125	4283611		
Unit				
Center	Ka.	Ka.	SO-18	DS-7
SiO$_2$	53.98	54.05	58.09	–
Al$_2$O$_3$	14.57	11.57	14.14	–
Fe$_2$O$_3$	4.93	5.98	7.61	–
MgO	4.41	4.24	3.34	–
CaO	6.63	5.66	6.38	–
Na$_2$O	1.72	3.2	3.7	–
K$_2$O	5.28	2.43	2.15	–
TiO$_2$	1.79	1.86	0.69	–
P$_2$O$_5$	0.97	0.88	0.804	–
MnO	0.06	0.05	0.39	–
LOI	4.8	9	1.9	–
Total	99.28	99.1	99.76	–
Ba	2106	893	507	–
Co	27.4	38.4	26.6	–
Cs	3.7	15.7	6.8	–
Hf	20	31.8	9.8	–
Nb	34.9	76.9	21.8	–
Rb	75	280	28	–
Sc	28	19	21.8	–
Cr	650.04	745.83	28	–
Sr	1113	746	404.3	–
Ta	2	4.8	7.2	–
Th	20.9	37.8	9.7	–
U	6.3	6.6	16	–
V	222	151	206	–
Zr	695	1081	248.2	–
Y	30.5	26.7	31.2	–
La	100	121	11.9	–
Ce	213	270	26.5	–
Pr	27.1	32.7	3.4	–
Nd	104.3	121.2	13.9	–
Sm	16.5	17	2.92	–
Eu	3.68	3.3	0.86	–
Gd	11.63	11.53	2.94	–
Tb	1.44	1.29	0.51	–
Dy	6.65	5.72	2.94	–
Ho	1.07	0.88	0.61	–
Er	2.7	2.3	1.79	–
Tm	0.38	0.31	0.28	–
Yb	2.3	2	1.75	–
Lu	0.3	0.3	0.27	–
Pb	0.9	1.5	–	20.4
Ni	56	258	–	56.8
Mg#	79.8	75.7	–	–

A 0.2-g sample aliquot was weighed into a graphite crucible and mixed with 1.5 g of LiBO$_2$ flux. The flux/sample charge was heated in a muffle furnace for 15 min at 1050 °C. The molten mixture was removed and immediately poured into 100 mL of 5% HNO$_3$ (American Chemical Society–grade nitric acid in deionize water). The major and trace element results are given in Table 5.1, and the detection limits of the geochemical analyses are given in Table 5.2.

5.2.2 Major Element Characteristics and Classification of the Volcanic Rocks

The volcanic rocks are classified on a SiO$_2$ versus K$_2$O+Na$_2$O (TAS) diagram (Figure 5.7).

Table 5.2 Detection levels of elements during the geochemical analyses of rock samples for ACME Laboratory.

Elements	Group 4A Det. Lim.	Upper Limit
SiO_2	0.01 %	100 %
Al_2O_3	0.01 %	100 %
Fe_2O_3	0.04 %	100 %
CaO	0.01 %	100 %
MgO	0.01 %	100 %
Na_2O	0.01 %	100 %
K_2O	0.01 %	100 %
MnO	0.01 %	100 %
TiO_2	0.01 %	100 %
P_2O_5	0.01 %	100 %
Cr_2O_3	0.002 %	100 %
LOI	0.1 %	100 %
C	0.01 %	100 %
S	0.01 %	100 %

Elements	Group 4A Det. Lim.	Group 4B Det. Lim.	Upper Limit
Au	–	0.5 ppb	100 ppm
Ag	–	0.1 ppm	100 ppm
As	–	1 ppm	10000 ppm
Ba	5 ppm	1 ppm	50000 ppm
Be	–	1 ppm	10000 ppm
Bi	–	0.1 ppm	2000 ppm
Cd	–	0.1 ppm	2000 ppm
Co	20 ppm*	0.2 ppm	10000 ppm
Cs	–	0.1 ppm	10000 ppm
Cu	5 ppm*	0.1 ppm	10000 ppm
Ga	–	0.5 ppm	10000 ppm
Hf	–	0.1 ppm	10000 ppm
Hg	–	0.1 ppm	100 ppm
Mo	–	0.1 ppm	2000 ppm
Nb	5 ppm*	0.1 ppm	50000 ppm
Ni	20 ppm	0.1 ppm	10000 ppm
Pb	–	0.1 ppm	10000 ppm
Rb	–	0.1 ppm	10000 ppm
Sb	–	0.1 ppm	2000 ppm
Sc	1 ppm	–	10000 ppm
Se	–	0.5 ppm	100 ppm
Sn	–	1 ppm	10000 ppm
Sr	2 ppm	0.5 ppm	50000 ppm
Ta	20 ppm*	0.1 ppm	50000 ppm
Th	–	0.2 ppm	10000 ppm
Tl	–	0.1 ppm	1000 ppm
U	–	0.1 ppm	10000 ppm
V	–	8 ppm	10000 ppm
W	–	0.5 ppm	10000 ppm
Y	3 ppm	0.1 ppm	50000 ppm
Zn	5 ppm*	1 ppm	10000 ppm
Zr	5 ppm	0.1 ppm	50000 ppm
La	–	0.1 ppm	50000 ppm
Ce	30 ppm*	0.1 ppm	50000 ppm
Pr	–	0.02 ppm	10000 ppm
Nd	–	0.3 ppm	10000 ppm
Sm	–	0.05 ppm	10000 ppm
Eu	–	0.02 ppm	10000 ppm
Gd	–	0.05 ppm	10000 ppm
Tb	–	0.01 ppm	10000 ppm
Dy	–	0.05 ppm	10000 ppm
Ho	–	0.02 ppm	10000 ppm
Er	–	0.03 ppm	10000 ppm
Tm	–	0.01 ppm	10000 ppm
Yb	–	0.05 ppm	10000 ppm
Lu	–	0.01 ppm	10000 ppm

A significant feature of the genesis and evolution of Miocene magmas in the voluminous Uşak-Güre basin's volcanic field is the absence of erupted basalt and the rarity of even mafic basaltic andesite (56.75 wt % SiO_2 or 4.08 wt % MgO). The lava samples of the Beydağ volcanic unit plot in a wide compositional range including shoshonite, latite, andesite, dacite, trachydacite and rhyolite (Figure 5.7a). These samples show high-K calc-alkaline to shoshonitic affinity (Figure 5.7b). Some samples from the Elmadağ caldera of the Beydağı volcanic unit also show ultrapotassic affinity according to Na_2O-K_2O diagram of Pecerillo & Taylor (1976) (Figure 5.7c).

However, according to the definition of Foley et al. (1987), the Kıran lava flows (U-140) and Yeniköy dike (U-153) are the only samples with high enough MgO (3.34–8.57 wt %) to be classified as ultrapotassic. With the exception of some of the most mafic lavas which are ferroan (Figure 5.7d), the samples are dominantly magnesian (or calc-alkaline in the sense of Miyashiro, 1974). The samples of the Payamtepe volcanic unit generally have higher K_2O contents than the Beydağı volcanic unit, and they plot above the alkaline–calc–alkaline discrimination line of Irvine & Baragar (1971). They are classified as ultrapotassic latite and trachyte/trachydacite. Among them, the only shoshonitic Kıran sample has the lowest SiO_2 content, plotting on the line between latite and shoshonite.

The Yeniköy NW–SE-trending dikes and the Karabacaklar lava flows are classified as trachyte/trachydacite and show an ultrapotassic affinity. The samples from the Karaağaç dikes are classified as either latite or andesite.

Volcanic rocks from the three calderas of the Beydağı volcanic unit exhibit increasing K_2O and Na_2O contents from Beydağ caldera in the south to Elmadağ caldera in the north. The Beydağı volcanic unit samples have K_2O and Na_2O contents varying in the range of 3.04–10.91 and 0.82–3.54 (wt % on an anhydrous base). Their SiO_2 and MgO contents range from 54.94 to 73.91 and from 0.13 to 4.40 (wt %), respectively. The Payamtepe volcanic unit samples have K_2O and Na_2O contents in the range of 5.21–10.04 and 1.56–5.96 (wt %), respectively, which are

similar to those of the Beydağı volcanic unit. The shoshonitic Kıran sample of the Payamtepe volcanic unit has lower SiO_2 and MgO contents than the Karabacaklar lava flows and the Yeniköy latite dikes (SiO_2=53.85 and MgO=8.57 wt %).

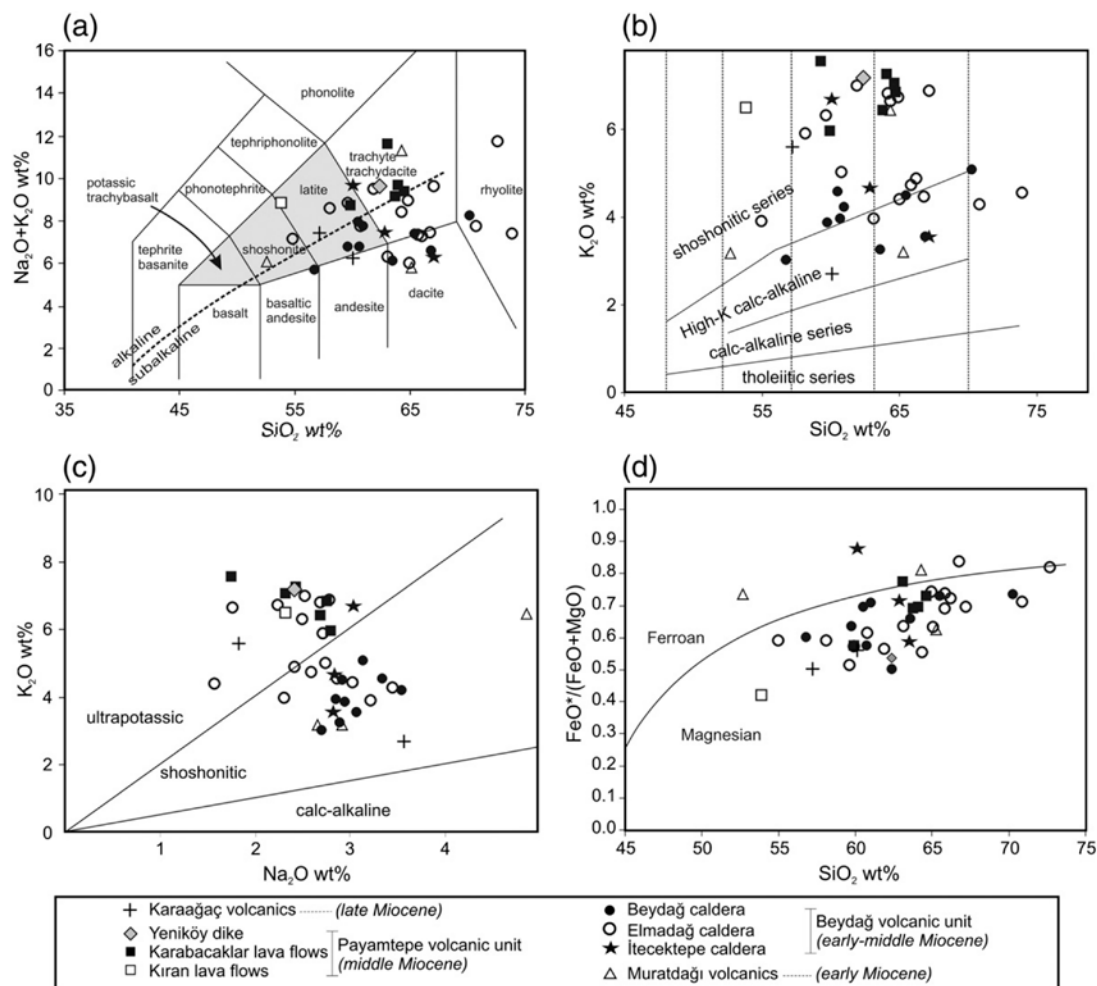Figure 5.7 Discrimination and classification diagrams for the volcanic rocks of the Uşak-Güre basin : (a) K_2O+Na_2O–SiO_2 (TAS) diagram of Le Maitre (2002); alkaline-subalkaline line is according to Irvine & Baragar (1971), I used potassic rock names in the shaded areas, (b) K_2O–SiO_2 diagram of Pecerillo & Taylor (1976). Data are plotted a water-free basis, (c) K_2O versus Na_2O diagram of Pecerillo & Taylor (1976), (d) FeO*/(FeO*+MgO) versus SiO_2 (dividing line from Miyashiro, 1974).

The volcanic rocks from the three calderas of the Beydağı volcanic unit show generally decreasing trends in Fe_2O_3(t), MgO and CaO with increasing SiO_2 contents (Figure 5.8). The K_2O contents of the samples from the Beydağ and Elmadağ calderas of the Beydağı volcanic unit are nearly constant as their silica contents increase. TiO_2 contents of the Beydağı volcanic unit samples show a slight

decrease with increasing silica. The Payamtepe volcanic unit samples also show decreases in $Fe_2O_3(t)$, MgO, CaO and TiO_2 with increasing SiO_2 contents (Figure 5.8).
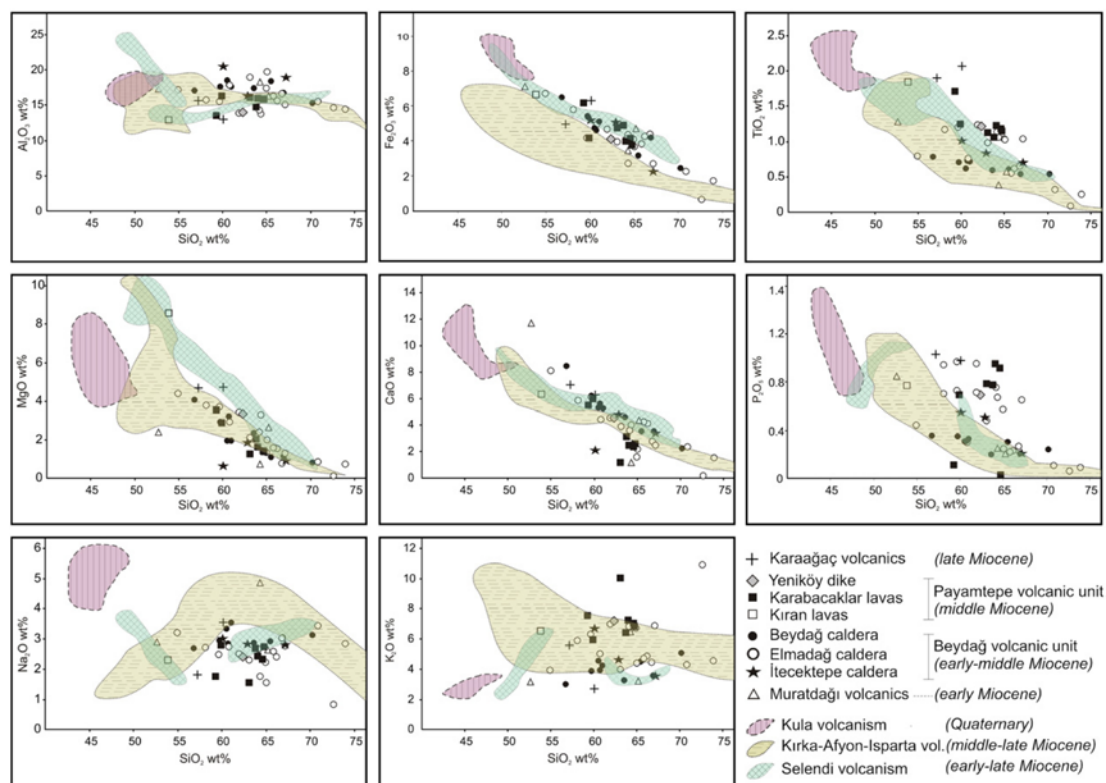

Figure 5.8 SiO_2 variation diagrams for selected major elements of the volcanic rocks in the Uşak Güre basin compared to selected suites from adjacent areas of Uşak-Güre basin. Data sources are: Ersoy & Helvacı, 2007; Ersoy et al., 2008 (for Selendi basin); Innocenti et al., 2005 (for Kula volcanic rocks); Floyd et al., 1998 (for Kırka and Afyon volcanic rocks); Aydar et al., 1995 (for Afyon volcanic rocks); and Francalanci et al., 2000 (for Kırka, Afyon and Isparta volcanic rocks).

5.2.3 Trace Element Characteristics

Trace element data from volcanic rocks of the Uşak-Güre basin is presented in Table 1. Nickel and Cr contents of the Beydağı volcanic unit samples vary in the range of 2–82 and 14–205 ppm. These values are 31–60 and 164–226 ppm for the Payamtepe volcanic unit samples, except for the one sample from shoshonitic Kıran sample which has 269 ppm Ni and 513 ppm Cr. Taking into account the high SiO_2 (54.0–73.9 wt%) and generally low MgO contents (4.4–0.1 wt%), the Ni and Cr contents of the Beydağı and Payamtepe volcanic units indicate that these rocks

represent highly evolved magmas (Figure 5.10). In this respect, sample U-140 of the shoshonitic Kıran rocks represents the most mafic volcanic rock in the region. Relatively higher Ni and Cr values are observed in the Karaağaç latite/andesite samples (56–258 and 650–745 ppm, respectively).

Selected trace element contents of the volcanic rocks of the Uşak- Güre basin are plotted against their SiO_2 contents (Figure 5.9). The samples from the three calderas of the Beydağı volcanic unit show decreasing trends in Ba and Sr. The İtecektepe caldera samples of the Beydağı volcanic unit show decreasing Rb with respect to increasing SiO_2 contents. Tantalum, Nb, Zr and Y contents are nearly constant for the Beydağı volcanic unit samples. These samples show a clear negative correlation between the V and SiO_2 contents. Barium and Rb contents of the Payamtepe volcanic unit increase, but Sr contents are nearly constant.

On a chondrite (C)-normalized REE diagram (Figure 5.10c), the samples from the Beydağı volcanic unit are characterized by selective enrichment in light rare earth elements (LREE). On this diagram, the Beydağı volcanic unit samples have Eu/Eu* values between 0.63 and 0.88. The Payamtepe volcanic unit has similar REE patterns to the Beydağı volcanic unit. The most mafic unit in the region, the shoshonitic Kıran rocks of the Payamtepe volcanic unit, have the highest LREE and relatively lower HREE contents with respect to the other rocks from the Payamtepe and Beydağı volcanic units. On the other hand, the shoshonitic Kıran rocks have higher LREE contents than the other units. Their Eu/Eu* values are between 0.72 and 0.81. The Beydağı and Payamtepe volcanic units are also characterized by enrichment in LREE and large ion lithophile elements (LILE) over HREE and high field strength elements (HFSE), producing negative anomalies in Ta, Nb and Ti on a primitive mantle (PM)-normalized multi-element diagram (Figures 5.10e, f and g). Samples from the Beydağı and Payamtepe volcanic units show negative P anomalies (e.g., Beydağı volcanic unit) that are most probably due to apatite fractionation in the more silicic volcanic rocks.
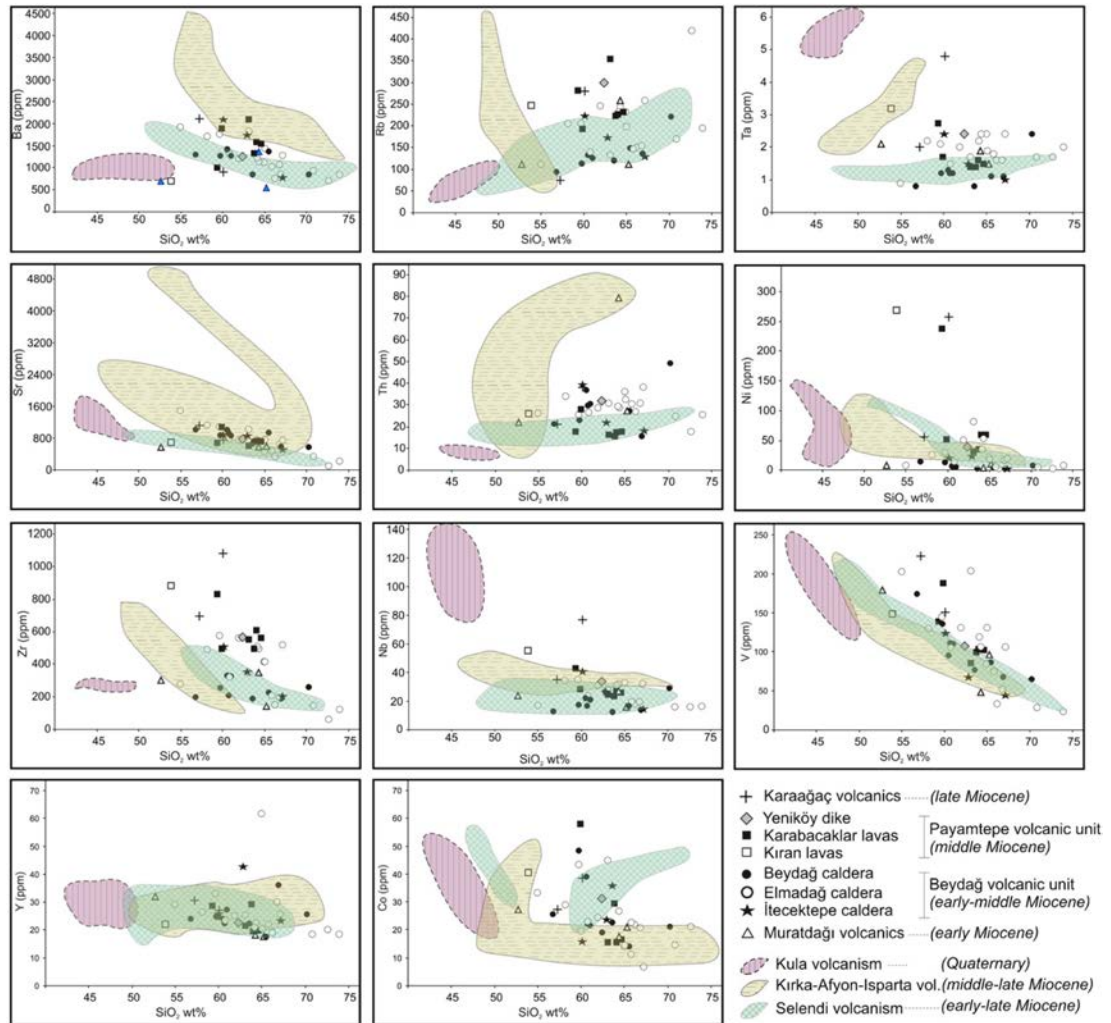
Figure 5.9 Variation of selected trace elements of the volcanic rocks in the Uşak-Güre basin compared to selected suites from adjacent areas of Uşak-Güre basin. Data sources are Ersoy & Helvacı (2007) and Ersoy et al. (2008) (for Selendi basin); Innocenti et al. (2005) (for Kula volcanic rocks); Floyd et al. (1998) (for Kırka and Afyon volcanic rocks); Aydar et al. (1995) (for Afyon volcanic rocks); and Francalanci et al. (2000) (for Kırka, Afyon and Isparta volcanic rocks).

5.2.4 Comparison with Volcanic units in Adjacent Basins

Despite the fact that Quaternary sodic alkaline Kula volcanic rocks (see Figure 5.1 for Kula region) are considered to have been derived from asthenospheric mantle, unaffected by subduction-related metasomatism (Güleç, 1991; Richardson & Bunbury, 1996; Seyitoğlu, 1997; Aldanmaz et al., 2000; Alıcı et al., 2002; Innocenti et al., 2005), the data are given for a comparison of the different magma sources through the Cenozoic interval.

The major and trace element contents of the several volcanic units from the adjacent Neogene basins are shown on Figures 5.8 and 5.9. These diagrams show that Neogene volcanic rocks from the Selendi basin located to the west of the Uşak-Güre basin has very similar $Fe_2O_3(t)$ and CaO trends but less similar MgO and Al_2O_3 trends.

The other major elements display discrepancies and have scattered trends with respect to SiO_2. The Kula and Selendi volcanic rocks have lower SiO_2 and higher MgO contents than the volcanic rocks of the Uşak-Güre basin. Major element variations of the volcanic rocks samples from the Kırka-Afyon-Isparta region located to the east of the Uşak-Güre basin (Figure 5.1) display some differences from the volcanic rocks of the Uşak-Güre basin. Although the negative trends of $Fe_2O_3(t)$, CaO and MgO and the nearly flat trend for Al_2O_3 versus SiO_2 are similar to the volcanic rocks of the Uşak-Güre basin , their major element variations are wider.

In addition, the Kırka-Afyon-Isparta volcanic rocks show more distinctive negative trends for TiO_2 and P_2O_5 versus silica. Ba Sr, Th, Nb, V and Y show comparable trends for all the volcanic rocks (Figure 5.9). Volcanic rocks of the Selendi basin and Kula volcanic rocks show positive trend for Rb and Th whereas the Kırka-Afyon-Isparta volcanic rocks show negative trends. In Figure 5.9, a gradual depletion of Ta from volcanic rocks in the Kula, Kırka-Afyon-Isparta, Uşak-Güre basin to Selendi basin is apparent. The Selendi, Kırka-Afyon-Isparta and Kula volcanic rocks show a slight negative trend in their Zr contents; volcanic rocks in the Uşak-Güre basin also have a weakly negative trend against SiO_2. Gradual depletion of V from volcanic rocks in the Uşak-Güre basin, Selendi and Kırka-Afyon-Isparta to Kula respectively are very distinctive (Figure 5.9).

Normalized-MORB and REE chondrite incompatible trace-element comparisons for each of the basins are shown in Figures 5.10 and 5.11. The MORB-normalized trace element patterns for the early Miocene volcanic rocks of the Uşak-Güre basin shows significant enrichment with respect to the early Miocene volcanic rocks in the Selendi basin, but the REE patterns of these rocks are similar.

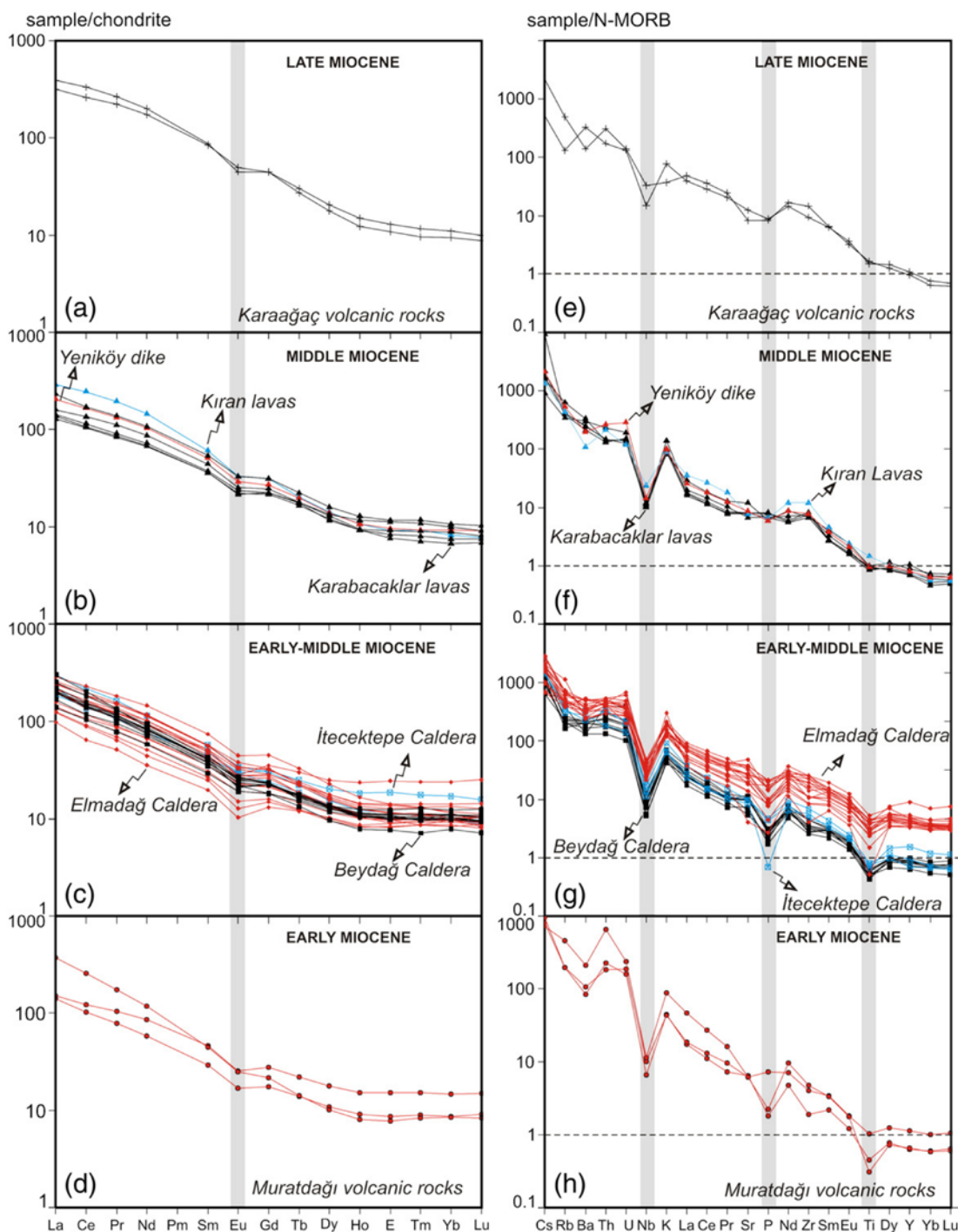Figure 5.10 Chondrite-normalized REE (a–c) and MORB-normalized (e–g) multi-element diagrams for the volcanic rocks of the Uşak-Güre basin . Normalizing values are from Sun & McDonough (1989).

Early–middle Miocene volcanic rocks in the Selendi and Uşak-Güre basin show similar NMORB and Chondrite-normalized trace element patterns, while the Kırka-Afyon-Isparta volcanic rocks are slightly enriched and show positive Pb anomalies.

The Quaternary Kula volcanic rocks, on the other hand, are characterized by smoother trace element patterns and have the lowest LREE contents, while the early–middle Miocene Selendi volcanic rocks show large Rb and Nb depletions. The Late Miocene Kırka-Afyon-Isparta volcanic units are characterized by enriched LILE patterns (Figures 5.10d, e and f). From the late Miocene to the Quaternary, an appreciable LREE enrichment is observed from the Miocene volcanic rocks of the Kırka-Afyon-Isparta, Selendi and Uşak-Güre basins to the Kula volcanic rocks, respectively (Figures 5.10d, e and f). The radiometric ages from the Beydağı and Payamtepe volcanic units are crucial for understanding the time of deposition of the İnay group. The youngest and oldest radiometric ages are important because the type sections of the İnay group (e.g. Ahmetler formation and Ulubey formation observed in extensive area of western Anatolia in NE–SW-trending basins) are taken from the Uşak-Güre basin. Based on our correlations, the deposition of the İnay group commenced as early as ~17 Ma in the north of the Uşak-Güre basin.

The $^{40}Ar/^{39}Ar$ dates of the Payamtepe volcanic unit restrict its activity to a period between 16.01±0.08 and 15.93±0.08 Ma. This evidence leads to two important observations regarding the evolution of Uşak-Güre basin: (1) the İnay group accumulated from late early Miocene (17.29 Ma), not early middle Miocene as proposed previously (Seyitoğlu, 1997), to middle Miocene (12.15 Ma) for the Uşak-Güre basin , and (2) the basin has been affected by an extensional tectonic regime since late early Miocene, and two different compositional volcanic activities are shown by the Beydağı volcanism (early–middle Miocene) and the Payamtepe volcanism (middle Miocene).

5.3 Discussion

5.3.1 Petrogenesis of the Volcanic Units

Variations in the major element abundances of the Uşak-Güre volcanic rocks display a complex petrogenetic evolution. It is apparent from the scatter on the major element diagrams (e.g. MgO, P_2O_5, TiO_2, K_2O) that the volcanic rocks are not part

of a single differentiation series; on the contrary, there are multiple magma series, each with its own parental magmas and differentiation trends (Figure 5.8).

The trends on the major and trace element Harker variation diagrams (Figures 5.8 and 5.9) likely suggest that fractional crystallization processes have played an important role in the genesis of the volcanic rocks in the Uşak-Güre basin, and the petrographic observations indicate that plagioclase was a major fractionating phase in the genesis of the volcanic rocks. This is geochemically evidenced by combined decreases in Sr and CaO, nearly flat or slightly decreasing Al_2O_3 contents and the Eu/Eu* values lower than 1. Decreases in CaO, Sc and V contents of the Beydağı and Payamtepe volcanic units may be explained by clinopyroxene fractionation.

Flat trends in the K_2O contents with respect to silica of the volcanics may also be indicative of fractionation of alkali feldspars. The presence of scarce amphibole in many of the samples indicates that this phase may also have influenced the geochemical evolution of the magmas, as suggested by the slightly decreasing trends in Y versus increasing SiO_2. The Zr contents of samples from the Beydağ volcanic unit slightly decrease with increasing silica indicating minor zircon fractionation. In addition, decreases in LREE contents with increasing SiO_2 may indicate apatite fractionation. Negative correlation between SiO_2 and Ni (and also Co) may reflect the effects of olivine fractionation, although no clear relationship exists for the Beydağı and Payamtepe volcanic units. Scattered trends of Ni and Co versus SiO_2 contents of the Beydağı and Payamtepe volcanic units may reflect magmatic mixing processes between evolved (low Ni-Co concentrations) and more primitive (high Ni-Co concentrations) magmas (Figure 5.9).

In the light of these data, and the petrographic observations, it is apparent that the geochemical compositions of the Beydağı and Payamtepe volcanic units were mainly modified by fractionation of plagioclase+clinopyroxene+olivine±amphibole+K-feldspar±apatite±zircon. Magma mixing processes may also have influenced the major and trace element variations of the volcanic rocks. Sr-Nd isotopic data from the Neogene volcanic units in western Anatolia indicate that large amounts of crustal

materials were involved in the genesis of the andesitic-dacitic volcanic rocks in Western Anatolia (e.g. Güleç, 1991; Aldanmaz et al., 2000). In the light of these observations, it is likely that fractional crystallization was accompanied by crustal assimilation. In order to better constrain the fractional crystallization and mixing processes, I have modelled trace element contents of the volcanic rocks (Figure 5.12).
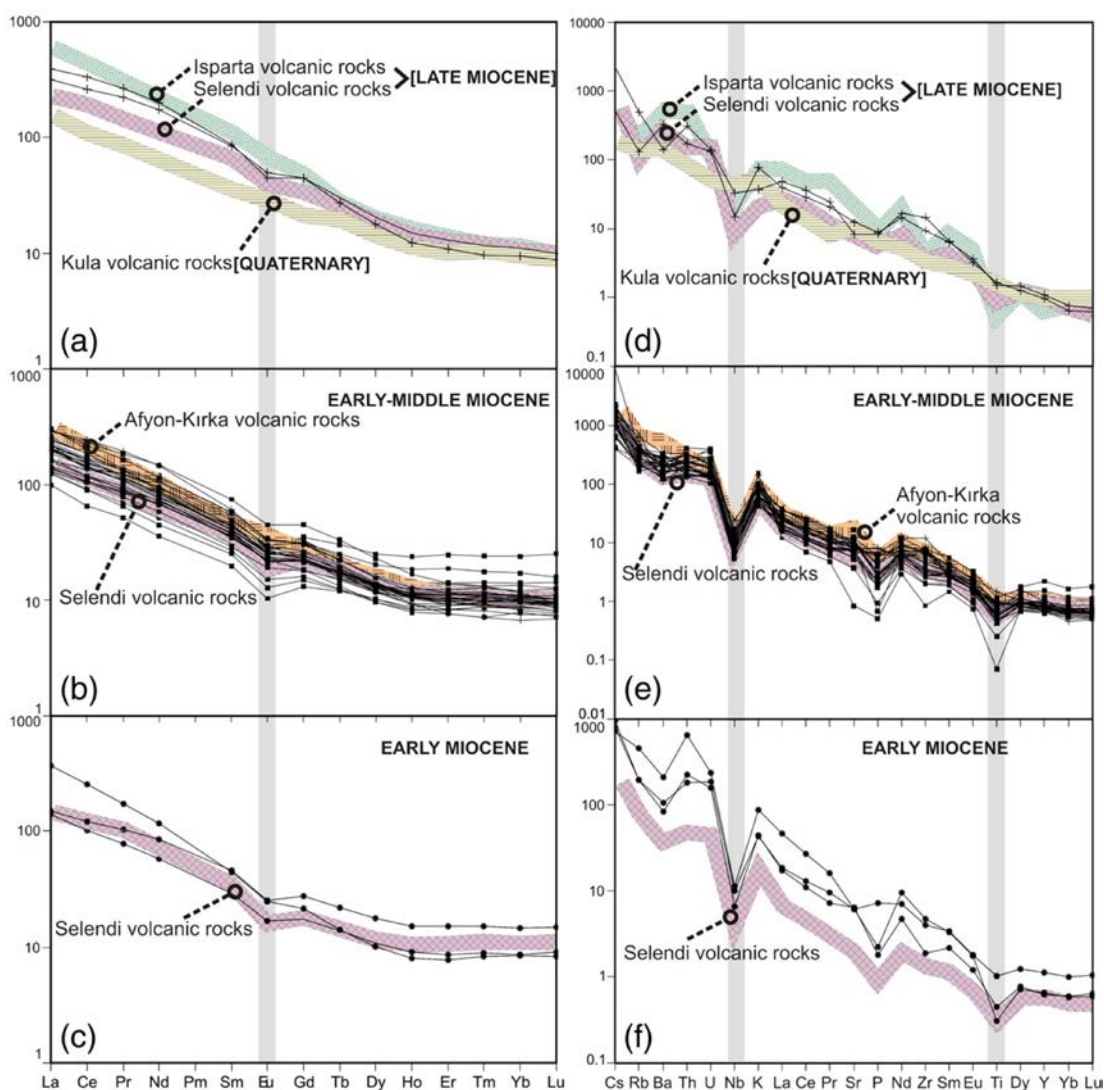

Figure 5.11 Chondrite-normalized REE (a–c) and MORB-normalized (e–g) multi-element diagrams for the volcanic rocks from the Uşak-Güre basin and adjacent basins. Normalizing values are from Sun & McDonough (1989).

As the major element interpretations indicate that plagioclase and clinopyroxene were the main fractionation phases in the genesis of the volcanics, Sc and V (which

are compatible in clinopyroxene) have been modeled against Sr (compatible for plagioclase). The fractionating mineral assemblage is chosen as plg(0.60)+cpx(0.20)+olv(0.10)±amp(0.10)+K-feld(0.10). The starting magma composition is accepted to be represented by sample U-80, which has the lowest SiO$_2$ and highest MgO contents among the Beydağı volcanic unit samples (SiO$_2$=53.64, MgO=4.30 wt%). The partition coefficients used in the models are given in Table 5.3. In order to explore the effects of the magma mixing with relatively primitive magmas, bulk mixing between sample U-80 and sample U-140 from the shoshonitic Kıran rocks (the most mafic sample in the region; SiO$_2$=52.42, MgO=8.34 wt%) and sample U-80 is also shown.
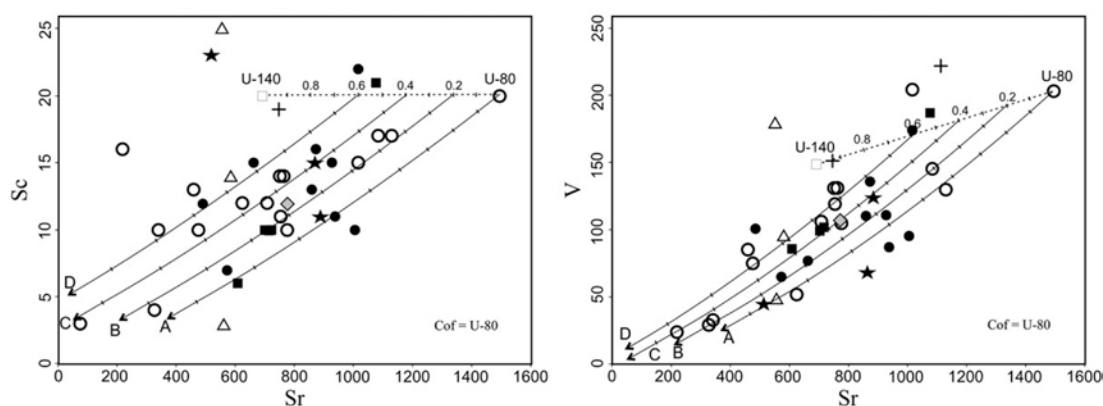
Figure 5.12 (a, b) Fractional crystallization and mixing models for the lavas from the Uşak-Güre basin. Dashed lines represent the bulk mixing between the sample U-140 (most mafic sample from the Payamtepe volcanic unit) and the sample U-80 (the most mafic sample from the Beydağ volcanic unit). Solid lines represent fractional crystallization trajectories. FC curves are calculated using several starting compositions representing by sample U-80 (A) and several degrees of mixing between U-80 and U-140 (B-D).

It is apparent from Figure 5.12 that the volcanic rocks from the Uşak-Güre basin are products of a complex petrogenetic evolution. Their genesis includes magma mixing and fractional crystallization processes which were likely accompanied by crustal assimilation. Complex relationships between these processes are likely responsible for the scattered patterns on the major and trace element Harker variation diagrams. The models are most compatible with samples of the Beydağı volcanic unit having been affected from ca. 0% to 60% mixing with the more mafic magmas of the Payamtepe volcanic unit, with plagioclase dominating the fractional

crystallization processes. The Karaağaç dikes are difficult to model because there is limited geochemical data.

The volcanic rocks of the Uşak-Güre basin show significant enrichments in LILE and LREE with negative Nb and Ta anomalies which are common characteristics of subduction-related enrichment processes. On a Ta/Yb versus Tb/Yb diagram, the volcanic rocks from the Uşak-Güre basin plot parallel to the mantle array with higher Th/Yb ratios, which also indicates that they have a subduction related chemical component to their genesis (Figure 5.12, e.g. Pearce, 1983). The volcanic rocks also show a trend of enrichment of incompatible elements which can be explained by fractional crystallization, supporting the fractionation histories modelled above.

Table 5.3 Mineral/liquid partition coefficients used in fractional crystallization models on Figure 5.9. From compilation of Rollinson (1993).

	Sr	V	Sc
Olivine	_	0.08	0.30
Clinopyroxene	0.08	1.10	3
Plagioclase	2.52	0.01	0.01
K-feldspar	2	0.01	0.01
Amphibole	0.30	15	10

Th/Yb versus Ta/Yb ratios of the volcanic rocks plot are above the mantle array (Figure 5.13). The shift to higher Th/Yb ratios is explained by either (1) subduction-related contributions to the mantle source of the volcanic rocks or (2) crustal contamination of the magmas in shallow level crustal magma chambers. As proposed previously (e.g. Yılmaz, 1989; Güleç, 1991; Aldanmaz et al., 2000), the high Th/Yb ratios of even the most mafic magmas indicate that their mantle source was affected by subduction-related components. The isotopic characteristics of the lavas also suggest a lithospheric mantle source that was metasomatized by subduction-related processes (Aldanmaz et al., 2000; Innocenti et al., 2005). Depletions of HFSE relative to mantle-normalized concentrations of Rb, Ba, K and Th (Figure 5.10) also suggest an enriched lithospheric mantle source for the volcanic rocks (e.g. Weaver &

Tarney, 1984; Thirlwall et al., 1994; Taylor & McLennan, 1995; Parat et al., 2005). In the light of these data, I propose that the wide-spectrum compositions of the volcanic rocks are related to (1) melting of heterogeneously metasomatized mantle lithosphere, (2) fractional crystallization and crustal contamination processes in shallow-level lithospheric magma chambers and (3) mixing processes. This interpretation accords with previous studies in western Anatolia (e.g. Yılmaz, 1989; Güleç, 1991; Aldanmaz et al., 2000; Innocenti et al., 2005; Ersoy et al., 2008).
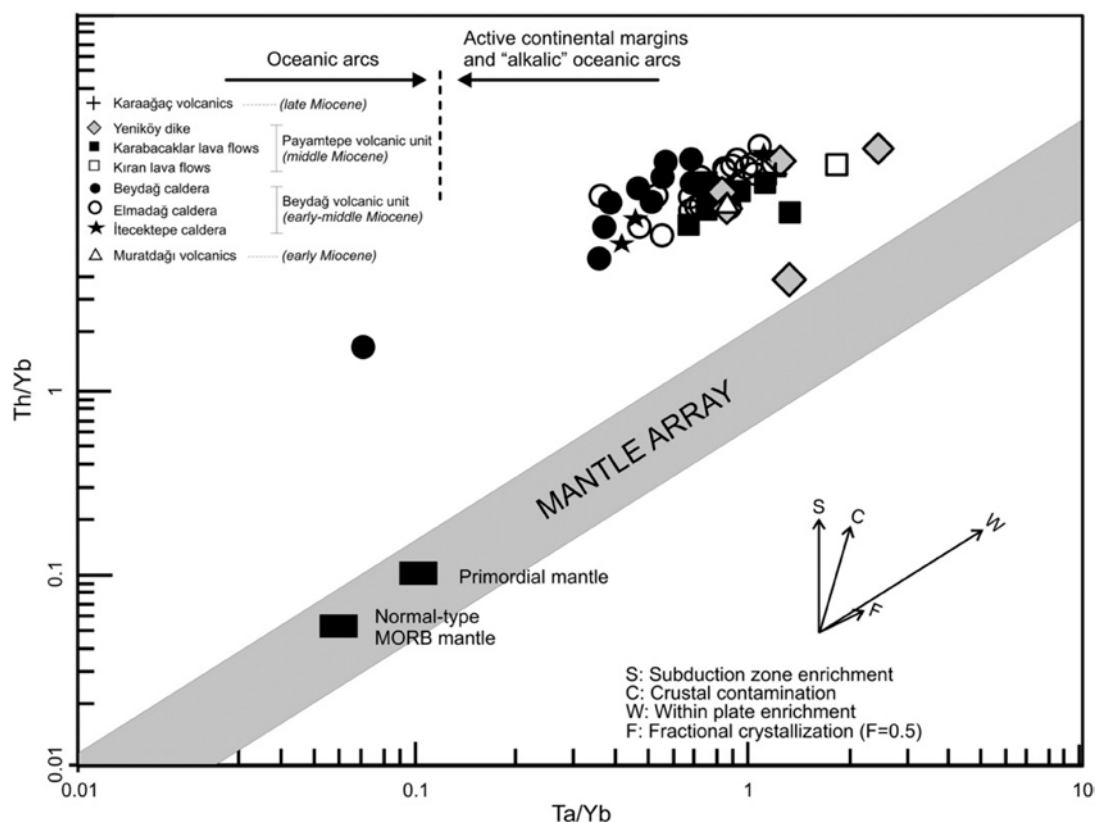
Figure 5.13 Th/Yb against Ta/Yb log-log diagram (after Pearce, 1983) for basic and intermediate volcanic rocks from the Uşak-Güre basin. The volcanic samples exhibit a consistent displacement from the mantle array indicating subduction-related metasomatism and/or crustal contamination.

5.3.2 Geodynamic Implications

The petrologic observations show that the Miocene volcanic units in the Uşak-Güre basin were derived from a lithospheric mantle source that had been heterogeneously enriched by subduction-related events. The timing of such an enrichment event is highly debated. Some authors suggest that the Neogene volcanic

units in western Anatolia were produced by the Hellenic subduction system that progressively migrated to the south from Eocene to Recent (Fytikas et al., 1984; Okay & Satır, 2000; Innocenti et al., 2005; Ring et al., 2010). Alternatively, Yılmaz (1989) suggested that the mantle source for the Neogene volcanism in the region was altered by a previous subduction of the northern branch of the Neotethys. According to this view, the mantle produced early–middle Miocene hybrid magmas that mixed with crustal-derived melts in a compressional tectonic regime (Yılmaz, 1989, 1990; Güleç, 1991).

Similarly, Aldanmaz et al. (2000) proposed that the early–middle Miocene volcanism resulted from previously metasomatized mantle in an extensional environment that was driven by partial delamination of sub-continental lithospheric mantle roots, with the mantle-derived melts subsequently contaminated in crustal reservoirs. On the other hand, as the volcanic rocks in this study clearly lie to the south of the İzmir-Ankara Suture Zone, the subduction of the northern-branch of the Neo-Tethys cannot be responsible for metasomatism of the mantle source. In this case, the metasomatic events were likely related to (1) ancient subduction (e.g. Proterozoic as proposed by Pe-Piper & Piper, 2001, 2007) or (2) Miocene activity of the Hellenic subduction zone (as proposed by Ring et al., 2010). Moreover, Seyitoğlu (1997) linked the Miocene volcanic activity to an extensional setting resulting from orogenic collapse of the thickened crust. This view also explains the time-dependent chemical variation of the volcanism (increasing amounts of mafic products).

The Quaternary Kula volcanics, with sodic-alkali OIB-type compositions, are presumed to be generated from decompressional melting of the asthenospheric mantle as the overlying lithosphere thinned (Yılmaz, 1989, 1990; Güleç, 1991; Seyitoğlu, 1997; Aldanmaz et al., 2000). Recently, Innocenti et al. (2005) suggested that these products were produced in a subduction system in which the nearly flattened and folded subducted slab tore allowing the rise of sub-slab mantle to produce the Quaternary Kula volcanism. However, mantle tomographic sections clearly indicate a steeply dipping subducted slab that is incompatible with this model

(Spakman et al., 1988; Faccenna et al., 2003; van Hinsbergen et al., 2005; Ring et al., 2010).

When the geological observations are considered, it is apparent that the Miocene volcanism in the study area was developed synchronously with the tectonic exhumation of the Menderes Core Complex. Exhumation of the massif was asymmetrical and occurred in distinct stages (e.g. Şengör, 1987; Seyitoğlu & Scott, 1996; Gessner et al., 2001; Purvis & Robertson, 2005; Ring et al., 2010; Ersoy et al., 2010). The volcano-sedimentary infill of the Uşak-Güre basin remains to the North of the asymmetrically uplifted Menderes Core Complex. Moreover, the volcanic rocks in western Anatolia are clearly restricted to the northern part of the Menderes Massif, and there is no significant volcanic activity further to the south as proposed by Pe-Piper & Piper (2001, 2007). These observations may be used to discuss the nature of the Miocene subduction system that produced the volcanic rocks. In light of the data from this study and previous suggestions, I hypothesize that the early–middle Miocene Uşak-Güre volcanic rocks were produced during orogenic collapse, during which the Menderes Core Complex was exhumed by extensional tectonics (Figure 5.14a).

The subduction-related metasomatized nature of the lithospheric mantle source of the volcanic rocks was most probably inherited from a previous subduction-related process, either during the Proterozoic or during retreating of the Hellenic subduction zone (e.g. Pe-Piper & Piper 2001, 2007; Ring et al., 2010). The extensional tectonics and subsequent formation of the Menderes Core Complex was probably driven by partial delamination of the sub-continental lithospheric mantle (e.g. Aldanmaz et al., 2000). Such a delamination event was likely responsible for upwelling of the asthenospheric mantle, near the center of the Menderes Core Complex, to produce the OIB-type sodic alkaline Quaternary Kula volcanism (Figure 5.14b).
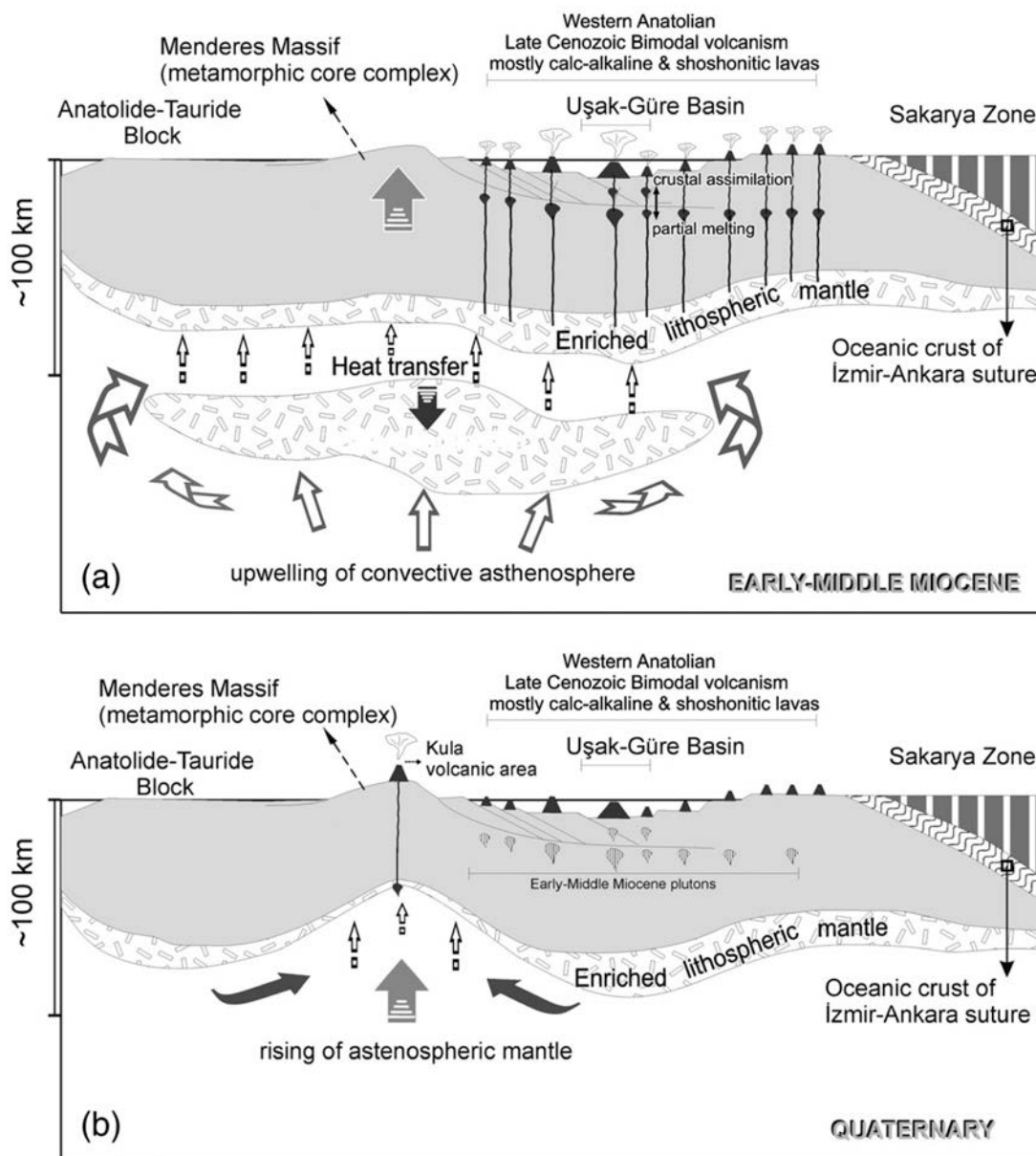
Figure 5.14 Cartoon diagram showing the (a) early–middle Miocene and (b) Quaternary geodynamic and magmatic evolution of Western Anatolia.

CHAPTER SIX
CONCLUSIONS

The combination of geologic mapping, detailed sedimentologic and structural evidence and collecting samples for geochemistry, from each of the evolutionary phases, have allowed us to characterise the temporal and spatial evolution of footwall and hangingwall deformation, physical volcanologic and petrogenetic constraints which is interpreted in the context of evolution of the Uşak-Güre basin during Miocene.

The results of stratigraphic and structural evolution of the thesis are summarised as:

(1) The new ^{40}Ar/^{39}Ar radiometric data demonstrate that Cenozoic volcanism commenced (17.29 Ma) with the emplacement of the Beydağı volcanic unit in the northern part of the Uşak-Güre basin, synchronously with deposition of the İnay group. The youngest radiometric age is obtained from the Beydağı volcanic unit in the Beydağı caldera (12.15±0.15 Ma) in the south, indicating that the Beydağı volcanism was active until the late middle Miocene, and that its activity migrated from north to south with time.

(2) The radiometric ages from the Beydağı and Payamtepe volcanic units are crucial for understanding the time of deposition of the İnay group. The youngest and oldest radiometric ages are important because the type sections of the İnay group (e.g. Ahmetler and Ulubey formations are observed in extensive area of western Anatolia in NE–SW-trending basins) are taken from the Uşak-Güre basin. Based on our correlations, the deposition of the İnay group commenced as early as ~17 Ma in the north of the Uşak-Güre basin.

(3) The ^{40}Ar/^{39}Ar dates of the Payamtepe volcanic unit restrict its activity to a period between 16.01±0.08 and 15.93±0.08 Ma. This evidence leads to two important observations regarding the evolution of Uşak-Güre basin: (1) the İnay

group accumulated from late early Miocene (17.29 Ma), not early middle Miocene as proposed previously (Seyitoğlu, 1997), to middle Miocene (12.15 Ma) for the Uşak-Güre basin, and (2) the basin has been affected by an extensional tectonic regime since late early Miocene, and two different compositional volcanic activities are shown by the Beydağı volcanism (early–middle Miocene) and the Payamtepe volcanism (middle Miocene).

(4) The study indicates three tectonic stages since the Early Cenozoic: the Early Miocene Deformation phase (D_2); the Middle Miocene Deformation Phase (D_3) and the Late Miocene Deformation Phase (D_4). Each of three phases indicates that the Uşak-Güre basin was affected by NE–SW-trending progressive extensional tectonics.

(5) This thesis also presents interpretations of depositional mechanism of the early Miocene Hacıbekir; the early middle Miocene İnay Groups and the Asartepe formation. The large-scale corrugations on the SDF are responsible for the sediment flux that formed the Hacıbekir Group. So, the Hacıbekir Group does not belong to the deposits of the Uşak-Güre basin. The Hacıbekir Group tectonically overlies the cataclastic rocks of the Menderes Massif, rather than unconformably as proposed previously (Seyitoğlu, 1997; Yılmaz et al., 2000; Çemen et al., 2006).

(6) Northeast-dipping low-angle detachment surfaces are clearly defined in both of the Uşak and Güre basin margins for the first time. Photomicrographs of the metamorphic rocks of the Menderes Massif as a footwall unit of the SDF show a transition from the ductile to brittle deformation. So, these textures and some mesoscopic structures in the field demonstrate the characteristics of the low-angle detachment fault along the SDF occurred at the beginning of the Miocene in Uşak-Güre basin. The ductile NNE-transport extensional structures are affected by a brittle NNE-transport extensional system through from Early Miocene to Late Miocene.

(7) The initial extensional system called the Early Miocene Deformation (D_2 Phase) is formed by low-angle normal faults with a ramp-flat geometry, which detach above an extensional detachment that cuts down into the schist and

metagranites on Güre margin. Displacement along the ramp-flat geometry of the low-angle normal faults has folded the hanging-wall rocks, which show folds with NE–SW-oriented axes, transverse to the extensional transport.

(8) The Menderes Massif which has been recognized as a metamorphic core complex, which results from a large-scale extension on the Gediz detachment fault, formed in response to rapid crustal extension that most likely occurred due to the gravitational collapse following contractile over-thickening of the crust of the Menderes Massif in the early middle Miocene. Following the D_2 extensional phase, fluvio-lacustrine İnay Group initiated their own deposition (17-15 Ma). NE–SW directed oblique accommodation faults deformed and cut the hanging wall of the GDF. These faults were responsible for the NE–SW directed Uşak-Güre basin (e.g. Selendi, Gördes, Demirci basins) with an accompanying huge volume of calc-alkaline and ultrapotassic volcanism both of the main fault extending the Güre margin and within the Uşak basin (Figure 3.7d).

(9) NE–SW oblique faults which were sustained faults as a consequence of extension were triggered by the isostatic uplift and exhumation of the Menderes core complex from Oligo-Miocene to late Miocene. Since the late Miocene NE–SW oblique and high angle faults uplifted the Uşak basin margin. These faults were responsible for the deposition of the Asartepe formation and also exhumation of the buried units of the basin (Figure 3.7e). Uşak basin margin was accentuated by the activity of high-angle faults with NEE–SWW orientation that produced as a dome shape structure (see Figure 3.2) since the late Miocene which is called the Late Miocene Deformation (D_4 Phase). High angle normal faults configured the present boundaries between the cover rocks of the Asartepe formation and the metamorphic basement. Locally these high angle normal faults cut the Early Miocene detachment fault with NEE–SWW orientation.

(10) I propose a probable transfer fault zone (Uşak–Muğla Transfer Zone) directly controlled by NE–SW-trending oblique slip normal faults which led to successive

extensional deformations since the middle Miocene on the eastern edge of the Menderes Massif Core Complex (Figure 3.8).

The results of physical volcanology studies of the thesis are summarised as:

(1) Volcanologic evolution of three volcanic edifices has been described for the first time in the western Anatolia. The stratovolcanoes were generated in a subaqueous-subaerial environment and all the volcanic sequences form complex successions of effusive-extrusive and explosive deposits with associated reworked deposits.

(2) Elmadağ stratovolcano includes eight distinct pyroclastic flows (ignimbrite; P_1-P_8), three debris flows (D_1-D_3), two block-and-ash flows (B_1 and B_2) and several undefined debris avalanche deposits; İtecektepe have three pyroclastic flows (P_1-P_3), two debris flow (P_1-P_2), three debris avalanche deposits (T_1-T_3); Beydağı exhibits seven pyroclastic flows (P_1-P_7), three debris flows (D_1-D_3) and several debris avalanche deposits.

(3) Accumulation of the debris flow and debris avalanche deposits occurred in a subaqueous environment by explosive fragmentation in the presence of water (İnay Lake). The products of the explosive volcanism and related magma-water interactions have been described for the first time in western Anatolia. The magma-water interactions have not only exposed within destruction areas of İtecektepe and Beydağı volcanic centers, but also out of Elmadağ volcano. This evidence indicates that accumulation of the lake sediments was still ongoing the post-destructive phase. I have also supplied evidences for subaqueous-subaerial effusive phase. Peperitic textures have been observed within Güre basin, especially in Zahman village, as evidenced by the jig-saw fit breccias clasts, lobate contacts with host rocks (lacustrine Ulubey formation, İnay Group) and occurrence at both bottom and top of the coherent lava facies (Zahman lava flows).

(4) Strong evidence is also present regarding to origin of three destructive structures. All evidence indicates that Elmadağ destructive area may be occurred by both mechanism of multi-stage sector collapses and intense tectonic deformations. Thickness and distributions of pyroclastic flow deposits of the Elmadağ area seem to be not enough to produce of the caldera structure, whereas İtecektepe and Beydağı deformation areas reflect a caldera structure. It is suggested that Beydağı destructive area display nested caldera structure based on its own elongation in circular shaping, wide-spread and thick pyroclastic flow deposits (e.g. ignimbrites) which widely covered by the lacustrine deposits (Ulubey formation) and similar volcanologic properties respect to other calderas in the world.

(5) Finally, the occurrence of volcanism and related gold bearing porphyry system in Beydağı volcanic edifice and destructive areas of Elmadağ and İtecektepe are tectonically controlled by the combined influence of the NE–SW oblique, strike-slip and high-angle faults on-land propagating destruction of these stratovolcanoes.

The results of geochemical and radiometric age studies of the thesis are summarised as:

(1) Three different volcanic units (Beydağı and Payamtepe volcanic units and Karaağaç dikes) were recognized within the Uşak-Güre basin using new mapping and radiometric age data. Our new ^{40}Ar/^{39}Ar radiometric data show that Cenozoic volcanism in the Uşak-Güre basin started (17.29 Ma) with the Beydağı volcanic unit, which is located in the northern part of the basin where it interfingers with the İnay group. The youngest radiometric age from the Beydağı volcanic unit is from the Beydağı caldera (12.15±0.15 Ma) in the south. Also, the ^{40}Ar/^{39}Ar dates of the Payamtepe volcanic unit restrict it to a period between 16.01±0.08 and 15.93±0.08 Ma.

(2) The volcanic rocks display a broad compositional range from basaltic trachyandesite to rhyolite and are high-K calc-alkaline to shoshonitic and ultrapotassic. The geochemical features of the volcanic rocks are comparable with

those of the other volcanic areas in western Anatolia, indicating that they were derived from enriched mantle lithosphere metasomatized by subduction related fluids. The volcanic rocks from the Uşak-Güre basin reflect a complex petrogenetic evolution.

(3) Their genesis includes magma mixing and fractional crystallization processes which were likely accompanied by crustal assimilation. The rocks of the Beydağı volcanic unit have been affected by~0–60% mixing with the more mafic magmas of the Payamtepe volcanic unit and subsequent plagioclase and pyroxene dominated fractional crystallization processes.

(4) Exhumation of the Menderes core complex accompanying the lithospheric-scale extensional fault systems provided natural conduits for the transport of calc-alkaline and potassic magmas in Uşak-Güre basin. The origin of the early–middle Miocene Uşak-Güre lavas in western Anatolia is best explained by delamination of lithospheric mantle slices that were heterogeneously enriched by previous subduction-related processes.

REFERENCES

Agostini, S., Doglioni, C., Innocenti, F., Manetti, P., Tonarini, S., & Savaşçın, M.Y. (2007). The transition from subduction-related to intraplate Neogene magmatism in the Western Anatolia and Aegean area. In: Beccaluva, L., Bianchini, G., Wilson, M., (Eds.), Cenozoic Volcanism in the Mediterranean Area: *Geological Society of America, Special Paper, 418,* 1-15.

Agostini, S., Doglioni, C., Innocenti, F., Manetti, P., & Tonarini, S. (2010). On the geodynamics of the Aegean rift. *Tectonophysics. 488,* 7-21.

Alçiçek, M.C., Ten Veen, J.H., & Özkul, M. (2006). Neotectonic development of the Çameli basin, southwestern Anatolia, Turkey. In: Robertson, A., Mountrakis, D., Brun, J.-P. (Eds.), Tectonic Development of the Eastern Mediterranean Region: *Geophysical Society of London Special Publication, 260,* 591-611.

Alçiçek, H. (2010). Stratigraphic correlations of the Neogene basins in southwestern Anatolia: Regional paleogeographical, paleoclimatic and tectonic implications. *Paleogeography, Paleoclimatology, Paleoecology, 291,* 297-318.

Aldanmaz, E., Pearce, J.A., Thirlwall, M.F., & Mitchell, J.G. (2000). Petrogenetic evolution of late Cenozoic, post-collision volcanism in western Anatolia, Turkey. *Journal of Volcanology and Geothermal Research, 102,* 67-95.

Aldanmaz, E. (2002). Mantle source characteristics of alkali basalts and basanites in an extensional intracontinental plate setting, western Anatolia, Turkey: Implications for multi-stage melting. *International Geology Review 44,* 440-457.

Aldanmaz, E., Pickard, M., Hanan, B.B., Furman, T., Kurkcuoglu, B., & Sayit, K. (2009). Geochemical Evolution of Miocene Volcanism in Western Anatolia, Turkey Related to Orogenic Collapse. *American Geophysical Union, Fall Meeting, 90,* 1770.

Alıcı, P., Temel, A., & Gourgaud, A. (2002). Pb-Nd-Sr isotope and trace element geochemistry of Quaternary extension-related alkaline volcanism: a case study of Kula region (western Anatolia, Turkey). *Journal of Volcanology and Geothermal Research 115,* 487-510.

Altunkaynak, Ş. (2007). Collision-driven slab breakoff magmatism in northwestern Anatolia, Turkey. *Journal of Geology, 115,* 63-82.

Aydar, E., Gourgaud, A., Deniel, C., Lyberis, N., & Gundoğdu, N. (1995). Quaternary volcanism of Central Anatolia (Turkey) – association of calc-alkaline and alkaline magmatisms in a zone of convergence. *Canadian Journal of Earth Sciences, 32,* 1058-1069.

Aydar, E., Bayhan, H,, & Gourgaud, A. 1998. Köroğlu caldera, mid-west Anatolia, Turkey: volcanological and magmatological evolution. *Journal of Volcanology and Geothermal Research, 335,* 279-288.

Aydar, E., Bayhan, H., & Gourgaud, A. 2003. The lamprophyres of Afyon stratovolcano, western Anatolia, Turkey: description and genesis. *Geomaterials, 335,* 279-288.

Belousov, A., Belousova, M., & Voight, B. (1999), Multiple edifice failures, debris avalanches and associated eruptions in the Holocene history of Shiveluch volcano, Kamchatka, Russia. *Bulletin of Volcanology, 61,* 324-342.

Bingöl, E. (1977). Geology and main rock unit petrology of Muratdağı. *Bulletin of the Geological Society of Turkey, 20,* 13-66.

Boccaletti, M., Manetti, P., & Peccerillo, A. (1974). The Balkanids as an instance of back-arc thrust belt: possible relation with the Hellenids. *Geological Society of America Bulletin, 85,* 1077-1084.

Bozkurt, E. (2001). Neotectonics of Turkey - a synthesis. *Geodinamica Acta, 14,* 3-30.

Bozkurt, E. (2003). Origin of NE-trending basins in western Turkey. *Geodinamica Acta, 16,* 61-81.

Bozkurt, E. (2004). Granitoid rocks of the southern Menderes Massif (southwestern Turkey): field evidence for Tertiary magmatism in an extensional shear zone. *International Journal of Earth Science, 93,* 52-71.

Bozkurt, E., & Park, R.G. (1994). Southern Menderes Massif—an incipient metamorphic core complex in Western Anatolia, Turkey. *Journal of the Geological Society, 151,* 213-216.

Bozkurt, E., & Oberhansli, R. (2001). Menderes Massif (Western Turkey): structural, metamorphic and magmatic evolution—a synthesis. *International Journal of Earth Science, 89,* 679-708.

Bozkurt, E., & Sözbilir, H. (2004). Tectonic evolution of the Gediz graben: field evidence for an episodic, two-stage extension in Western Turkey. *Geological Magazine, 141,* 63-79.

Bunbury, J. M.R (1996). The Kula volcanic field, western Turkey: The development of a Holocene alkali basalt province and the adjacent normal-faulting graben: *Geological Magazine, 133,* 275-283.

Candan, O., Çetinkaplan, M., Oberhansli, R., Rimmele, G. & Akal, C. (2005). Alpine high-P/low-T metamorphism of the Afyon Zone and implications for the metamorphic evolution of Western Anatolia, Turkey. *Lithos*, *84,* 102-124.

Cas, R.A.F., & Wright, J.V. (1987). *Volcanic Successions: modern and ancient: a geological approach to processes, products and successions, London.* Allen and Unwin Press, 528.

Catlos, E.J., & Çemen, İ. (2005). Monazite ages and the evolution of the Menderes Massif, Western Turkey. *International Journal of Earth Sciences, 94,* 204-217.

Catlos, E.J., Baker, C.B., Soronsen, S.S., Çemen, İ., & Hançer, M. (2008). Monazite geochronology, magmatism, and extensional dynamics within the Menderes Massif, Western Turkey. *IOP Conference Series: Earth and Environmental Science, 2,* 012013.

Collins, A.S., & Robertson, A.H.F. (2003). Kinematic evidence for late Mesozoic-Miocene emplacement of the Lycian Allochthon over the Western Anatolia Belt, SW Turkey. *Geolological Journal, 38,* 1-16.

Çemen, İ., Goncuoglu, M.C., & Dirik, K. (1999). Structural evolution of the Tuzgolu Basin in central Anatolia, Turkey. *Journal of Geology, 107,* 693-706.

Çemen, İ., Catlos, E.J., Göğüş, O., & Özerdem, C. (2006). Postcollisional extensional tectonics and exhumation of the Menderes Massif in Western Anatolia extended terrane, Turkey. *Geological Society of America Special Paper*, *409,* 353-379.

Çiftçi, N.B., & Bozkurt, E. (2009). Evolution of the Miocene sedimentary fill of the Gediz Graben. *Journal of Sedimentary Geology, 216,* 49-79.

Çiftçi, N.B., & Bozkurt, E. (2010). Structural evolution of the Gediz Graben, SW Turkey: temporal and spatial variation of the graben basin. *Basin Research*, *22,* 846-873.

Çoban, H., & Flower, M.F.J. (2007). Late Pliocene lamproites from Bucak, Isparta (southwestern Turkey): Implications for mantle 'wedge' evolution during Africa-Anatolia convergence. *Journal of Asian Earth Science, 29,* 160-176.

Daley, B. (1971). Diapiric and other deformational structures in a Oligocene argillaceous limestone. *Sedimentary Geology, 6,* 29-51.

Dewey, J.F., Hempton, M.R., Kidd, W.S.F., Saroğlu, F., & Şengör, A.M.C. (1986). Shortening of continental lithosphere: The neotectonics of Eastern Anatolia—A young collision zone. In: Coward, M.P., Ries, A.C. (Eds.), Collision zone tectonics: *Geological Society of London Special Publication, 19,* 3-36.

De Rosa, R. (1999). Compositional modes in the ash fraction of some modern pyroclastic deposits: their determination and significance. *Bulletin of Volcanology, 61,* 162-173.

Dilek, Y., & Altunkaynak, Ş. (2007). Cenozoic crustal evolution and mantle dynamics of post collisional magmatism in western Anatolia. *International Geology Review, 49,* 431-453.

Doglioni, C., Agostini, S., Crespi, M., Innocenti, F., Manetti, P., Riguzzi, F., & Savaşçın, Y. (2002). On the extension in Western Anatolia and the Aegean sea. In: Rosenbaum, G., Lister, G. S. (Eds.), Reconstruction of the Evolution of the Alpine–Himalayan Orogen: *Journal of the Virtual Explorer, 8,* 169-184.

Doglioni, C., Tonarini, S., & Innocenti, F. (2009). Mantle wedge asymmetries and geochemical signatures along W- and E-NE-directed subduction zones. *Lithos, 113,* 179-189.

Edmonds, M., Herd, R.A., & Strutt, M.H. (2006). Tephra deposits associated with a large lava dome collapse, Soufriére Hills Volcano, Montserrat, 12–15 July 2003. *Journal of Volcanology and Geothermal Research, 153,* 313-330.

Ercan, T., Dinçel, A., Metin, S., Türkecan, A., & Günay, E. (1978). Geology of the Neogene basins in Uşak region. *Bulletin of the Geological Society of Turkey, 21,* 97-106.

Ercan, T., Satır, M., Kreuzer, H., Türkecan, A., Günay, E., Çevikbaş, A., Ateş, M., & Can, B. (1985). The interpretation of new chemical, isotopic and geochronologic data from the Cenozoic volcanics of western Turkey. *Bulletin of the Geological Society of Turkey, 28,* 121-136.

Ercan, E., Satır, M., Sevin, D., & Türkecan, A. (1996). Some new radiometric ages from Tertiary and Quaternary volcanic rocks from West Anatolia. *Bulletin Mineral Research and Exploration Institute (Turkey), 119,* 103-112.

Erdoğan, B., & Güngör, T. (2004). The problem of the core-cover boundary of the Menderes Massif and an emplacement mechanism for regionally extensive gneissic granites, Western Anatolia (Turkey). *Turkish Journal of Earth Sciences*, *13,* 15-36.

Erkül, F., Helvacı, C., & Sözbilir, H. (2005). Evidence for two episodes of volcanism in the Bigadic borate Basin and tectonic implications for western Turkey. *Geological Journal, 40,* 545-570.

Ersoy, E., & Helvacı, C. (2007). Stratigraphy and geochemical features of the Early Miocene bimodal (ultrapotassic and calc-alkaline) volcanic activity within the NE-trending Selendi Basin, Western Anatolia, Turkey. *Turkish Journal of Earth Science, 16,* 117-139.

Ersoy, E., Helvacı, C., Sözbilir, H., Erkül, F., & Bozkurt, E. (2008). A geochemical approach to Neogene–Quaternary volcanic activity of western Anatolia: An example of episodic bimodal volcanism within the Selendi Basin, Turkey. *Chemical Geology, 225,* 265-282.

Ersoy, E.Y., Helvacı, C., & Sözbilir, H. (2010). Tectono-stratigraphic evolution of the NE–SW- trending superimposed Selendi basin: Implications for late Cenozoic crustal extension in Western Anatolia, Turkey. *Tectonophysics, 488,* 210-232.

Ersoy, E.Y., Helvaci, C., & Palmer, M. (2011). Stratigraphic, structural and geochemical features of the NE–SW trending Neogene volcano-sedimentary basins in western Anatolia: Implications for associations of supra-detachment and transtensional strike-slip basin formation in extensional tectonic setting. *Journal of Asian Earth Sciences*, *41,* 159-183.

Faccenna, C., Jolivet, L., Piromallo, C., & Morelli, A. (2003). Subduction and the depth of convection in the Mediterranean mantle. *Journal of Geophysical Research, 108,* 2099.

Fierstein, J., Hildreth, W., & Calvert, A.T. (2011). Eruptive history of South Sister, Oregon cascades. *Jounal of Volcanology and Geothermal Research, 207* (3-4), 145-179.

Floyd, P.A, Helvacı, C., & Mittwede, S.K. (1998). Geochemical discrimination of volcanic rocks associated with borate deposits: an exploration tool. *Journal of Geochemical Exploration, 60,* 185-20.

Foley, S.F., Venturelli, G., Green, D.H., & Toscani, L. (1987). The ultrapotassic rocks: characteristics, classification, and constraints for petrogenetic models. *Earth-Science Reviews, 24,* 81-134.

Francalanci, L., Innocenti, F., Manetti, P., & Savaşçin, M.Y. (2000). Neogene alkaline volcanism of the Afyon-Isparta area, Turkey: petrogenesis and geodynamic implications. *Mineralogy and Petrology, 70,* 285-312.

Francalanci, L., Vougioukalakis, G.E., Perini, G., & Manetti, P. (2005). A West-East traverse along the magmatism of the South Aegean volcanic arc in the light of

volcanological, chemical and isotope data. In: Fytikas, M., Vougioukalakis, G.E. (Eds.). The South Aegean Active Volcanic Arc, Present Knowledge and Future Perspectives: Amsterdam, *Elsevier book series Developments in Volcanology 7,* 65-111.

Freundt, A., Wilson, C.J.N., & Carey, S.N. (2000). Ignimbrites and block-and ash flow deposits. In: Sigurdsson H, Houghton B, McNutt S.R, Rymer H, Stix, J. (Eds.). *Encyclopedia of volcanoes* (581-599). San Diego: Academic Press.

Fytikas, M., Innocenti, F., Manetti, P., Mazzuoli, R., Peccerillo, A., & Villari, L. (1984). Tertiary to Quaternary evolution of volcanism in the Aegean region. In: Dixon, J.E., & Robertson, A.H.F. (Eds.). The Geological Evolution of the Eastern Mediterranean. *Geological Society London Special Publication, 17,* 687-699.

Gautier, P., Brun, J.P., Moriceau, R., Sokoutis, D., Martinod, J., & Jolivet, L. (1999). Timing, kinematics and cause of Aegean extension: a scenario based on a comparison with simple analogue experiments. *Tectonophysics, 315,* 31-72.

Gawthorpe, R.L., & Leeder, M.R. (2000). Tectono-sedimentary evolution of active extensional basins. *Basin Research*, *12,* 195-218.

Geological Map (1:500000) of Turkey–İzmir (2002). Publication of Mineral Research and Exploration Institute of Turkey.

Genç, Ş.C., & Yılmaz, Y. (1997). An example of the post-collisional magmatism in norrthwestern Anatolia: the Kızderbent volcanics (Armutlu peninsula, Turkey). *Turkish Journal of Earth Sciences, 6,* 33-42.

Genç, Ş.C., Karacık, Z., Altunkaynak, S., & Yılmaz Y. (2001). Geology of a magmatic complex in the Bodrum peninsula, SW Turkey. In: Dora, O.Ö., Özgenç İ., Sözbilir, H. (Eds.). *Proceedings of the International Earth Sciences Colloquium on the Aegean region*, 63-68.

Gessner, K., Ring, U., Johnson, C., Hetzel, R., Passchier, C.W., & Güngör, T. (2001). An active bivergent rolling-hinge detachment system; central Menderes metamorphic core complex in western Turkey. *Geology, 29,* 611-614.

Glodny, J., & Hetzel, R. (2007). Precise U–Pb ages of syn-extensional Miocene intrusions in the central Menderes Massif, western Turkey. *Geological Magazine, 144* (2), 235-246.

Görür, N., Sakınç¸ M., Barka, A., Akkök, R., & Ersoy, S. (1995). Miocene to Pliocene paleogeographic evolution of Turkey and its surroundings. *Journal of Human Evolution*, *28,* 309-324.

Güleç, N., 1991. Crust-mantle interaction in western Turkey: implications from Sr and Nd isotope geochemistry of Tertiary and Quaternary volcanics. *Geological Magazine 128,* 417-435.

Helvaci, C., & Yağmurlu, F. (1995). Geological setting and economic potential of the lignite and evaporite-bearing Neogene basins of Western Anatolia, Turkey. *Israel Journal Earth Sciences*, *44,* 91-105.

Helvacı, C., & Alonso, R.N. (2000). Borate deposits of Turkey and Argentina; a summary and geological comparison. *Turkish Journal of Earth Science, 24,* 1-27.

Helvacı, C., Ersoy, Y., Sözbilir, H., Erkül, F., Sümer, Ö., & Uzel, B. (2009). Geochemistry and ^{40}Ar/^{39}Ar geochronology of Miocene volcanic rocks from the Karaburun Peninsula: Implications for amphibole-bearing lithospheric mantle source, Western Anatolia. *Journal of Volcanology and Geothermal Research, 185,* 181-202.

Hetzel, R., Passchier, C.W., Ring, U., & Dora, O.Ö. (1995). Bivergent extension in orogenic belts; the Menderes Massif (south Western Turkey). *Geology (Boulder)*, *23,* 455-458.

Innocenti, F., Agostini, S., Di Vincenzo, G., Doglioni, C., Manetti, P., Savaşçın, M.Y., & Tonarini, S. (2005). Neogene and Quaternary volcanism in Western Anatolia: magma sources and geodynamic evolution. *Marine Geology, 221,* 397-421.

Innocenti, F., Agostini, S., G., Doglioni, C., Manetti, P., & Tonarini, S. (2010). Geodynamic evolution of the Aegean: constraints from the Plio-Pleistocene volcanism of the Volos–Evia area. *Journal of the Geological Society, London 167,* 475-489.

Irvine, N., & Baragar, W.R.A. (1971). A guide to chemical classification of the common volcanic rocks. *Canadian Journal of Earth Science, 8,* 523-548.

Işık, V., & Tekeli, O. (2001). Late orogenic crustal extension in the northern Menderes Massif (western Turkey); evidence for metamorphic core complex formation. In: Bozkurt, E., Oberhänsli, R. (Eds.), Menderes Massif (western Turkey); structural, metamorphic and magmatic evolution. *International Journal of Earth Science, 89,* 757-765.

Işık, V., Tekeli, O., & Seyitoğlu, G. (2004). The ^{40}Ar/^{39}Ar age of extensional ductile deformation and granitoid intrusion in the northern Menderes core complex: implications for the initiation of extensional tectonics in Western Turkey. *Journal of Asian Earth Sciences*, *23,* 555-566.

İnci, U. (1984). Stratigraphy and organic properties of bituminous shales of Demirci and Burhaniye. *Geological Society of Turkey Bulletin, 5,* 27-40.

İnci, U. (1998). Lignite and carbonate deposition in Middle Lignite succession of the Soma Formation, Soma coalfield, western Turkey. *International Journal of Coal Geology, 37,* 287-313.

Jackson, J., & McKenzie, D. (1988). Rates of active deformation in the Aegean Sea and surrounding areas. *Basin Research, 1,* 121-128.

Jolivet, L. (2001). A comparison of geodetic and finite strain pattern in the Aegean, geodynamic implications. *Earth and Planetary Science Letters, 187,* 95-104.

Juras, S., Miller, R., & Skyman, P. (2010). Technical Report for the Kısladag Gold Mine, Turkey. January 2010.

Justet, L., & Spell, T.L. (2001). Effusive eruptions from a large silicic magma chamber: the Bearhead Rhyolite, Jemez volcanic field, NM. *Journal of Volcanology and Geothermal Research, 107,* 241-264.

Kano, K., & Takarada, S. (2007). Cone-building block-and-ash flows: the Senyama volcanic products of O'e Takayama volcano, SW Japan. Bulletin of Volcanology, 69, 563–575.

Karacık, Z. (2006). Stratigraphy and volcanology of the Türkbükü volcanics: products of a stratovolcano in the Bodrum Peninsula, SW Anatolia. *Geological Journal, 41,* 145-162.

Karacik, Z., & Yılmaz, Y. (1998). Geology of the ignimbrites and the associated volcano-plutonic complex of the Ezine area, northwestern Anatolia: *Journal of Volcanology and Geothermal Research, 85,* 251-264.

Karaoğlu, Ö., Helvaci, C., & Ersoy, E.Y. (2010). Petrogenesis and $^{40}Ar/^{39}Ar$ Geochronology of the Volcanic Rocks of the Uşak and Güre basins, western Türkiye. *Lithos*, *119 (3-4),* 193-210.

Koçyiğit, A., Yusufoğlu, H., & Bozkurt, E. (1999). Evidence from the Gediz graben for episodic two-stage extension in western Turkey. *Journal of Geological Society, London, 156,* 605-616.

Koçyiğit, A., Ünay, E., & Saraç, G. (2000). Episodic graben formation and extensional neotectonic regime in west Central Anatolia and the Isparta Angle: a case study in the Akşehir–Afyon graben, Turkey. In: Bozkurt, E., Winchester, J.A., & Piper, J.D.A. (Eds.). Tectonics and magmatism in Turkey and the surrounding area, *Geological Society of London, Special Publication, 173,* 405-421.

Krainer, K., & Spötl, C. (1998). Abiogenic silica layers within a fluvio-lacustrine succession, Bolzano Volcanic Complex northern Italy: a Permian analogue for Magadi-type cherts? *Sedimentology, 45,* 489-505.

Kreemer, C., Holt, W.E., & Haines, A.J. (2003). An integrated global model of present-day plate motions and plate boundary deformation. *Geophysical Journal International, 154,* 8-34.

Le Maitre, R.W. (2002). *Igneous Rocks: a Classification and Glossary of Terms*: *Recommendations of the International Union of Geological Sciences Subcommission on the Systematics of Igneous Rocks.* Cambridge; Cambridge University Press.

LePichon, X., & Angelier, J. (1979). The Hellenic arc and trench system: A key to the neotectonic evolution of the eastern Mediterranean area. *Tectonophysics, 60,* 1-42.

Lipman, P.W., & Sawyer D.A. (1985). Mesozoic ash-flow caldera fragments in southeastern Arizona and their relation to porphyry copper deposits. *Geology, 13,* 652-656.

Lips, A.L.W., Cassard, D., Sözbilir, H., Yılmaz, H., & Wijbrans, J.R. (2001). Multistage exhumation of the Menderes Massif, western Anatolia (Turkey). *International Journal of Earth Sciences, 89,* 781-792.

Manville, V. (2002). Sedimantary and geomorphic responses to ignimbrite emplacement. Readjustment of the Waikato River after the AD 181 Taupo Eruption, New Zeland. *Journal of Geology, 110,* 519-541.

Marcoux, E., & Milési, J.P. (2000). Volcanism and epithermal gold deposits. In Leyrit, H., & Montenat, C. (Eds.). Volcaniclastic rocks from magma to tephra. *Gordon and Breach Science Publishers;* 235-251.

Marrett, R.A., & Allmendinger, R. W. (1990). Kinematic analysis of fault-slip data. *Journal of Structural Geology.*

McKenzie, D. (1978). Active tectonics of the Alpine-Himalayan belt, the Aegean Sea and surrounding regions. *Geophysical Journal of the Royal Astronomical Society, 55,* 217-254.

Miyashiro, A. (1974). Volcanic rock series in island arcs and active continental margins. *American Journal of Science, 274,* 321-355.

Mueller, W.U., & Corcoran, P.L. (2001). Volcano-sedimentary processes operating on a marginal continental arc: the archean Raquette Lake formation, Slave Province, Canada. *Sedimentary Geology.* (141-142), 169-204.

Okay, A., & Siyako, M. (1993). The revised location of the İzmir-Ankara Suture in the region between Balıkesir and İzmir. In: S. Turgut (Ed.). (333-355). *Tectonics and Hydrocarbon Potential of Anatolia and Surrounding Regions*.

Okay, A.İ., & Satır, M. (2000). Coeval plutonism and metamorphism in a latest Oligocene metamorphic core complex in northwest Turkey. *Geological Magazine, 5,* 495-516.

Okay, A.İ., Zattin, M., & Cavazza, W. (2010). Apatite fission-track data for Miocene arabia-Eurosia collision. *Gelogy, 38,* 35-38.

Ortner, H. (2007). Styles of soft-sediment deformation on top of a growing fold system in the Gosau Group at Muttekopf, Northern Calcereous Alps, Austria: Slumping versus tectonic deformation. Sedimentary Geology, 196 (1-4), 99-118.

Özer, S., & Sözbilir, H. (2003). Presence and tectonic significance of Cretaceous rudist species in the so-called Permo-Carboniferous Göktepe Formation, central Menderes metamorphic massif, western Turkey. *International Journal of Earth Science, 92,* 397-404.

Parat, F., Dungan, M.A., & Lipman, P.W. (2005). Contemporaneous Trachyandesitic and Calk-alkaline Volcanism of the Huerto Andesite, San Juan Volcanic Field, Colorado, USA. *Journal of Petrology, 46,* 859-891.

Pearce, J.A. (1983). Role of the sub-continental lithosphere in magma genesis at active continental margins. In: Hawkesworth, C. J., Norry, M. J. (Eds.), Continental basalts and mantle xenoliths. (230-249). Nantwich: Shiva Publishing.

Pe-Piper, G., & Piper, D.J.W. (2001). Late Cenozoic, post-collisional Aegean igneous rocks: Nd, Pb and Sr isotopic constraints on petrogenetic and tectonic models. *Geological Magazine, 138,* 653-668.

Pe-Piper, G., & Piper, D.J.W. (2007). Neogene backarc volcanism of the Aegean: new insights into the relationship between magmatism and tectonics. In: Beccaluva, L., Bianchini, G., Wilson, M. (Eds.), Cenozoic Volcanism in the Mediterranean Area. *Geological Society of America, Special Publications* (418), 17-31.

Özer, S., & Sözbilir, H. (2003). Presence and tectonic significance of Cretaceous rudist species in the so-called Permo-Carboniferous Göktepe Formation, central Menderes metamorphic massif, western Turkey. *International Journal of Earth Science, 92,* 397-404.

Purvis, M., & Robertson, A. (2004). A pulsed extension model for the Neogene-Recent E-W-trending Alaşehir Graben and the NE–SW-trending Selendi and Gördes Basins, western Turkey. *Tectonophysics*, *391,* 171-201.

Purvis, M., & Robertson, A. (2005). Miocene sedimentary evolution of the NE-SW-trending Selendi and Gördes basins, western Turkey: Implications for extensional processes. *Sedimentary Geology, 174,* 31-62.

Rimelle, G., Oberhansli, R., Goffe, B., Jolivet, L., Candan, O., & Çetinkaplan, M. (2003). First evidence of high-pressure metamorphism in the "Cover Series" of the southern Menderes massif. Tectonic and metamorphic implications for the evolution of SW Turkey. *Lithos*, *71,* 19-46.

Ring, U., Johnson, C., Hetzel, R., & Gessner, K. (2003). Tectonic Denudation of a late Cretaceous–Tertiary collisional belt: regionally symmetric cooling patterns and their relation to extensional faults in the Anatolide belt of Western Turkey. *Geological Magazine*, *140,* 421-441.

Ring, U., & Layer, P.W. (2003). High-pressure metamorphism in the Aegean, eastern Mediterranean: underplating and exhumation from the Late Cretaceous until the Miocene and Recent above the retreating Hellenic subduction zone. *Tectonics, 22,* 1022.

Ring, U., & Collins, A.S. (2005). U–Pb SIMS dating of synkinematic granites: timing of core complex formation in the northern Anatolide belt of Western Turkey. *Journal of the Geological Society*, *162,* 289-298.

Ring, U., Will, T., Glodny, J., Kumerics, C., Gessner, K., Thomson, S.N., Güngör, T., Monie, P., Okrusch, M., & Drüppel, K. (2007). Early exhumation of high-pressure rocks in extrusion wedges: the Cycladic blueschist unit in the eastern Aegean, Greece and Turkey. Tectonics, *26, TC2001.*

Ring, U., Glodny, J., Will, T., & Thomson, S. (2010). The Hellenic Subduction System: High Pressure Metamorphism, Exhumation, Normal Faulting, and Large-Scale Extension. *Annual Review of Earth and Planetary Sciences, 38,* 45-76.

Ring, U., & Glodny, J. (2010). No need for lithospheric extension for exhuming (U)HP rocks by normal faulting. *Journal of the Geological Society, 167,* 225-228.

Rollinson, H.R. (1993). *Using Geochemical Data: Evaluation, Presentation, Interpretation.* London: Prentice Hall.

Rossetti, D.F. (1999). Soft-sediment deformational structures in late Albian to Cenomanian deposits, Sao Luis Basin, northern Brazil: evidences for paleoseismicity. *Sedimentology,* *46,* 1065-1081.

Rytuba, J.J. (1994). Evolution of Volcanic and Tectonic Features in Caldera settings and Their Importance in the localization of Ore Deposits. *Economic Geology, 89,* 1687-1696.

Rytuba, J.J., Arribas, A., Jr., Cunningham, C.G., McKee, E.H., Podwysock, M.H., Smith, J.G., Kelly,W.C., & Arribas, A. (1990). Mineralized and unmineralized calderas in Spain Part II, Evolution of the Rodalquilar caldera complex and associated gold-alunite deposits: *Mineralium Deposita, 25,* 29-35.

Sato, H., Fujii, T., & Nakada, S. (1992). Crumbling of dacite dome lava and generation of pyroclastic flows at Unzen volcano. *Nature, 360,* 664-666.

Schneider, J.L., & Fisher, R.V. (1998). Transport and emplacement mechanisms of large volcanic debris avalanches: evidence from the northwest sector of Cantal volcano (France). *Journal of Volcanology and Geothermal Research, 83,* 141-165.

Seyitoğlu, G. (1997). Late Cenozoic tectono-sedimentary development of the Selendi and Uşak-Güre basin: a contribution to the discussion on the development of east-west and north trending basins in western Turkey. *Geological Magazine, 134,* 163-175.

Seyitoğlu, G., & Scott, B. (1991). Late Cenozoic crustal extension and basin formation in West Turkey. *Geological Magazine, 128,* 155-166.

Seyitoğlu, G., & Scott, B. (1992). Late Cenozoic volcanic evolution of the northeastern Aegean region. *Journal of Volcanology and Geothermal Research, 54,* 157-176.

Seyitoğlu, G., & Scott B. (1994). Late Cenozoic basin development in west Turkey: Gördes Basin tectonics and sedimentation. *Geological Magazine, 131,* 631-637.

Seyitoğlu, G., & Scott, B. (1996). The cause of N-S extensional tectonics in western Turkey: Tectonic escape vs. backarc spreading vs. orogenic collapse. *Journal of Geodynamics, 22,* 145-153.

Seyitoğlu, G., Işik, V., & Çemen, İ. (2004). Complete Tertiary exhumation history of the Menderes Massif, Western Turkey: an alternative working hypothesis. *Terra Nova*, *16,* 358-364.

Seyitoğlu, G.**,** Alçiçek, M.C., Işık, V., Alçiçek, H., Mayda, S., Varol, B., Yılmaz, I., & Esat, K. (2009). The stratigraphical position of Kemiklitepe fossil locality (Eşme, Uşak) revised: Implications for the Late Cenozoic sedimentary basin development and extensional tectonics in western Türkiye. *Neues Jahrbuch für Geologie und Palaeontologie, 251,* 1-15.

Sözbilir, H., 2001. Extensional tectonics and the geometry of related macroscopic structures: field evidence from the Gediz Detachment, Western Turkey. *Turkish Journal of Earth Science 10,* 51-67.

Sözbilir, H. (2005). Oligo-Miocene extension in the Lycian orogen: evidence from the Lycian molasse basin, SW Turkey. *Geodinamica Acta*, *18,* 257-284.

Sözbilir, H., Sari., B., Uzel, B., Sümer, Ö., & Akkiraz, A. (2010). Tectonic implications of transtensional supradetachment basin development in an extension-parallel transfer zone: the Kocaçay Basin, western Anatolia, Turkey. *Basin Research, 23,* 423-448.

Spakman, W., Wortel, M.J.R,, & Vlaar, N.J. (1988). The Hellenic subduction zone: a tomographic image and its geodynamic implications. *Geophysical Research Letters, 15,* 60-3.

Spell, T.L., & McDougall, I. (2003). Characterization and calibration of $^{40}Ar/^{39}Ar$ dating standards. *Chemical Geology, 198,* 189-211.

Staudacher, T.H., Jessberger, E.K., Dorflinger, D., & Kiko, J. (1978). A refined ultra high vacuum furnace for rare gas analysis. *Journal of Physical Earth Science Instrumentation, 11,* 781-784.

Sun, S.S., & McDonough, W.F. (1989). Chemical and isotopic systematics of oceanic basalts: implications for mantle compositions and processes. In Saunders, A. D., & Norry, M. J. (Eds.). Magmatism in the Oceanic Basin. *Geological Society of London, Special Puplication,* 313-345.

Şengör, A.M.C., & Yılmaz, Y. (1981). Tethyan evolution of Turkey: a plate tectonic approach. *Tectonophysics, 75,* 181-241.

Şengör, A.M.C., Yilmaz, Y., & Sungurlu, O. (1984). Tectonics of the Mediterranean Cimmerides: nature and evolution of the western termination of Paleo-Tethys. In The Geological Evolution of the Eastern Mediterranean, Dixon, J.E, Robertson, A.H.F. (Eds.). *Geological Society London*, *Special Puplication, 17,* 77-112.

Şengör, A.M.C., Görür, N., & Şaroğlu, F. (1985). Strike-slip deformation, basin formation and sedimentation: strike-slip faulting and related basin formation in zones of tectonic escape: Turkey as a case study. *Society for Economic Paleontologists and Mineralogists Special Publication, 37,* 227-264.

Şengör A.M.C. (1987). Cross-faults and differential stretching of hanging walls in regions of low-angle normal faulting: examples from western Turkey. In: Coward, M.P., Dewey, J.F., Hancock, P. (Eds.). Continental Extensional Tectonics. *Geological Society London Special Puplications, 28,* 575-589.

Taylor, S.R., & McLennan, S.M. (1995). The geochemical evolution of the continental crust. *Reviews of Geophysics, 33,* 241-265.

Thirlwall, M.F., Smith, T.E., Graham, A.M., Theodorou, Hollings, N.P., Davidson, J.P., & Arculus, R.J. (1994). High field strength element anomalies in arc lavas; source or process? *Journal of Petrology, 35,* 819-838.

Thompson, S.N., & Ring, U. (2006). Thermochronologic evaluation of postcollision extension in the Anatolide orogen, Western Turkey. *Tectonics*, 25 (3), TC30005.

Ulusoy, I., Çubukçu, E., Aydar, E., Labazuy, P., Gourgaud, A., & Vincent, P.M. (2004). Volcanic and deformation history of the Bodrum resurgent caldera system (southwestern Turkey). *Journal of Volcanology and Geothermal Research, 136,* 71-96.

Ustaömer, P.A., Ustaömer, T., Collins, A.S., & Reischpeitsch, J. (2009). Lutetian arc-type magmatism along the southern Eurasian margin: New U-Pb LA-ICPMS and whole-rock geochemical data from Marmara Island, NW Turkey. *Mineralogy and Petrology, 96,* 177-196.

Uzel, B., & Sözbilir, H. (2008). A First record of strike- slip basin in western Anatolia and its tectonic implication: The Cumaovası basin as an example. *Turkish Journal of the Earth Science, 17,* 559-591.

van Hinsbergen, D.J.J., Hafkenscheid, E., Spakman, W., Meulenkamp, J.E., & Wortel, R. (2005). Nappe stacking resulting from subduction of oceanic and continental lithosphere below Greece. *Geology, 33,* 325-328.

van Hinsbergen, D.J.J. (2010). A key extensional metamorphic complex reviewed and restored: the Menderes Massif of western Turkey. *Earth Science Review, 102,* 60-76.

van Hinsbergen, D.J.J., Dekkers, M.J., Bozkurt, E., & Koopman, M. (2010). Exhumation with a Twist: Paleomagnetic Constraints on the Evolution of the Menderes Metamorphic Core Complex, Western Turkey. *Tectonics* 29, TC3009.

Verge, N. (2000). The tectonics and consequences of mid-Oligocene to earliest Miocene detachment-facilitated, large magnitude NNE–SSW horizontal extension/vertical thinning of the earlier tectonically thickened continental lithosphere of western Anatolia. İzmir: Proceedings of International Earth Science Colloquium Aegean Region.

Weaver, B.L., & Tarney, J. (1984). Empirical approach to estimating the composition of the continental crust. *Nature, 310,* 575–577.

Yağmurlu, F., Savaşçın, M.Y., & Ergün, M. (1997). Relation of alkaline volcanism and active tectonism within the evolution of Isparta Angle, SW Turkey. *Journal of Geology, 105,* 717-728.

Yılmaz, Y. (1989). An approach to the origin of young volcanic rocks of western Turkey. In Şengör, A.M.C. (Ed.). *Tectonic evolution of the Tethyan region* (159-189). Kluwer Academic Publishers.

Yılmaz, Y. (1990). Comparison of young volcanic associations of western and eastern Anatolia formed under a compressional regime: a review. *Journal of Volcanology and Geothermal Research, 44,* 1-19.

Yılmaz, Y., Genç, Ş. C., Gürer, F., Bozcu, M., Yılmaz, K., Karacık, Z., Altunkaynak, Ş., & Elmas, A. (2000). When did western Anatolian grabens begin to develop? In: E. Bozkurt, J.A. Winchester, and Piper, J.A.D. (Eds.), Tectonics and Magmatism in Turkey and Surrounding Area. *Geological Society London, Special Puplication, 173,* 131-162.

Yılmaz, Y., Genç, Ş.C., Karacık, Z., & Altunkaynak Ş. (2001). Two contrasting magmatic associations of NW Anatolia and their tectonic significance. *Journal of Geodynamics, 31,* 243-271.